R-1064 (02)

UCRL-16246
SPRING 1965

NASA CR70522

GPO PRICE $ _____

CFSTI PRICE(S) $ _____

Hard copy (HC) _____

Microfiche (MF) _____

ff 653 July 65

SEMIANNUAL REPORT
BIOLOGY and MEDICINE

DONNER LABORATORY
and DONNER PAVILION

UCRL-16246
UC-48 Biology and Medicine
TID-4500 (45th Ed.)

DONNER LABORATORY AND DONNER PAVILION

LAWRENCE RADIATION LABORATORY - UNIVERSITY OF CALIFORNIA
BERKELEY, CALIFORNIA

SEMIANNUAL REPORT — BIOLOGY AND MEDICINE

SPRING 1965

John H. Lawrence, M.D., Editor
Tove Neville, Associate Editor

Contract W-7405-eng-48

Examples of mouse lymphoma ascites cells following irradiation. Above is a tripolar mitosis. Cell below shows an "anaphase bridge" between groups of chromosomes. For pi-meson irradiation effects see p.101.

TABLE OF CONTENTS

Classification and Evolution of Patterns of Erythropoiesis in Polycythemia Vera as Studied by Iron Kinetics

Myron Pollycove, H. Saul Winchell and John H. Lawrence

Diverse patterns of erythropoiesis have been described in polycythemia vera. Increased erythropoiesis is present, but patients may have normal (1, 2) or shortened red-cell life span (3, 4). Splenic sequestration of red cells and extramedullary erythropoiesis may or may not be present (3, 4, 5). A relative or absolute decrease in red-cell volume may occur, and some patients may die with a refractory anemia (3, 6). The present work is directed toward classification of the diverse patterns, and definition of the evolutionary history of erythropoiesis in this disease. Possible bases for the pattern of evolution of erythropoiesis documented in this work are discussed. Sixty-four patients with polycythemia vera were studied by means of iron kinetics. Seven of these patients had repeat iron-kinetic studies over a 12-year period. The clinical course and pathologic findings at postmortem examination on the patients were correlated with iron-kinetics findings.

MATERIALS AND METHODS

Except where indicated, patients reported in the series were diagnosed as having polycythemia vera on the basis of: a) an increased circulating red-cell volume exceeding 34 ml/kg body wt; and, b) exclusion of disorders associated with secondary erythrocytosis. Tumors associated with secondary erythrocytosis were excluded on the basis of complete medical evaluation during clinic visits and subsequent long-term follow-up of the patient's course and, when applicable, postmortem findings. Arterial blood-oxygen saturation was performed in patients where the possibility of chronic pulmonary disease or right to left cardiac and vascular shunts was present. All patients were evaluated by members of the medical group, and in most cases therapy and long-term follow-up were performed at the Donner Laboratory clinic. Complete records were kept of all pertinent medical information concerning procedures performed elsewhere throughout the entire course of the patient's disease.

Iron-kinetic studies were performed according to the techniques of Pollycove and Mortimer (7). Ten to forty microcuries of radioactive ^{59}Fe, ferrous citrate, specific activity 5-25 μCi per microgram, were used. This amount was added to sufficient fresh autologous plasma and the mixture incubated at 37°C for 20-30 min to insure binding of all iron to the beta-1 globulin transferrin. Five to twenty milliliters of the labeled fresh plasma were injected intravenously with a calibrated syringe. During the 14 days following injection, serial blood samples were analysed for plasma and erythrocyte radioactivity and surface measurements of radioactivity over the liver, spleen and sacral bone marrow were made, as

described previously (7, 8). Plasma and erythrocyte radioactivities were measured by counting 2- or 3-ml samples in a well scintillation counter with 2-inch or 3-inch sodium iodide crystals and 6-inch or 4-1/2-inch lead shielding. The counter efficiency was approximately 16% for ^{59}Fe, the background approximately 20 counts per minute. All samples were counted for sufficient time periods to accumulate over 2,000 counts above background to insure satisfactory counting statistics. Blood samples were centrifuged at 2,000 g for 15 min twice to obtain plasma free of erythrocytes. It was necessary to take care in drawing and manipulating the blood to avoid hemolysis which, after significant labeling of erythrocytes occurs, would produce erroneously high concentration of radioiron in plasma. Concentration of iron in plasma was determined by the modification of Peters and co-workers of the Ramsey method (9). Hematocrits were determined on all samples (Wintrobe). Plasma and red-cell volumes were determined independently by the ^{59}Fe and ^{32}P dilution methods. Surface counting rates were obtained from mobile scintillation counters over liver, spleen and sacrum. External monitoring values are expressed as a fraction of the zero time extrapolate value.

Plasma-radioiron curves obtained over a 14-day period were analyzed for iron incorporation into hemoglobin by first correcting the curves for hemolytic feedback of iron into the plasma and then analyzing the resulting curves in the fashion previously described by Pollycove and Mortimer (7). Where there is neither hemolytic nor marked storage feedback of iron into the plasma, the radioiron-plasma-disappearance curve falls exponentially throughout the first 10- to 14-day period of observation. Therefore, in the absence of marked feedback from stores, it was assumed that whenever the plasma-radioiron curve reached an early asymptote during the first two-week period that this asymptotic value was primarily the result of radioiron feedback from hemolysis. By: a) assuming that extramedullary hemolytic feedback of radioiron into the plasma was proportional to the amount of radioiron incorporated in circulating erythrocytes; and, by b) assuming that the asymptote reached by the plasma-radioiron curve during the first two weeks was due primarily to hemolytic feedback of iron into the plasma, a curve could be drawn which approximates the extramedullary hemolytic feedback function of radioiron to plasma (see Fig. 2 and Fig. 4). When intramedullary hemolysis is present, causing the plasma-radioiron-clearance curve to reach an asymptote much earlier than the time of maximum incorporation of radioiron into erythrocytes, hemolytic feedback of radioiron into the plasma is estimated by a function having the shape of normal red-cell ^{59}Fe-incorporation curve but more rapid and displaced in time so as to coincide with the point at which the plasma radioiron reaches its asymptote (see Fig. 3). On subtraction of this hemolytic feedback curve from the measured plasma-radioiron concentration, a curve with two or three exponential components was obtained, which was analyzed in the fashion previously described by Pollycove and Mortimer.

Measurement of platelet survival was performed using ^{32}DFP in a manner described previously (10). White-blood-cell counts were performed in a routine fashion. Differential counts were done on Jenner-Giemsa stained air-dried blood films. Platelet counts were determined by the phase contrast technique. All cell counting was done in duplicate.

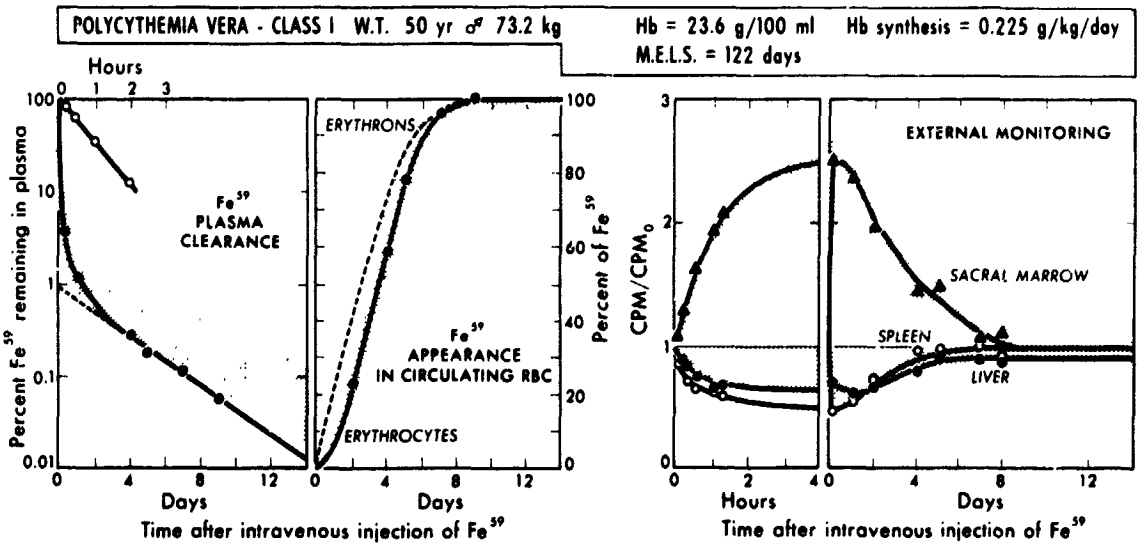

Figure 1. In polycythemia Class I ^{59}Fe kinetics, plasma-iron turnover is increased and normal patterns of radioiron incorporation into circulating red cells and external monitoring over sacral bone marrow, liver and spleen are seen. Analysis of plasma-radioiron data (7) yields increased values for rate of hemoglobin synthesis, but mean erythron life span is within normal limits (i.e., increased red-cell volume is proportional to increased erythropoiesis).

MUB-6190

RESULTS

^{59}FE-KINETICS PATTERNS: ERYTHROPOIETIC CLASSES I, IIa, IIb, III The iron-kinetics results obtained from studies of 64 patients with polycythemia vera (Table 1) can be classified into four distinct patterns. The first pattern is characterized by a normal RBC life span and is exemplified by the data and results shown in Fig. 1. External monitoring data are similar to that seen in normal subjects (7), with a rapid accumulation of iron in the bone marrow and subsequent complete release. There is no evidence of splenic sequestration of red cells nor any evidence of extramedullary hemopoiesis. The pattern of appearance of ^{59}Fe in circulating RBC is within normal limits. Plasma-iron turnover is increased above normal values (class average of nine patients not given previous radiation therapy from Table 2 is 0.040 mg/kg/hr ± σ = 0.016, normal being 0.019 ± σ = 0.004). Analysis of plasma-radioiron data obtained during a two-week period according to the kinetics model of Pollycove and Mortimer (7) shows increased hemoglobin synthesis (same class average on Table 2 is 0.172 g/kg/d ± σ = 0.046, normal being 0.089 ± σ = 0.014) and a normal mean erythron life span, (same class average from Table 2 = 118 days ± σ = ± 13.6 normal being 117 days ± σ = 7.5). This pattern is designated polycythemia Class I.

Class II is characterized by shortened red-cell survival in the absence of extramedullary erythropoiesis. This class is subdivided into two groups; Class IIa, in which red-cell hemolysis occurs after release from the bone marrow (usually with splenic sequestration and destruction); and Class IIb, in which the majority of red-cell hemolysis occurs in the narrow

Table I. Iron kinetics in polycythemia vera.

Patient	Sex	Age at time of Dx	Treatment before study: Rx before Fe^{59} kinetics	Treatment before study: Time before Fe^{59} study of last Rx (yr)	Maximum recorded RBC vol. (ml/kg) [24-33]	Time after Dx max. RBC vol. measured (yr)	Hematologic values at time of Fe^{59} kinetics [normal values]: Time from Dx to study (yr)	WBC ($No./mm^3$) [5 000-10 000]	Platelets ($No./mm^3$) [250 000-500 000]	Hemoglobin (g/100 ml) [14.0-16.0]	RBC volume (ml/kg) [24-33]	Plasma volume (ml/kg) [27-45]	Serum iron (μg/100 ml) [70-170]	Plasma iron turnover (mg/kg/hr) [0.019 ± .004]	Calculated Hgb synthesis (g/kg/day) [0.089 ± .014]	Mean erythron life (days) [117 ± 7.5]	Erythropoietic site: Marrow	Spleen	Liver	Time from Dx to death (yr)
Polycythemia vera Class I																				
W. S.	M	19	None	--	59.4	1.2	1.2	5 900	290 000	21.0	56.8	32.2	85	0.020	0.124	139	+	0	0	--
A. L.	F	50	None	--	48.4	0.0	4.3	60 600	360 000	18.2	48.4	33.7	89	0.044	0.116	112	+	0	0	--
W. T.	M	50	None	--	90.3	0.9	0.5	8 400	224 000	23.6	85.8	24.2	230	0.061	0.225	122	+	0	0	14.5[a]
F. W.	M	52	None	--	68.5	0.0	0.0	17 600	290 000	22.3	60.3	32.5	130	0.029	0.188	134	+	0	0	11.7
R. G.	M	55	None	--	58.3	1.1	0.4	25 500	340 000	19.6	52.6	35.2	119	0.037	0.128	127	+	0	0	--[b]
A. E.	M	56	None	--	54.6	0.0	1.0	9 600	255 000	18.2	54.6	47.8	190	0.032	0.185	96	+	0	0	7.3
P. P.	F	63	None	--	64.1	0.0	0.0	13 400	405 000	22.4	52.6	37.2	117	0.044	0.177	101	+	0	0	2.5
A. J.	M	64	None	--	87.8	0.0	0.2	11 000	250 000	25.1	87.7	47.4	72	0.053	0.261	111	+	0	0	12.3[a]
J. C.	F	69	None	--	48.6	0.0	0.2	11 200	330 000	21.0	48.6	32.4	118	0.040	0.147	116	+	0	0	3.4
C. M.	F	56	Y^{90}	2.3	62.8	2.3	2.3	10 500	224 000	27.0	62.8	19.8	120	0.030	0.153	132	+	0	0	16.7
Polycythemia vera Class IIa																				
D. S.	M	13	None	--	48.6	0.1	0.6	8 900	210	18.9	43.0	34.0	80	0.036	0.217	68	+	0	0	--
J. W.	M	14	None	--	41.1	0.1	0.8	8 800	235	13.7	34.4	25.5	88	0.026	0.130	81	+	0	0	--
M. J.	M	27	None	--	40.5	5.8	3.0	20 800	770 000	16.5	36.0	37.9	86	0.022	0.124	99	+	0	0	--
G. S.	M	32	None	--	70.8	0.7	0.7	14 800	620 000	16.7	41.5	41.4	89	0.050	0.320	41	+	0	0	--
L. H.	F	32	None	--	43.2	0.0	3.0	9 900	625 000	19.8	43.2	39.0	210	0.067	0.269	51	+	0	0	--
L. H.	M	50	None	--	42.8	3.1	0.0	8 050	360 000	17.6	39.6	42.0	170	0.025	0.151	86	+	0	0	--
H. T.	M	51	None	--	34.2	3.9	3.0	11 700	380 000	18.5	34.7	37.5	113	0.015	0.051	62	+	0	0	--
E. A.	M	66	None	--	65.2	0.5	0.5	11 500	310 000	19.0	44.1	44.8	82	0.084	0.452	39	+	0	0	--
R. J.	M	67	None	--	41.0	0.0	0.5	10 700	675 000	18.9	41.8	33.4	149	0.030	0.182	71	+	0	0	--
D. C.	M	43	splenectomy[c]	0.4	50.2	0.2	0.0	17 900	640 000	19.1	49.1	36.0	75	0.044	0.224	68	+	0	0	8.6[d]
H. M.	M	43	P^{32}	0.8	46.0	0.0	11.0	18 000	300 000	21.4	46.0	27.9	200	0.050	0.218	68	+	0	0	16.4[a]
A. P.	F	51	P^{32}	2.0	48.0	1.7	4.7	6 900	330 000	13.4	26.0	20.7	121	0.026	0.171	47	+	0	0	8.5[b]
H. K.	M	57	P^{32}	0.5	61.1	3.2	3.2	6 600	283 000	20.2	49.7	36.0	140	0.051	0.276	58	+	0	0	13.2[b]
R. G.	F	64	P^{32}	2.0	41.2	2.9	8.2	7 650	507 500	16.9	32.7	38.7	139	0.034	0.192	41	+	0	0	--
Polycythemia vera Class I-IIa, iron-deficient																				
B. T.	M	6	None	--	44.5	0.0	0.0	7 400	275 000	20.0	44.5	34.3	50	0.028	0.154	75	+	0	0	--
L. P.	F	9	None	--	59.2	0.1	0.2	10 150	300 000	20.0	59.2	38.5	35	0.035	0.243	44	+	0	0	--
E. C.	F	37	None	--	65.6	0.0	0.5	9 300	255 000	20.6	65.6	30.7	46	0.045	0.246	60	+	0	0	--
L. P.	M	40	None	--	38.3	0.0	10.2	8 400	435 000	13.4	38.3	55.6	62	0.039	0.244	58	+	0	0	--
M. G.	F	52	None	--	52.2	0.0	0.0	8 300	350 000	17.1	52.2	45.4	60	0.054	0.256	60	+	0	0	--
G. B.	F	55	None	--	62.2	3.1	0.2	9 300	215 000	19.1	40.5	34.9	36	0.020	0.132	60	+	0	0	--
C. F.	M	63	None	--	48.0	0.0	0.3	11 850	275 000	15.0	35.4	36.4	20	0.023	0.127	57	+	0	0	3.1[b]
A. L.	F	68	None	--	70.9	3.8	3.0	10 000	190 000	16.7	69.7	41.5	31	0.069	0.402	43	+	0	0	4.8
C. M.[c]	M	71	None	--	105.8	0.1	0.2	17 900	230 000	20.0	98.7	43.3	35	0.131	0.571	42	+	0	0	3.5
F. R.	M	72	None	--	61.5	3.3	3.0	26 400	550 000	13.4	43.4	71.7	23	0.064	0.254	47	+	0	0	6.1[f]
F. J.	M	75	None	--	71.8	0.0	0.5	19 550	180 000	18.2	71.8	36.7	41	0.030	0.200	33	+	0	0	0.8[f]
E. P.	F	78	None	--	40.6	0.0	0.0	59 350	850 000	11.3	40.6	51.5	10	0.018	0.114	47	+	0	0	
L. M.	F	28	splenectomy[c]	9.6	49.9	0.0	9.0	20 100	705 000	15.3	49.9	52.6	28	0.038	0.220	67	+	0	0	--
M. O.	F	38	P^{32}	0.3	60.2	12.3	13.0	4 600	270 000	16.2	53.1	46.2	54	0.062	0.251	63	+	0	0	19.0[b]
R. H.	M	48	P^{32}	1.5	66.3	7.7	10.0	16 700	410 000	16.1	26.3	40.5	56	0.041	0.286	29	+	0	0	13.2[b]
R. G.	F	52	P^{32}	3.0	63.3	7.9	11.5	24 800	240 000	10.9	27.4	50.9	37	0.021	0.131	60	+	0	0	16.3[a]
J. M.	M	63	P^{32}	5.6	50.0	9.0	9.0	21 000	955 000	16.7	40.8	52.0	19	0.034	0.195	59	+	0	0	--[e]

Table 1. Iron kinetics in polycythemia vera. (Continued)

Polycythemia vera Class IIb																		
C. P.	M	45	P^{32}	2.5	44.8	11.[illegible]	18.0	2850	270 000	11.0	21.1	58.7	159	0.078	0.432	18	+	0	0	18.4[f]
M. M.	F	56	P^{32}	0.5	51.5	17.9	12.0	3350	180 000	8.2	13.3	46.6	134	0.034	0.217	19	+	0	0	19.0[f]
Polycythemic vera Class III																		
W. I.	M	44	None	--	52.3	16.8	13.0	26 300	260 000	13.6	35.8	51.9	23	0.039	0.233	26	+	+	+	17.0
E. P.	F	45	None	--	58.3	0.0	0.9	27 000	200 000	16.2	54.6	51.7	130	0.097	0.372	49	+	+	0	--
V. L.	F	46	None	--	g	--	18.0	14 500	210 000	9.3	33.2	78.7	48	0.105	0.528	20	+	+	+	21.8[e]
C. T.	F	58	None	---	45.8	0.0	10.0	204 000	300 000	13.1	45.8	71.4	59	0.061	0.381	37	0	+	+	12.0[e]
J. B.	F	70	None	--	46.0	0.0	0.0	9500	206 800	12.3	49.5	68.0	111	0.081	0.476	26	+	+	0	--[h]
J. G.	M	76	None	--	58.8	0.1	0.0	20 900	280 000	17.4	58.8	44.9	19	0.049	0.258	37	+	+	+	2.7
A. F.	F	42	P^{32}	2.7	49.6	19.0	25.0	12 700	200 000	10.3	17.5	46.3	59	0.028	0.184	32	+	+	+	29.0
H. G.	F	46	P^{32}	1.0	g	--	5.0	2700	30 500	7.2	20.5	45.6	155	0.049	0.252	27	+	+	+	6.0
O. C.	F	45	P^{32}	10.0	g	--	6.8	35 000	106 000	7.6	30.1	87.9	203	0.118	0.735	8	+	+	+	8.6[e,h]
M. P.	F	47	P^{32}	2.6	81.6	10.0	10.0	6800	60 000	10.0	28.0	69.7	49	0.085	0.467	18	0	+	+	--
R. H.	M	48	P^{32}	0.5	66.3	7.3	12.5	9700	375 000	8.8	23.0	51.5	100	0.083	0.423	13	+	+	0	12.9[e]
J. L.	M	49	P^{32}	1.3	55.8	5.8	17.0	7650	290 000	13.0	27.4	48.0	121	0.065	0.350	25	+	+	0	21.5[e]
K. ?.	F	49	P^{32}	1.5	52.0	6.8	4.0	18 800	980 000	12.4	33.7	36.6	65	0.066	0.225	36	+	+	+	--
S. S.	M	54	P^{32}	0.7	61.9	0.8	6.0	44 000	760 000	6.4	37.8	113.2	5	0.033	0.196	40	+	+	+	7.8
R. G.	M	55	P^{32}	4.2	58.3	0.4	12.0	7800	255 000	11.4	25.4	52.9	54	0.044	0.298	24	+	+	+	--
R. W.	M	55	spleen irrad.[c]	13.6	68.0	0.0	0.0	46 300	425 000	14.7	68.0	31.1	40	0.072	0.173	28	+	+	+	4.5
P. N.	M	56	P^{32}	0.8	g	--	3.6	22 700	140 000	8.9	30.7	46.2	80	0.092	0.258	31	0	+	+	5.0
H. K.	M	57	P^{32}	0.4	61.1	3.2	8.0	9600	200 000	12.9	35.7	40.9	31	0.067	0.453	18	0	+	+	13.2
J. J.	M	60	P^{32}	0.6	68.7	5.1	7.0	13 500	88 000	8.3	27.1	71.1	97	0.177	0.964	8	+	+	+	7.3[e,h]
W. M.	M	62	P^{32}	0.8	73.3	8.3	9.0	25 700	190 000	13.6	49.6	53.7	44	0.061	0.201	67	0	+	+	10.8[e]
C. F.	M	63	P^{32}	0.6	48.0	0.0	2.5	72 500	210 000	12.0	36.1	41.1	17	0.040			+	+	+	3.1
L. Y.	F	64	P^{32}	0.4	56.9	2.8	1.0	13 200	240 900	21.1	49.7	30.3	200	0.089	0.369	46	+	+	0	3.6[e]
K. L.	F	65	P^{32}	1.5	60.0	4.0	9.0	11 300	320 000	10.7	26.8	55.8	71	0.061	0.296	31	+	+	0	13.2[e]
B. L.	M	69	P^{32}	0.9	51.1	6.8	12.0	12 000	210 000	9.3	19.3	50.0	84	0.046	0.276	24	+	+	0	14.1[e]
F. S.	M	75	P^{32}	2.9	g	--	3.0	27 250	180 000	9.0	25.2	67.5	112	0.045	0.081	34	+	+	+	3.7[e]

a. Developed clinical findings of myeloid metaplasia (Class III) subsequent to study.

b. Developed clinical and iron kinetics findings of myeloid metaplasia (Class III) subsequent to study. For iron kinetics values at the time of repeat study see patient under results of Class III.

c. Not used in averaging in "treatment with P^{32}" group.

d. Developed terminal refractory anemia.

e. Myeloid metaplasia diagnosed by iron kinetics subsequently confirmed at post mortem examination.

f. Acute leukemia at post mortem examination.

g. Red cell volume determination not performed at the time hemoglobin and hematocrit elevated in these cases. However, in each case hemoglobin values in excess of 20.0 grams were recorded and leucocytosis and in some cases thrombocytosis was present and the patient had the clinical findings of polycythemia vera.

h. Myeloid metaplasia in spleen diagnosed by iron kinetics subsequently confirmed by splenectomy or splenic aspiration.

i. Development of myeloid metaplasia subsequent to study demonstrated at post mortem examination.

Table II. Averaged values of data from Table I (mean ±σ)

Measured parameter [normal values]	Class I		Class IIa		Class I - IIa c Fe deficiency		Class IIb		Class III	
	No P^{32} Rx (9)	P^{32} Rx (1)	No P^{32} Rx (9)	P^{32} Rx (4)[b]	No P^{32} Rx (12)	P^{32} Rx (4)[b]	No P^{32} Rx (0)	P^{32} Rx (2)[c]	No P^{32} Rx (6)	P^{32} Rx (18)[b]
Age at time of Diagnosis (Dx)	53.1 ±13.6	56.0	39.1 ±18.2	53.8 ± 7.7	52.2 ±23.6	49.5 ± 9.7	—	45 0 56 0	56.5 ±12.7	55.9 ± 8.95
Maximum recorded RBC volume - ml/kg	64.4 ±14.5	62.8	47.5 ±11.6	49.1 ± 7.4	60.1 ±17.5	60.0 ±10.01	—	44.8 51.5	52.2 ± 5.7	60.3 ± 9.2
Time after Dx maximum RBC volume measured (yr)	1.2 ± 0.5	2.3	1.6 ± 2.0	2.0 ± 1.3	0.6 ± 1.3	9.6 ± 2.8	—	11.5 17.9	— —	6.0 ± 4.8
Time from Dx to death (yr)	8.6 ± 4.5	16.7	— —	9.5 ± 6.2	3.7 ± 1.8	— —	—	18.4 19.0	13.4 ± 7.1	10.7 ± 6.9
Time from Dx to Fe^{59} kinetics study (yr)	0.9 ± 1.23	2.3	1.3 ± 1.2	6.8 ± 3.0	1.5 ± 2.8	11.4 ± 2.3	—	18.0 18.0	7.0 ± 7.1	8.5 ± 5.7
WBC - (No./mm^3) [5 000 - 10 000]	18 000 ±16 000	10 500	11 583 ± 3 746	9 788 ±4 757	16 383 ±14 128	16 775 ± 7 591	—	2 850 3 350	50 366 ±68 984	19 605 ±16 531
Platelets - (No./mm^3) [250 000 - 500 000]	305 000 ±55 000	224 000	531 666 ±208 415	368 750 ±159 513	384 167 ±217 865	468 750 ±287 967	—	270 000 180 000	242 800 ±39 062	268 583 ±232 028
Hemoglobin (g/100 ml) [14.0 - 16.0]	21.3 ± 2.2	22.0	17.7 ± 1.8	18.0 ± 3.1	17.1 ± 3.0	15.0 ± 2.4	—	11.0 8.2	13.7 ± 2.6	10.7 ± 3.3
RBC volume (ml/kg) [24 - 33]	60.8 ±14.3	62.8	41.6 ± 8.8	38.6 ± 9.6	55.0 ±18.0	36.9 ±11.0	—	21.1 13.3	46.3 ± 9.3	30.2 ± 8.8
Plasma volume (ml/kg) [32 - 45]	35.8 ± 7.1	19.8	38.2 ± 3.9	34.6 ± 4.5	43.4 ±11.0	47.4 ± 4.5	—	58.7 46.6	61.1 ±12.2	57.5 ±19.1
Serum iron (µg %) [70 - 170]	128 ± 9	120	119. ±44	150 ±30	37 ±15	42 ±15	—	159 134	65 ±42	90 ±60
Plasma iron turnover -mg/kg/hr - [0.019 ± 0.004][a]	0.040 ± 0.016	0.030	0.039 ± 0.022	0.040 ± 0.011	0.046 ± 0.03	0.040 ± 0.015	—	0.078 0.034	0.072 ± 0.024	0.069 ± 0.035
Calculated Hgb Synthesis - g/kg/day [0.089 ± 0.014][a]	0.172 ± 0.046	0.153	0.211 0.11	0.214 ± 0.040	0.244 ± 0.124	0.216 ± 0.059	—	0.432 0.217	0.375 ± 0.106	0.355 ± 0.209
Mean erythron life span (days) [117 ± 7.5][a]	118 ±13.6	132	66.1 ±18.7	54 ±10.4	52.2 ±11.0	52.8 ±13.8	—	18 19	34.7 ±11.6	28.2 ±14.2

a. Normal values derived from dat.. on 13 normal subjects.

b. Patients treated by splenectomy or splenic radiation are not included .n averaging values.

c. Values of each of the two patients in this class are listed separately.

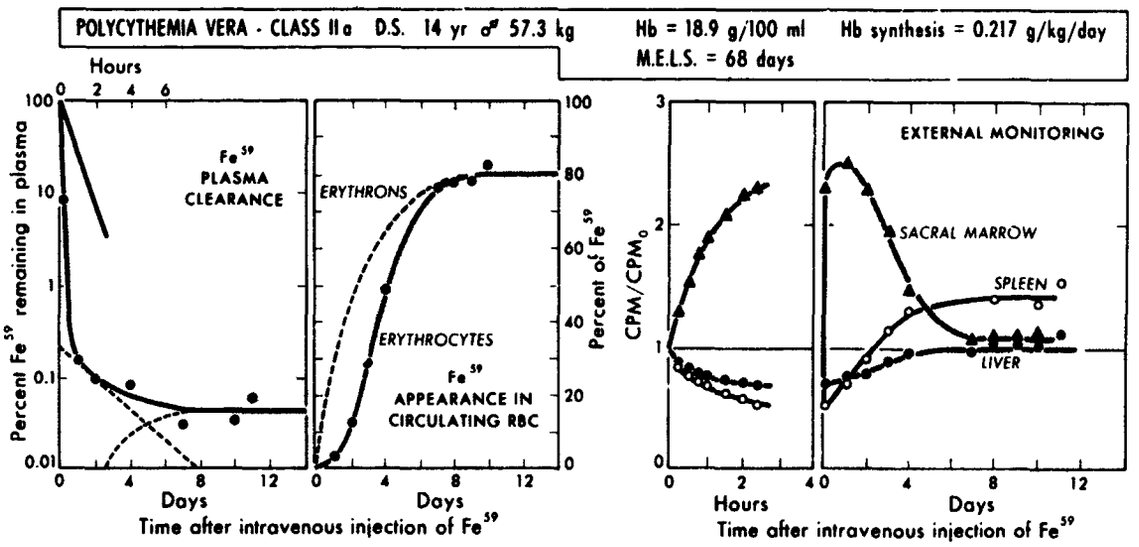

Figure 2. In polycythemia Class IIa ^{59}Fe kinetics, plasma-iron turnover is increased with the plasma-radioiron curve reaching an asymptote at the time maximum incorporation of ^{59}Fe in RBC is reached. If hemolysis is marked, the maximum incorporation of ^{59}Fe in RBC may be below the normal range. External monitoring over sacral bone marrow and liver have normal patterns, but the spleen usually shows a secondary rise above baseline indicating splenic sequestration of red cells. By correcting the plasma-radioiron curve for extramedullary hemolytic feedback (see Materials and Methods section) a curve having two or three exponential components is obtained. Analysis of plasma-radioiron data thus corrected for hemolytic feedback yields increased values for rate of hemoglobin formation and shortened mean erythron life span.
MUB-6191

prior to release into the circulating blood (intramedullary hemolysis). Figure 2 is a typical example of the iron-kinetics pattern designated polycythemia vera Class IIa. In this class there is again rapid accumulation of iron in the sacral marrow with subsequent prompt, virtually complete release as the iron leaves the marrow in circulating red-blood cells. Generally, there is a secondary rise in the counting rate over the spleen indicating splenic sequestration of red blood cells. The shape of the curve representing net ^{59}Fe incorporation into circulating RBC may be within normal limits, but when there is considerable shortening of red-cell survival the maximum net incorporation of ^{59}Fe into circulating RBC is depressed below normal values. Plasma-iron turnover is increased above normal values (class average of nine patients not given previous radiation therapy in Table 2 is 0.039 mg/kg/hr $\pm \sigma$ = 0.022). The kinetic analysis of plasma-radioiron-clearance curves demonstrates increased hemoglobin synthesis (same class average in Table 2 is 0.211 g/kg/d $\pm \sigma$ = 0.114). Shortened red-cell life span is seen (same class average = 66.1 days $\pm \sigma$ = 18.7), and the plasma radioiron becomes constant between six to ten days, in keeping with hemolytic feedback of radioiron into the plasma from red cells destroyed in the spleen. This iron-kinetic pattern is similar to that

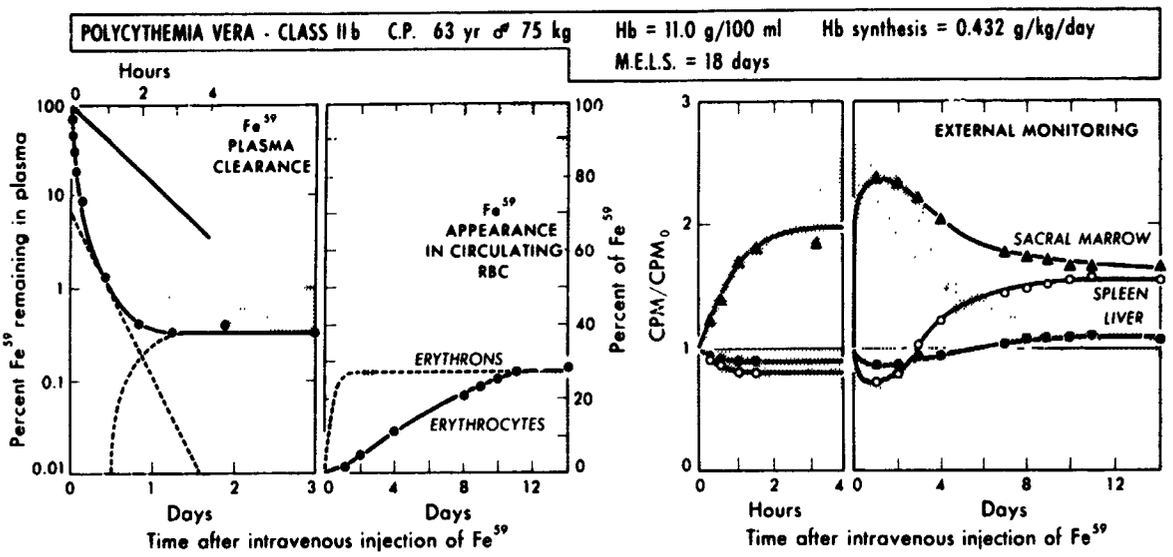

Figure 3. In polycythemis Class IIb ^{59}Fe kinetics, plasma-iron turnover is increased with the plasma-radioiron curve reaching an asymptote much earlier than the time of maximum incorporation of ^{59}Fe into circulating RBC. The appearance of radioiron in circulating RBC is markedly delayed and mean erythron hemoglobinization time is markedly prolonged (7). The external monitoring curve over the sacral bone marrow fails to return to baseline with net retention of radioiron, and the spleen curve frequently shows a variable secondary rise indicating splenic sequestration of RBC. This pattern is identical to that seen in the megaloblastic anemias and Thalassemia major (8), indicating intramedullary hemolysis of erythrocytes and their precursors. When the plasma-radioiron curves are corrected for intramedullary hemolysis (see Materials and Methods section) and the resultant curves are analyzed, hemoglobin synthesis is found to be markedly increased and mean erythron life span is markedly shortened.

MUB-6192

seen in congenital spherocytic anemia and a variety of acquired hemolytic anemias characterized by extramedullary hemolysis (8).

In Class IIb there is markedly shortened red-cell survival, which is predominantly the result of intramedullary hemolysis. This has been studied in only two patients, both of whom had been treated with ^{32}P and were noted to be rapidly deteriorating 18 years following the initial diagnosis of polycythemia vera. In both of these cases anemia was rapidly progressive and hepatosplenomegaly was not marked. External monitoring, as shown in Fig. 3, demonstrates a rapid initial accumulation of iron in the sacral marrow with markedly delayed and incomplete secondary release. Plasma-iron turnover is increased (in case shown in Fig. 3 was 0.078 mg/kg/hr). There is no evidence of extramedullary erythropoiesis in liver or spleen. Kinetic analysis of plasma-radioiron data of the patient shown in Fig. 3 revealed a markedly increased hemoglobin synthesis of 0.432 mg/kg/d with a markedly shortened RBC

life span of 18 days. Maximum incorporation of radioiron into circulating red blood cells is delayed and markedly decreased. A very early hemolytic feedback of iron to plasma is observed in the plasma-radioiron curve. The mean effective erythron-hemoglobinization time (7) is markedly prolonged, correlating with the incomplete release of radioiron from the sacral bone marrow. This pattern is similar to that seen with refractory anemia with erythroid hyperplasia, thalassemia major and the megaloblastic anemias, and is interpreted as representing severe intramedullary hemolysis (8). This is substantiated by the finding of marked erythroid hyperplasia in the bone marrow without an increase of circulating reticulocytes in these patients at the time of kinetic analysis.

The iron-kinetics pattern designated as Class III is characterized by extramedullary hemopoiesis in spleen and sometimes in liver. An example of this class can be seen in Fig. 4. There is an initial accumulation of iron in the spleen and sometimes in the liver with subsequent release as the iron leaves these organs in newly formed red cells. There may or may not be evidence of red-cell production within the bone marrow (see Table 1). The incomplete net release of radioiron from the spleen is interpreted as representing splenic sequestration in addition to splenic production of red blood cells. Plasma-iron turnover is generally greater than that seen in Classes I and IIa (Class III average of six patients not given previous radiation therapy in Table 2 was 0.072 mg/kg/hr $\pm \sigma = 0.024$). Kinetic analysis of the plasma-radioiron data reveals further increase in hemoglobin synthesis (same class average in Table 2 = 0.375 g/kg/d $\pm \sigma = 0.106$) and a further shortening of the mean erythron life span, (same class average in Table 2 = 34.7 days $\pm \sigma = 11.6$). There is marked early hemolytic feedback of iron into the plasma as seen in the plasma-radioiron data. The appearance of ^{59}Fe in circulating RBC is early and rapid, but the maximum net incorporation of radioiron into circulating red cells is distinctly reduced as a result of the destruction of red cells, primarily within the spleen.

In addition to the above mentioned groups there are those polycythemic patients without evidence of myeloid metaplasia or intramedullary hemolysis who were iron deficient at the time of the study. Because of the shortened mean erythron life span and variable splenic sequestration of red cells seen in iron deficiency *per se* (8), these patients could not be differentially classified between Class I and Class IIa. Consequently the iron-kinetics values obtained for members of this group were the result of the abnormalities of iron deficiency superimposed upon the values of Classes I and IIa (see Tables 1 and 2).

EFFECT OF RADIATION THERAPY ON PATTERNS OF ERYTHROPOIESIS Tables 1 and 2 summarize the results of individual iron-kinetic studies correlated with clinical and pathologic features of each of the 64 patients studied. The results were organized according to the classes defined above. In each class the patients who had received no radiation therapy (^{32}P, ^{90}Y, X ray) prior to the time of the iron-kinetic study are listed separately from those patients who had received previous radiation therapy. In all cases, those patients without radiation therapy had received only venesection. In the group that had radiation therapy prior to the study, only those patients are included who had their last course of radiation

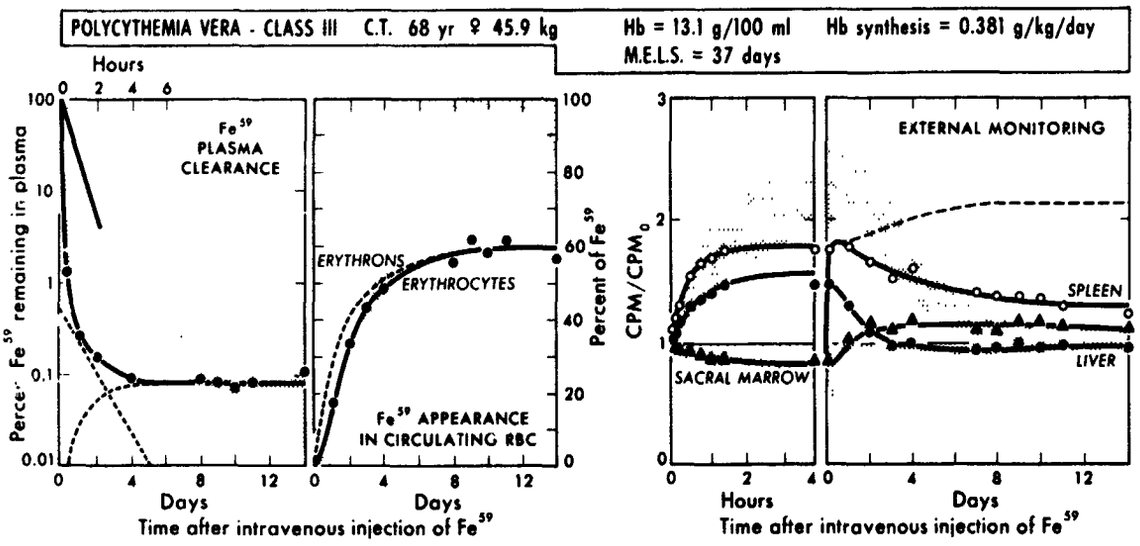

Figure 4. In polycythemia Class III ^{59}Fe kinetics, plasma-iron turnover is increased with the plasma-radioiron curve reaching an asymptote at the time maximum incorporation of radioiron into circulating RBC is reached. ^{59}Fe rapidly appears in circulating RBC, but the maximum incorporation of radioiron into circulating RBC is subnormal because of early hemolysis. Erythropoiesis may or may not be present in bone marrow or liver (see Table 1). The external monitoring curve over a site in which erythropoiesis is present shows an initial rise in counting rate with a subsequent fall concurrent with the appearance of radioiron in circulating erythrocytes. Splenic sequestration of RBC is frequently present resulting in incomplete loss of radioiron from the spleen with failure of the spleen curve to return to baseline values. When splenic sequestration of RBC exceeds splenic erythropoiesis, a spleen curve is obtained similar to the broken line shown on the right hand portion of this figure, in which the magnitude of the secondary rise in counting rate over the spleen exceeds the initial maximum counting rate seen at the end of the first 24 hr. Correction of the plasma-radiciron curve for "extramedullary" type hemolysis and analysis of the resulting curves yields increased rates of hemoglobin synthesis and decreased mean erythron lifespans (Tables 1 and 2).

MUB-6193

therapy more than five months prior to the iron-kinetics study, eliminating those patients in whom the acute affects of radiation would affect red-cell kinetics.

At the time of ^{59}Fe-kinetics study, 10 patients were in Class I (nine untreated by radiation); 14 patients were in Class IIa (nine untreated by radiation); 25 patients were in Class III (six untreated by radiation); two patients were in Class IIb and 17 patients were in iron-deficiency-combined Classes II and IIa (12 patients untreated by radiation). Four of these patients appear in two groups because of change in erythropoietic class determined by repeat iron kinetics study (see Table 3). Within each group the results obtained on patients who had received prior radiation therapy were comparable to those obtained on patients who had not received radiation therapy prior to the time of the study. However, the mean values for red-cell volume and body hemoglobin in treated patients in Classes IIa and III tend to be somewhat lower than in untreated patients in these categories.

INCIDENCE OF IRON DEFICIENCY Of 43 polycythemic patients witnout myeloid metaplasia (Classes I and II with and without iron deficiency), 17 were found to be iron deficient at the time of the study (serum iron < 70 μg %), and of 25 patients having myeloid metaplasia (Class III) 13 patients were found to be iron deficient at the time of the study (Table 1). These results demonstrate the very high frequency with which iron deficiency (resulting from either spontaneous blood loss or phlebotomy) complicates the course of polycythemia vera. Since iron deficiency per se results in decrease in mean erythron life span and increased rate of hemoglobin synthesis, this factor contributes significantly to the abnormalities in erythropoiesis seen in this disease (8).

IRON-KINETICS DIAGNOSIS OF MYELOID METAPLASIA The iron-kinetics evidence for localization of erythropoiesis in a given area depends upon the demonstration of an initial rapid increase in counting rate over the given area with subsequent decrease of counting rate over these sites, simultaneous with the corresponding appearance of radioiron in circulating erythrocytes. However, under the circumstances in which splenic sequestration of red cells exceeds splenic erythropoiesis, (see legend Fig. 4) a delayed secondary rise in the counting rate over the spleen may obliterate evidence of the initial release of iron from the spleen.

In each patient in whom the iron kinetics study was interpreted to demonstrate myeloid metaplasia, the finding was confirmed clinically, (i.e., clinical evidence included the combinations of findings of marked hepatosplenomegaly, marked anisocytosis, poikilocytosis, circulating nucleated red cells, platelet and white-cell abnormalities). Three patients, classified in Class III by iron kinetics, had the diagnosis of myeloid metaplasia confirmed by splenic aspiration or splenectomy. In 11 patients the iron-kinetics diagnosis of myeloid metaplasia was confirmed at postmortem examination (two of which had previous confirmation by splenic aspiration or splenectomy). In two patients in whom a secondary delayed rise in splenic counting rate was noted, suggesting splenic sequestration and destruction of red cells in excess of splenic erythropoiesis, subsequent splenectomy resulted in cessation of the need for supportive transfusions and increased hemoglobin concentration (patients J. B. and O. C. Table 1).

HEPATIC ERYTHROPOIESIS AND IRON DEFICIENCY In all seven cases listed in Table 1 in which myeloid metaplasia was present in the spleen but not in the liver, the serum iron was within normal limits at the time of the study (Table 1). (There was one additional patient, not included in Tables 1 and 2, in whom only a partial iron-kinetics study was performed, erythropoiesis was present only in the spleen and the serum iron was low -- M. D., Table 3). In 13 out of 18 cases where myeloid metaplasia was present in the liver as well as the spleen the patients were iron deficient at the time of study (Table 1). In the remaining five cases where erythropoiesis was present in the liver but the serum iron was not depressed, there was evidence for excessive splenic sequestration and destruction of red cells in the spleen with an average mean erythron life span = 21.6 d. In one case (J. J. Table 3) an initial iron-kinetic study revealed erythropoiesis in spleen but not in the liver and a repeat iron-kinetics study two years later revealed erythropoiesis in both liver and spleen. In the second study there was marked splenic sequestration of red cells with a marked increase in serum-iron turnover and increased hemoglobin synthesis with markedly reduced mean erythron life span. These results suggest that as net hemoglobin synthesis increases, myeloid metaplasia first occurs in the spleen and when further reduction in mean erythron life span and further increase in hemoglobin synthesis occur, either because of superimposition of iron deficiency or marked shortening of RBC survival with splenic sequestration of red cells, myelopoiesis may then be seen in the liver.

BLOOD VOLUME CHANGES The blood volume (sum of independently measured red-cell volume and plasma volume) is increased in all classes of polycythemia studied (11). The greatest increase is seen in Class III (mean values for blood volume for the various classes from Table 2 for patients not given radiation therapy prior to study are in Class I = 96.6 ml/kg, Class IIa = 79.8 ml/kg, Class IIb = 69.9 ml and Class III = 107.4 ml/kg). The increase in blood volume in the members of Class III was roughly correlated with the degree of hepatosplenomegaly present and was associated with a markedly expanded plasma volume. Because of the markedly increased blood volume the red-cell volume (ml RBC/kg body wt.) was frequently found to be in the normal range though the hemoglobin concentration indicated an anemia.

EVOLUTION OF ERYTHROPOIETIC PATTERNS Two patients initially found to be in Class I, and one patient initially found to be in Class IIa, as well as one patient initially found to be in iron deficiency Classes I and IIa, during their subsequent course developed myeloid metaplasia as determined by clinical criteria alone (see above). One patient initially found to be in Class IIa and two patients initially in iron-deficiency Classes I and IIa during their subsequent course were found to develop myeloid metaplasia as determined by histologic examination at postmortem examination in addition to clinical criteria (see Table 1). In one patient initially in Class I and one patient initially in Class IIa, as well as three patients initially in Class IIa, as well as three patients initially in iron deficiency Classes I and IIa, the transition to Class III (myeloid metaplasia) was initially demonstrated by repeat iron-kinetics studies in addition to clinical criteria (see Table 3). The two patients found to be in Class IIb at the time of iron kinetics had no evidence of preceding myeloid metaplasia and thus would have been classified in Classes I and IIa earlier in their course. The time from diagnosis to

Table III. Hematologic values of patients at the time of repeat iron kinetics studies

nt	Class	Time from Dx to study (years)	Last Radiation Rx prior to study (years)	WBC (No./mm^3)	Platelets (No./mm^3)	Hgb (g %)	RBC Vol. (ml/kg)	Plasma Vol. (ml/kg)	Serum Fe (μg %)	Plasma Fe turnover (mg/kg/hr)	Calculated Hb synthesis g/kg/day	Net mean Erythron life span (days)	Erythropoietic site		
													Marrow	Spleen	Liver
.	I	0.4	None	25 5000	340 000	19.6	52.6	35.2	119	0.037	0.128	127	+	0	0
.	III	12.0	4.2	7 800	255 000	11.4	25.4	52.9	54	0.044	0.298	24	+	+	+
.	II_a	3.2	0.5	6 600	280 000	20.2	49.7	36.0	140	0.051	0.276	58	+	0	0
.	III	8.0	0.4	9 600	200 000	12.9	35.7	46.9	31	0.067	0.453	18	0	+	+
	III	5.0	0.3	8 200	220 000	14.2	66.7	68.3	48	0.124	0.751	23	+	+	0
	III	7.0	0.6	13 500	88 000	8.3	27.1	71.1	97	0.177	0.964	8	+	+	+
.	III	0.9	None	27 000	200 000	16.2	54.6	51.7	130	0.097	0.372	49	+	+	0
.	III	13.5	6.0	13 500	9 000	13.0	36.3	58.7	76	0.094	0.545	22	+	+	0
.	I-II_a c Fe deffic.	10.0	1.5	16 700	410 000	16.1	26.3	40.5	56	0.041	0.286	29	+	0	0
.	III	12.5	0.5	9 700	375 000	8.8	23.0	51.5	100	0.083	0.425	13	+	+	0
.	I-II_a c Fe deffic.	0.3	None	11 850	775 000	15.0	35.4	36.4	20	0.023	0.127	57	+	0	0
.	III	2.4	0.6	72 500	210 000	12.0	36.1	41.4	17	0.040	--	--	+	+	+
.	I-II_a c Fe deffic.	13.0	0.3	4 600	270 000	16.2	53.1	46.2	54	0.062	0.251	63	+	0	0
.[a]	III	18.0	1.8	14 200	220 000	12.1	--	--	28	0.065	--	--	+	+	0

artial Study -- radioiron clearance from plasma was not obtained after the first day, making calculation of Hb synthesis impossible. This study not included
data in Tables I and II.

study of patients in Classes IIb and III (mean times for untreated groups being 18.0 years and 7.0 years respectively -- Table 2) is significantly longer than patients in Classes I and IIa, (mean time for untreated groups being 0.9 years and 1.3 years respectively -- Table 2), suggesting that patients in the former classes had had their disease for a longer period of time than patients in the latter classes. Many patients who were found to be in Class III at the time of the iron-kinetics study previously had clinical histories and hematological findings that suggested that earlier in their course myeloid metaplasia had not been present. These results indicate that patients in Classes I and IIa are in earlier phases of their disease than patients in Classes IIb and III. As time passes many patients in Classes I and IIa may progress into Class III (myeloid metaplasia) or a few may progress into Class IIb (refractory anemia with erythroid hyperplasia and intramedullary hemolysis).

In all patients in whom repeat iron-kinetic studies were performed during the course of their disease, calculated hemoglobin synthesis increased simultaneous with a shortening of mean erythron life span and decreasing hemoglobin-concentration values during their second study (see Table 3). This same pattern is seen when plasma-iron turnover and hemoglobin synthesis are related to the mean time after diagnosis of untreated patients in Classes I, IIa and III, as seen in Fig. 5. An even greater rate of hemoglobin synthesis and shortening of mean erythron life span is seen in the two patients in Class IIb (time from diagnosis to study = 18 years).

As can be seen from Tables 1, 2 and 3, and in Fig. 5, there is a rough direct correlation between hemoglobin synthesis and white-blood-cell count (3, 11). Since, at least in part, the white blood count is a reflection of white-cell-production rate one may postulate that during the course of polycythemia vera the rate of white-cell production increases in a fashion similar to the rate of red-cell production. The concept that white-cell production is increased in certain patients with polycythemia vera has been previously postulated (12) and gains some support from published work (13).

As can be seen from Tables 1 and 2, patients in Class III tend to have lower platelet counts than patients in Classes I and IIa. Since, following their release from the bone marrow, the platelets (similar to the red cells) spend the major portion of their functional life in the blood, the finding that their concentration, similar to the hemoglobin concentration, tends to be decreased in patients in Class III suggests that, as with red cells, the functional survival of platelets is decreased in patients in this class. The concept that platelet survival parallels RBC survival in this disease gains support from ^{32}DFP platelet studies which we performed in two polycythemic patients. In both patients platelet survival was shortened roughly in proportion to shortening of RBC survival. In one patient in erythropoietic Class IIa, the mean platelet survival was 5.2 days, and in the other patient in erythropoietic Class III the mean platelet survival was 2.4 days (normal 8-12 days).

DISCUSSION

In polycythemia vera there is a shortening of red-cell life span as the disease progresses, which is incompletely compensated by an increase in red-cell synthesis, resulting

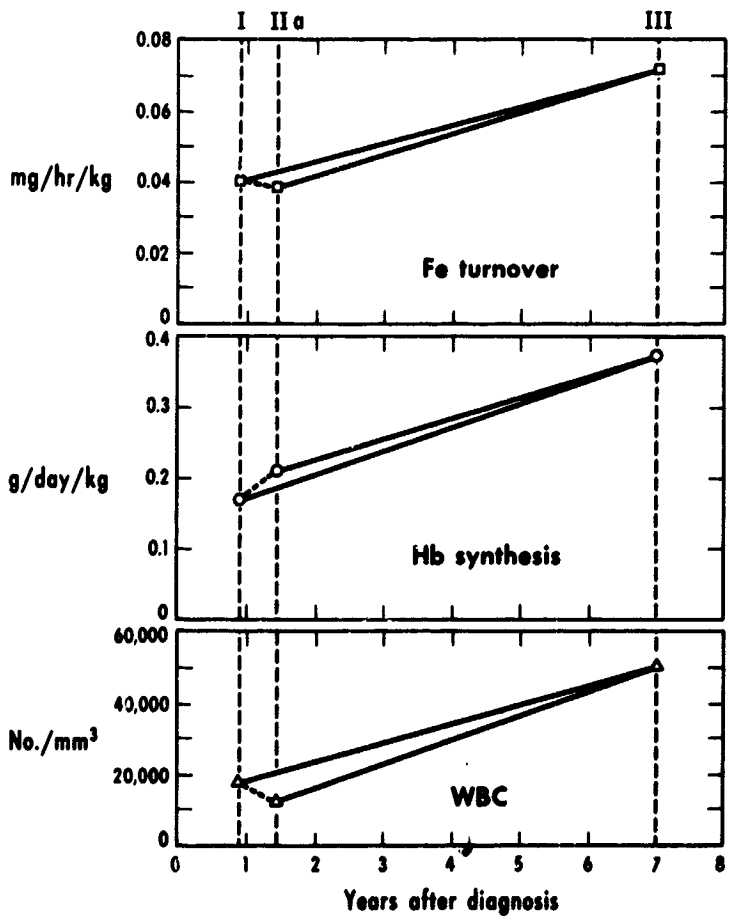

Figure 5. Mean values for plasma-iron turnover, hemoglobin synthesis and white-blood-cell (WBC) count of patients not receiving radiation therapy prior to study in Classes I, IIa, and III are plotted as a function of time from diagnosis to study.

MUB-6292

in a progressive decrease of red-cell volume. This occurs whether or not X ray or radioisotopes are used in therapy and appears to be a result of the natural history of the disease. Splenic sequestration of red cells is correlated with this shortening of red-cell survival. As the disease progresses and the rate of hemoglobin synthesis increases, myeloid metaplasia may appear at first in the spleen. The close association of hepatic myeloid metaplasia with marked splenic sequestration of red cells and iron deficiency suggests that hepatic erythropoiesis occurs when red-cell survival is markedly shortened with marked splenic destruction or with the additional complication of further decrease of red-cell survival due to iron deficiency. It is possible that iron deficiency leads to nonspecific selective advantage of the liver for erythropoiesis relative to the non-iron deficient state (e.g., large plasma-iron perfusion rate of liver).

In certain cases an abrupt marked shortening in mean erythron life span may occur prior to the development of myeloid metaplasia, as a result of marked intramedullary destruction of red cells (Class IIb). The development of this situation appears ominous since in both of these cases with prior ^{32}P therapy, death ensued within a year of the iron-kinetic study. Patients without myeloid metaplasia who have a terminal severe anemia with marrow showing erythroid hyperplasia have been described by others in the course of polycythemia vera not

treated by radiation therapy (6). Whether the situation which we have described as polycythemia vera Class IIb is identical with the erythroleukemia-type picture described by others or is a state preceding the development of acute leukemia is open to speculation.

It is suggested that the pattern of evolution of granulocyte and platelet kinetics in polycythemia vera may be similar to that of the red cells as discussed above. Since as with red cells, the platelets spend the major portion of their functional life span in the blood, the tendency for lowered values of both platelet and hemoglobin concentration in Class-III patients suggests that during the course of polycythemia vera the platelets, as well as the red cells, have decreasing functional survival with incompletely compensatory increased production. Two studies of platelet survival in this disease are consistent with this hypothesis. Similarly, since the concentration of white cells in the blood appears to be relatively independent of the "functional survival" of the white cell, the tendency towards increasing white-cell counts as the duration of the disease increases may primarily reflect increasing rates of white-cell production. If these speculations are correct, then the course of changes in the red cells, white cells and platelets in polycythemia vera, can be described in terms of the progressive emergence of clones of hematopoietic cells which have selective advantage for reproduction but have altered functional capacity or shortened functional survival. Whether the emergence of such altered cell clones may be caused by mutational events, replication error, viral-induced cell changes, or in response to adnormal humoral stimuli involves second order speculation at the present time.

The results of this study have two therapeutic implications in the treatment of myeloid metaplasia (Class III) appearing in the course of polycythemia vera. The frequent finding of iron deficiency in these patients suggests usefulness of iron therapy in the treatment of their anemia. In those patients in whom splenic sequestration of red cells appears to exceed splenic erythropoiesis (as evidenced by a secondary increase in amplitude of external monitoring counting rate over the spleen) splenectomy should be of aid in reducing the anemia.

The pattern of evolution of erythropoiesis described above applies to patients whether or not they received radiation therapy or phlebotomy alone. The present series is too small for determining whether or not there is any statistical difference in the rate of evolution of erythropoietic patterns in this disease in patients treated with radiation versus those treated by phlebotomy alone.

CONCLUSIONS

Patients with polycythemia vera may be classified according to their erythropoietic pattern. Erythropoiesis is abnormally increased in all classes. Class I is characterized by normal red-cell life span. Class II is characterized by shortened red-cell life span: in Class IIa the shortened red-cell survival is related to splenic sequestration of RBC; in Class IIb the markedly shortened red-cell survival is predominantly related to intramedullary hemolysis. Class III is characterized by extramedullary erythropoiesis. Patients in Classes I and IIa are in relatively earlier phases of their disease and frequently are found to develop red-cell kinetics of Class III as their disease progresses. Conversely, patients in Classes

IIb and III are generally late in the course of their disease and have previous hematologic findings that suggest that they originally had the red-cell kinetic patterns of Classes I and IIa.

As the duration of their disease increases, patients with polycythemia vera generally have progressive shortening of red-cell life span which is incompletely compensated by progressive increase in red-cell production with resultant progressive decrease in circulating red-cell volume. However, total blood volume is maintained elevated as plasma volume increases. Similar changes may occur in white-cell and platelet production and in functional survival in this disease. These changes occur whether or not the patient is given radiation therapy. It is suggested that the natural history of the disease may be characterized by progressive emergence of hematopoietic cell clones that have a selective advantage for reproduction associated with altered functional survival.

The results suggest the potential usefulness of iron or splenectomy in polycythemic patients with myeloid metaplasia (Class III) and anemia dependent upon the presence of the frequent finding of iron deficiency or the occasional finding of splenic sequestration of red cells in excess of splenic erythropoiesis.

ACKNOWLEDGMENTS

The authors wish to thank N. Kusubov for her excellent technical assistance.

Portions of this work were performed with the aid of funds from the United States Atomic Energy Commission and the National Institute of Health Grant CA-01440.

REFERENCES

1. London, I. M.; Shemin, D.; West, R., and Rittenberg, D.; J. Biol. Chem. 179:463-84, 1949.
2. Nathan, D. G.; Berlin, N. I.; Blood 14:668, 1959.
3. Lawrence, J. H.; in Modern Medical Monographs, New York, Grune and Stratton, 1955.
4. Wasserman, L. R.; Bull. N. Y. Acad. Med. 30:343, 1954.
5. Nakai, G. S.; Craddock, C. G.; Gigueroa, W. G.; Ann. Internal Med. 2:419, 1962.
6. Perkins, J.; Israels, M. C. G., and Wilkinson, J. F.; Quart. J. of Med. New Ser. 33, No. 132:499, 1964.
7. Pollycove, M., and Mortimer, R.; J. Clin. Invest. 40:753, 1961.
8. Pollycove, M.; in Thannhauser's Textbook of Metabolism and Metabolic Disorders, Vol. 2, edited by N. Zollner and S. Estren, New York, Grune and Stratton, 1964, Chpt. 15.
9. Peters, T.; Giovanniello, T. J.; Apt, L.; and Ross, J. F.; J. Lab. Clin. Med. 8:280, 1956.
10. Pollycove, M.; in Proceedings of the International Conference on Peaceful Uses of Atomic Energy, 2nd Geneva, Vol. 26, Geneva, United Nations, 1958, 167-171.
11. Berlin, N. I.; Lawrence, J. H., and Gartland, J.; Amer. J. Med. 9:747, 1950.

12. Dameshek, W.; Blood 6:372-375, 1951.
13. Mauer, A. M., and Jarrold, R.; Blood 22:125, 1963.

Received June, 1965.

Whole-Body Counting of ^{47}Ca and ^{85}Sr

Thornton Sargent, John A. Linfoot and Elsa L. Isaac

Since the pioneering work of Bauer, Carlsson and Lindquist with ^{45}Ca there has been increasing anticipation that with use of isotopes such as ^{47}Ca, ^{45}Ca, and ^{85}Sr, and application of compartment theory, the complex problem of calcium metabolism would be clarified. The recent status of compartment models and isotope technique was well summarized at an IAEA Symposium in 1962 (1). In spite of the considerable amount of able research work reported to date, however, the tangible advances have been disappointing contrasted, for instance, to the success of compartment theory in describing iron metabolism (2).

The reasons for the greater difficulty with calcium are several: it is widely distributed in tissue and does not travel rapidly through one-way metabolic steps such as iron through bone marrow; many of the compartments are difficult to sample, and some of the major compartments may not even have been identified yet; little is known on a physiologic basis about the manner in which calcium enters and leaves its major site in the body, the skeleton.

The ultimate object of understanding calcium metabolism is the clinical application of this knowledge. Yet with a few exceptions, some of which will be mentioned later, variations in compartment parameters reported to date have not correlated with the disease states measured. That is, the values of parameters found in patients with bone diseases have usually not varied significantly from one disease to another nor from normal subjects to patients.

The parameters usually determined are the size of the exchangeable calcium pool, E, and the bone accretion rate, A. On the basis of the various models that have been proposed, these parameters are determinable by taking serial blood samples and collecting stool and urine after injection of a single dose of ^{45}Ca or ^{47}Ca. The pool size is determined from the plasma specific-activity curve from one to seven days extrapolated to the zero intercept, and bone-accretion rate is determined by the difference in turnover between the plasma and excreta. This measure of bone-accretion rate suffers from several basic defects. First, it is essentially a calculated difference between two measured rates, always a statistically risky process. Second, it is always assumed that during the course of the study no radioisotope has re-entered the pool because of resorption of label already deposited in bone. The resorption rate has rarely been measured, nor have measurements been carried out long enough to determine the effect of components with smaller slopes on the slope and intercept of the component representing the exchangeable pool. Aubert and Milhaud (3) have reported that errors may be as high as 35% due to neglecting the later components of retention curves.

Heaney and Whedon (4), for instance, discuss the later components they found in plasma curves. They take the point at which the curve on semi-log plot breaks as the time at which bone resorption begins and assume that the slope prior to this accurately represents the K of plasma clearance. There is no reason to suppose that bone resorption has not occurred prior to this, yet their calculations apparently are based on this assumption. It is difficult to see how any of the reports to date can have much meaning unless they have included a measured value of resorption rate in their calculations. The difficulties of measuring resorption are many, both in tracer studies and morphologically. The tetracycline markers used extensively show only resorption from calcium deposited by osteons in cortical bone; virtually nothing is known of resorption in cancellous bone (1).

The pool size and bone-accretion rate have been the parameters most commonly calculated and reported, primarily because they are the easiest to derive from the simplest tracer measurements. In addition to the question of accuracy of such measurements mentioned above, there is no a priori reason to assume that these parameters will change in every kind of bone disease. While in a few conditions marked changes in E and A have been found, such as in osteomalacia and hypoparathyroidism, in many other diseases these parameters have been found to be not markedly altered. One of the most common bone diseases, osteoporosis, has been studied extensively by tracer techniques, some authors finding the bone-accretion rate normal and some finding it reduced (5). Belcher et al. (6), for example, have found normal bone-accretion rate and increased resorption rates in osteoporosis, although this may have been due to differences in data obtained compared to other workers.

Because resorption rate will affect all calculations of bone metabolism, it is surprising that whole-body counters have not been more extensively employed in its measurement. Once ^{85}Sr is incorporated into bone, it is probably treated physiologically very much like calcium. The slope of the retention curve of this isotope in the body should be closely related to the resorption rate of bone.

WHOLE-BODY COUNTING

STRONTIUM 85 Studies of bone metabolism with whole-body counters have been relatively infrequent; they have been well reviewed by Cederquist (7). Although many reports have appeared on various types of scanning methods, they will not be considered here unless they were used to gather essentially the same information as whole-body counting, namely whole-body retention as a function of time. Both ^{47}Ca and ^{85}Sr are useful for these studies as they are both gamma emitters, but ^{85}Sr has been used most often because of its more favorable half-life of 64 days and the interest in strontium metabolism in its relation to the more hazardous isotope ^{90}Sr. However, because strontium only partly mimics calcium physiologically, it is ultimately necessary to use both isotopes if bone metabolism itself is to be studied.

Apparently the earliest complete study on long term ^{85}Sr retention was that of Bishop et al. (8), using two entirely normal subjects. Cohn et al. (9) reported long term retention in ten patients, nine of whom had diseases known to involve the skeleton; six of the

ten however were considered to have normal bone metabolism, whereas four had marked abnormalities of calcium metabolism. A sum of three exponential terms adequately fit the data, and values of the slope of the longest component and its intercept are reported for each patient. For the patients without bone disorders the mean half-time of this component was 843 days, and the mean intercept representing the fraction of the injected dose retained in this compartment was 0.245. For the patients with bone disease the half-times were much shorter and the intercepts higher. Both authors (8, 9) found that the data were adequately fitted by three exponential terms but could also be fitted well by a power function after 30 days. Suguri et al. (10), in a study on a single healthy male, found similar results and parameters for the equations. Cohn (9) discusses the relative merits of the two types of equation to fit the data and reports he found that either equation fit equally well within the period of time for which data could be obtained and within the statistical accuracy of the data. When he extrapolated the curves for each type of equation, however, the power function predicted far greater retention at later times. While ultimately the choice of the best description of long term data may affect our concept of bone metabolism, for the present it is probably adequate to accept the half-time as determined by retention out to 200 to 300 days as the "final" slope.

MacDonald (11) and MacDonald et al. (12) found differences in metabolism of ^{85}Sr in osteoporotics, but confirmation of these will probably have to await studies over a longer period than those reported to date.

Cederquist (7) studied a series of patients with and without osseous metastases, using his scanning geometry primarily with ^{85}Sr but also in a few cases with ^{47}Ca. He found that percentage retention of the isotope as a function of time varied widely in patients with osseous metastases, covering a range wider than but including that of patients without skeletal involvement, and also normal volunteers. He concluded that a short-term retention study in itself did not yield useful clinical information. However, it would seem that there must be significance in these widely varying retention figures if sufficient other data were at hand since the variations may result from physiological processes it would be extremely interesting to know about. However, information other than roentgenography must be obtained in order to assess their significance. Cederquist found that the ratio of the counts in the prone position to those in the supine position was distinctly and consistently higher in patients with skeletal involvement, being greater than unity in such cases and less than unity in normals and patients without bone disease. This difference in ratio appeared within a day or two, sometimes even after a few hours, and remained thereafter. The difference in ratio was attributed to more rapid uptake of the isotope by lesions in the bone, primarily the cancellous bone of the spine, whether the lesions were osteolytic or osteoblastic. Rapid uptake in the spine would place the isotope closer to the crystal in the prone position and yield the higher ratio. Since the difference in ratio appears so soon after injection, ^{87m}Sr may be an even more useful isotope for this type of study; its lower energy gamma, because of its increased absorption by tissue, should enhance the ratio effect. Although this clinically useful method may be considered a scanning technique, rather than a whole-body measurement, the great improvement in agreement between excreta and whole-body retention found with this method (7) more than justifies its consideration here.

Errors in whole-body counting due to the effects of the geometry of crystal detector with respect to the subject were recognized early and have been dealt with in various ways, as is well summarized by Cederquist (7). The chair is clearly the poorest geometry, although after an initial period of tissue equilibration of about two weeks, the retention curve from the chair geometry is reasonably parallel to that from the one-meter arc geometry, and excreta collections yield retention reasonably close to that from the one-meter arc (13). For this reason, some workers (9, 14) have used the arc for early counts and the chair for greater sensitivity when the activity has decayed to lower levels. Cederquist (7) and his colleagues at Lund have developed a scanning method in which the patient is counted both prone and supine; variations in counting due to change in location of the isotope appear to be evened out and excellent agreement was obtained with excreta measurements. Taylor et al. (15) have also developed a scanning method and obtain less good agreement with excreta measurements; apparently their counting was done in supine position only. Belcher and Dudley (16), scanning over subjects prone and supine, and Korey et al. (17) with scanning crystals above and below the patient, have also found good agreement between excreta and whole-body counting. Cohn et al. (18) normalize whole-body data to excreta data at ten days for both ^{47}Ca and ^{85}Sr; for ^{47}Ca they use excreta data only for the first four days and normalized whole-body counting thereafter.

CALCIUM-47 Although this isotope has been used rather extensively in blood and scanning studies of calcium metabolism, its use with whole-body counters has been relatively limited. The 1.31-MeV gamma ray makes it very useful for in vivo counting, but its short 4.7-day half-life, although giving a relatively low integral radiation dose to the patient, limits in vivo retention studies to 40 days or less. An early study (13) reports results on one normal and two cases of acromegaly, and other reports (7, 15-17) are brief or report only a few short-term studies of calcium retention.

Cohn et al. (19) have reported studies with ^{47}Ca in two normals and a case of partial parathyroid deficiency. In addition to whole-body counting, they collected urine and feces, took blood samples and counted a sample of the bone compartment by placing a collimated counter over the knee for a period of only ten days. On the basis of a three compartment model, a solution was obtained from the data with a computer program; this method of data handling will be discussed in more detail below. On a low-calcium diet the patient with parathyroid deficiency exhibited a greatly reduced urinary excretion, as expected in any person on such a diet, and the serum calcium fell as expected in parathyroid deficiency. Although the bone-accretion rate and the total exchangeable pool did not change appreciably, the vascular-extravascular-soft tissue compartment shrank and the exchangeable bone compartment increased. While these changes are consistent with partial hypoparathyroidism, and the use of all possible data makes the solution more convincing, the changes in data observed were rather small and the normal subjects were not studied on an equivalent low calcium diet as a control.

Sargent et al. (14) reported whole-body-counter studies in a small group of patients with osseous metastases of mammary carcinoma, acromegaly, and patients without known bone disease. Pronounced differences were found between the whole-body retention of ^{47}Ca

at 20 to 35 days of those patients with osseous metastases and acromegaly and those without skeletal involvement. The patients with osseous metastases had much more rapid loss of radiocalcium, and one patient after treatment, had greater than normal retention. These observations were considered consistent with their disease. Six cases of acromegaly showed retention of ^{47}Ca considerably above normal, the increase apparently being correlated with the degree of severity of the disease. This study and that of Cederquist (7) would seem partially to refute the notion that the advantages of whole-body counting lie chiefly in the realm of long term studies (20). On the other hand Cederquist (7) feels that long term studies are of limited value, and regrettably did not study any of his patients over a long period. It is hoped that this paper will demonstrate that both short- and long-term studies are not only valuable but necessary for a complete understanding of bone metabolism.

COMPARTMENT MODELS Numerous models of skeletal metabolism have been proposed, recently reviewed by Heaney (21). Most of them are approximately equivalent but vary in the number of compartments and in the extent of simplifications made for the sake of solving the resulting equations. The primary and almost sole contributor of models in which whole-body counting is used has been Cohn's group at Brookhaven National Laboratory, although Glass and Nordin (22) and Glass et al. (23) have recently entered this field.

Initially Cohn et al. (9) studied long term strontium turnover and simply fit the whole-body-counter data to a sum of three exponentials, without attempting to calculate pool sizes or accretion rates. In the next paper (18) a four compartment model was employed, in which the tracer was required to move from plasma (I) through the exchangeable bone pool (II) to the initial "fixed" bone pool (III). It was then pictured as moving from III to IV, the latter also being in bone, and resorption from IV returned tracer to II. An analogue computer was used to generate a function for each compartment such that their sums fit the experimental data. It was recognized that this solution was only one of several possible, but it could be concluded that the body handles strontium very similarly to calcium as far as skeletal accretion is concerned. The observed differences in whole-body retention of calcium and strontium could be accounted for by preferential renal excretion of strontium as reported by other workers, with possibly a small preferential resorption of strontium from bone.

In subsequent papers (19, 24) the early model was abandoned in favor of a three compartment model, with the plasma-extracellular-intracellular pool, 1, exchanging independently with an exchangeable bone pool, 2, and with stable bone, 3. The size and exchange rate of 2, the exchangeable bone pool, is determined primarily by two points of the plasma-activity curve in the first 24 hr, and resorption from 3 returning to 1 is considered to be zero over the ten-day period of the study. All possible data that could be collected: plasma, whole-body, urine, feces, and collimated counts over the knee, were utilized to obtain a solution of the differential equations of the model by the IBM 7094 computer program developed by Berman (25). The accuracy of fit of the data to curves calculated by the computer from the derived parameters, and the reproducibility of these parameters in repeat studies on the same subjects six months later, led the authors to describe this solution as precise and the model as unique. At the end of the paper (24), however, and supported by private

communication, it appears that when the study is extended to 30 days the model no longer works. Undoubtedly another model can be developed which the data will fit, and it might also be predicted that when data out to 300 days are utilized this 30-day model will not fit either. It is difficult to see how any model can be expected to describe calcium metabolism adequately unless it reflects long-term calcium turnover, i.e., the bone-resorption rate.

METHODS

The present study was undertaken on a relatively limited class of patients, essentially those who had been selected for pituitary irradiation with the 900-MeV alpha beam of the 184-in. cyclotron at Berkeley. Initially only ^{47}Ca was used, and some of these results have already been reported (14). As it became apparent that the usefulness of the studies was severely limited by the lack of information as to long term retention, we began using ^{85}Sr simultaneously. The patients were counted at frequent intervals initially to obtain fairly detailed ^{47}Ca retention data, and then at intervals for up to one year for the long-term ^{85}Sr retention.

The techniques used have largely been described previously (13, 14). When ^{85}Sr was injected in addition to ^{47}Ca, the ^{85}Sr was injected first, the patient counted immediately, and then the ^{47}Ca was injected and the patient counted again. The energy range used for the ^{47}Ca counts was 1.18 to 1.42 MeV, for ^{85}Sr, 0.44 to 0.58 MeV. The number of counts added to the ^{85}Sr range by the ^{47}Ca was calculated from this sequence of counts for each patient. It was found for these energy ranges that the average ratio of the number of counts in the ^{47}Ca peak to the number of counts from ^{47}Ca in the ^{85}Sr peak region was 0.531, with a range from 0.508 to 0.570. The two patients with metastatic cancer had much lower values, 0.415 and 0.427.

The data from patients are presented in Table 1 with pertinent clinical information and categories by disease. The patients were on diets of approximately 900 mg calcium intake per day for the first week of the study, returning to their normal diet after that; all patients were completely ambulatory, and usually seen on an out-patient basis. Except for those patients for whom it is indicated that the study was begun a year or more post-treatment, all were studied at the time irradiation was begun. Ordinarily the growth-hormone levels fall gradually after heavy-particle pituitary irradiation, and although improvement in subjective symptoms may occur earlier, striking metabolic effects are usually not detectable until a year or more after treatment (26).

The data were treated and analyzed without reference to any specific mathematical solution of compartment models. The following assumptions were made, however:

1. The retention curve of calcium as seen by the whole-body counter consists of two exponential components.

2. The two ^{47}Ca slopes, which are obtained on the assumption of two compartments, represent respectively: a) the net rate of loss from the body of the injected tracer in the exchangeable pool primarily via urine and feces; b) the rate of loss of tracer that has been fixed in bone and resorbed; some fraction of this is then again fixed in bone whereas the remainder is excreted as in a). This effect, and the rate of transfer from the pool to fixed bone, cannot be calculated from whole-body-counter measurements alone. The extrapolated intercept of

Table 1. Summary of clinical data on patients

Patient	Age, Sex	Enlargement of sella	Plasma growth hormone mμg/ml	Serum Ca	Serum P	Urinary calcium mg/24 hr	Clinical description (BrCa = breast cancer)
JV	17 M	+++	22.9	10.3	5.2	334	Very active acromegaly
MH	23 M	++	43.5	10.6	5.5	330	Very active acromegaly
JMa	23 M	+++	63.0	9.5	6.7	81	Very active acromegaly
JMn	30 M	+++	34.5	10.0	4.8	487	Very active acromegaly
KP	27 F	+	23.0	9.6	4.6	190	Very active acromegaly, galactorrhea, amenorrhea
IB	31 M	++	106.0	9.6	5.3	248	Very active acromegaly
HB	33 M	++	-	9.4	4.2	145	Active acromegaly
DU	45 M	++	98.0	9.3	5.2	342	Very active acromegaly
JMy	46 M	++	47.9	10.4	5.1	296	Very active acromegaly, ulcer therapy
AS	44 M	+++	58.2	9.6	5.4	218	Very active acromegaly
MT	62 F	+	9.3	10.0	4.0	126	Mildly active acromegaly, diabetes mellitus
JH	66 F	+	16.3	10.2	5.2	174	Moderately active acromegaly
MD	48 F	+	13.4	10.6	3.5	149	Mildly active acromegaly, arthritis
CH	39 M	+++	99.0	9.2	4.7	382	Very active acromegaly; ulcer and androgen therapy
DT	40 F	+++	4.3	10.4	4.7	-	Inactive; surgical hypophysectomy, panhypopituitarism
OR	55 M	+++	4.5	9.5	3.8	314	Inactive; previous pituitary irradiation, panhypopituitarism
FS	47 M	++	24.0	9.7	4.0	269	Active acromegaly; previous pituitary irradiation inadequate
LB	54 F			9.8	3.5	180	BrCa; cutaneous metastases; ovariectomized (hypophysectomized)
VH	40 F			9.8	4.4	82	BrCa; osteolytic metastases; ovariectomized
EK	50 F			9.1	3.1	112	BrCa; carcinoma en cuirasse; spinous metastases; postmenopausal
PL	47 F			16.1	-	-	BrCa; extensive osteolytic metastases; radiation oophorectomy
GS	49 F			14.1	2.5	565	BrCa; carcinoma en cuirasse; ovariectomized
JR I	56 F			11.0	3.9	264	BrCa; osteolytic metastases; ovariectomized (hypophysectomized)
JR II	57 F			10.5	4.2	132	As above, 1 yr after pituitary irradiation and chemotherapy
BC I	35 F			10.3	5.0	12	BrCa; extensive osteoblastic metastases; ovariectomized; (hypophysectomized)
BC II	36 F			8.8	2.5	52	As above; 7 months after pituitary irradiation and steroid therapy
RC	17 M			10.2	3.5	224	Cushing's disease; no evident catabolic changes; elevated 17 OHCS, normal 17 KS
RS	45 F			9.8	2.8	316	Cushing's disease; mild osteoporosis, amenorrhea, muscle weakness; elevated 17 OHCS, normal 17 KS
JT	69 M			11.4	3.6	-	Extensive Paget's disease of the bone, lesions of the lumbar vertebrae and pelvis; alkaline phosphatase 55 Bodansky units

the slope of the bone component b) to injection time represents the fraction of the injected dose which was incorporated into bone, and the intercept of the exchangeable pool slope represents the remainder of the tracer, which was excreted.

3. Strontium, once it is incorporated into bone, is handled in the same way as calcium, and hence the "final" slope of ^{85}Sr-retention curve represents the slope of the ^{47}Ca curve over the same period of time, if the half-life of the ^{47}Ca were long enough to permit measurements for so long. This assumption does not require that equal fractions of strontium and calcium be incorporated initially, only that the resorption rate of calcium and strontium be the same. It is inaccurate, however, in that strontium once resorbed will re-enter the pool and be subject to preferential renal excretion before being again accreted into new bone. This effect would make the "final" ^{85}Sr slope greater than the ^{47}Ca slope, but the effect must be small because the fraction of ^{85}Sr resorbed over the entire course of the study is small itself.

The data points were fitted with curves that were sums of single exponentials by using the program developed by Berman (25) for the IBM 7094 computer. The best fit curve is obtained by an iterative least-squares process. By supplying initial estimates of slopes and intercepts, curves can be fitted with any desired number of exponential components.

It was found here, as it has been by others (8, 9, 10), that the ^{85}Sr-retention curve is fitted best by three components; two components give a poor fit, especially in the first five or ten days. The values of the slopes and intercepts were designated according to the following system for the computer input, and are referred to in this way in the text as well. Subscript 4 refers to calcium, 7 to strontium; λ's are the slopes in days $^{-1}$, the half-time thus being $t_{1/2} = \frac{0.693}{\lambda}$; σ's are the intercepts, expressed as a fraction of unity. For strontium, λ_{01}, λ_{02}, λ_{03} represent respectively the largest, medium, and smallest slopes, corresponding to the shortest, medium, and longest half times; σ_{41}, σ_{42}, σ_{43} represent the corresponding intercepts. For calcium, λ_{05} and λ_{06} are the large and small slopes or short and long half-times respectively, and σ_{75} and σ_{76} their intercepts. These relationships are shown graphically in Fig. 1a.

The initial estimates for the computer were first obtained for ^{85}Sr by graphical analysis. The λ_{03} for ^{85}Sr was then applied to the graph of each patient's ^{47}Ca-retention curve, with the intercept adjusted to yield approximately a two-component curve. This intercept and the slope of the other component and its intercept were then given to the computer as initial estimates for the ^{47}Ca curve. Also given to the computer were all the ^{85}Sr and ^{47}Ca data points and instructions to consider λ_{06} and λ_{03} as dependent variables. This instruction is based on the third assumption mentioned earlier, that the turnover of strontium and calcium in bone as seen by the whole-body counter are the same. The single value obtained for λ_{03} and λ_{06} is, of course, determined almost entirely by the ^{85}Sr data points, since no ^{47}Ca remains at the time this slope is seen, but as determined by the computer it is compatible with the number of compartments and with the other σ's and λ's calculated. No other dependence between the calcium and strontium curves is specified.

A group of patients in whom ^{47}Ca only had been used, prior to use of ^{85}Sr, was also studied with the computer program, as follows. Since the λ_{03} did not vary significantly in the 12 patients with acromegaly studied with ^{85}Sr, the mean value of λ_{03} obtained for these patients, 0.00094, was given to the computer as a fixed value for λ_{06}. This value is quite close to Cohn's mean of 0.00087 (9). The computer could then calculate values for σ_{76}, σ_{75} and λ_{05}, without dependence on ^{85}Sr data which did not exist for these patients. Similarly, a mean value of 0.0027 was obtained from the two patients with metastasized breast cancer studied with ^{85}Sr, and used as a fixed λ_{06} for the patients in this category studied with ^{47}Ca only. Two other patients, LS without known bone metastases and BC with osteoblastic metastases, were assigned fixed values of 0.00094. The values of σ_{76}, σ_{75} and λ_{05} are relativiely insensitive to changes in λ_{06} so this procedure is fairly accurate since the approximate value of λ_{06} is known for each disease.

Published data (8, 10) for three normal subjects using ^{85}Sr only were also given to the computer for calculation. Values given for Cohn's six patients (9) were taken directly from his work.

The fitting of curves to data points and determination of slopes and intercepts performed by the computer can, of course, be done by hand but involves considerable estimation of goodness of fit, especially with regard to the choice of σ_{76}. The choice of values by the computer on the basis of the iterative least squares method is much simpler, and it is more convincing that the best fit has been found. Since the value of σ_{76} as found here appears to have the most meaningful correlation with disease, the best value for it is most important.

RESULTS

The slopes and intercepts as determined by the computer are presented in Table 2. The standard deviation shown for each value was not based on counting statistics for each datum point, but on the deviation of the data points from the computer-derived curve and the accuracy with which the parameters could be assigned because of these deviations. Those patients for whom the $\lambda_{03}/\lambda_{06}$ value is listed as "fixed" were those in whom ^{47}Ca only was used, as described earlier, and thus there are no ^{85}Sr parameters listed for them.

The ^{85}Sr component represented by σ_{41} and λ_{01} has not been attributed any physiological meaning by other authors, although it might conceivably be associated with a renal excretion process that does not occur for calcium, such as excretion of ionic strontium. The values obtained for the patients varied widely, with means of 0.40 and 0.64 for σ_{41} and λ_{01} respectively. These are lower and higher respectively than the values for normals obtained by Cohn and calculated here from the data of Bishop et al. (8) and Surguri et al. (10). These two parameters may be strongly affected by the values of the other parameters, which are themselves affected by the diseases studied, or σ_{41} and λ_{01} may be directly affected by the disease, the latter seeming the less likely. It might be noted that in two cases, patient JMn and normal JFL, the values for σ_{41} and λ_{01} reached the high or low limits imposed on the computer, which in effect means that only two compartments are required to fit the retention

Table 2. Computer-derived values of slopes and intercepts of ^{85}Sr and ^{47}Ca retention curves, assuming two components for ^{47}Ca and three for ^{85}Sr; λ_{06} taken as dependent on λ_{03}

Patient	Sr		Sr	Ca	Sr	Ca	Sr	Ca	Sr/Ca
	σ_{41}	λ_{01}	σ_{42}	σ_{75}	σ_{43}	σ_{76}	λ_{02}	λ_{05}	$\lambda_{03}/\lambda_{06}$
JV	-	-	-	.33±.02	-	.69±.01	-	.15±.02	.00091 fixed
MH	.34±.09	.51±.15	.14±.08	.35±.02	.52±.01	.64±.02	.10±.06	.12±.02	.00102±.0001
JMa	-	-	-	.32±.02	-	.65±.02	-	.09±.02	.00091 fixed
JMn	.01 limit	8.0 limit	.55±.05	.40±.02	.45±.01	.59±.02	.17±.03	.10±.02	.0012±.0003
KP	.25±.06	1.1±.4	.36±.05	.34±.02	.39±.01	.62±.01	.16±.03	.24±.03	.0019±.0003
IB	.46±.06	.32±.06	.06±.05	.38±.02	.46±.03	.59±.02	.04±.05	.08±.01	.0012±.0002
HB	-	-	-	.39±.01	-	.59±.01	-	.13±.01	.00091 fixed
DU	.48±.04	.51±.07	.12±.02	.42±.02	.40±.03	.55±.03	.04±.03	.07±.01	.00062±.0005
JMy	.11±.05	.04±.03	.69±.06	.50±.02	.23±.02	.48±.01	.31±.04	.14±.02	.00075±.0 026
AS	.30±.04	1.6±.5	.45±.03	.42±.02	.26±.01	.56±.02	.13±.01	.12±.02	.00021±.0002
MT	.75±.04	.29±.03	.07±.04	.68±.02	.18±.01	.34±.02	.05±.03	.15±.01	.00095±.0003
JH	-	-	-	.50±.04	-	.44±.03	-	.07±.01	.00091 fixed
MD	-	-	-	.66±.03	-	.30±.02	-	.09±.01	.00091 fixed
CH	.50±.09	.76±.2	.28±.08	.59±.02	.22±.01	.37±.02	.13±.04	.13±.01	.00095±.0003
DT	.68±.03	.35±.02	.13±.02	.59±.01	.19±.01	.41±.01	.04±.01	.12±.01	.00033±.00016
OR	.26±.05	.72±.2	.39±.05	.48±.01	.35±.01	.50±.01	.13±.02	.12±.01	.0014±.0001
FS	.25±.14	.72±.5	.56±.13	.64±.03	.18±.01	.38±.02	.12±.02	.12±.02	.00098±.0004
LB	.42±.46	.20±.13	.39±.46	.78±.13	.20±.02	.26±.13	.09±.05	.03±.01	.0024±.0006
VH	.16±.11	.83±.64	.60±.11	.58±.02	.23±.01	.45±.02	.18±.03	.11±.01	.0029±.0002
EK	-	-	-	.79±.05	-	.24±.06	-	.09±.02	.0027 fixed
PL	-	-	-	.67±.02	-	.36±.02	-	.14±.01	.0027 fixed
GS	-	-	-	.59±.02	-	.37±.01	-	.10±.01	.0027 fixed
JR I	-	-	-	.59±.01	-	.42±.01	-	.15±.01	.0027 fixed
JR II	-	-	-	.39±.01	-	.60±.01	-	.12±.01	.0027 fixed
BC I	-	-	-	.22±.01	-	.78±.01	-	.06±.01	.00091 fixed
BC II	-	-	-	.51±.1	-	.45±.1	-	.03±.01	.00091 fixed
LS	-	-	-	.66±.02	-	.34±.02	-	.05±.01	.00091 fixed
RC	.53±.14	.59±.25	.27±.14	.63±.03	.20±.02	.33±.03	.11±.06	.10±.01	.0041±.0007
RS	.71±.04	.66±.08	.23±.04	.74±.02	.05±.01	.23±.01	.11±.02	.19±.01	.00034±.0006
JT	.20±.06	1.1±.6	.39±.05	.33±.03	.41±.03	.64±.02	.06±.01	.34±.07	.0034±.0003
Bishop GEH	.49±.2	.30±.2	.29±.2	-	.23±.02	-	.06±.04	-	.0010±.0006
Bishop JFL	.55±.07	10 limit	.25±.06	-	.20±.01	-	.07±.02	-	.0015±.0003
Sgri,1	.68±.1	.27±.04	.17±.1	-	.18±.01	-	.07±.04	-	.00016±.0005
Cohn,6		.28		-	.24±.01	-	.05	-	.00087±.0001

curve in these cases. The intercepts σ_{42} and σ_{75} for ^{85}Sr and ^{47}Ca are essentially obtained by difference from the other intercepts.

The slopes λ_{02} and λ_{05} are the slopes of the corresponding components of strontium and calcium. If these two elements are handled identically by the body with the exception of renal excretion, then λ_{02} and λ_{05} might be expected to be the same in any individual. Examination of these values in Table 2 reveals that they are sometimes close in value but sometimes not, those patients in whom they are most different being those in whom λ_{01} or σ_{41} are the most extreme, namely patients JMn, JMy and JT. This suggests that the computer obtained a poor solution for λ_{01} and σ_{41} for these patients, that an error of geometry or data occurred or that these patients handled strontium in some unusual way. The mean values for all patients were 0.116 for λ_{02} (^{85}Sr) and 0.134 for λ_{05} (^{47}Ca), which are reasonably close, but the lack of agreement in many individual cases suggests that the assumptions made as to the physiology of these elements, or in calculation of the values, are not adequate.

The intercepts σ_{43} and σ_{76} represent respectively the fractions of the injected ^{85}Sr and ^{47}Ca, which were ultimately fixed in bone. They are related to the bone-accretion rate, but not directly, this rate being calculated from plasma clearance in various ways by different authors as discussed earlier. The calcium intercept must represent the fraction of any calcium entering the bloodstream, which is ultimately deposited in bone. Thus it seems clear that if intercepts are found that are higher than normal, something abnormal is occurring in calcium deposition; either a reduced exchangeable pool size, and increased bone-accretion rate, or both.

In Fig. 1b, σ_{43} and σ_{76} are plotted for each patient; a line was fitted through them by hand. This line has a slope of almost exactly one, and intersects $\sigma_{43} = 0$ at $\sigma_{76} = 0.18$; such a line is described by $y = a\,x + b$, where $y = \sigma_{76}$, $x = \sigma_{43}$, $a = 1$ and $b = 0.18$. That is, the strontium intercept is equal to the calcium intercept minus 0.18, and this is true to a good degree of approximation for all the patients studied here, as will be seen later in Fig. 2. The physiologic meaning of this relationship is not immediately apparent.

The calcium intercepts σ_{76}, found by application of the strontium slope λ_{03} to the calcium data points, are shown in Fig. 2 for each patient. Those patients for whom ^{47}Ca data only was available, and a fixed λ_{03} was assigned, are shown as open circles. In accordance with the previously described relationship ($\sigma_{43} = \sigma_{76} - 0.18$) the strontium intercepts σ_{43} are plotted on the same figure with a scale 0.18 lower than the σ_{76} scale. Of the ten patients with active acromegaly, all except JMy have calcium intercepts of 0.55 or higher. Of those seven patients with relatively inactive or treated acromegaly, only patient OR had an intercept greater than 0.45. Of the patients with metastasized breast cancer, only LB and EK had markedly low intercepts, although VH, EK, PL, GS and JR were known to have metastatic lesions of the bone. As will be noted later, however, the two of these patients who had ^{85}Sr studies, LB and VH, both had markedly large values for the "final" slope λ_{03}.

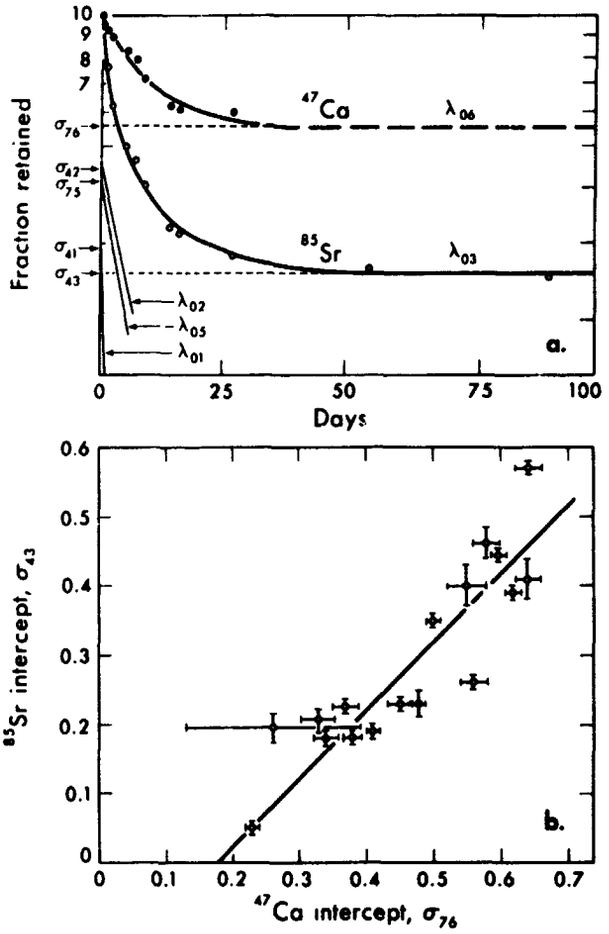

Figure 1. (a) Data points, computer-derived curves, slopes and intercepts in a typical patient, AS. (b) Correlation between σ_{43} and σ_{76}.
MUB-6666

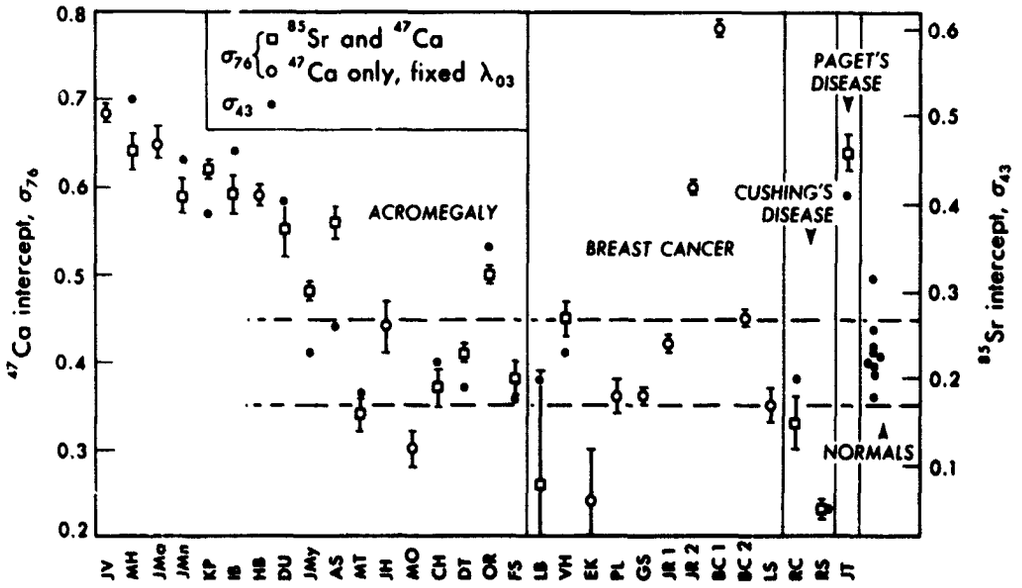

Figure 2. Calcium and strontium intercepts for all patients.
MUB-6666

Two of the breast cancer patients, JR and BC, were studied twice (Fig. 2). JR, with osteolytic lesions, showed a σ_{76} greatly increased with treatment 2, compared to before 1. BC, on the other hand, with osteoblastic malignancy, showed a much higher intercept before treatment 1 than after 2. Presumably treatment slowed the lytic activity in JR, allowing greater incorporation of calcium, whereas in BC the osteoblastic activity was suppressed by treatment and calcium incorporation was thus reduced.

The two patients with Cushing's disease (from bilateral adrenal hyperplasia) were disparate in age. Patient RS was a 45-year-old woman and her σ_{43} and σ_{76} intercepts were markedly low, in accord with the known antianabolic effects occurring in hyperadrenocorticism Patient RC was only 17 years old when studied. The rapid turnover of bone (high λ_{03}, Fig. 3) and the normal value of the intercepts σ_{76} and σ_{43} (as opposed to the low values for patient RS) observed in the latter case may be related to his age, the short duration of clinical symptoms, or other factors that were not apparent in his metabolic studies.

The high intercept and large λ_{03} in the case of Paget's disease are in general agreement with the case studied by Cohn (9).

Although no subject with normal calcium metabolism was studied completely here, patient LS had no known bone metastases and her calcium-retention curve was almost identical to that of other patients with no calcium abnormalities reported earlier (14). The value of her σ_{76} intercept, the σ_{76} values of the patients with treated or inactive acromegaly, the correlation between σ_{76} and σ_{43} as plotted in Fig. 2, and the values of σ_{43} from other workers shown in Fig. 2, all suggest that the normal range for σ_{76} probably lies between 0.35 and 0.45 and for σ_{43} between 0.17 and 0.27. The need for truly complete studies of normal subjects of a variety of ages is apparent. Nevertheless, severe cases of acromegaly can clearly be differentiated from normal or inactive acromegalics by their high calcium intercept.

The "final" slope of ^{85}Sr found for each patient is shown in Fig. 3; normal values from the literature are also shown. The patients with acromegaly, with the exception of KP, have values that are entirely within the range of normals. The only patients with values above normal, i.e., with short biological half-times of strontium in bone, are: the two patients with metastasized breast cancer, in whom the high turnover rate could be considered to reflect the osteolytic effect of the metastases on bone; RC, the young boy with Cushing's disease, discussed earlier; and JT, with Paget's disease in which rapid remodeling of bone is known to be characteristic.

Thus it appears that in acromegaly the incorporation of calcium into bone is increased but once incorporated its turnover is normal. This is presumably owing to the effect of the excessive amounts of growth hormone produced by the pituitary adenoma for which they were treated. Such an effect of growth hormone, although entirely plausible, has not been demonstrated by other means.

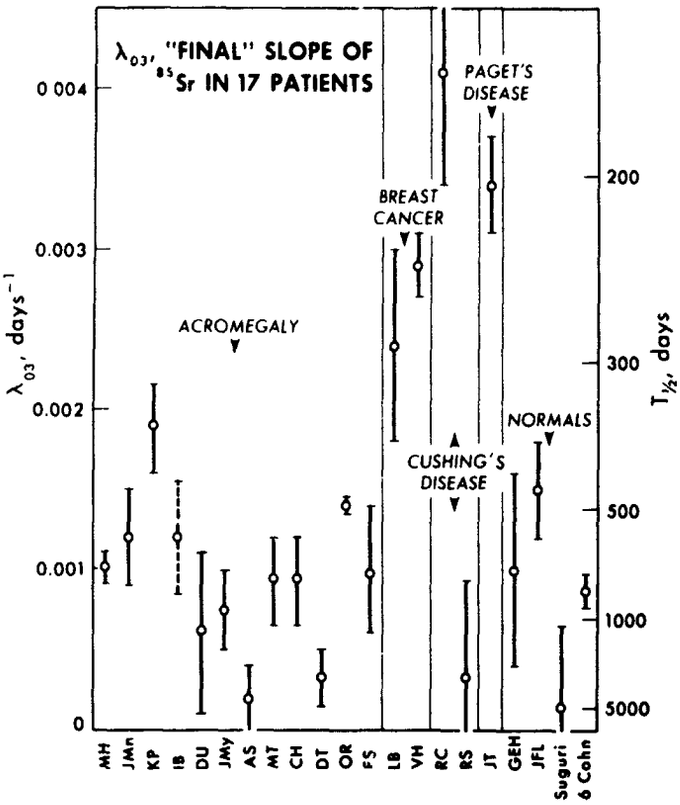

Figure 3. ^{85}Sr slope λ_{03} for 17 patients. MUB-6667

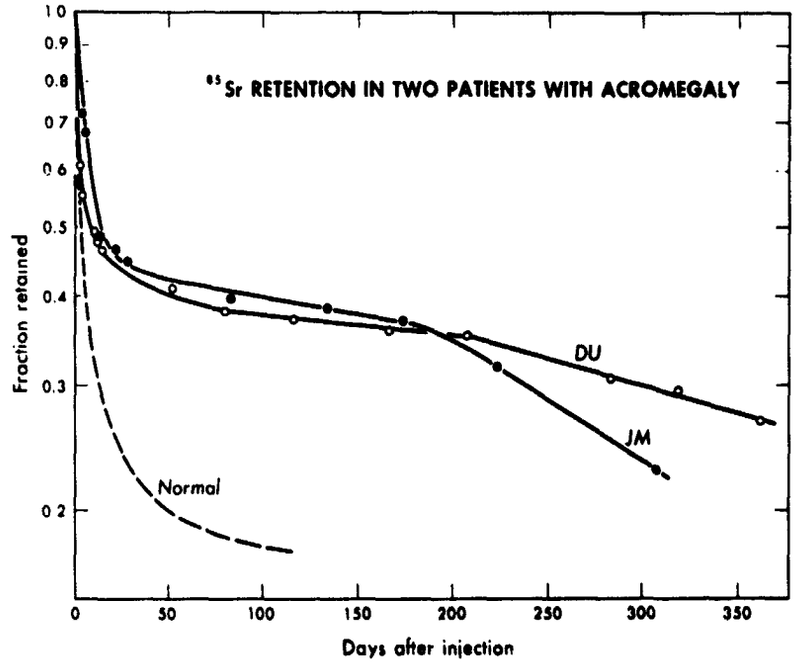

Figure 4. Two patients with acromegaly; ^{85}Sr resorption changes about 200 days after treatment. MUB-6667

Figure 4 shows an interesting effect noted in only two of the acromegalic patients, JMn and DU. All patients were studied at the beginning of their two week course of pituitary irradiation therapy, and marked reduction in growth hormone levels and other metabolic changes usually do not occur until about a year after treatment (26). Among these later effects are actual resorption, radiologically demonstrable, of excessive bone growth of the hands, jaws and feet. In these two patients at about 200 days the slope of the ^{85}Sr-retention curve increased markedly, which could only be accounted for by an increased resorption of bone. Other clinical signs at about this time also indicated improvement, such as reduction of headaches, improvement in glucose tolerance and fall in serum phosphorus. Since both untreated acromegalics and those studied several years after treatment have normal values of λ_{03}, it would appear that in the interval of one to two years after treatment the resorption rate is altered to return bone size to normal. It would appear from this that growth hormone is prominently involved in the homeostasis of skeletal metabolism.

CONCLUSIONS

It is clear that whole-body counting alone will not lead to completely satisfactory solutions to the understanding of calcium metabolism. Plasma sampling is certainly the simplest additional data to obtain, and this was done on a small sample of the patients reported here. However, calculations of bone-accretion rates by the methods of various authors, including the computer program of Berman (25), have not yielded results that are compatible with each other or with the diseases in question and thus have not been reported here. It is felt that blood sampling for only eight to ten days cannot be used with accuracy for reasons stated earlier. With beta counters now available, which have backgrounds of the order of one or two counts per minute and which can take samples of up to 2 ml of plasma, it should be possible to count ^{45}Ca in the blood for much longer periods.

The fundamental assumption used in the work reported here is that the "final" ^{85}Sr slope is the same as that of calcium, and that this slope can be applied to the ^{47}Ca curve to obtain a complete equivalent whole-body-retention curve for ^{47}Ca for up to one year. Although no independent results confirm that these assumptions are valid, they are at least internally consistent for the following reasons: 1) the curves chosen by the computer are good fits and do not suggest the presence of a third component as did the ^{85}Sr data. 2) The only dependency relationship demanded in the computer program was that between λ_{03} and λ_{06}, yet the values for the intercepts of these slopes bore a constant relationship to each other (Figs. 1b and 2). 3) The mean values of the faster slopes, λ_{02} and λ_{05}, were close to each other, although less close when individual patients are considered. Furthermore, on the basis of what is known of the metabolism of these elements, the assumption is reasonable.

It is felt that this study clearly indicates that both ^{47}Ca and ^{85}Sr should be used if one is to obtain a complete picture of calcium turnover in a patient by whole-body counting. Differences in calcium metabolism are clearly seen, which have not been reported previously using other methods. It is equally clearly indicated that whole-body counting alone is not enough; long-term blood studies with ^{45}Ca will be required, and preferably a measure of other compartments as well, before a comprehensive and accurate mathematical model for calcium

metabolism can be developed and tested. In this kind of study, the whole-body counter provides the indispensable and only practical means of measuring the turnover of isotope in bone.

ACKNOWLEDGMENTS

Grateful acknowledgment is made to Mona Boaz for technical assistance and to Mark Horovitz and Penny Collom for the computer analyses.

REFERENCES

1. Medical Uses of Ca^{47}, Vienna, IAEA, 1964.
2. Pollycove, M.; in Eisenstoffwechsel: Beiträge zur Forschung und Klinik, edited by W. Keiderling, Stuttgart, George Thieme Verlag, 1959, pp. 20-40.
3. Aubert, J. P., and Milhaud, G.; Biochim. Biophys. Acta 39:122, 1960.
4. Heaney, R. P., and Whedon, D. G.; J. Clin. Endocrinol. Metab. 18:1246, 1958.
5. Bone Metabolism in Relation to Clinical Medicine, edited by H. A. Sissons, Lippincott, Philadelphia, 1963, p. 124.
6. Belcher, E. H.; Fraser, R.; Gutteridge, G. F.; Joplin, J. F., and Robinson, C. J.; in Medical Uses of Ca^{47}, Vienna, IAEA, 1964, p. 102.
7. Cederquist, E.; Acta Radiol. Suppl. 232, 1964.
8. Bishop, M.; Harrison, G. E.; Raymond, W. H. A.; Sutton, A., and Rundo, J.; Intern. J. Radiation Biol. 2:125, 1960.
9. Cohn, S. H.; Spencer, H.; Samachson, J.; and Robertson, J. S.: Radiation Res. 17:173, 1962.
10. Suguri, S.; Ohtani, S.; Oshino, M., and Yanagishita, K.; Health Phys. 9:529, 1963.
11. MacDonald, N. S.; in Proc. Symp. Whole-Body Counting, Vienna, IAEA, 1962, p. 501.
12. MacDonald, N. S.; Figueroa, W. G., and Urist, M. R.; University of California at Los Angeles Report UCLA-12-538, Biology and Medicine, 1964.
13. Sargent, T. W.; in Proc. Symp. Whole-Body Counting, Vienna, IAEA, 1962, p. 447.
14. Sargent, T.; Linfoot, J. A.; Stauffer, H., and Lawrence, J. H.; J. Nucl. Med. 5:407, 1964.
15. Taylor, D. M.; Trott, N. G.; Rinsler, M. G., and Vennart, J.; Brit. J. Radiol. 36:732, 1963.
16. Belcher, E. A., and Dudley, R. A.; in Medical Uses of Ca^{47}, Vienna, IAEA, 1964, p. 9.
17. Korey, K. R.; Greenberg, E.; Kenny, P.; Laughlin, J. S.; Merlino, M., and Weber, D.; in Medical Uses of Ca^{47}, Vienna, IAEA, 1964, p. 5.
18. Cohn, S. H.; Lippincott, S. W.; Gusmano, E. A., and Robertson, J. S.; Radiation Res. 19:104, 1963.
19. Cohn, S. H.; Bozzo, S.; Glatstein, N.; Constantinides, C.; Litvak, J., and Gusmano, E. A.; Metabolism 13:1356, 1964.
20. Cohn, S. H.; in Progress in Atomic Medicine, edited by J. H. Lawrence, New York, Grune and Stratton, in press.
21. Heaney, R. P.; Clin. Ortho. 31:153, 1963.
22. Glass, H. I., and Nordin, B. E. C.; Phys. Med. Biol. 8:387, 1963.
23. Glass, H. I.; Clarson, D. G., and Burns, H. G.; Phys. Med. Biol. 9:57, 1964.

24. Cohn, S. H.; Bozzo, S. R.; Jesseph, J. E.; Constantinides, C.; Huene, D. R., and Gusmano, E. A.; Formulation and Testing of a Compartmental Model for Calcium Metabolism in Man, in press.

25. Berman, M.; Shawn, E., and Weiss, M. F.; Biophys. J. 2:275, 1962.

26. Linfoot, J. A., and Greenwood, F. C.; J. Clin. Endocrinol. and Metab., in press.

Received June, 1965.

Organ Visualization with Scintillation-Camera Techniques

Leonard R. Schaer and Hal O. Anger

The use of radioactive isotopes in clinical medicine has become widespread. One application is obtaining pictures of organs wherein gamma-ray-or positron-emitting isotopes have concentrated. These pictures enable one to outline functional parts of the organ, and observe anatomical irregularities that can be interpreted in the light of clinical symptoms. The most commonly used machine for this purpose is the well-known radioisotope scanner. With this technique, a directional scintillation counter moves back and forth across an organ while progressing slowly in the transverse direction until the organ being studied has been fully covered or scanned. At the same time, a mechanically coupled light beam is modulated and a picture of the distribution of activity in the organ is printed on photographic film. A major limitation of scanners is the length of time required for each scan or picture. Often 30 min or more are required for a simple scan. Taking large numbers of pictures at different times or from different angles is, therefore, seldom attempted.

We wish to briefly describe the clinical use of the scintillation camera (1-4), a relatively new electronic instrument for taking radioisotope pictures of internal organs without scanning. It contains an 11-1/2-in.-diameter by 1/2-in.-thick sodium iodide crystal viewed by a hexagonal array of nineteen 3-in.-diameter photomultiplier tubes. Scintillations produced in the crystal by gamma rays are shown on an oscilloscope as bright flashes of light that correspond in position with the original scintillations. These flashes are recorded over a period of time (anywhere from a few seconds to several minutes) on polaroid film.

Images from gamma-ray-emitting substances are projected onto the scintillator by either a pinhole collimator or a multichannel collimator. Pinhole collimators give the best combination of resolution and sensitivity for small objects such as the thyroid gland. Multichannel collimators, a 1,165-hole collimator for medium-energy gamma rays and a 4,000-hole one for lower energy gamma rays, give the best combination for larger objects such as the brain, liver and kidneys.

A special situation exists for positron-emitting isotopes whereby the gamma-ray collimators can be eliminated, and improved sensitivity and resolution obtained. A positron is a positively charged electron that travels a short distance in tissue and then combines with a negative electron. An annihilation reaction then occurs and two 0.51-MeV gamma rays are produced that travel away in exactly opposite directions. A second gamma-ray detector, called the focal detector, is placed below the patient so that both gamma rays are detected in coincidence. The currently used focal detector has a single 9- × 1-1/2-in. crystal viewed by

seven photomultiplier tubes. From the position of the two simultaneous scintillations in the two detectors, the point of origin of the gamma-ray pair in the subject is determined, and a flash of light in a corresponding position is shown on the oscilloscope.

The principal features of the scintillation camera can be described as follows: 1. In most instances the entire organ involved can be exposed at one time. 2. Each exposure is of relatively short duration. When short half-life isotopes are used, high specific activity can be injected and excellent pictures obtained with exposures lasting only a few seconds. In most studies, however, exposure time is four to five minutes. When reduction of radiation dose is desired, the exposure time can be lengthened to compensate for the smaller quantity of radioactive material injected. 3. Multiple views can be taken, i.e., anterior, lateral, and oblique, by merely positioning the patient or the camera. Moreover, repeated exposures can be taken as the study progresses. 4. A special feature of the scintillation camera is the adaptability for taking motion pictures of isotopes as they pass through organs.

CLINICAL USES

The clinical uses of the scintillation camera are best shown by a brief discussion of the various organs studied.

BRAIN More than 100 brain tumor suspects have been examined using gallium-68-EDTA as the tracer compound (4). Gallium 68 is a positron emitting isotope with a half-life of 68 min. It is the decay daughter of germanium 68 (^{68}Ge), and a simple device called a "positron cow" (5) is used to obtain the gallium at any time. Usually 400 to 600 μCi are injected intravenously, and five minute exposures are taken starting 30 min later. Figure 1a shows a right lateral projection of a brain scintiphoto study. The arrows point to an area of increased concentration of ^{68}Ga, localized in a meningioma. The two intense white areas at the bottom are small ^{68}Ge markers placed at the corner of the right eye, and in front of the right ear for orientation purposes. Figure 1b is the same projection rephotographed through a diffusion filter. The latter converts variations in the number of dots per unit area to different shades of gray. By blurring the distracting dot patterns so that they are no longer visible, the gross variations are left intact and become more obvious.

Technetium 99m in the form of pertechnitate ion is another short half-life isotope (6.04 hr) that is advantageously used with the scintillation camera. Large amounts of this isotope can be injected without excessive radiation to the patient, and excellent pictures are obtained in about one minute. Figure 2 shows the results of a ^{99m}Tc brain scintiphoto study in a patient who previously had a meningioma surgically removed. Figure 2a shows a right lateral projection with the arrow pointing to a region of increased concentration of the isotope. It is believed that permanent vascular changes remaining after surgery explain the increased concentration in this area. A concentration of isotope is also apparent in the salivary glands and the mouth. Figure 2b represents a posterior projection of the same patient with arrows again pointing to the lesion. The vertical sinus is seen in the midline. Approximately 6.5 mCi of ^{99m}Tc were injected intravenously five minutes before these pictures were taken.

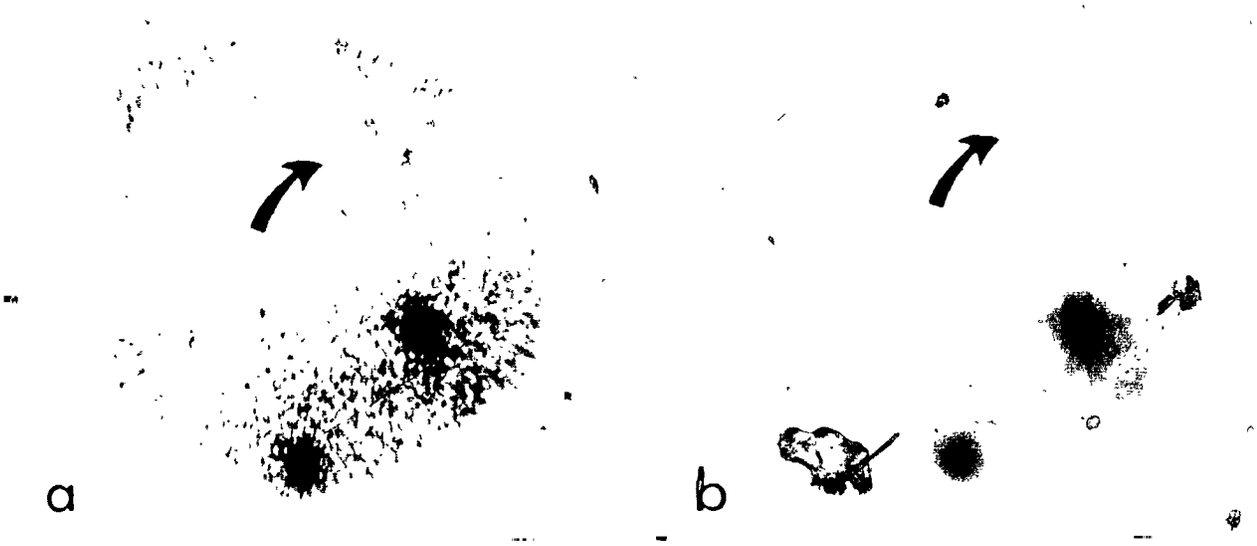

Figure 1a. Right lateral projection ^{68}Ga brain study. Arrows indicate lesion.

Figure 1b. Same study photographed through diffusion filter.

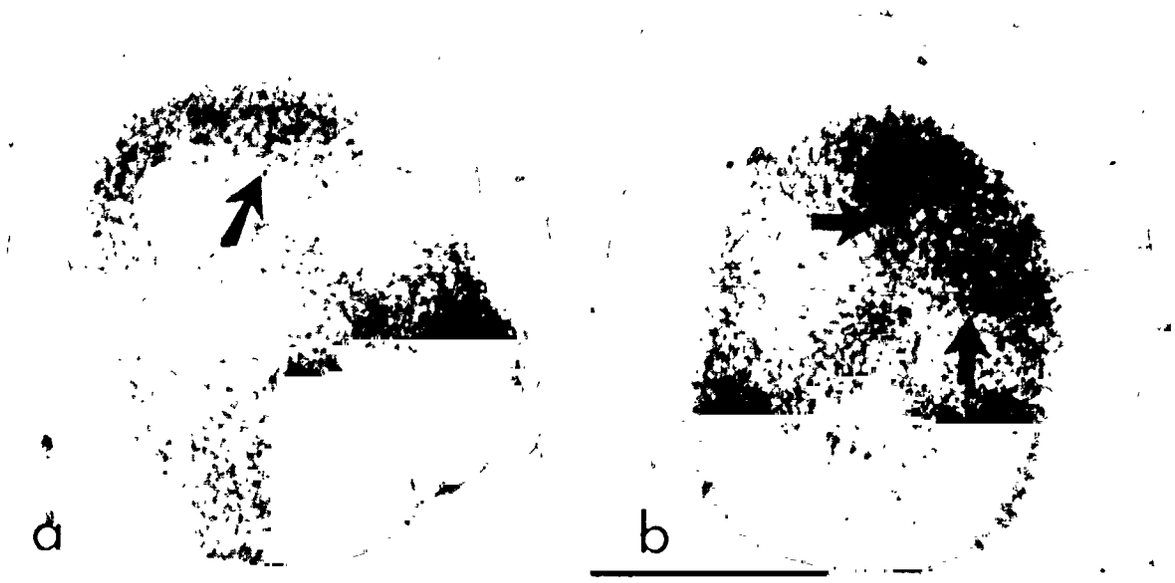

Figure 2a. Right lateral projection of brain using ^{99m}Tc. Arrows indicate lesion. Note concentration of material in salivary glands.

Figure 2b. Posterior projection of same patient. Arrows indicate lesion. Vertical sinus is visible.

THYROID Historically the thyroid has been the organ most widely studied by scanning methods and customarily only a frontal projection is obtained. Obvious difficulty can arise with such a study if a lesion is located posteriorly. The scintillation camera is now fitted with a triple aperture pinhole collimator, which allows one frontal and two oblique views of the thyroid to be taken with a single exposure. Figure 3 is a diagram representing the type of picture that is obtained using the triple-aperture pinhole collimator. The frontal view of both lobes of the thyroid is seen in the center of the field. Representative cold nodules are indicated in the upper left pole and in the mid-right pole. Enlarged oblique views of the left and right lobe are shown at the sides of the field. The relative position of the cold nodules is again represented by the dashed circles.

A clinical example is seen in Fig. 4. A standard dose of sodium iodide 131 was administered to the patient 24 hr preceding the study. A five-minute exposure is seen in Fig. 4a. Although the frontal view of the thyroid appears suspicious in the region of the lower right pole, the study might be interpreted as inconclusive. However, in the enlarged oblique view of the right lobe, the area of decreased concentration is easily seen. In like manner, the frontal projection shown in Fig. 4b appears relatively normal, but an area of decreased concentration is observed in the left oblique view.

LIVER Iodine 131-Rose Bengal is taken up by hepatic cells, which allows for good visualization of this organ. Tumors are always seen as "negative" areas because they do not take up the isotope. Since the liver is a large organ, conventional scanning proves to be a lengthy procedure. Sometimes so much time elapses during the scanning that the Rose Bengal begins to leave the liver and pass into the common bile duct, thus interfering with proper completion of the scan. The scintillation camera is able to take a picture of an entire normal-sized liver with a single five-minute exposure. Usually pictures are taken 5 min after intravenous injection of the ^{131}I-Rose Bengal. Lateral and oblique pictures are taken as desired and indicated. Follow-up pictures taken later or the next day are used to ascertain the patency of the bile duct. In some instances we have been able to take moving pictures of the material passing through the bile ducts, thus ruling out obstruction. Figure 5a is a hepatic scintiphoto which shows the frontal projection of the entire liver. Figure 5b is the same picture rephotographed through the diffusion filter. It shows more clearly the "negative" area (indicated by arrow), which represents a metastatic tumor to the liver from the colon. The intense area on the left side of the picture is caused by ^{131}I-Rose Bengal, which has concentrated in the gallbladder.

SPLEEN Using mercury 203-bromomercurihydroxypropane (BMHP) according to the technique of Wagner et al. (6), we have found that excellent visualization of the spleen is possible. Approximately 100 μCi of this material are drawn up into a syringe attached to a stopcock. The stopcock is attached to a hypodermic needle which is then placed in a vein. About 10 ml of blood are withdrawn, and the syringe is detached from the stopcock. The blood and the ^{203}Hg-BMHP are gently mixed and allowed to incubate for one minute. The material is then reinjected. Figure 6 shows the results of such a study in a patient. By positioning patient under the camera, various projections were obtained with 5-min exposures.

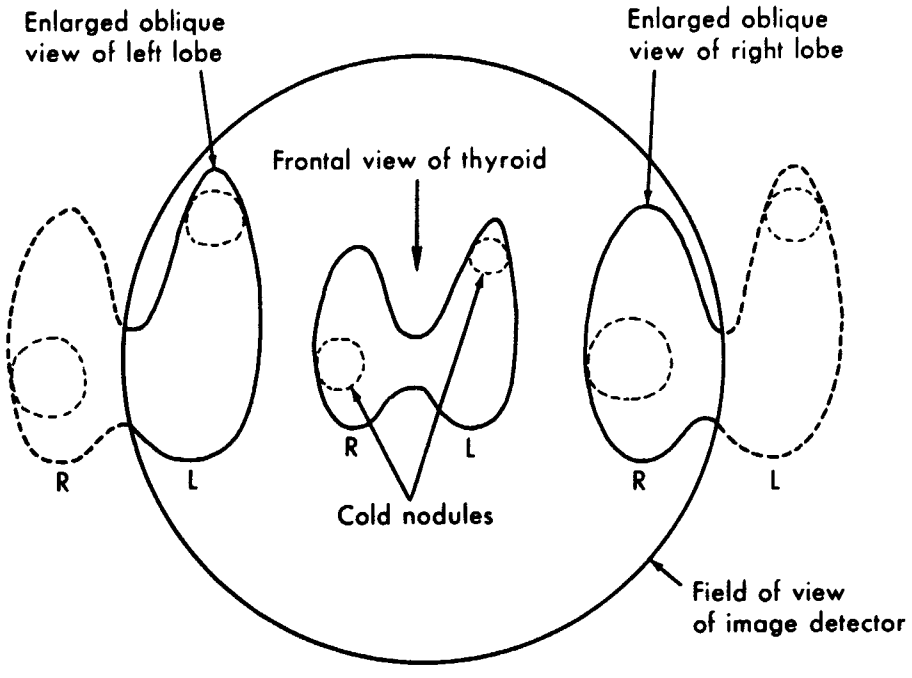

Figure 3. Diagrammatic representation of picture obtained using triple pinhole collimator for thyroid scintiphotos.

KIDNEYS Conventional scanning techniques are limited to anatomical delineation of renal tissue. In some instances, conclusions may be drawn from the relative intensity of the pictures obtained to give indirect evidence for alteration of renal blood flow. We have used ^{203}-Hg-labeled chlormerodrin with the scintillation camera for anatomic study of the kidneys. In 90% of the patients, both kidneys can be photographed at one time. In addition, since exposure times can be very short, we are able to demonstrate the passage of ^{131}I-Hippuran through the kidneys. Figure 7 shows a complete anatomical and dynamic study of the kidneys in a normal individual. Figure 7a is a picture of ^{203}Hg-chlormerodrin-labeled kidneys, as seen from the posterior projection. Once the kidneys have been properly located and studied in this fashion, the patient remains lying beneath the scintillation camera. Then 200 μCi of ^{131}I-Hippuran are injected intravenously and time-lapse moving pictures are taken (each frame lasting 15 sec). Still exposures are taken at intervals, as indicated by the captions beneath the figure. In addition, twin recording graphs of the activity passing through each kidney are now possible at the same time. Figure 8 shows a study of the kidneys in a seven-year old boy with leukemia. Because of an elevation in blood pressure, attention was directed to the possibility of leukemia-cell infiltration in the renal tissue. Figure 8a is a posterior projection of the kidneys obtained with ^{203}Hg-labeled chlormerodrin. This five-minute exposure shows both kidneys to be enlarged, with the right kidney greater in size than the left. In addition, an area of decreased uptake of material is seen in the lower pole area of the right kidney. In order to evaluate the function of these kidneys, an ^{131}I-Hippuran study was carried out. The results of this study are shown in Fig. 8b-f. Little material is seen to concentrate in either kidney until approximately eight minutes has elaspsed. Material continued to be concentrated up to 21 min following the injection of the isotope. Follow-up study on the same child after he received 100 R of X-ray therapy to the left kidney is seen in Figs. 8g-k. The spectacular change in the concentration of ^{131}I-Hippuran in the left kidney tissue is apparent.

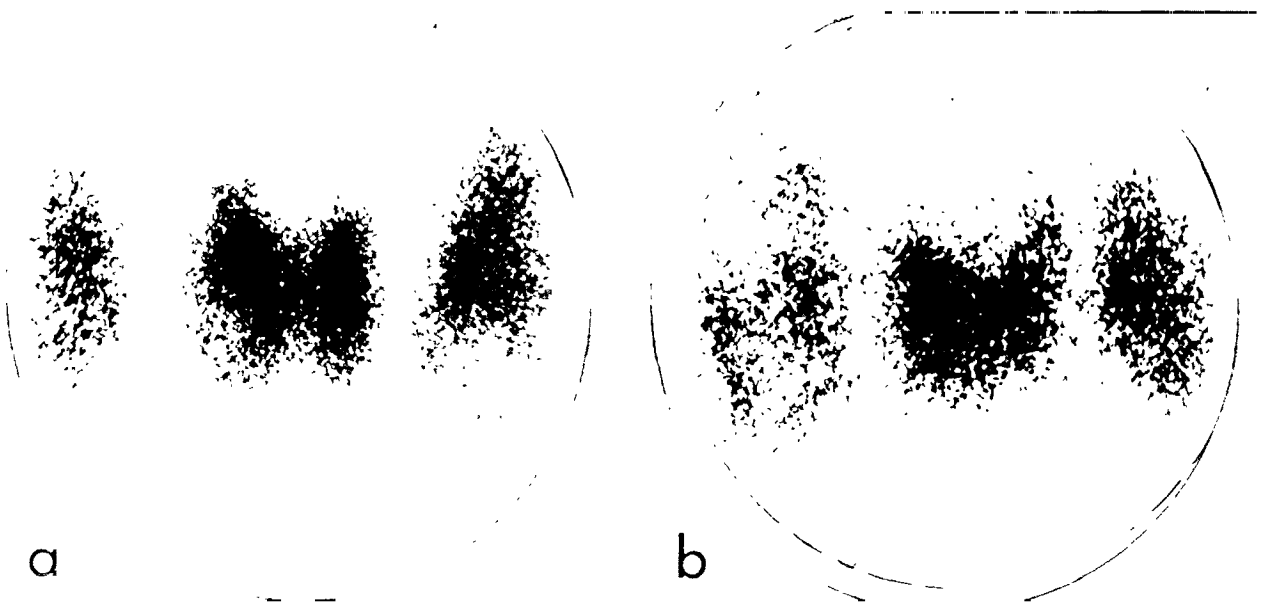

Figure 4a. Thyroid scintiphoto showing area of decreased concentration in lower right pole.

Figure 4b. Thyroid scintiphoto showing decreased concentration in left oblique view.

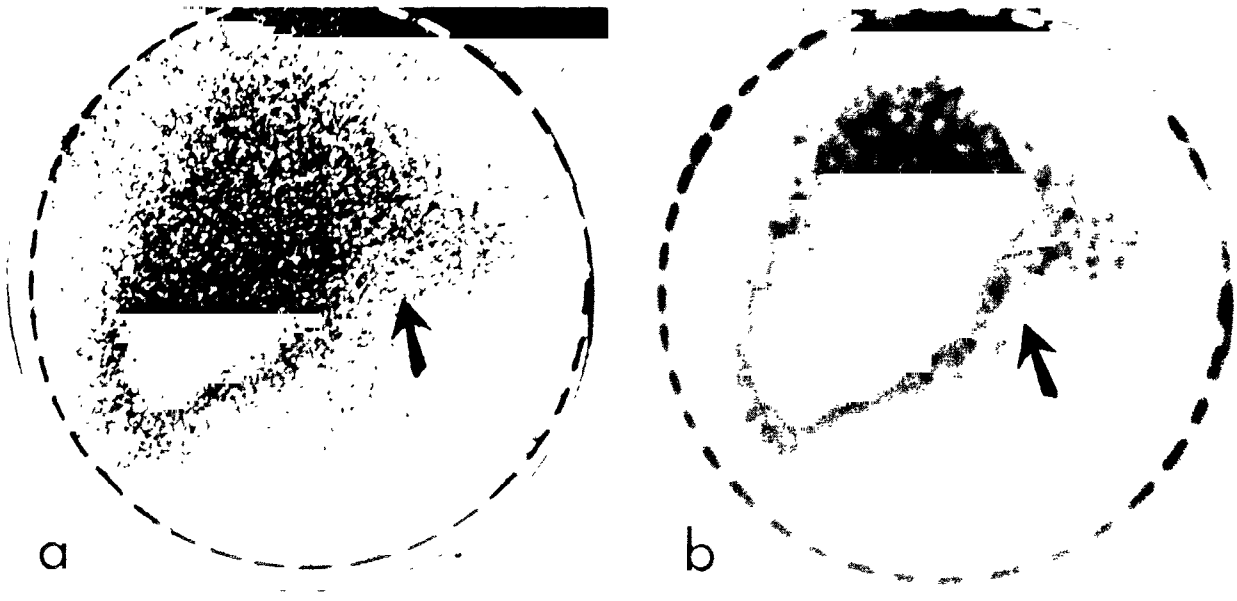

Figure 5a. Frontal view of liver using ^{131}I-Rose Bengal.

Figure 5b. Same picture rephotographed through diffusion filter. Arrows indicate negative area, representing metastatic tumor. Gallbladder is seen as bright area in normal location.

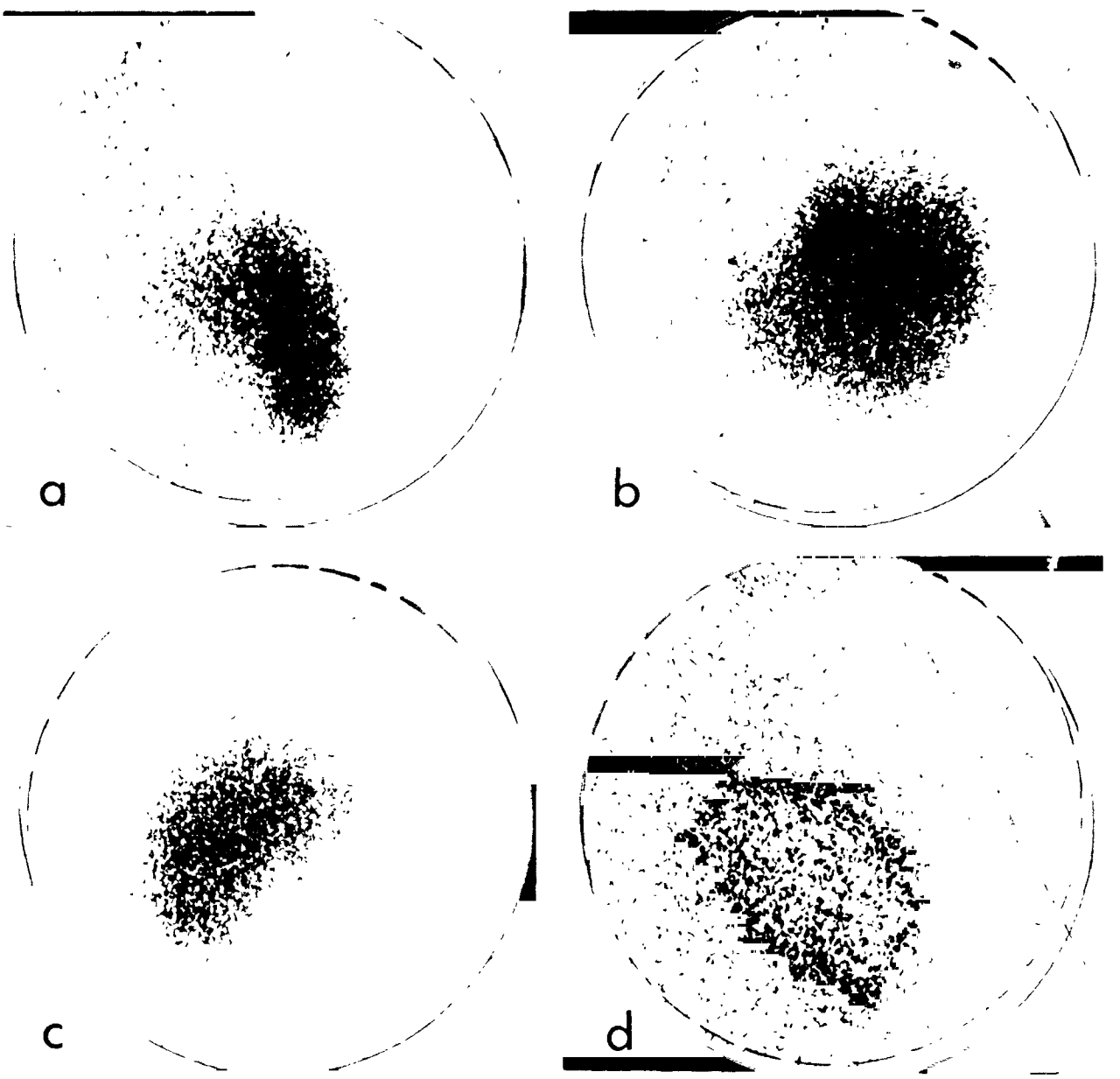

Figure 6. Scintiphoto of normal spleen taken with ^{203}Hg-BMHP, (a) anterior projection, (b) left lateral projection, (c) posterior projection, (d) right anterior oblique projection.

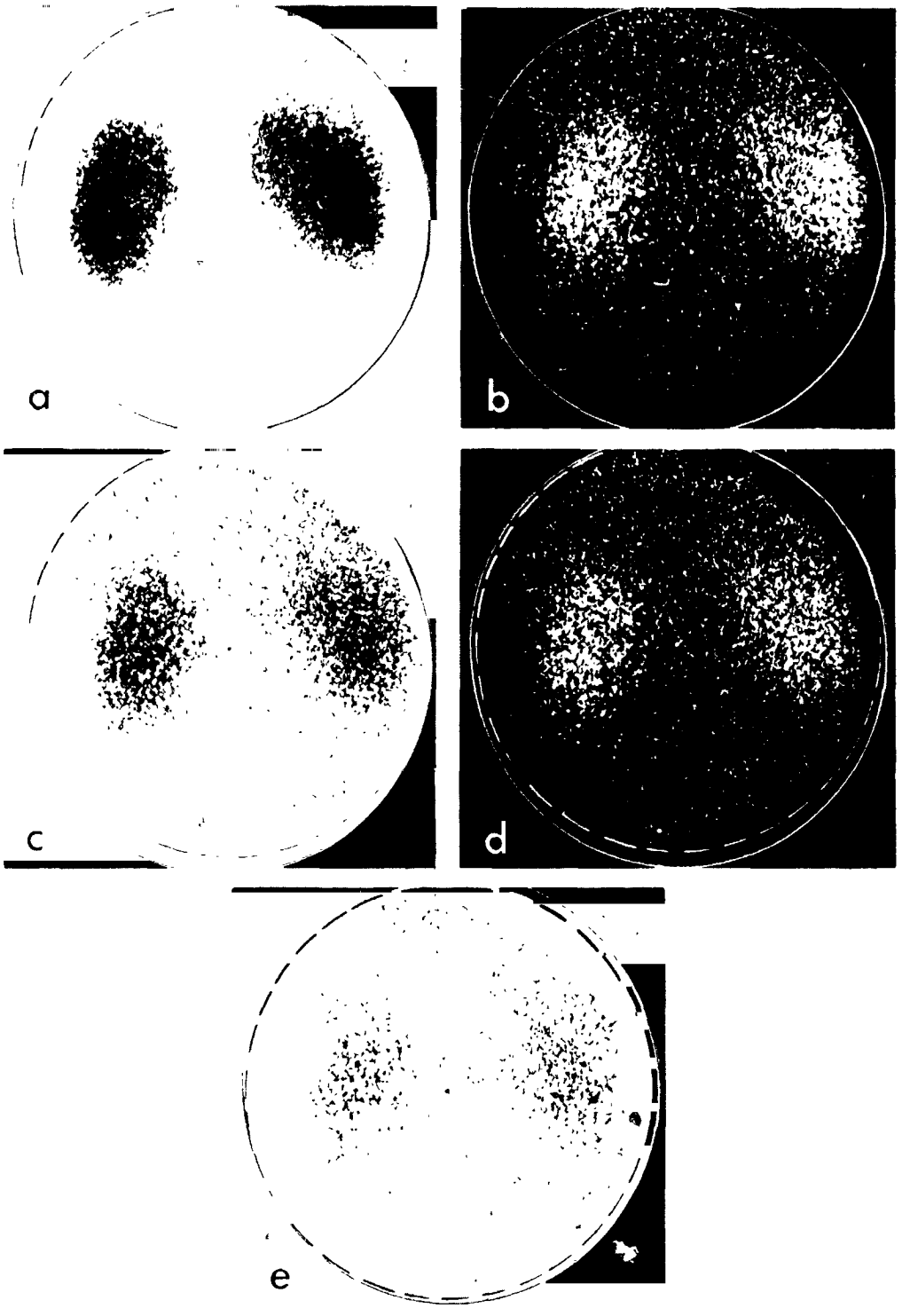

Figure 7. Renal scintiphotos showing normal renal anatomy (all posterior views); (a) picture taken with ^{203}Hg-chlormerodrin, (b-e) stop motion ^{131}I-Hippuran study. Pictures exposed during interval: (b) 1 to 2 min after injection, (c) 2 to 4 min after injection, (d) 4 to 6 min after injection, (e) 6 to 8 min after injection.

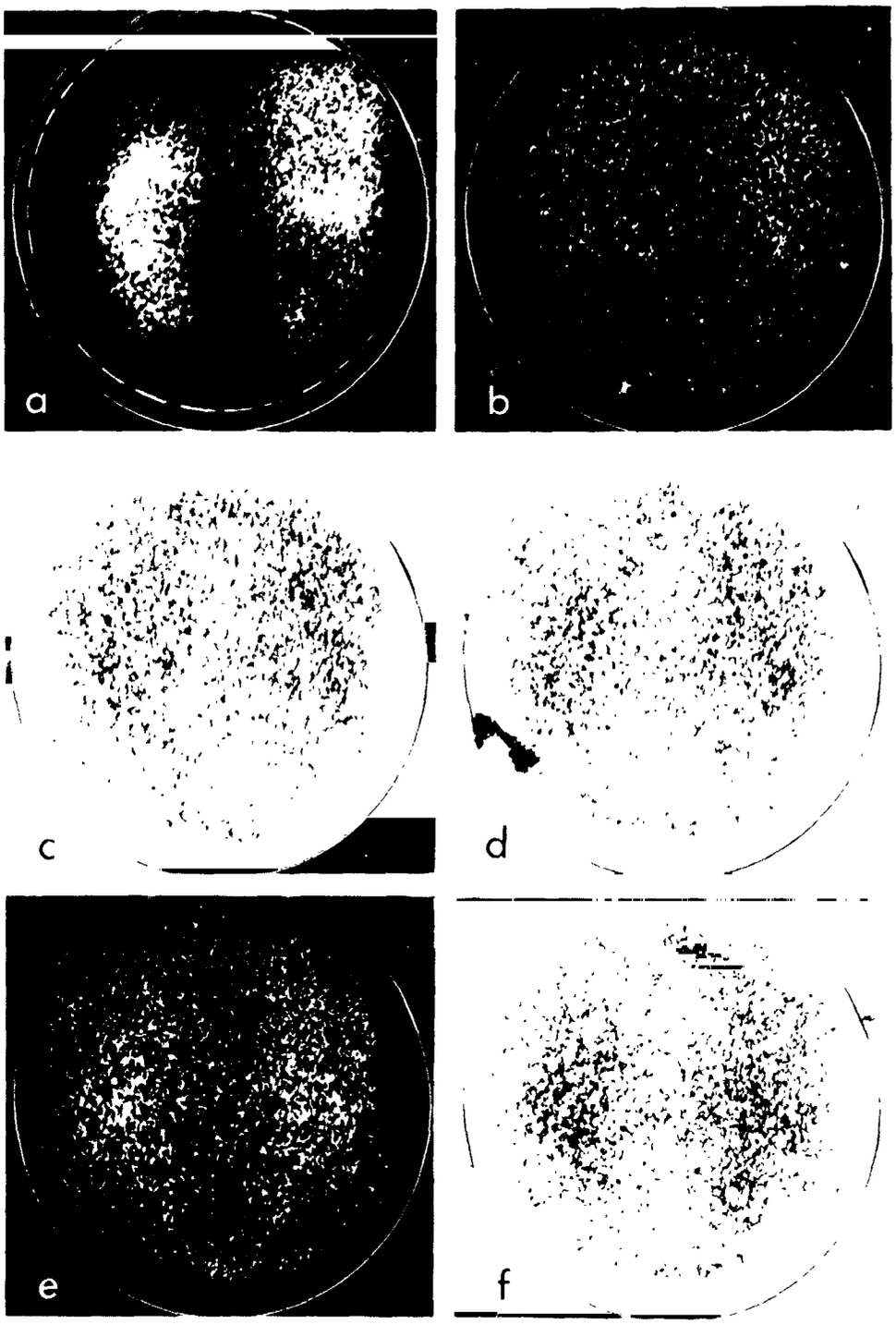

Figure 8. Renal scintiphotos of a child with leukemic infiltration of the kidneys (posterior projection); (a) picture taken with ^{203}Hg-chlormerodrin, (b-f) stop motion ^{131}I-Hippuran study. Pictures exposed during intervals: (b) 1 to 2 min after injection, (c) 2 to 4 min after injection, (d) 4 to 6 min after injection, (e) 8 to 10 min after injection, (f) 12 to 14 min after injection, (g-k) ^{131}I-Hippuran renal scintiphoto study on same patient after radiation therapy to left kidney. Pictures taken during interval: (g) 1 to 2 min after injection, (h) 2 to 4 min after injection, (i) 4 to 6 min after injection, (j) 6 to 8 min after injection, (k) 12 to 14 min after injection.

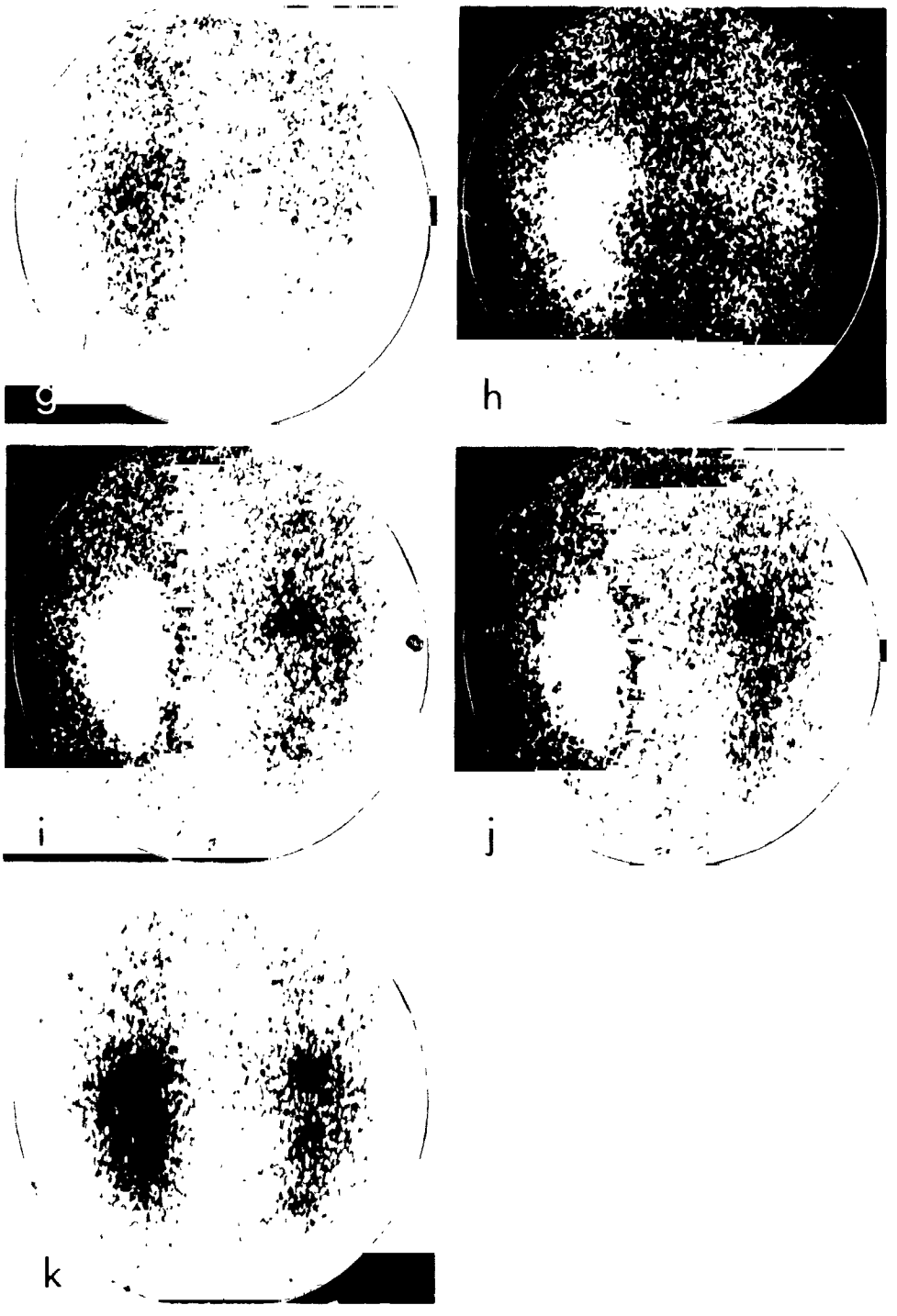
g
h
i
j
k

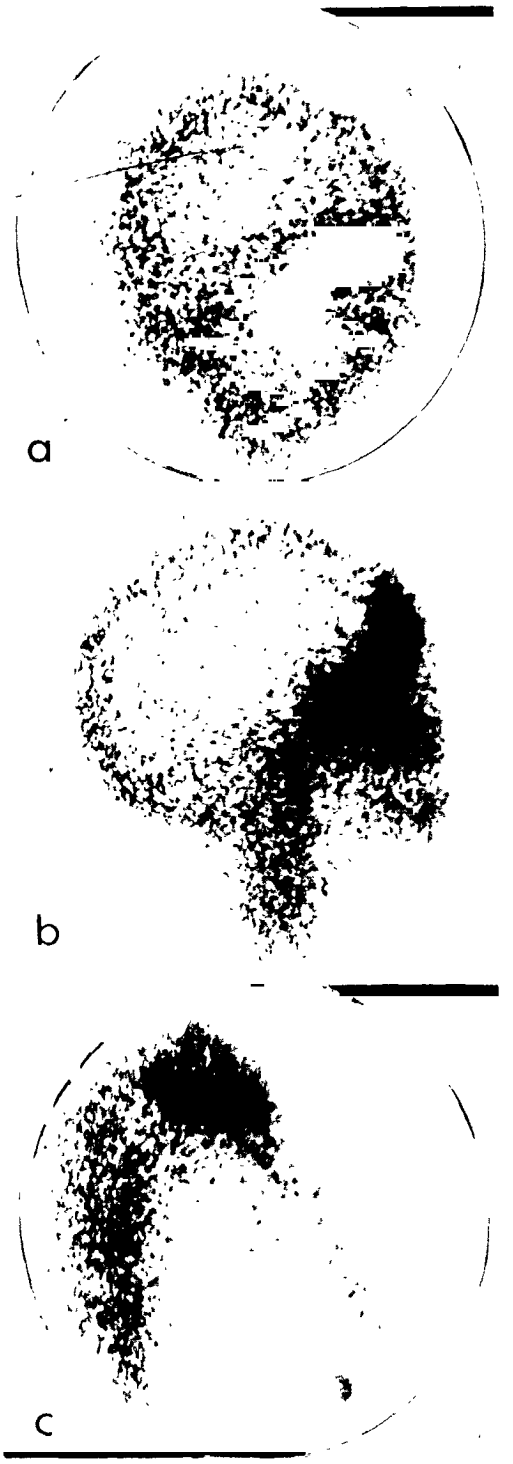

Figure 9. Sodium fluoride-18 distribution in head of child with fibrous dysplasia of the bone above the left orbit; (a) frontal view, (b) right lateral projection, (c) left shoulder girdle showing normal epiphysis.

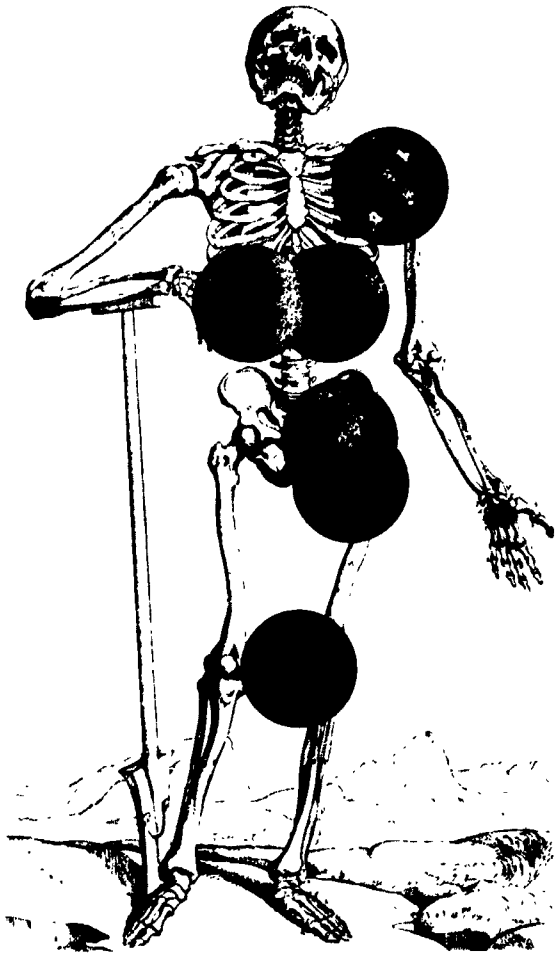

Figure 10. Bone-marrow distribution in patient with erythrocytosis secondary to cyanotic heart disease. Pictures were taken 16 hr after injection of positron emitting ^{52}Fe (courtesy Dr. D. C. Van Dyke).

BONE Fluorine 18, a positron emitter with a half-life of 1.8 hr, has been employed to demonstrate bone tumors and other abnormalities. About 200 μCi of sodium fluoride 18 are injected intravenously and pictures are taken starting at least one hour later. Exposures last three minutes per field and each field is nine inches in diameter. The table the patient lies on is moved in order to photograph different areas of the skeleton. Compensation for decay of the isotope is made by progressively longer exposures. Figure 9a shows a frontal projection of the head of a child studied with sodium fluoride 18. This patient has fibrous dysplasia of the bone above the left orbital area, and there is a striking concentration of the isotope in this region. Figure 9b shows the right lateral projection of the same patient. Figure 9c shows the upper portion of the left humerus with the expected increased concentration in the epiphysis.

BONE MARROW By administering iron 52, another positron emitter, the distribution of functioning bone marrow can be demonstrated (7). About 100 μCi are injected and pictures taken 16 hr later. Exposure time is five minutes for each nine-inch area. Figure 10 shows the bone marrow in a patient with cyanotic heart disease, with secondary erythrocytosis. Areas of functioning bone marrow are easily seen as indicated.

SUMMARY

With the scintillation camera, photographs of radioactive substances can be taken *in vivo* with short exposure times compared to those necessary with conventional radioisotope scanners. Oblique and other projections of organs can be easily taken. Motion pictures can be made of dynamic processes where indicated. Representative studies of various organs are presented.

ACKNOWLEDGMENTS

The authors gratefully acknowledge the assistance of Jean Luce and Yukio Yano.

REFERENCES

1. Anger, H. O.; Van Dyke, D. C.; Gottschalk, A.; Yano, Y., and Schaer, L. R.; Nucleonics 23, No. 1:57, 1965.
2. Anger, H. O.; J. Nucl. Med. 5:515, 1964.
3. Anger, H. O.; Nucleonics 21, No. 10:56, 1963.
4. Anger, H. O. and Gottschalk, A.; J. Nucl. Med. 4:326, 1963.
5. Yano, Y. and Anger, H. O.; Semiannual Report, Donner Laboratory, Lawrence Radiation Laboratory, UCRL-11387, 1964.
6. Wagner, H. N.; Weiner, I. M.; McAfee, J. G., and Martinez, J.; Ann. Internal Med. 113:696, 1964.
7. Anger, H. O. and Van Dyke, D. C.; Science 144:1587, 1964.

Received May, 1965.

Virus Particles Associated with Immune Responses in Ehrlich Ascites Tumor Cells

Josephine L. Barr and Thomas L. Hayes

The results of immunological studies by Biggs and Eiselein (1) have indicated the presence of a particulate antigenic factor in one subline of Ehrlich ascites tumor cells that can produce an immunity against innoculated ascites tumor cells of this type, (designated Type A by Biggs and Eiselein (1)). By filtration techniques, this antigenic factor was associated with a particle size somewhere between 100 mμ and 450 mμ. Ehrlich ascites tumor cells of another subline (Type B), tested by them under identical conditions, exhibited no such particulate antigen (1). In view of the well-known association of certain tumors and virus particles (2-4), an attempt was made to examine these cell lines with the electron microscope to see if there were distinguishing morphological characteristics of the two sublines of Ehrlich ascites tumor cells.

METHODS

Ascites tumor cells Type A and Type B were obtained from the peritoneal cavity of mice 7 to 9 days after challenge and placed immediately in cold (4 °C) 1% veronal-acetate buffered osmium tetroxide. Fixation was carried out in a 10-ml centrifuge tube, and the peritoneal fluid was diluted 1 to 10 by the fixative solution. Fixation was allowed to proceed for one-half hour at room temperature. The cells were then spun down in a clinical centrifuge in a hood for 2 min at full speed. The supernatant fluid was decanted and 70% ethyl alcohol was added.

Cells were gently agitated, allowed to stand for 5 min and were then again sedimented, supernated, decanted and 100% ethyl alcohol added. A second change of 100% ethyl alcohol was carried out and the cells remained in this solution for 10 min. Cells were then placed in a 1 to 1 solution of 100% ethyl alcohol and N-butyl methachrylate for 10 min, were then sedimented and resuspended in a mixture of 85% butyl and 15% methyl methachrylate for 10 min. After sedimenting and decanting, a mixture of 85% butyl and 15% methyl methachrylate with 2% benzol peroxide (w-v) was added to the centrifuge tube, and the cells were allowed to stand for 10 min. Plastic (BEEM) capsules were filled with partially polymerized 85-15 methachrylate and catalyst, and the cells were added to the top of the capsule. The capsules were covered and spun so that the cells sedimented to the bottom of the capsule. Polymerization was completed in a 40 to 45 °C oven. Sections were cut with an LKB ultramicrotome and were observed in an Hitachi HU-11 electron microscope.

Figure 1. Subline A ascites tumor cell. V = virus particles. Magnification x 20,500.

Figure 2. Subline A ascites tumor cell. V = virus particles. Magnification x 88,500.

Figure 3. Subline B ascites tumor cell. No virus particles are seen. Magnification x 17,000.

Figure 4. Subline B ascites tumor cell. No virus particles are seen. Magnification x 88,500.

RESULTS AND DISCUSSION

Figure 1 shows a typical cell of Type A ascites tumor at low magnification, and accumulations of virus particles at the cell surface in regions near the poles of the cell can be seen. Figure 2 shows these particles at higher magnification and demonstrates the structure of outer membrane and inner dense core that has previously been associated with tumor viruses (2-4). The average diameter of these virus particles was 800 Å and they could be demonstrated in a majority of the cells of Type A. No particles of this morphology were found in the cytoplasm or nucleus of the cell. The cell surface was quite active showing many microvilli, and the virus particles were found in the extracellular space between these villi.

Figure 3 shows a low magnification picture of a Type B ascites tumor cell. No virus particles were seen on the surface of the cells. In higher magnification, Fig. 4, the active cell surface with microvilli is apparent but no virus particles are present.

Using the study by Biggs and Eiselein of two sublines of ascites tumor cells in the peritoneal fluid of mice,we had an opportunity to observe the ultrastructure and associated particles of tumors grown in the same animal species and at the same site within the animal. The correlation between the observed virus particles in Type A cells and the immunological competence of this cell line would suggest that the antigenic substance formed by Type A ascites tumor cells is a virus particle of 800 Å diameter that is found at the outer surface of the cell. The pore size of 1,000 to 4,500 Å, shown by Biggs and Eiselein to pass the antigenic material, is roughly compatible with this virus particle. The ascites tumor systems as developed here offer an opportunity to study closely related tumor species with varying immunity responses and present the possibility of correlating immunological data with morphological information obtained by the use of the electron microscope.

SUMMARY

Virus particles have been demonstrated in a subline of ascites tumor cells that are capable of inducing an immune response. These particles are of a size that is roughly compatible with the size of the antigenic material,as shown by filtration data. No such particles were found in a second ascites tumor subline that has been shown to have no antigenic material of this size range. It is suggested that the antigenic material is this virus particle.

ACKNOWLEDGMENTS

We are indebted to Dr. Max Biggs and John Eiselein for supplying the samples of Ehrlich ascite tumor cells, types A and B, used in this electron microscopic study.

REFERENCES

1. Biggs, M. W., and Eiselein, J. E.; Lawrence Radiation Laboratory Report UCRL-12450, 1965.
2. Negroni, G.; Advances in Cancer Research, Vol.7, New York, Academic Press, 1963, pp. 515-561.
3. Andrewes, C.; Brit. Med. J. 1:653, 1964.

4. Amano, S., and Ichikawa, Y.; in Electron Microscopy, 5th International Congress for Electron Microscopy, Vol. 2, Philadelphia, Academic Press, 1962, p. MM-2.

Received June, 1965.

A Preliminary Curve Relating Dose in Time to Pituitary Histologic Change Following 910-MeV Alpha-Particle Irradiation

Joseph J. Hazel, Larry W. McDonald and Alexander Gottschalk

The present report represents a retrospective attempt to establish a dose-effect curve relating dose and time to an arbitrarily chosen level (50% or more) of destructive cellular change in the pituitary gland following its irradiation with 910-MeV alpha particles from the 184-in. synchrocyclotron. Fifty-six cases were studied, representing advanced carcinoma of the breast with widespread metastases and including seven patients with diabetes showing diabetic retinopathy. These cases were treated with pituitary irradiation in an attempt to produce an hypophysectomy in the hope of influencing the course of their disease. These patients all had normal pituitary glands except for three who showed metastases in the gland from the carcinoma of the breast at autopsy. All the present cases came to autopsy at times ranging from slightly more than two months to several years after treatment. The pituitary gland was studied in each case by one pathologist, and the amount of histological damage was assessed using the same set of criteria.

The pituitary irradiation was carried out by a method previously described (1). The plateau region of the 910-MeV alpha-particle beam was utilized. The patients were placed in individual masks and were treated in 12 planes through a sagittal body axis while the head was rotating through a 70° arc. The treatment set up is represented in Fig. 1. Maximum tumor dosages at the center of the pituitary gland ranged from 10,800 rads in 14 days to 36,500 rads in 12 days. The cases were assessed at autopsy at 2 1/2 months or more following the irradiation to the pituitary gland, and a level of 50% or more of cellular damage in the pituitary was used as a criterion of significant ablation in an effort to construct a time-dose-effect curve.

CASE HISTORIES

In an effort to assess the level of pituitary damage in terms of functional changes, target-end-organ hormone values of a number of cases showing more than 50% damage and a corresponding number showing less were compared. It was obvious that those cases with greater histologic pituitary change showed a greater decrease in function of target end organs. Likewise, the objective clinical responses of the patients were reviewed and were seen to follow the same general pattern (Table 1). Two typical case histories are presented, one of which showed more than 50% destructive pituitary change and the other less than 50% change.

Mr. J. D. was a 47-year-old male seen in October of 1958 for carcinoma of the left breast with metastases to bones. He had had a left mastectomy in May, 1957, and was well

Figure 1. The treatment set up for pituitary irradiation showing the patient in the mask and the angles of rotation.
JHL-2897

Figure 2. A case in which the percent destruction was estimated at 25%. The stalk and posterior lobe are seen at the upper left hand corner. Increased amounts of supporting tissue appear in the area of the middle lobe.

Table 1.

Patient	Pituitary dose	% destruction	Objective response	Replacement therapy for hypopituitarism
(Breast Carcinoma)				
1	21,000 in 12 days	50%	No	Yes
2	18,600 in 11 days	50%	No	Yes
3	21,000 in 12 days	95%	Yes	Yes
4	27,000 in 22 days	50%	No	Yes
5	27,000 in 13 days	75%	Yes	Yes
6	24,300 in 12 days	95%	Yes	Yes
7	30,600 in 12 days	95%	Yes	Yes
8	18,600 in 9 days	50%	No	No
9	17,000 in 5 days	70%	Yes	Yes
10	25,000 in 12 days	>50%	Yes	Yes
11	21,000 in 12 days	60%	Yes	Yes
12	24,000 in 12 days	50%	No	Yes
13	21,000 in 12 days	50%	Yes	Yes
14	21,000 in 12 days	70%	No	No
15	24,600 in 12 days	95%	No	Yes
16	27,000 in 13 days	90%	No	Yes
17	27,000 in 12 days	60%	No	No
(Diabetic Retinopathy)				
18	21,600 in 12 days	>50%	Yes	Yes
19	21,600 in 12 days	99%	Yes	Yes
20	24,000 in 12 days	99%	No	Yes
21	21,000 in 13 days	30%	Yes	Yes

Eight of 17 breast carcinoma patients and two of three diabetic patients above the 50% pituitary-destruction line were judged to have had an objective clinical response to the radiation. All of the responders showed at least 50% destructive pituitary changes except for one diabetic showing a response at 30%. Two breast carcinoma patients survived at least 3 1/2 months without response at 95 and 90% destruction, and one diabetic showed no response at 99% glandular destruction.

Hypopituitarism was a function of dosage--85% of the cases having 50% or more (50-99%) pituitary destruction showed evidence of hypopituitarism as compared to 50% with less than 50% destruction (10-49%).

until November of that year when he developed pain in the left hip. He was found to have metastatic disease in the left pelvis and received a course of local X-ray therapy in June, 1958, and again in September with little improvement in the pain. When seen in October the presence of extensive osteolytic metastatic disease in the left femur and left pelvis was noted. In addition he had palpable supraclavicular and posterior cervical lymph nodes. Following evaluation he received 27,000 rads of alpha-particle radiation to the pituitary in six treatments over a 12-day period. One month following the irradiation he developed symptoms and signs of hypopituitarism which were controlled with appropriate replacement therapy. Two and one half months after the therapy he began to experience relief of the pain in the left hip and leg. This relief continued and the pain disappeared. He was able to return to full activity. Six months after the therapy X-ray pictures began to show evidence of healing in the metastatic lesions of the pelvis. Ten months after the therapy there was evidence of further healing and remineralization with solid appearing bony trabeculae. He remained well until approximately 14 months after the therapy when the pain again began to return, and over the next 2 to 3 months he began to show evidence of increasing metastatic disease throughout the skeleton. His subsequent course was gradually downhill with more widespread metastatic disease becoming evident. This case represents a useful and worthwhile palliative response for a matter of over a year after having received his pituitary irradiation. At autopsy 30 months after therapy the pituitary gland revealed 95% destructive changes.

Mrs. N. G., a 31-year-old female, was seen in July of 1961, two and one-half years after having had a right radical mastectomy for carcinoma of the breast. In October of 1960 she developed a recurrence in the chest wall and in February of 1961 some supraclavicular nodes appeared. These had been treated with local radiation therapy. When seen here she had a number of cutaneous nodules scattered over the chest wall and had developed a node in the left axilla. Following evaluation she received a dose of 17,000 rads to the pituitary with the alpha-particle beam in six treatments over a 12-day period. Two months following the irradiation an increase in the number and size of the cutaneous nodules was noted, and the appearance of new lymphadenopathy in the neck region was manifest. Metastatic disease in the spine became evident and she began to have some difficulty in swallowing due to infiltration of metastatic disease in the upper cervical area. There was no evidence of hypopituitarism at this time. All of these symptoms gradually progressed over the course of the next 5 months and she expired with extensive metastatic disease 8 months after having completed her pituitary irradiation without showing evidence of hypopituitarism. At autopsy there was judged to be approximately 5% destructive change in the pituitary.

RESULTS

Histological changes ranged from the loss of a few glandular cells, with a reticulin framework remaining, to a more complete destruction of tissue with occasional hemorrhage. On Mallory-Heidenhain stains it often appeared that basophils were selectively preserved, but this was not a consistent finding. In a few instances where differential cell counts were done, no marked shifts in relative cell numbers were found. In no instance did it appear that a primary tumor was arising in the pituitary. Occasionally, metastatic tumor was present in the gland. Sclerosis of blood vessels and fibrous thickening of the capsule of the pituitary

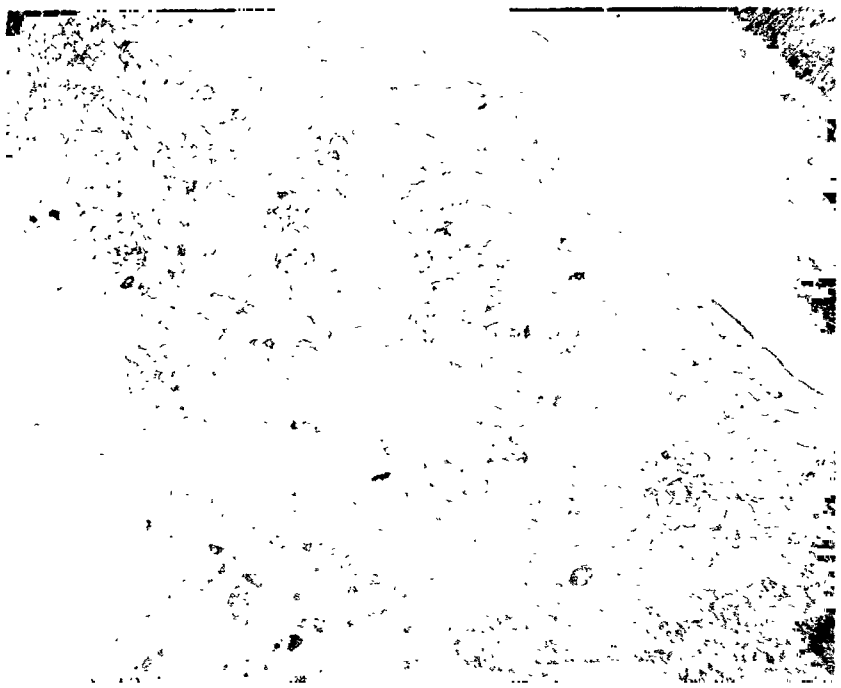

Figure 3. Case number 4 in which the percent destruction was estimated at 50%. In this mid-saggital section the percent destruction is about 65%. When compared with other sections however, the final destruction was estimated at 50% (see Fig. 4).

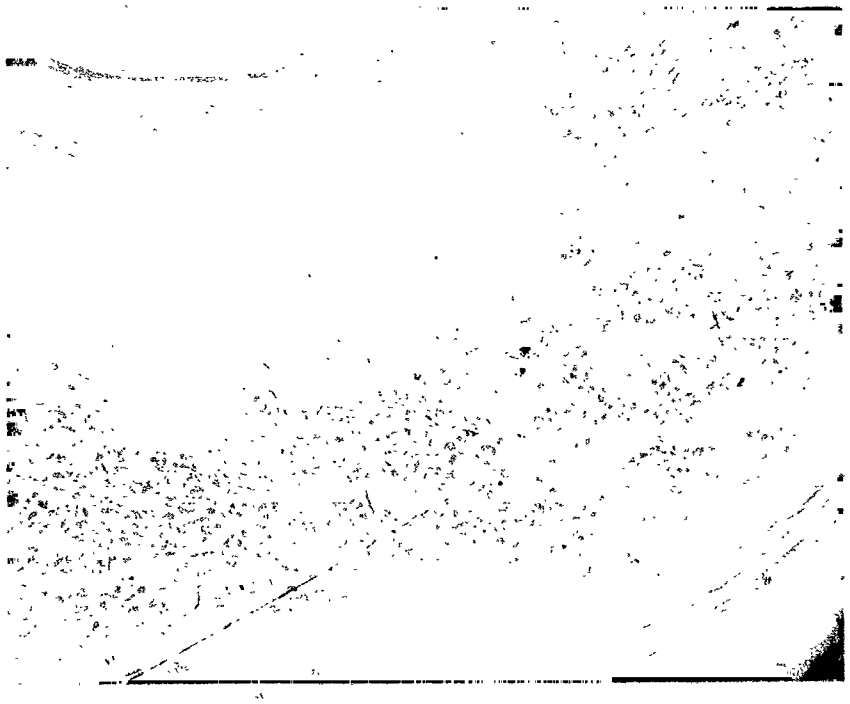

Figure 4. Same as Fig. 3 but from superior horizontal section. Increased amounts of collagenous supporting tissue are present, but more than 50% of the glandular tissue appears to remain.

Figure 5. Case number 16, in which an estimated 90% of the gland was destroyed. All glandular cells have been lost from the central part of the field, only the supporting framework remains.

were often seen, especially in those cases where destruction of the gland was estimated at about 50%.

All estimates of the percentage of destruction of the gland were made without prior knowledge of the radiation dose to the pituitary. When destruction was minimal (Fig. 2) it was difficult to be sure one was not observing an area of fibrosis which is frequent within the anterior pituitary. Generally, however, the radiation produced more empty spaces where the glandular cells had died and disappeared.

In addition, many of the remaining glandular cells showed pyknotic changes and retraction of cytoplasm. It is likely that these cells had marked functional impairment. When glandular tissue loss was estimated at between 25 and 75%, one often saw a great deal of variation in the degree of cell loss between different sections (Figs. 3 and 4). At least five sections were taken of each pituitary. These were the mid-saggital, right and left superior horizontal, and right and left inferior horizontal. In addition, right and left middle horizontal sections were taken in many instances. When the degree of destruction was 75% or more, the nuclei of remaining cells were all pyknotic and the cytoplasm was retracted. The remaining cells tended to be grouped in bands near the capsule (Fig. 5).

DISCUSSION AND SUMMARY

On the basis of the pathological evaluation of the cellular destructive changes as assessed by the same pathologist, the curve relating dose and time with 50% destructive

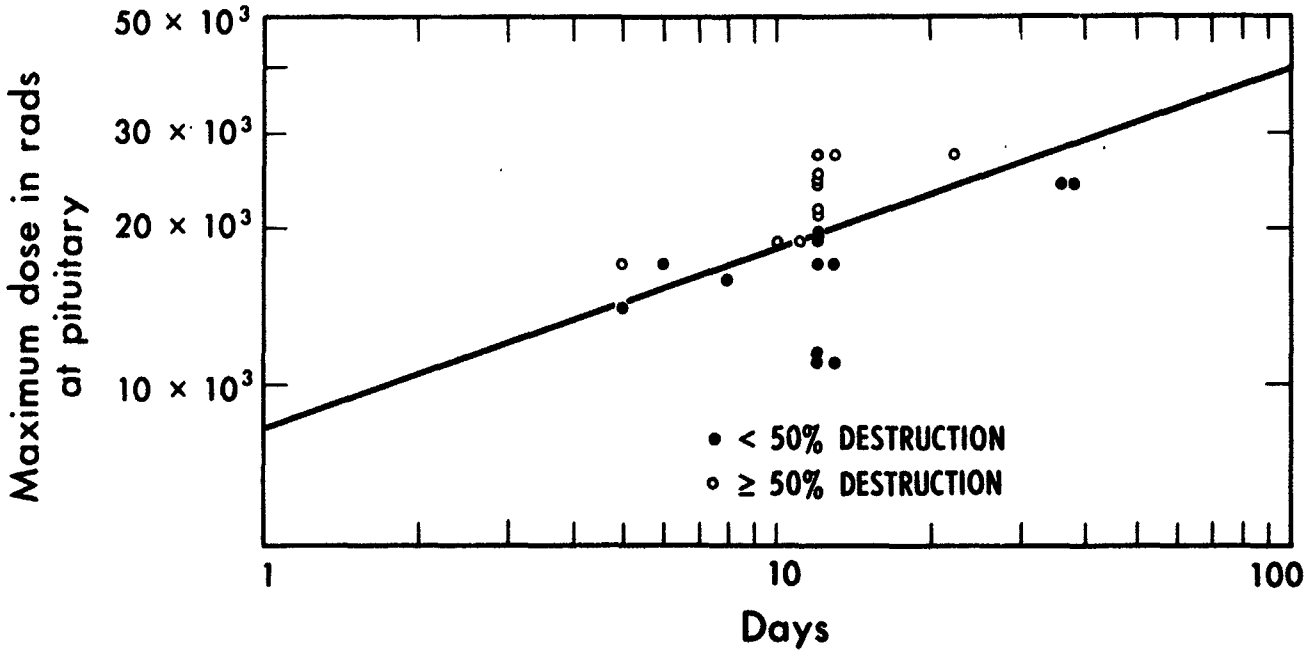

Figure 6. The time-dose curve relating to 50% cellular destruction in pituitary. The white dots represent 50% or more destruction.

MUB-7820

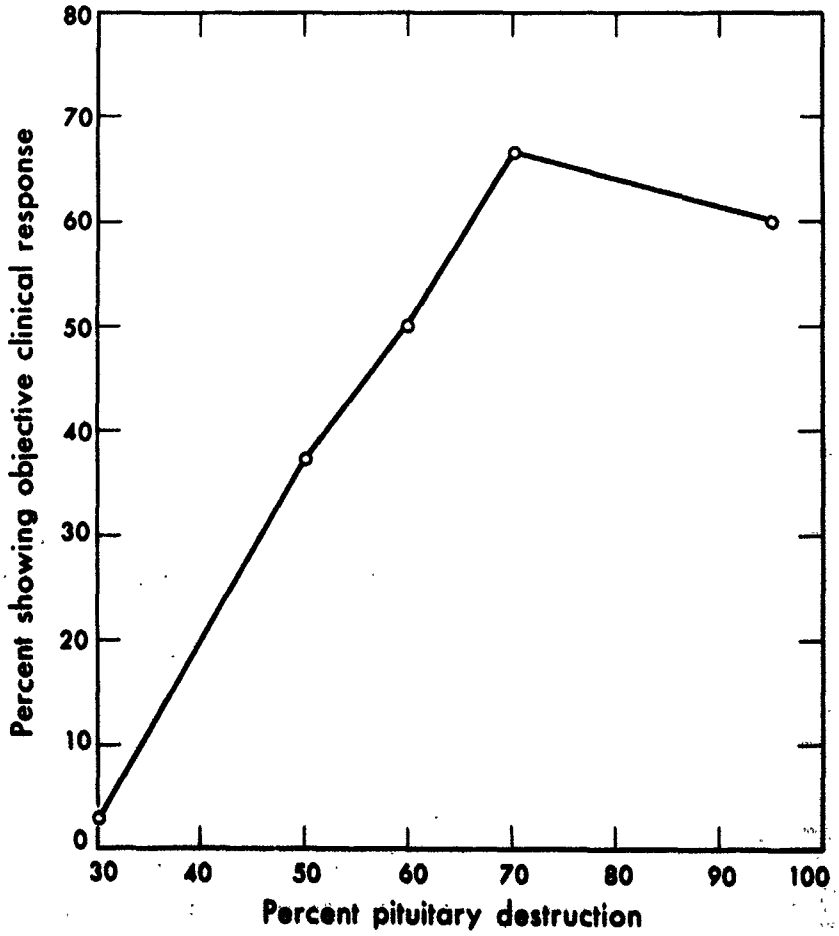

Figure 7. Pattern in the 11 responders of the 21 cases with 50% or more pituitary destruction out of the total 56 cases reviewed.

MUB-7821

change was drawn. This is presented in Fig. 6. It is seen that the resultant is linear and extrapolates to approximately 8,500 rads in a single treatment to co-relate with 50% or more pituitary damage histologically. The validity of this extrapolation from multiple observations to a single value remains somewhat uncertain and awaits confirmatory evidence using single treatments below and above this range. It is anticipated that the slope of the curve is valid and will hold for other levels of pituitary damage. From Fig. 6 it is seen that a dosage level of approximately 17,000 rads in 5 days was the minimum associated with 50% destruction of the pituitary in these cases.

In comparing the doses used here to those found to cause necrosis of the pituitary with intrapituitary implantation of yttrium-90 seeds or pellets, values of 400,000 rads at 1 mm from the cluster or 100,000 rads at 3 mm are quoted (2). One hundred thousand rads are felt to be approximately the level for pituitary necrosis using the implantation technique. Eighty per cent of 49 cases so treated showed complete histological necrosis (2). The zone of necrosis was 2 to 4 mm wide. In our reported cases treated with external radiation the system of rotation localized the high-dose radiation in the pituitary gland with the maximum value quoted in the center and a falloff laterally at the margins of the pituitary to perhaps about 70% of this value. A complete pituitary destruction was not found in any of our cases and it was not felt that this was necessary to obtain a functional ablation of the pituitary and a clinical response. This same observation has also been recorded by Notter (2). However, it should be mentioned that regeneration of the pituitary after partial destruction has been cited by Edelstyn et al. (3). It is tentatively suggested by our figures, Fig. 7, that approximately 70% or greater destructive change in the pituitary results in a clinical response in the majority of patients.

The present small study allows for the tentative establishment of a time-dose-effect curve relating to a level of pituitary destruction using irradiation with the plateau of a 910-MeV alpha-particle beam.

REFERENCES

1. Lawrence, J. H.; Tobias, C. A.; Born, J. L.; Gottschalk, A.; Linfoot, J. A.; Kling, R. P.; J. A. M. A. 186:263, 1963.
2. Notter, G.; Acta Radiol. Suppl. No. 184, 1959.
3. Edelstyn, G. A.; Gleadhill, C. A., and Lyons, A. R.; Brit. J. Surg. 51:32-40, 1964.

Received June, 1965.

Technique of Patient Alignment for Pituitary Irradiation with High-Energy 910-MeV Alpha Particles

Alexander Gottschalk

The high-energy alpha-particle beam provides a unique method of pituitary irradiation. The virtual absence of side scatter and the ease of collimation permit accurate placement in tissue with a precision that is difficult if not impossible to achieve with super voltage or orthovoltage electromagnetic irradiation. Although the high-energy (plateau) portion of the alpha-particle beam is low LET irradiation and thus of comparable RBE to electromagnetic irradiation (1) an excellent depth-dose distribution is obtained by rotating the patients head during treatment. The combination of a precisely defined beam and an exact system of rotation provides a geometric means of delivering a very large dose to the pituitary while sparing the vital peripituitary structures. It is the purpose of this article to outline the method by which pituitary irradiation is accomplished.

HEAD ROTATION

The essential feature of this facet of treatment is the construction of an individualized lucite mask for each patient. This is done by first placing quick setting moulage over the head and face, including the nose but not the mouth. From the moulage, a plaster cast of the head is moulded. This is bivalved along the coronal plane, and the mask is made by vacuum-forming heated lucite over the plaster. Holes for the eyes and nostrils are made, and the two halves of the mask are bolted together. Although the mask is virtually skin tight--motion of more than 0.5 mm is impossible--the mask may be comfortably worn for periods up to 1 1/2 hr. Head rotation is easily accomplished, and made exactly reproducible on a daily basis by attaching the mask to a mechanical head rotator.

Three coordinate planes are used to describe the position of the patient in the medical cave of the 184-in. synchrocyclotron. The patient assumes the supine position for therapy. The X-axis is the line running from head to toe, the Y-axis is the line from anterior to posterior, i.e., from the eyes to the occiput, and the Z-axis (the axis of the heavy particle beam) from side to side, i.e., in the coronel plane from one temporal region to the other. A complex dual system of rotation is used--first, the head is constantly rotated through an arc of 70° with the X-axis acting as the center of rotation. Secondly, the body is rotated through an arc of 66° in discrete steps. Here the center of rotation is the Y-axis, and the body is moved along the coronal plane. Motion is through a 6° arc, so that 12 successive planes are treated with the body stationary for each treatment. Figure 1 schematically illustrates the three coordinate planes, and the two methods of rotation.

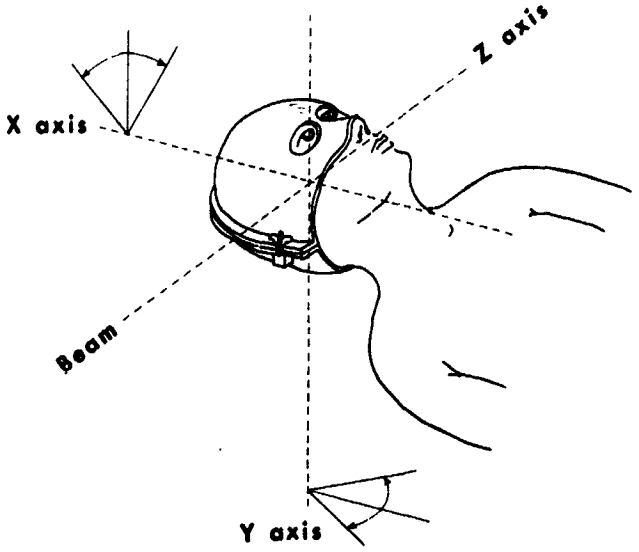

Figure 1. Schematic drawing illustrating orientation planes and axes of rotation for pituitary irradiation.

MUB-1636

MODIFICATION OF ROTATION FOR THE BRAGG PEAK

Although the precise details of a therapy regimen using the Bragg Peak have not been rigidly elucidated, observations now available suggest the following features will be used for pituitary therapy with the Bragg Peak.

The mask will be modified either by bivalving along the saggital plane, or by developing a seamless mask. This is necessary because a water jacket must be present between the collimator face and the lateral aspect of the mask to insure a constant path length of the beam. The side of the mask, consequently, must be smooth to permit the water jacket to abut against the mask fully with no air gaps created.

In addition, in an effort to eliminate air pockets inside the patient, the ear canals need to be filled with unit density material.

Finally, it will be necessary to avoid those rotation quadrants which include the mastoid air cells and petrous bones. The strip of calvarium just caudal to this region, however, appears to be of uniform thickness. As a result it may be possible to use rotation with the Bragg Peak and thus, further increase the depth dose advantage.

The actual pituitary alignment will not differ from that to be described for the high-energy (plateau) alpha beam.

LOCALIZATION OF THE PITUITARY

Patient alignment has been simplified enormously in the past several years because of the development of a polaroid X-ray spot filming device that emancipates the radiologist from the delay of conventional wet developing and the inconvenience of handling wet film. The adaptation, by Way Pratt, of an intensifying screen to fit the Land-Polaroid Camera now permits excellent quality spot X-ray films to be taken with a 10-sec dry developing time.

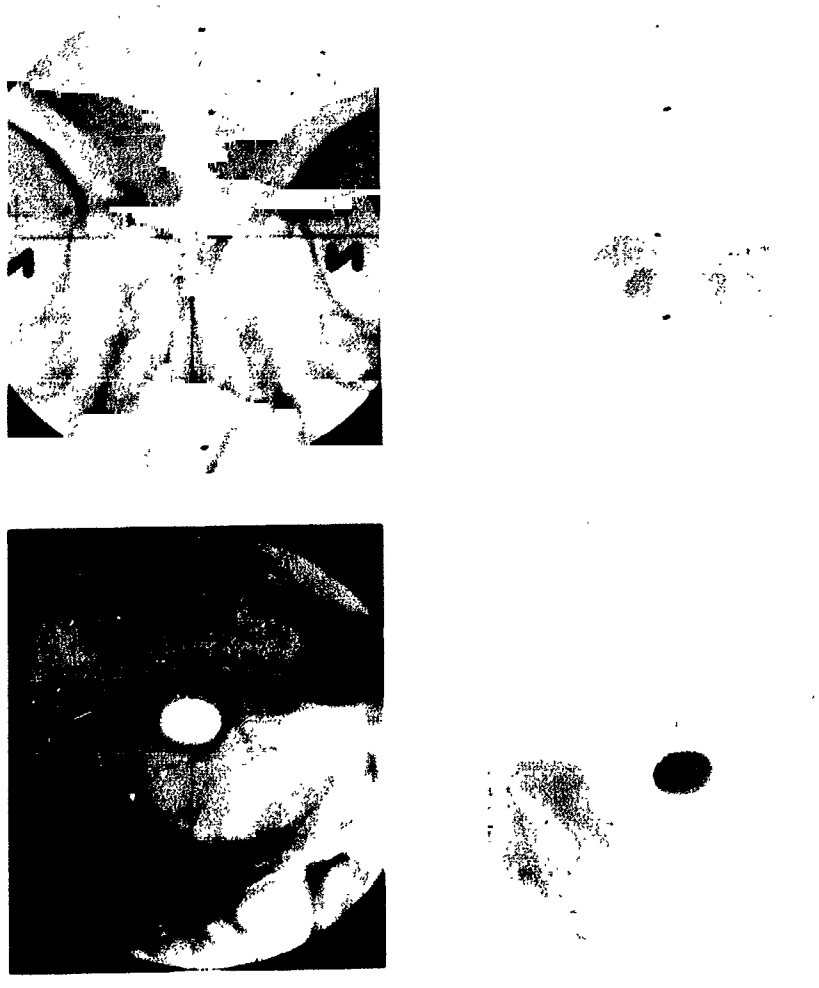

Figure 2. Alignment spot roentgenograms. (a) Upper left--frontal view, note how overlying ethmoid air cells obscure floor of sella. (b) Upper right autotomogram--the floor of the sella stands out clearly. (c) Lower left and right--Beam spot laterals illustrating precision of realignment. The unmagnified beam appears small in relation to the magnified sella.

JHL-4074

These films are so rapidly obtained that the use of fluoroscopy is no longer indicated. The initial X ray is exposed after the patient is positioned so that the Z axis is two centimeters anterior to and two centimeters cranial to the external auditory canal. Proper placement of the beam on the lateral projection is readily achieved because the bony contour of the sella turcica is easily seen outlining the pituitary fossa.

The difficult portion of pituitary alignment is the identification of the floor of the sella on the frontal projection. DiChiro has pointed out that this is possible from routine skull X rays in a high percentage of cases (2). However, the overlying ethmoid air cells can cause confusing projections in this region. The use of the "autotomogram" is frequently of great value in identifying the sellar floor with certainty. The "autotomogram" is taken by exposing

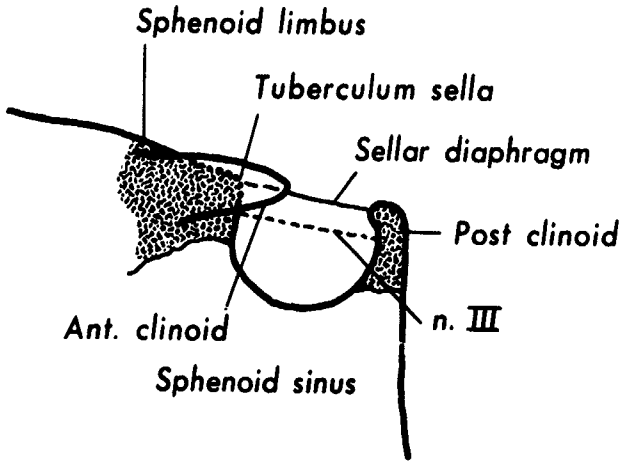

Figure 3. Schematic drawing demonstrating some of the peripituitary anatomy in the lateral view.
D4-1311

the frontal X-ray spot film with the patients head rotating through a 10° arc. This blurs out the anterior structures--i.e., orbits, ethmoid cells, glabella and so forth--leaving the region of the sella (the center of rotation) in sharp relief. The sellar floor is usually well seen on the autotomogram and with this view as a guide, can be identified on the routine frontal spot film. The alignment is thus completed by rotating the head until the interorbital center (i.e. central point between the inner margins of the orbits--a point well up anterior to the sella) and the center of the sella are lined up at the center of rotation. This insures that the head is in a true vertical position. In practice, because the tolerance of the mask is but 0.5 mm , it is sufficient to have this much leeway between the two points, if the sellar floor is precisely centered.

Finally, the center point of body plane rotation is established by drawing a line joining the superior aspects of both orbits. This should then be made parallel to the Z axis. Millimeter coordinate systems--accurate to 0.1 mm--are available for each of the three coordinate planes. Consequently, once correct alignment is achieved, the coordinates are recorded. Realignment prior to subsequent therapy is always necessary because of the slightly different angle the patient holds his head each time he gets into his mask; but future adjustments are invariably minor, and easily made.

It has been the practice to obtain a beam spot at the end of each alignment to check the final lateral position of the sella. This is made by a double exposure of a short pulse of heavy-particle irradiation and a lateral spot X-ray film. If minor adjustments are necessary another beam spot should be obtained. The position of the patient after alignment is complete is always documented by a final beam spot--lateral X-ray, and a frontal X ray. A typical example of alignment X-rays is shown in Fig. 2.

COLLIMATOR SELECTION

The short focal-spot-to-film distance in the medical cave produces a magnification error of about 20%. As a result, the spot films are not well suited to aid in selecting the appropriate pituitary-shaped collimator. For this purpose, a lateral skull X-ray, taken at a 6-foot focal-spot-fo-film distance, is now a part of the preirradiation work up for each

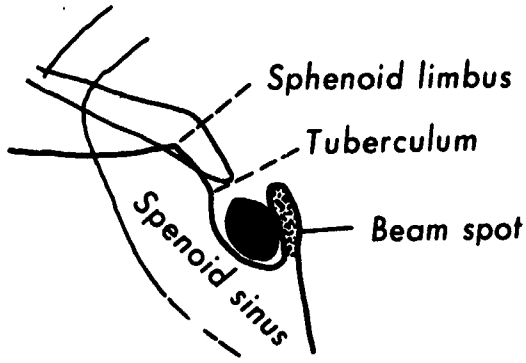

a b

Figure 4. Anatomic variation of the tuberculum. (a) Beam spot lateral. (b) Sketch of 4a illustrating the anatomic position of the tuberculum, in this case it is quite inferior to the sphenoid limbus instead of in its usual position 6 mm horizontal to the limbus.

patient. This film is used to select the aperture. In general, the smaller elipses are used in most instances (e.g. 6.25 × 9.5 cf 6.5 × 11.5 mm), but occasionally, a circular shape is appropriate. Since isodose curves are available for these geometrically regular shapes only, the use of other configurations is less common.

PERIPITUITARY ANATOMY AND ANATOMIC VARIATION OF THE SELLA

Joplin has provided a detailed account of the anatomy of this region (3). Certain aspects, however, have a particular application to heavy-particle therapy. A most important structure is the sellar diaphragm. This runs between the anterior edge of the posterior clinoid, and the tuberculum sella (see Fig. 3). The optic chiasm is always above the diaphragm. It is my practice to locate precisely the diaphragm on the spot film, to be sure the beam is always inferior to it.

Lateral to the sella, the closest important vital structure is the third cranial nerve (see Fig. 3). Its course can be described approximately as a tangent to the inferior surface of the anterior clinoids running parallel to the sellar diaphragm. As a general rule, it can be considered to lie about 13 mm lateral to the center of the sella. Joplin (3) states that at the level of the tuberculum the normal range is 23 to 39 mm, while at the dural perforation it is 20 to 27 mm. The adjacent temporal lobe is 2 mm further lateral. Although the carotid

a

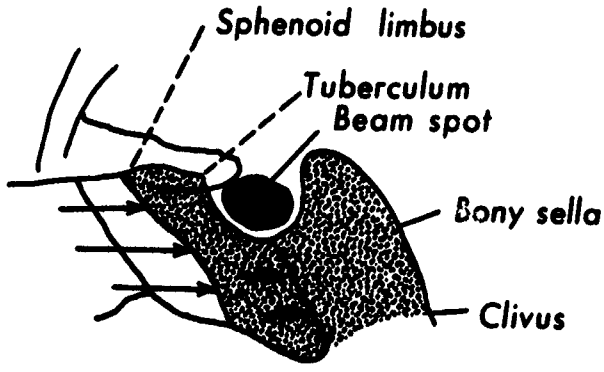

b

c

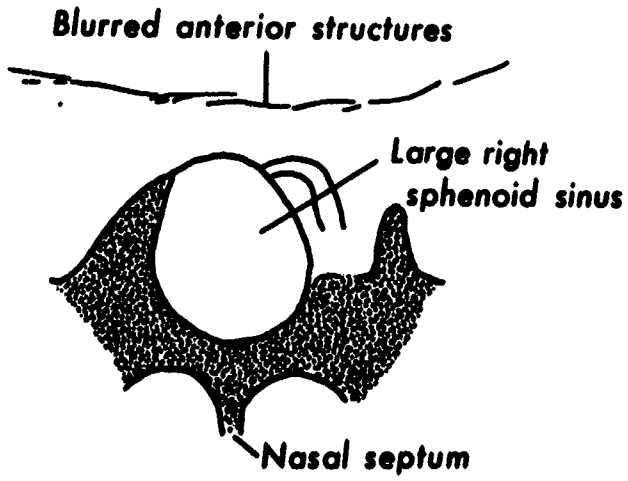

d

Figure 5. Bony sella. (a) Beam spot lateral. (b) Sketch of 5a. Note that the posterior wall of the left sphenoid sinus (three slender arrows) extends well anterior to the sellar floor; while the right sphenoid sinus terminates (two thick arrows) at the sellar floor. (c) Autotomogram. (d) Sketch of 5c. Only the right sphenoid sinus is well seen. Because of the bony sella, the sellar floor is not definitely identified.

siphon is in close proximity to the sella as well, it is our experience that this large vessel is extremely radioresistent.

With the isodose curves presently available (4) for the normal sized pituitary collimator--i.e., an ellipse about 7 × 10 mm in diameter--the third nerve receives about 20 to 25% of the total dose delivered, the adjacent temporal lobe about 15 to 20%. Recently, post-mortum histologic study of the brains of several of the pituitary irradiation patients (5) revealed that microscopic changes in the temporal lobe can be correlated to a dose of 5,500 rads of heavy particles delivered over 12 days. It is my practice to limit the dose to the temporal lobes--i.e., 15 mm lateral to the center of the sella--to a maximum of 4,000 rads in 12 days. This provides a reasonable margin of safety. The third nerve, a peripheral nerve, can be expected to tolerate higher doses than the brain, so that the temporal lobe dose is the limiting factor.

Two important anatomic variations should be mentioned because they can effect the proper alignment. In some cases, the tuberculum sella is not a discrete sharp point forming an angle of about 90° with the pituitary fossa. Rather, it drops obliquely from the sphenoid limbus to make a very slight prominence (see Fig. 4). In these cases there is a real danger of mistaking the limbus for the tuberculum, thus running a risk of including the optic chiasm in the beam.

Secondly, the success of the autotomogram depends on the presence of an air filled sphenoid sinus under the floor of the sella. Occasionally, the sella is composed largely of bone. In these cases (see Fig. 5) it is impossible to visualize the sellar floor with this technique. Occasionally it is possible to utilize a calcified pineal or falx to confirm the vertical interior midline, but usually one must rely for meticulous alignment using the anterior facial structures such as the inner orbital margins.

SUMMARY

The technique of patient alignment prior to pituitary irradiation with high-energy alpha particles is described, and a consideration of dose-limiting factors and anatomic variability discussed.

ACKNOWLEDGMENTS

The author is indebted to the cyclotron crew under the direction of James Vale; to physicists John T. Lyman, Jerry Howard, and David Love for the appropriate dosimetry; to Janette Cornell for nursing care; and to R. Way Pratt for expert help in positioning patients.

REFERENCES

1. Tobias, C. A.; Anger, H. O., and Lawrence, J. H.; Am. J. Roentgenol. 67:1-27, 1952.
2. DiChiro, G.; Am. J. Roentgenol. 84:26, 1960.
3. Joplin, G. F.; Radiologic Anatomy of Pituitary and Surrounding Structures; unpublished post-graduate thesis.
4. Lyman, J. T.; Personal communication.

5. McDonald, L. W.; Born, J. L.; Lawrence, J. H., and Lyman, J. T.; Semiannual Report, Donner Laboratory, Lawrence Radiation Laboratory, UCRL-11033:41, 1963.

Received September, 1964.

Radiosensitivity of the Vestibular Apparatus of the Rabbit

Larry W. McDonald, Gerald A. King and Cornelius A. Tobias

Experiments showing the labyrinth to be sensitive to the effects of ionizing radiation date back at least to 1905 when Ewald (1) showed that glass beads containing 3 mg of radium bromide, when placed in the vicinity of the labyrinth of the pigeon for a few hours, caused effects like those of removal of the labyrinth. Thielemann (2) made observations of the inner ear after X-ray exposure of mice. As confirmed by other later experiments, perilymphatic hemorrhage was seen with higher doses, especially in the cochlea and about the ampullae. Studies have been made of hearing in patients receiving cobalt-60 gamma irradiation for tumors of the head and neck (3). These showed some decrease in the hearing threshold and some perceptive hearing loss with temporary recruitment attributed to transient vasculitis. With doses above 500 R, Kelemen (4) regularly found perilymphatic edema about the vestibular part of the inner ear. The cupula was resistant up to doses of 1,000 to 2,000 R when disintegration of the cupulae and cristae was seen. It was not possible from his studies to determine a precise threshold above which changes always occurred. Generally the cochlea showed more evidence of change than the cupula and crista. No recent references to studies of vestibular function following radiation in man have been found, except for those of Moskovskaya (5) who reported observations that he interpreted as increased excitability of the vestibular apparatus. The observed phenomena consisted of shakiness in gait, dizziness, nausea on turning the head, pallor, tendency toward perspiration, reduction of blood pressure and changes in postrotational nystagmus. These symptoms were reduced in two to three weeks but persisted and were still present after five years. The increased excitability of the vestibular apparatus was thought to be due to weakening of the inhibitory action of the cerebral cortex. The total tumor radiation dose given was 5,000 to 12,000 R.

Sveshnikov (6) made a study of the effects of proton beams and ^{60}Co gamma rays on the function of the labyrinth of dogs. Six dogs were irradiated with the proton beam (apparently whole body) and 10 with a single dose or fractionated doses of ^{60}Co γ-radiation. The testing for vestibular function was done by rotational methods with recording of vestibulo-somatic and autonomic reflexes. In addition, caloric tests were made. The details of the study are not clear from the available translations. Sveshnikov interpreted the findings as showing a diminution of the threshold and reactivity of the vestibular apparatus. With the proton beam (510 MeV) the changes were pronounced with doses of 500 to 350 rads only at the climax of radiation sickness. Somewhat similar effects were observed with γ-radiation in doses of 200 R, 350 R and 500 R, more marked effects being seen with single exposures.

The above literature review is not intended to be complete but is given to show the previous approaches to the study of the radiosensitivity of the vestibular apparatus to ionizing radiation. The review of papers in the past four years is complete with regard to the vestibular apparatus as distinct from the cochlea. In all of the previous studies, the radiation dose received by the vestibular apparatus has been poorly defined as in the radium studies where no attempt was made to determine a dose effect relationship, or the radiation was given as whole-body or whole-head irradiation. In the latter case it was never certain whether the effects were due to direct effects on the vestibular apparatus or to abscopal effects and radiation sickness.

Knowledge of the radiosensitivity of the vestibular apparatus is needed so that appropriate precautions may be taken in the therapeutic irradiation of the head and neck and so the risk of damage to the vestibular apparatus of man in space travel may be estimated. In addition, there is a need for knowledge of the effect of other stressful conditions such as high termperatures, high and low g-forces and general status of nutrition and hydration on the radiosensitivity of the vestibular apparatus to irradiation.

Our ultimate interest is in the effects of radiation on the vestibular apparatus of man. It would be less hazardous to project results of animal experiments to man if the study is limited to only the vestibular apparatus. Since the morphology of the vestibular apparatus in man is nearly identical to that of mammalian species in general, the effects in the experimental animal should qualitatively be like those in man. Previous studies have failed to limit the radiation to the inner ear and have also failed to explore the radiosensitivity of the vestibular apparatus down to the threshold levels both for functional and ultrastructural damage.

The present study was undertaken in order to determine the sensitivity of the rabbit semicircular canal system to alpha-particle-beam irradiation limited to the inner ear. These initial studies are limited to testing of the effect of such radiation on postrotational nystagmus. Morphological studies of the crista ampularis will be made now that methods of radiation and functional testing have been established. Later studies are planned for the study of radiosensitivity of the otolith organ of the utricle.

MATERIALS AND METHODS

Male New Zealand white rabbits weighing between 1 and 2 kg (7-10 weeks old) were used throughout this study. In order to localize the labyrinth in radiographs, a 1.5 kg animal was heparinized, anesthetized with pentobarbitol, and the head and upper extremities of the animal were perfused for about 30 min with neutral buffered formalin. The head was then removed and frozen in liquid nitrogen. The head in the frozen state was sawed into serial frontal sections through the vicinity of the inner ear with a band saw. Each section was 0.5 to 0.7 cm thick. The cochlea and semicircular canals were located in these sections, and fragments of lead were placed in both cochlea. The semicircular canals were located 2 mm behind and 1 mm above the location of the lead fragments. The sectioned head was allowed to thaw, and the sections were all taped together and radiographs taken of the head as shown in Fig. 1. The beam of the cyclotron was directed through the points indicated by the arrows.

Figure 1. Radiograph of reconstructed rabbit head showing fragments of lead in cochlea bilaterally. This is a slightly oblique lateral view, magnification factor × 2. The tips of the arrows are in the semicircular canals.

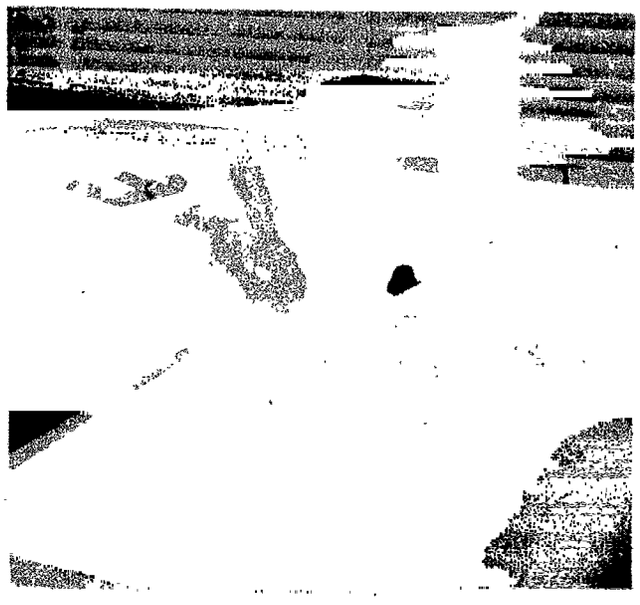

Figure 2. Animal rotating device. The reversing switch and variable speed rheostat are located to the right of the timer.
JHL-4648

Radiations were given with a 910-MeV alpha-particle beam produced in the 184-in. cyclotron at Berkeley. A 3/8-in. beam-defining aperture was used. The beam was passed through the labyrinth at an angle of 40° anterior and 20° superior to the transverse line joining the two labyrinths. At this angle the cerebellum and medulla are not included in the radiation field. No rotational techniques were used in irradiation, and only the plateau portion of the Bragg curve was used. The dosimetry methods were similar to those described by Birge, Anger and Tobias (7). Unilateral right sided doses of 475, 998 and 1,512 rads were given to different animals. Bilateral doses of 500 rads were given to two animals. Following irradiations the animals were rotated in the apparatus shown in Fig. 2. Except for experimental animals number 41 and 48, all rotations were counter-clockwise. In earlier groups of animals, rotation rates were 40, 20 and 15 sec for 10 revolutions. In later rotations, which include the last two graphed rotations of animals number 3, 4, 5, 41, 48, 118 and 120, somewhat slower rotation rates were included. All rotation rates are given as reciprocals in seconds per 10 revolutions. The animals were rotated until all nystagmus stopped and then rotation was stopped by turning off the electric power and catching the rotar of the device with one hand. The time from stopping of the rotation to the last sweep of the slow component of the nystagmus was taken as the duration of the postrotational nystagmus. Seven control animals were tested every one or two weeks for periods ranging from three to five weeks (see Figs. 3 and 4). Irradiated animals were tested at one or two days to one week following irradiation and then generally at weekly intervals (Fig. 5).

RESULTS

The results of rotation of control animals are shown graphically in Figs. 3 and 4. Rotations in Fig. 4 were made in clockwise and counter-clockwise directions, and only maximum durations of nystagmus are shown in the figure, regardless of the direction of rotation. In Fig. 5 are plotted the results with the experimental animals. Here only the last rotation (D) of animals numbered 3, 4, and 5 was in both directions and again only the maximum duration of nystagmus is recorded. For animals number 41 and 48 only the preirradiation (A) testing was in one direction only (counter-clockwise), and all other rotations were in both directions, again only the maximum duration of nystagmus being shown in the graph.

DISCUSSION

In these studies, we have found the highly damped pendulum model of function of the semicircular canal to be applicable. In this model, as proposed by van Egmond (8), the crista and cupula act as a tight swinging door (Fig. 6) which prevents any actual flow of the endolymph, at least if the system is functioning at its most efficient levels. Angular acceleration produces a deflection of the crista and cupula by the rotational shift in the mass of the endolymph fluid in the semicircular canal. The restoring force is in the elasticity (and possibly smooth muscle tonus) of the crista and cupula.

According to van Egmond (8) the differential equation of a torsion pendulum as applied for a model of the function of the semicircular canal may be given as follows:

$$\theta \ddot{\epsilon} + \pi \dot{\epsilon} + \Delta\epsilon = 0$$

where the terms are defined as:

θ = moment of inertia of endolymph,

π = moment of friction at unit angular velocity,

Δ = directional momentum at unit angle caused by cupula,

ϵ = angular deviation of endolymph in relation to the skull,

$\dot{\epsilon}$ = first derivative of ϵ with respect to time, i.e., angular velocity of the endolymph,

$\ddot{\epsilon}$ = 2nd derivative of ϵ, i.e., angular acceleration of endolymph.

All angles are taken at the center of the semicircular canal. The approximate solution of this second order linear differential equation as given by van Egmond is:

$$\epsilon = \gamma \frac{\theta}{\pi} \left(e^{\frac{-\Delta t}{\pi}} - e^{\frac{-\pi t}{\theta}} \right)$$

where $\gamma = \dot{\epsilon}$, the angular velocity of the endolymph, and with the limiting conditions of $\epsilon = 0$ when $t = 0$.

The impulse given to the endolymph when rotation is stopped is equivalent to some factor of the rotation rate. At some minimum deviation of the endolymph (ϵ_{min}) nystagmus will stop. Since the moment of friction for the endolymph, π, is fairly large, the moment of inertia, θ, is small and t is near a maximum, the term $e^{\frac{-\pi t}{\theta}}$ will be very small at ϵ_{min}, and may be neglected. By taking logarithms, rearranging the terms of the equation and lumping all constant terms into a single constant K, the equation becomes:

$$\log \gamma = -k_1 + \frac{\Delta}{\pi} t$$

$$\text{and } \log \frac{1}{\gamma} = k_1 - \frac{\Delta}{\pi} t$$

$$\text{and } \log R = k - \frac{\Delta}{\pi} t$$

where R = seconds per 10 revolutions.

The constant $\frac{\pi}{\Delta}$ for man is according to van Egmond's work (8) about 8 sec. This was determined in man using the subjective sensation of rotation as the end point for ϵ_{min}. The average for the testing of the seven control rabbits shown is 11 sec. This is a little higher than the value for man (different end point used), but much lower than the value found by Groen et al. for the elasmobranch fish (Raja Clavata) (9). As can be seen from Fig. 5, both animals receiving bilateral radiation of 500 rads to the labyrinth have a marked reduction in $\frac{\pi}{\Delta}$ (i.e., the slope is markedly increased as the data are plotted). In addition there is a shift of the curves to the left following irradiation (i.e., the duration of nystagmus has decreased for all rates of rotation). In the case of animal no. 48, the last testing 5 1/2 weeks following irradiation (curve D) shows $\frac{\pi}{\Delta} > 20$. The large value here is due to testing error when the duration of nystagmus is less than 5 sec. The decrease in $\frac{\pi}{\Delta}$ can also be seen in the animal (no. 5) receiving 1,512 rads to the right labyrinth only.

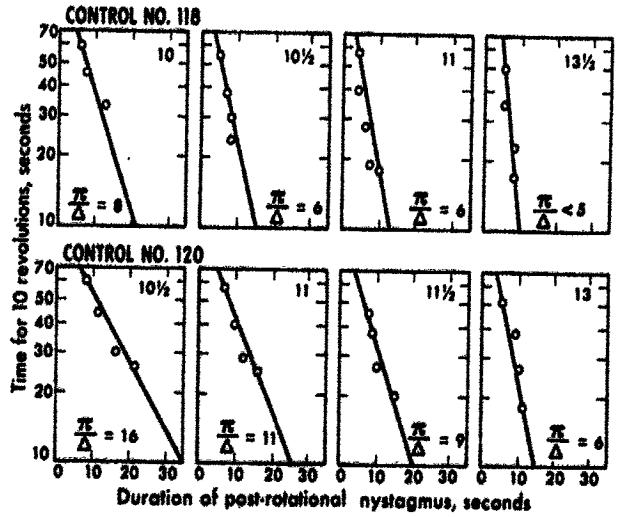

Figure 3. All rotations were counter-clockwise in this group of control animals. $\frac{\pi}{\Delta}$ is a factor of the reciprocal of the slope of each curve.

MUB-5005

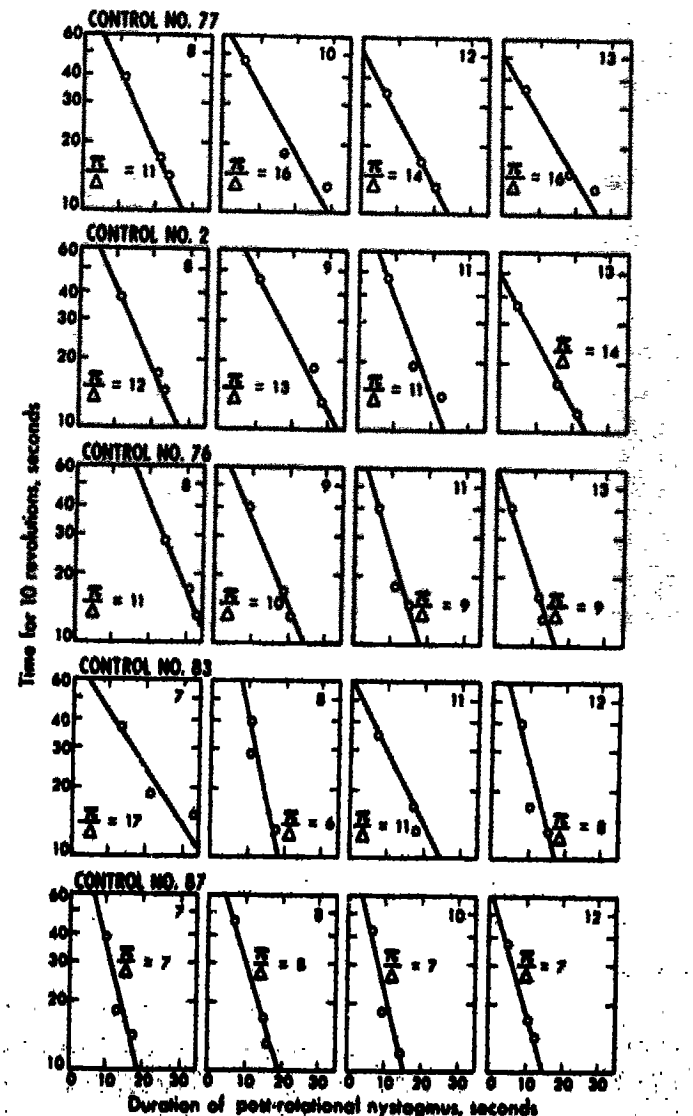

Figure 4. All rotations were done in both directions in this group of control animals. The maximum duration of nystagmus is that plotted in each instance, regardless of the direction of rotation.

MUB-5006

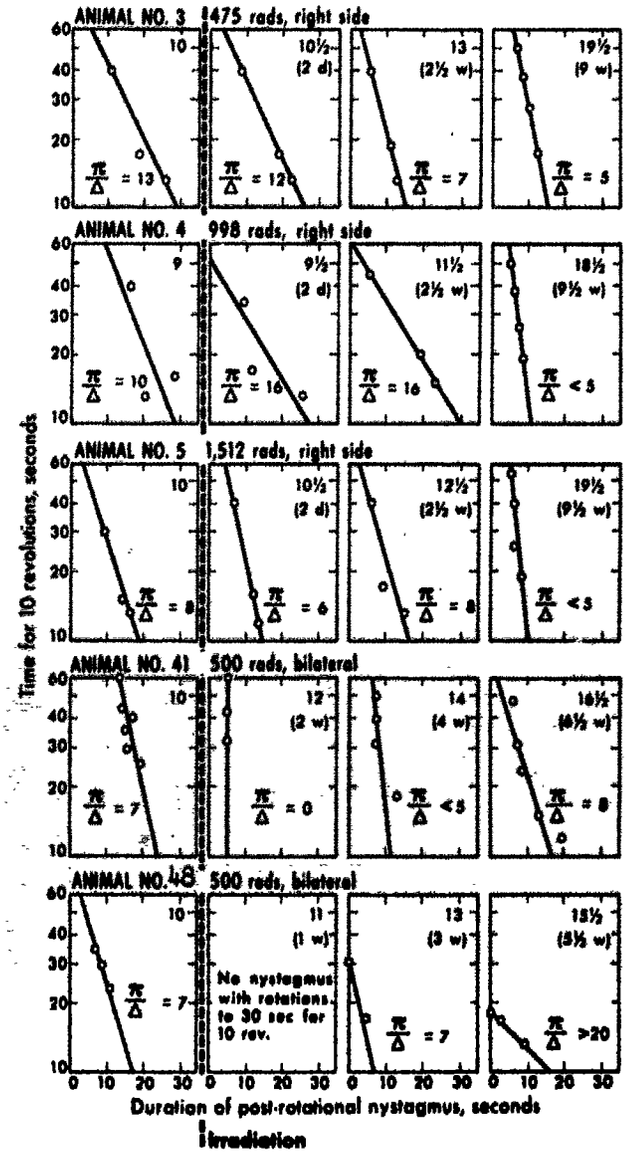

Figure 5. Irradiated animals with doses as indicated. Rotations were counter-clockwise for animals no. 3, 4, and 5 except for the last testing, "D", where rotations were in both directions. For animals no. 41 and 48, only the pre-irradiation "A", testing was counter-clockwise alone. The other animals were tested with rotations in both directions. Only the maximum duration of nystagmus is recorded, regardless of rotation direction.

MUB-5004

The zero intercept varies greatly among both experimental and control animals. Most values range between 30 to 51 deg/sec (70 to 120 seconds per 10 revolutions). This is more than 10 times greater than the value of 2.5 deg/sec found for man by van Egmond. This difference probably reflects a much reduced sensitivity of the testing methods used in these rabbits. No effect of radiation on this intercept can be made out from the data. From these two bilaterally irradiated animals, it appears that 500 rads are well above the threshold for an effect of particle irradiation upon the function of the semicircular canal. More animals irradiated at lower doses will be needed to determine a precise threshold.

In further studies it is planned to determine the threshold of the radiosensitivity of the semicircular canal function and, in addition, to determine at what time following irradiation the functional changes appear. During these further studies, we plan to determine if ocular counter rolling can be used satisfactorily as a test of macula utriculi function in the

Figure 6. Section of normal vestibule showing ampulla (a) with crista (c), utricle (u), perilymphatic space (p), nerve to ampulla (n), vestibular ganglion (g) in internal acoustic meatus and petrous portion of temporal bone (b). The cupula of the crista has been lost in this preparation. The stubs of cilia appear as irregular serrations on the convex surface of the crista. The semicircular canal joins the ampulla at the left margin of the photomicrograph. Neutral buffered formalin perfusion fixation, decalcified with EDTA and stained with H and E. (× 55)

rabbit. If so, the radiosensitivity of this vestibular function will also be determined. In order to make a comparison of particle and electromagnetic ionizing irradiation, we also plan to irradiate the whole head of some animals with ^{60}Co γ-radiation at doses comparable to those of the heavy-particle irradiation. The animals will be tested for vestibular function in order to compare the biological effectiveness of the two types of ionizing radiation. In addition, the Bragg peak will be placed in the inner ear to compare the effect of very high LET radiation to other radiations used.

Exploration of the exact nature of the change in the labyrinth which produced the functional effect also remains to be done. Since the constant $\frac{w}{\Delta}$ appears to be reduced with irradiation, it must be concluded that either w(moment of friction) decreases or

Δ (directional momentum caused by cupula) increases, or both. It is known that the protein content of the endolymph is higher than that of spinal fluid (10). Any dilution of the endolymph would lead to a decrease in viscosity and a decrease in π (moment of friction). Since radiation is known to increase the loss of fluid from the capillary bed, this might be a mechanism of radiation effect, but this fluid escape is accompanied by large amounts of protein which would produce the reverse effect.

The perilymphatic edema with a dose of 500 R observed by Kelemen (4) would cause a decrease in the cross-sectional area of the semicircular canal with an increase in the surface relative to the cross sectional area. This relative increase in surface would increase π (moment of friction), which is a reverse effect of what has been observed in the present experiments.

A change in the elasticity of the crista and the cupula with an increase in Δ (directional momentum caused by the cupula) seems to be a more likely cause of the functional change. Small changes in the degree of polymerization of ground substance mucopolysaccharide, smooth muscle fibrils and basement membrane proteins could have a profound effect on the elasticity of the crista and cupula.

On the other hand, it is possible that a decrease in the radial length of the cupula-crista structure would lead to a loss of efficiency due to endolymph leaking over the cupula. This would effectively decrease the moment of friction, but would also decrease the directional momentum (Δ) caused by the cupula, so that a change in $\frac{\pi}{\Delta}$ can not be predicted.

A final possibility is that the effect might occur directly on neural tissue, such as the ciliated sensory cells, on the nerve fibers or on Scarpa's ganglion, which is also in the radiation field. Such a direct effect would not be in keeping, however, with the known effect of radiation on the function of other nerve tissue, although electroencephalographic changes have been observed with doses well below 500 rads.

A number of experimental studies could be undertaken to determine what the important structural alterations might be. At the present time only one such study is being planned and this is intended to examine the crista ampularis and cupula with both the light microscope and electron microscope. The problems involved in such studies are difficult because the delicate soft tissues of the vestibule are completely embedded in the temporal bone. Glutaraldehyde perfusion techniques, which preserve the fine structure well, have been developed here, but suitable methods for embedding in plastic and then localising the crista for ultra-thin sectioning remain to be devised. Several technical approaches appear feasible.

From the present studies it appears that the vertigo of acute radiation sickness may be due to a direct effect on the functional state of the vestibular apparatus rather than effects on the central nervous system, gastrointestinal tract, or indirect effects due to changes in the state of hydration, tissue necrosis, etc. The experimental work of Graybiel (11) and his associates indicate that the nausea and vertigo of motion sickness in man are entirely

vestibular in origin and he prefers the term vestibular sickness. Thus it seems likely that all vertigo may have its origin in the vestibular apparatus.

SUMMARY

A method of radiating the inner ear of the rabbit with an alpha-particle beam without significant exposure of the brain has been devised. Long lasting changes in semicircular-canal function of the rabbit have been demonstrated with doses of 500 rads. The approaches used to determine the threshold of radiosensitivity of the semicircular-canal function and the radiosensitivity of the macula utriculi are described. Structural changes are discussed which may account for the functional alterations observed. Work being undertaken to study the structural changes is described.

REFERENCES

1. Ewald, C. A.; Zentr. Physiol., 19:298, 1905.
2. Thielemann, M.; Fortschr. Gebiete Roentgenstrahlen 37:563, 1928.
3. Borsanyi, S.; Blanchard, C. L., and Thorne, B.; Ann. Otol., Rhinol. Laryngol. 70:255, 1961.
4. Kelemen, G.; Acta Oto-Laryngologica Suppl. 184, 1963.
5. Moskovskaya, N. V.; Vestn. Otorinolaring. 21:59, 1959.
6. Sveshnikov, A. A.; Med. Radiol. 8:48, 1963 (JPRS Translation TT: 63-41278).
7. Birge, A. C.; Ant r, H. O., and Tobias, C. A.; in Radiation Dosimetry, edited by G. J. Hine and G. L. Brownell, New York, Academic Press, 1956, p. 623.
8. Egmond, A. A. J. van; Groen, J. J.; and Jongkees, L. B. W.; J. Physiol. 110:1, 1949.
9. Groen, J. J.; Lowenstein, O.; and Vendrick, A. J. H.; J. Physiol. 117:329, 1952.
10. Citroen, L.; Exley, D.; and Halpike, C. S.; Brit. Med. Bull. 12:101, 1956.
11. Graybiel, A.; in Neurological Aspects of Auditory and Vestibular Disorders, edited by W. S. Fields and B. B. Alford, Springfield, Ill., Chas. C. Thomas Co. 1964, p. 248.

Received January, 1965.

Pion Studies with Silicon Detectors

Mudundi R. Raju, Henry Aceto and Chaim Richman

This study was initiated because of recent interest in negative pions for therapeutic applications (1-4). When a negative pion is brought to rest in a medium, say tissue, it may be captured by a constituent nuclei, resulting in "star" events. In such interactions about 20% of the total rest energy of the π^- meson, that is, approximately 30 MeV, appears in the form of α particles and protons with ranges less than 1 mm in biological tissue (2). It is very important to know the energy distribution of this pion star. Some measurements of the energy of these star fragments have been made using a diffusion cloud chamber (5) and emulsions (6). Semiconductor detectors are used in the present investigation to look at the pion beam passing through various thicknesses of absorbing material and finally to measure the energy distribution of negative pion stars in silicon. Until recently it was not possible to use semiconductor detectors for detecting particles producing a very small ionization, such as γ rays or very fast particles, because the ionization was near minimum. This limitation is due to the fact that these detectors had only a very small thickness. Now the technology has been imporved and detectors several mm thick are available (see reference 7 for example).

Semiconductor detectors have been extensively used for the detection of low-energy particles (8). There have been very few studies on application of these detectors to the detection of high-energy particles at the minimum-ionizing region. Miller et al. (9) were able to observe a good peak for 750-MeV/c π^- by using a silicon p-n junction detector. In addition, they differentiated a mixture of positive pions and protons of 750 MeV/c momentum. The resolution they obtained for the detection of these high-energy particles is of the order of approximately 34%, which is in reasonable agreement with the Landau effect. Van Putten et al. (10) determined the most probable energy loss and energy-loss distribution of negative pions at 1.50 and 2.55 BeV/c, using a gold-doped silicon crystal. The results confirmed the density effect as described by Sternheimer (11). Koch et al. (12) measured the most probable energy loss of relativistic mesons and protons (0.5 to 1.5 BeV/c) as a function of momentum for silicon.

In practice a pi-meson beam contains an appreciable contamination of μ mesons and electrons. Lithium-drifted silicon detectors made as described by Goulding and Hansen (13) were employed here to analyze the composite beam, both directly and after the beam was degraded by absorbers. Measurements were made for both positive and negative pions. The measurements of most probable energy-loss for pions in silicon were made and compared with predicted values. Finally, sufficient Lucite absorber thickness was used to degrade the

beam so that a substantial number of pions stopped in the silicon detector. The detector was then used to measure the energy distribution of π^- stars in silicon.

CALIBRATION

The experimental setup is shown in Fig. 1. The test pulse generator is used to simulate detector pulses and to check the linearity of the electronic systen . An ^{241}Am alpha source and a ^{207}Bi internal-conversion electron source are used for calibrating the pulse-generator output in terms of energy. Calibration and linearity checks are made for every experiment. The Berkeley heavy-ion linear accelerator (Hilac) accelerates nuclei to an energy of 10.38 MeV per nucleon. For helium nuclei the energy of the primary beam is 41.52 MeV. The beam comes out through a vacuum column with a 1-mil aluminum window. The detector is enclosed by a housing, in order that a vacuum can be maintained, with a 1-mil Mylar window. The entire detector-holder assembly is surrounded with a 1/4-mil aluminum electronic shield. By applying the correction for the degradation of the energy of the primary beam through these foils, the energy of the primary beam seen by the detector is found to be 40 MeV. A typical spectrum produced by totally absorbed α particles is shown in Fig. 2. In a detector where a particle is stopped, the resolution is a function of the detector and the electronic system. Values for full width at half maximum from 2 keV upwards, depending upon the type of experiment, have been obtained by many workers with semiconductor detectors exposed to monoenergetic particles, giving resolutions much less than 1%. Full width at half maximum obtained in this measurement is 0.62 MeV, giving a resolution of 1.5% when the detector is operated at room temperature. This poorer resolution is partly due to momentum spread of the beam and partly due to noise in the amplifier. However, better resolutions can be obtained by operating the detector at low temperature and using better amplifiers.

The energy of the beam, determined by using earlier calibration, is 39.88 MeV, which agrees very well with the primary energy of 40 MeV. This agreement confirms the calibration and linearity of the system up to 40 MeV. Further experiments with α particles confirm the linearity of the system up to an investigated energy of 85 MeV.

DETERMINATION OF DETECTOR THICKNESS

The thickness of the detector depletion layer determines the energy loss for particles passing completely through the detector. In our case, the depletion layer extends almost through the entire physical thickness of the detector except for a few mils on the Li side. In order to measure this depletion thickness we determine the maximum energy deposited in the detector. The range of the α particle whose energy corresponds to this maximum energy is then obtained from range-energy tables (14). The 910-MeV alpha beam is degraded so that the energy of the emergent beam is close to the energy corresponding to the range of the alpha beam in the detector. The response of the two detectors used in the present investigations for a degraded primary beam of 910-MeV α particles is shown in Figs. 3 and 4.

For α particles whose range is greater than the depth of the depletion region, the charge-pulse amplitude from the detector increases with decreasing alpha energy until the energy corresponds to the depletion thickness of the detector. A further decrease in alpha

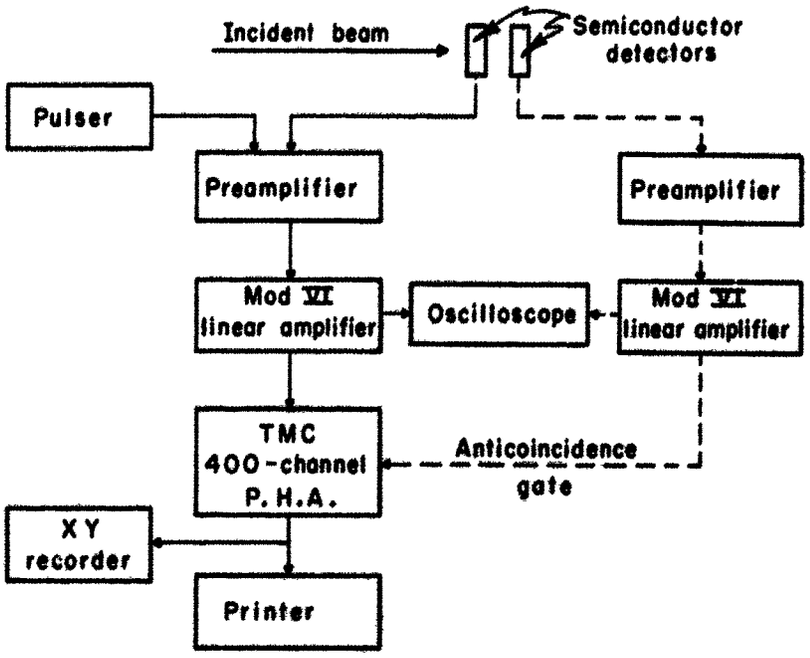

Figure 1. Experimental setup.

MUB-4136

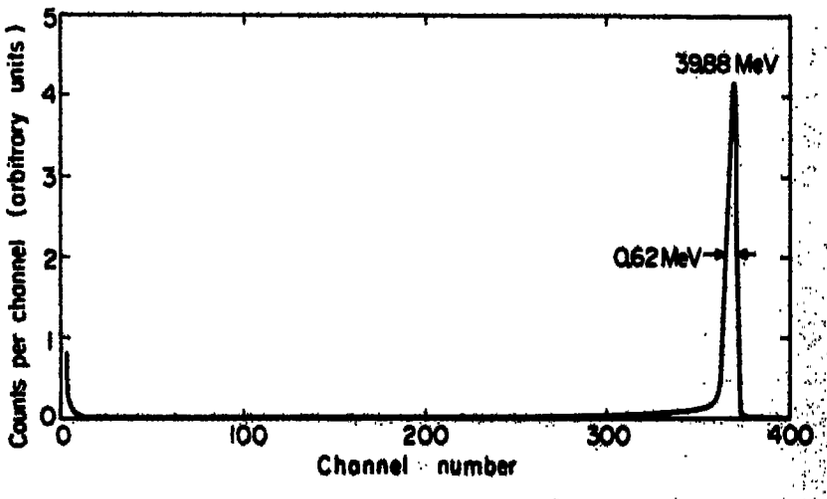

Figure 2. Spectrum of Hilac α beam.

MUB-6093

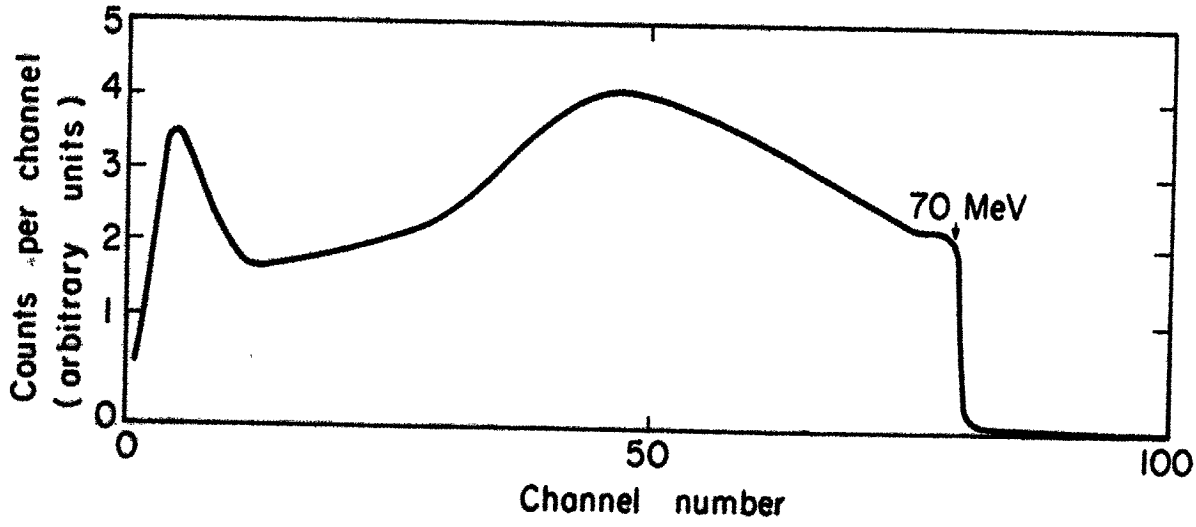

Figure 3. α Spectrum for detector used with 365-MeV π^- beam.
MUB-6092

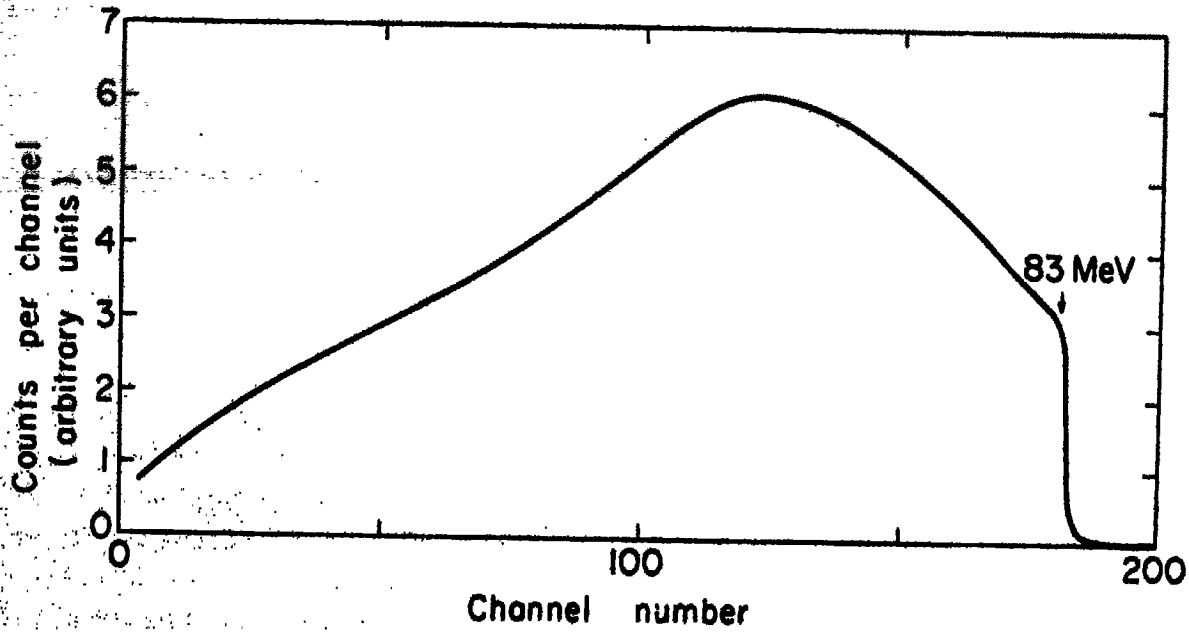

Figure 4. α Spectrum for detector used with 95-MeV π^+ beam.
MUB-6091

energy will cause a proportional decrease in charge pulse. It can be seen from Figs. 3 and 4 that the maximum cutoff energies for the two detectors used (corresponding to the range in the detector) are 70 and 83 MeV, respectively. The corresponding ranges from range-energy tables are 0.45 and 0.61 g/cm^2 respectively (14). The physical thicknesses of the detectors as determined with a micrometer are 6% greater than these values. This difference is due to the dead layer on the Li side. The experimental accuracy in the determination of detector thickness is within about 2%.

PRODUCTION OF NEGATIVE AND POSITIVE PIONS

The Berkeley 184-inch synchrocyclotron produces an intense beam of 732-MeV protons, and in their outer orbit they strike a 2-inch-thick beryllium target. When these protons collide with beryllium nuclei, π^0, π^+, and π^- mesons are produced. The experimental arrangement for π^- is shown in Fig. 5. To get a π^+ beam, all the magnetic fields are reversed, including that of the cyclotron. The magnetic lens system remains unchanged for pions of the same energy. The bending magnet removes particles of different $H\rho$ than the pions that are being used. The cyclotron produces pions in a range of energies of hundreds of MeV. In our experiments, we used π^- of 370 MeV and both π^+ and π^- of 95 MeV.

The cyclotron pulses 64 times per second, thus giving 64 coarse groups of pions per second. The mode of operation can be controlled so that these groups of pions can be spread out over either of two periods of time. The "short spill" mode spills the beam over a period of approximately 400 μsec. The auxiliary dee mechanism of the cyclotron makes it possible to spread each group of pions over a longer period of 8 msec. The long-spill operation results in a cyclotron duty cycle of about 54%, compared with 2.5% for the short spill. Long-spill operation is used throughout the experiment. Hence, for the detector exposed to pions at rates of about 10^3/sec, accidental counting loss should be negligible.

EXPERIMENTAL RESULTS OF dE/dx MEASUREMENTS

365-MeV π^- BEAM Pion beams are always produced with muon and electron contamination. Depending on the energy of the pion beam and the focusing setup, the relative percentage of muons and electrons with respect to pions varies (15). The percentage contamination varies inversely with energy, and at 365 MeV the percentage contamination of muons and electrons is very small.

Figure 6 shows the detector response obtained with 365-MeV π^- mesons. These pions are close to the minimum-ionizing region. There is a distinct pion peak whose corresponding energy is close to the theoretically predicted value. The resolution is about 33%, which is in reasonable agreement with the Landau effect (16). As we increased the thickness of the copper absorber in the beam, the energy of the pion would be lowered and hence the dE/dx would increase, with a concomitant increase in the energy spread. The experimental and theoretical values are in close agreement down to a residual energy of 164 MeV. At lower energies this agreement is lacking because of the uncertainty of the determination of residual energy which results from the constant increase in energy spread. The experimental values of energy loss in the 0.45-g/cm^2-thick silicon detector, compared to the theoretical values as calculated with

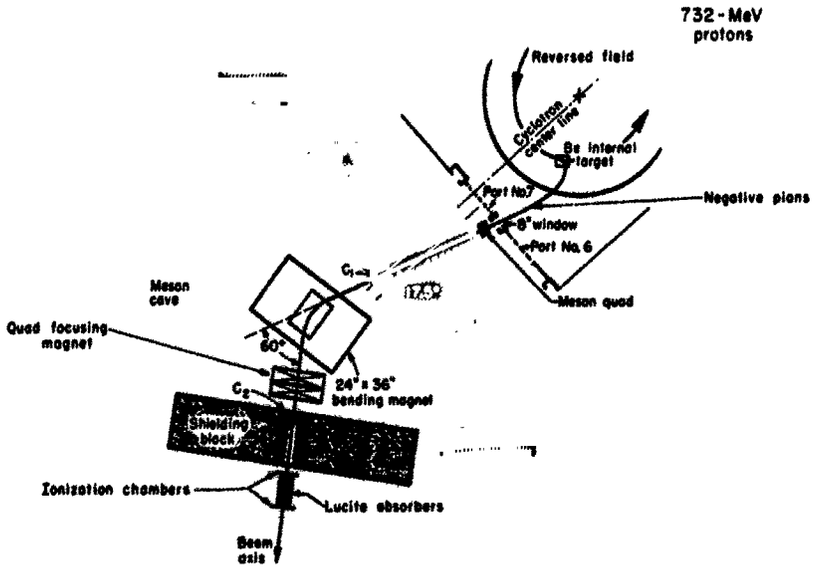

Figure 5. π-Meson experimental arrangement.
MUB-966

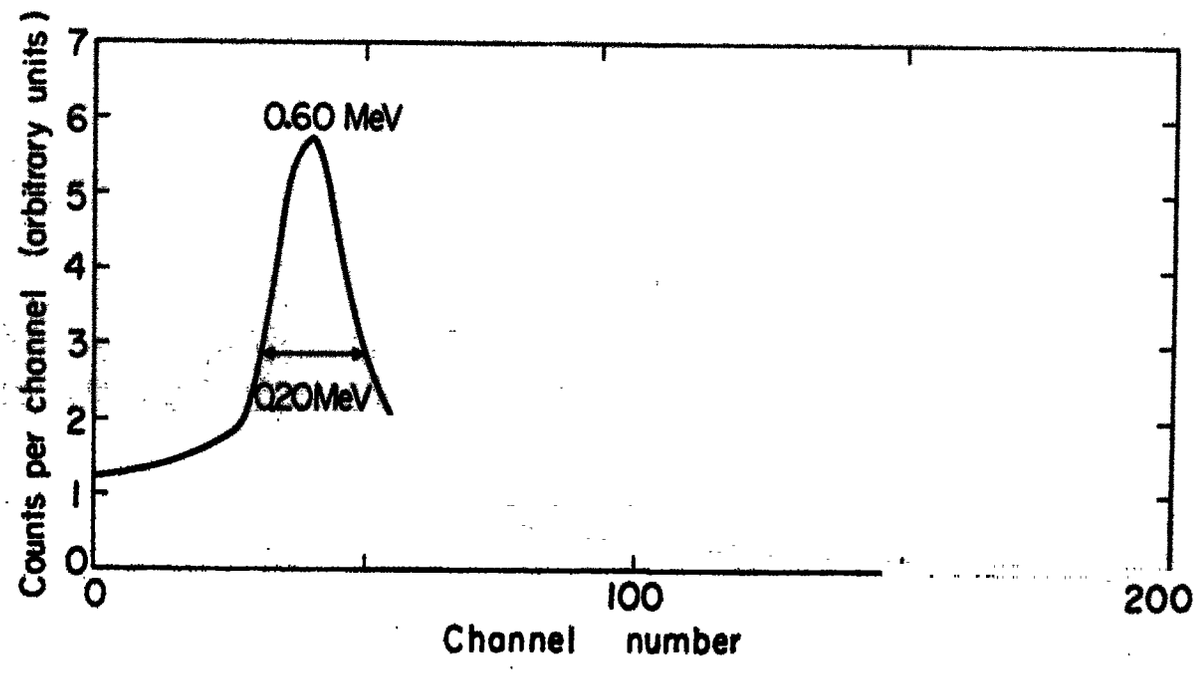

Figure 6. Detector response to 365-MeV π^- beam.
MUB-6094

Table 1. 365-MeV π^- beam in 0.45-g/cm^2 silicon detector

Thickness of copper absorber (in.)	Residual energy (MeV)	Energy loss (MeV)	
		Theory	Experiment
0	365	0.596	0.60
2	295	0.602	0.60
4	230	0.616	0.63
6	164	0.660	0.66
8	92	0.794	0.82

the Landau approximation, are shown in Table 1. The residual energies of the degraded beam are determined by using the range-energy tables of Rich and Madey (17).

95-MeV π^+ BEAM Figure 7 shows the result obtained with a 95-MeV π^+ beam whose muon and positron contamination is very small. Figures 8 through 10 show the same beam degraded by various thicknesses of Lucite. A number of features of these data are interesting. First, the resolution is in reasonable agreement with the Landau effect. Secondly, the peaks are shifted to higher energies as the thickness of the Lucite absorber is increased. Very interesting things are observed close to the end of the range. Figure 8 shows the response of the detector for a 95-MeV π^+ beam degraded with 7.5 in. of Lucite. This thickness of Lucite is 1 in. less than the range of these pions. A small peak at 1.15 MeV is noticed in addition to the 1.98-MeV π^+ peak. This small peak is due to μ^+ particles formed by the decay of π^+ mesons. Figure 9 shows the response of the detector for the beam degraded by 8.5 in. of Lucite, which corresponds to the Bragg-peak position. Both the muon and pion peaks are shifted to higher energies. At 10 in. of Lucite, which is beyond the range of pions, the pion peak has disappeared and the peaks indicating positrons at 0.87 MeV and muons at 1.32 MeV remain. At 9.5 in. of Lucite plus 3/8 in. copper (because of the lack of space, copper is used to substitute for an equivalent thickness of Lucite), which is beyond the range of pions and muons, only the electron peak at 0.92 MeV is observed, as shown in Fig. 10.

95-MeV π^- BEAM Unlike the other two beams, this beam is contaminated with approximately 25% electrons and approximately 10% muons. Figure 11 shows the response of the 95-MeV (189-MeV/c) negative pion beam, including its muon and electron contamination. Two peaks, at 0.87 and 1.05 MeV, are clearly visible. They are produced by electrons and pions, respectively. The muon contamination, being relatively small, is hidden in the distribution of electrons and pions. Figures 12 through 15 show the response of the detector for various thicknesses of Lucite introduced in the beam. It can be noticed that as the absorber thickness increases, the relative height of the pion peak decreases in comparison with the electron peak. This result is due to a higher nuclear collision cross section of pions in comparison with electrons. The results obtained with a time-of-flight system confirm this behavior. As the thickness of Lucite increases, the electron peak remains at the position corresponding to about 0.87 MeV whereas the pion peak shifts to higher energies. This is because the electrons of initial momentum 189 MeV/c are still in the minimum-ionising

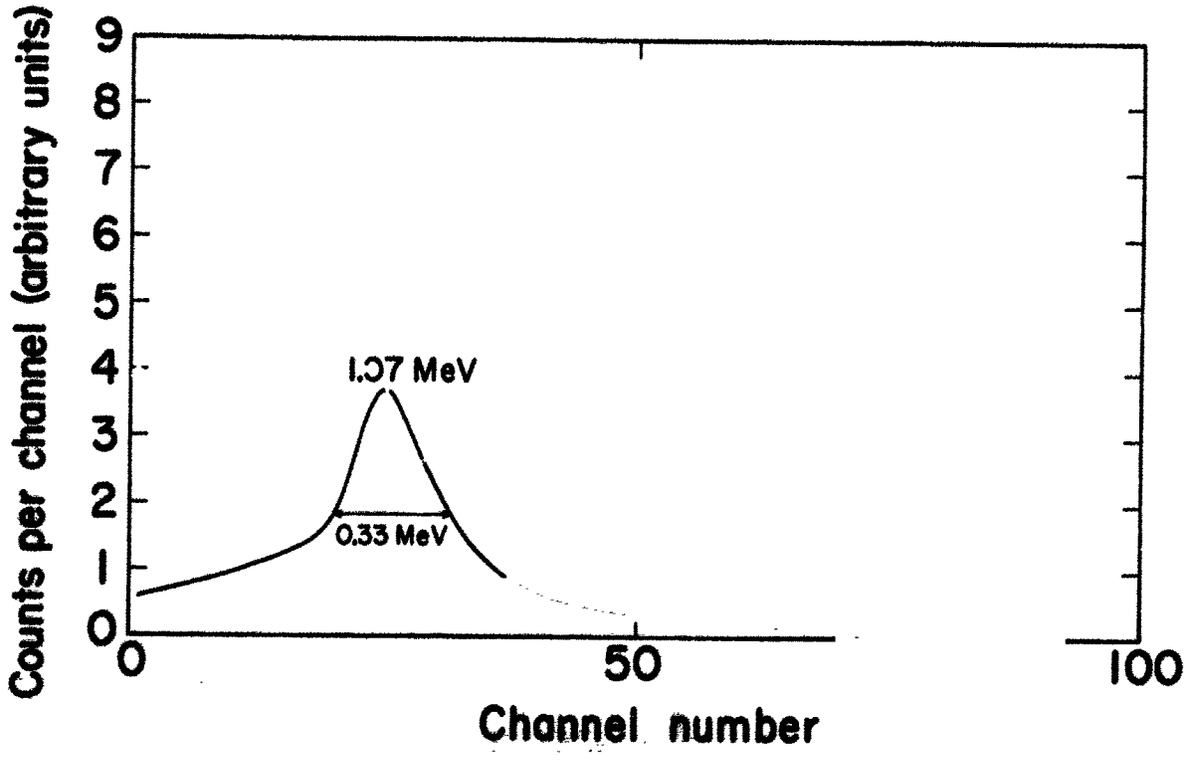

Figure 7. Detector response to 95-MeV π^+ beam.
MUB-4137

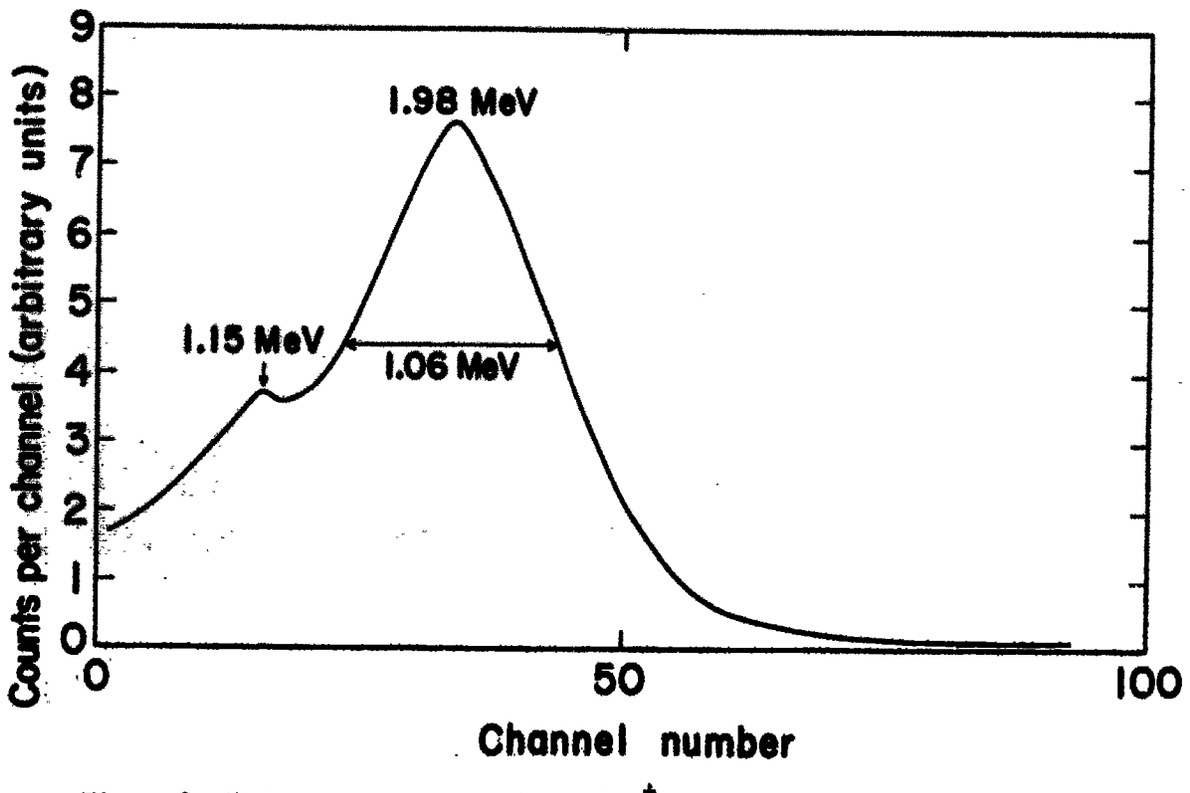

Figure 8. Detector response to 95-MeV π^+ beam degraded by 7.5 in. of Lucite.
MUB-4140

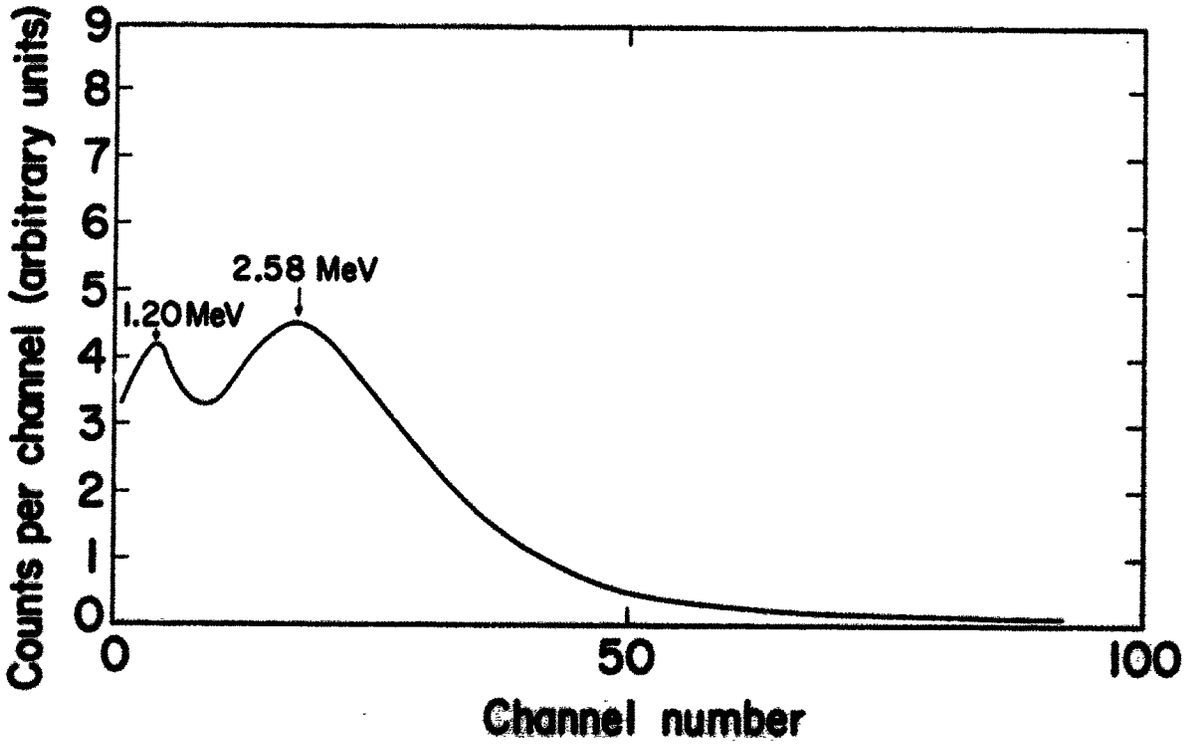

Figure 9. Detector response to 95-MeV π^+ beam degraded by 8.5 in. of Lucite.
MUB-4141

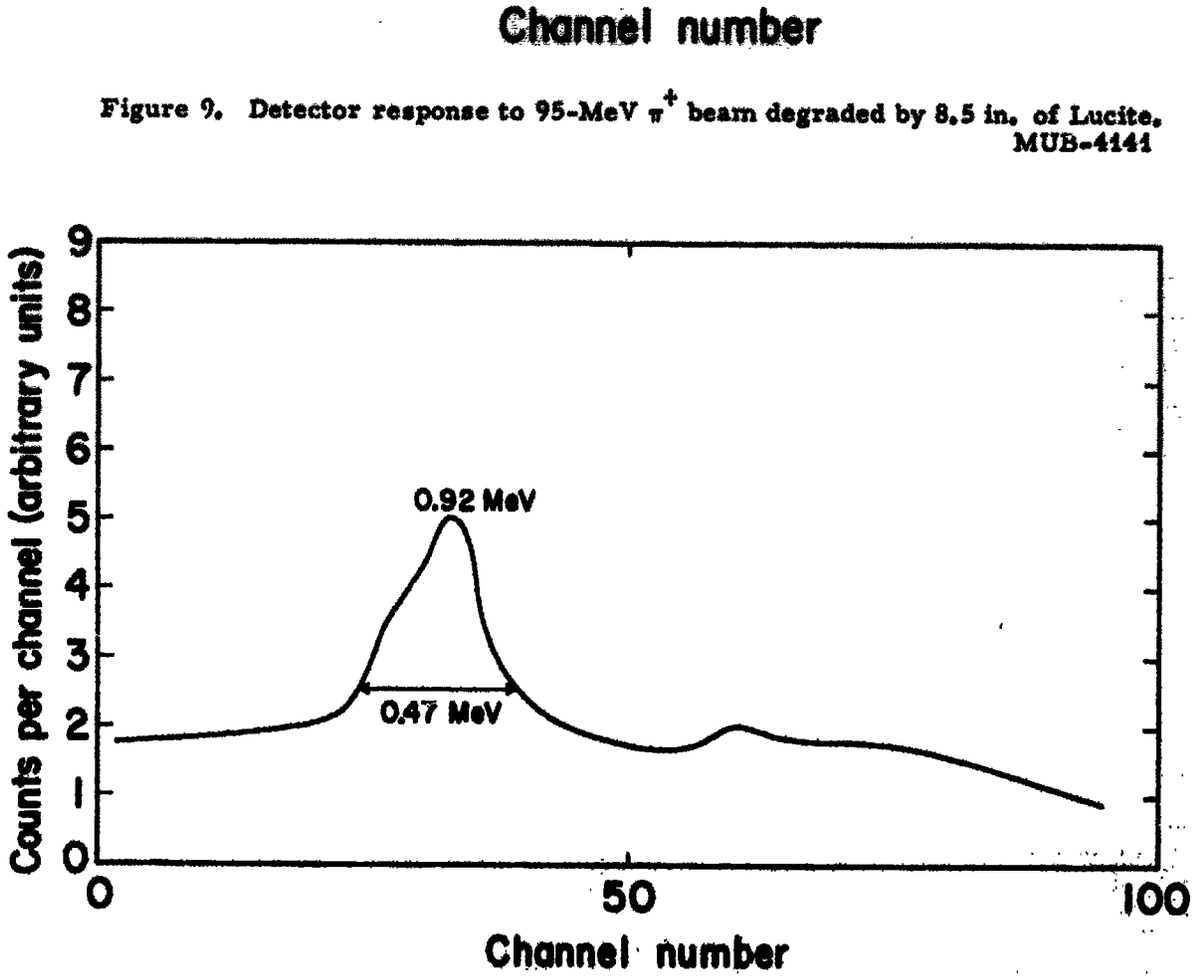

Figure 10. Detector response to 95-MeV π^+ beam degraded by 9.5 in. of Lucite and 3/8 in. of copper.
MUB-4142

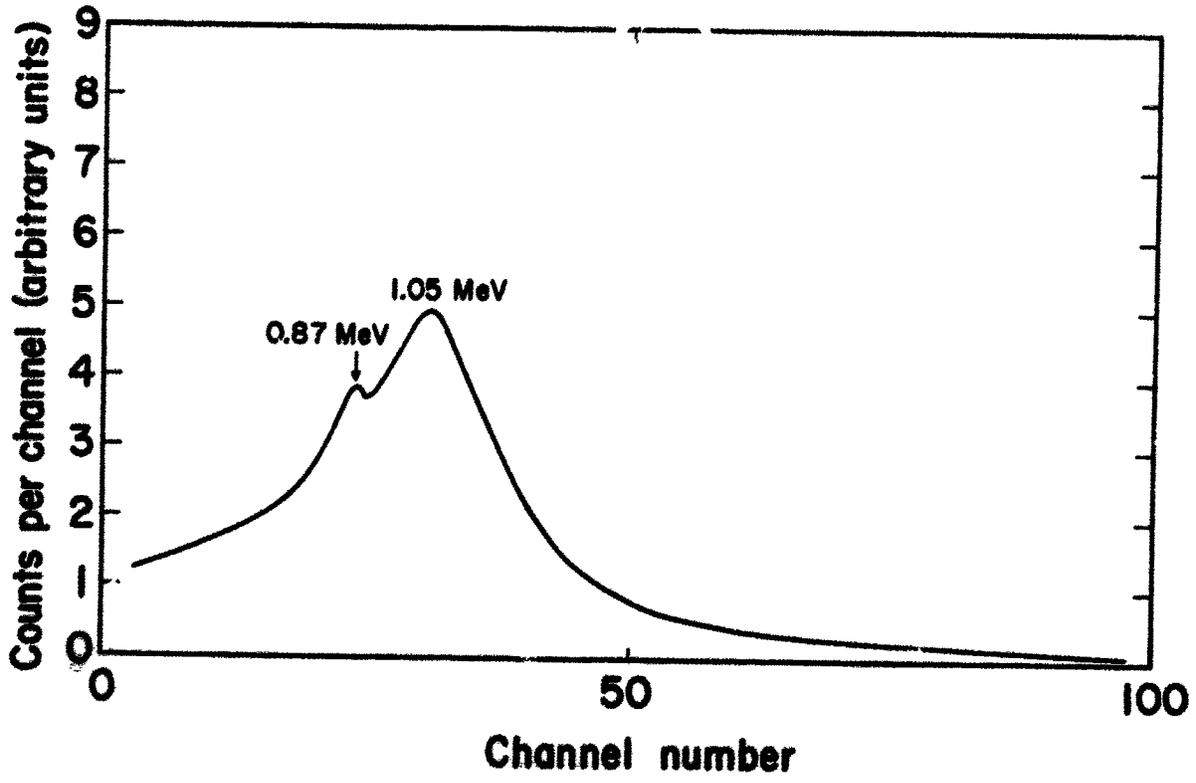

Figure 11. Detector response to 95-MeV π^- beam.
MUB-4138-A

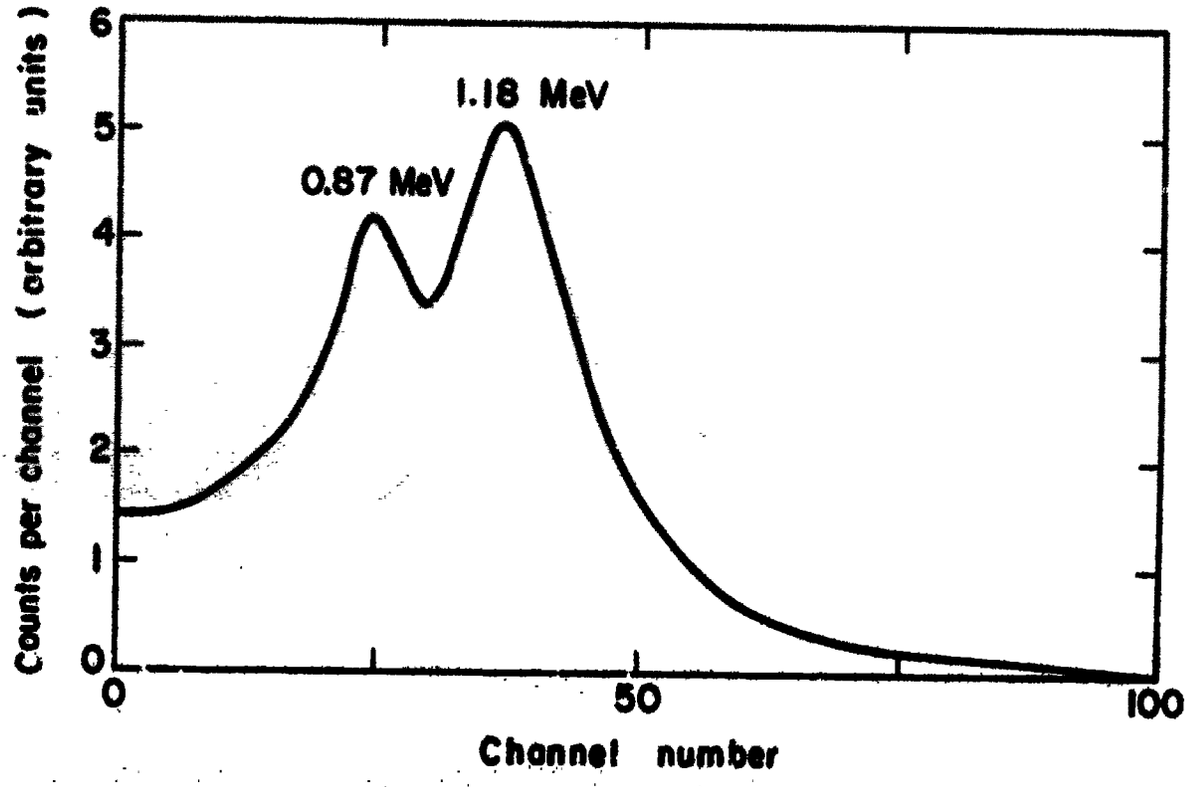

Figure 12. Detector response to 95-MeV π^- beam degraded by 3 in. of Lucite.
MUB-6089

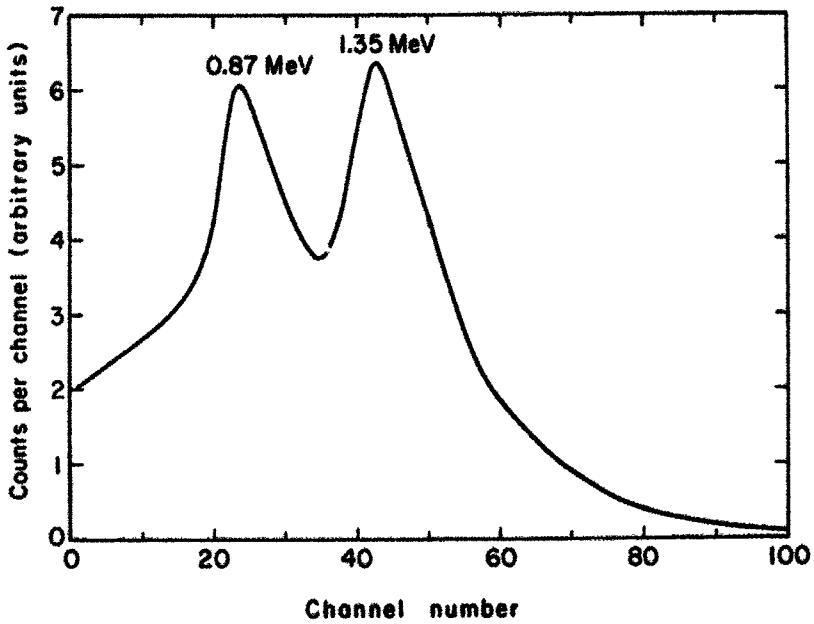

Figure 13. Detector response to 95-MeV π^- beam degraded by 5 in. of Lucite.
MUB-4135

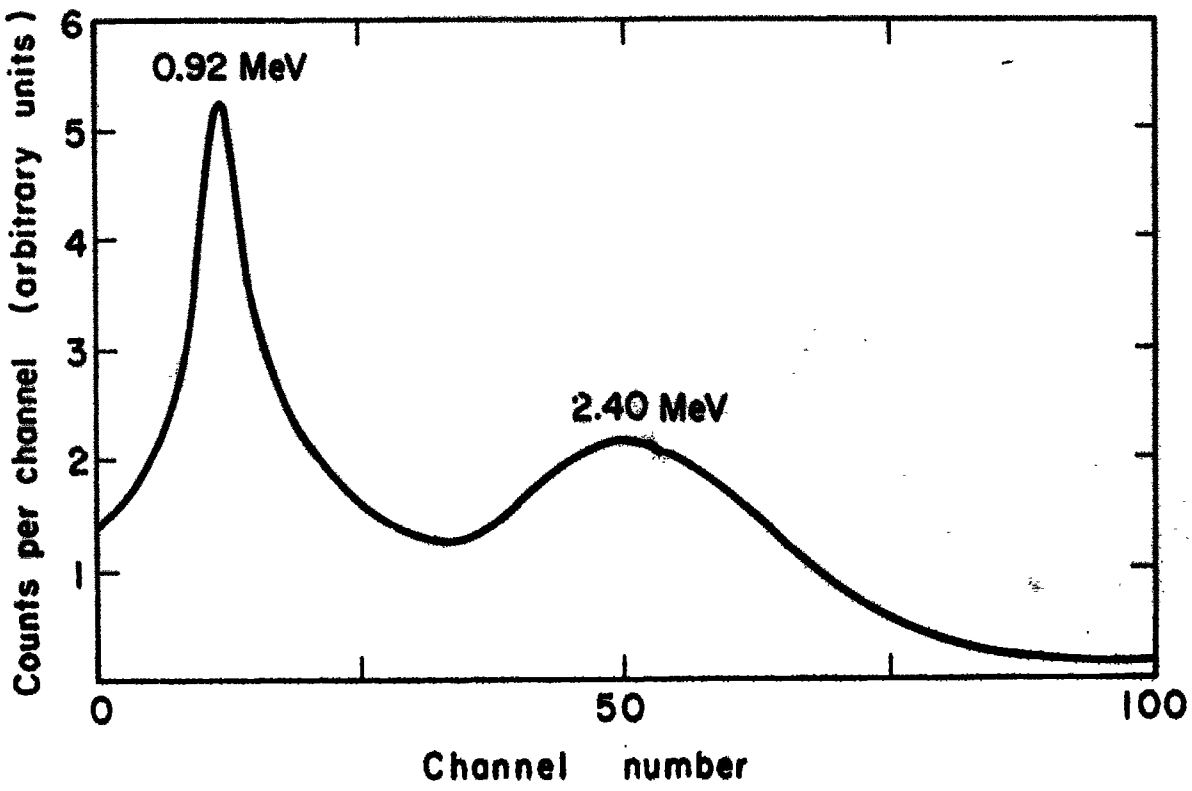

Figure 14. Detector response to 95-MeV π^- beam degraded by 8 in. of Lucite.
MUB-6095

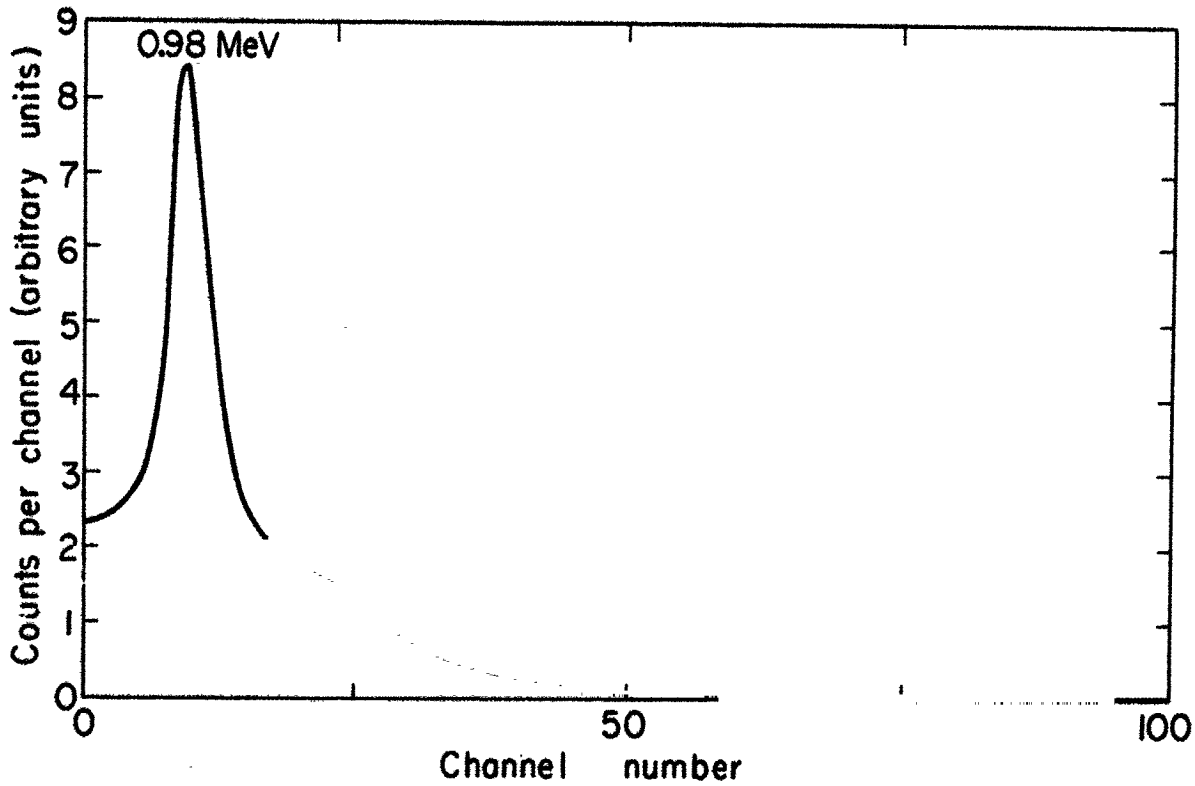

Figure 15. Detector response to 95-MeV π^- beam degraded by 10 in. of Lucite.
MUB-6090

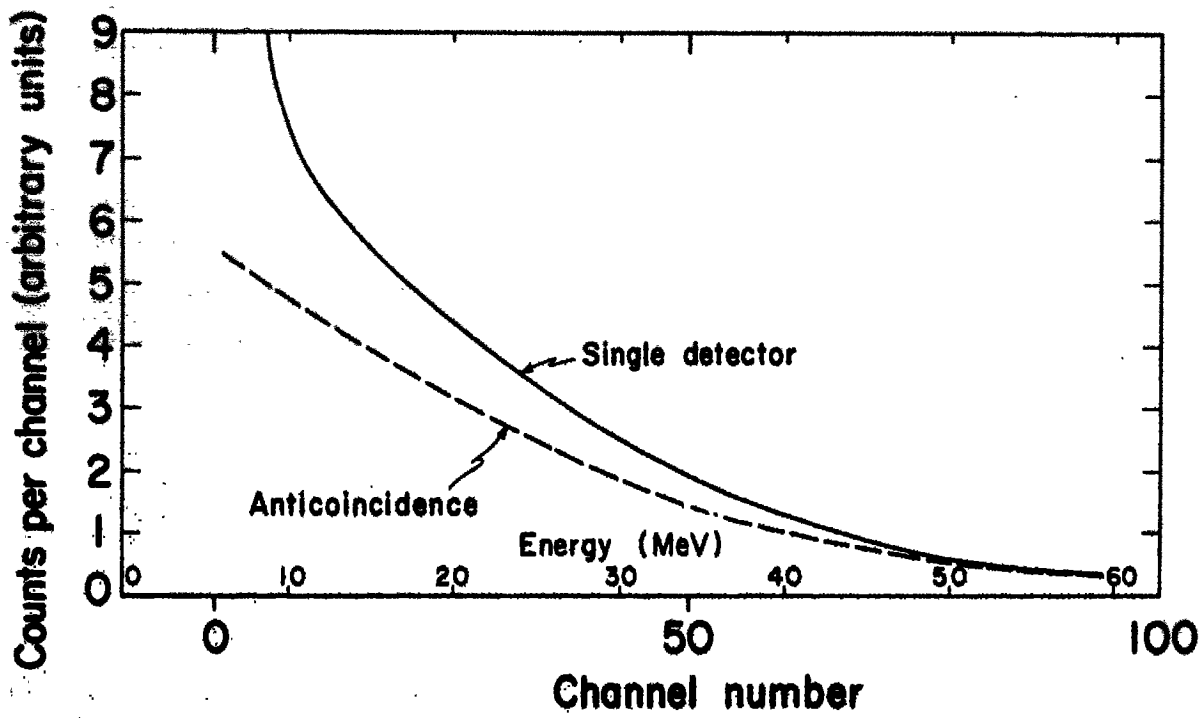

Figure 16. Energy distribution of pion stars.
MUB-4139

Table 2. 95-MeV π beam in 0.61 g/cm^2 Si detector

Thickness of Lucite absorber (in.)	Residual energy (MeV)	Theoretical energy loss (MeV)		Experimental energy loss (MeV)	
		Landau	Vavilov	π^+	π^-
0	95	1.08	1.05	1.07	1.05
2	80	1.17	1.13	1.13	1.12
3	72	1.23	1.19		1.18
4	63	1.32	1.28	1.28	1.28
5	54	1.45	1.40		1.35
6	44	1.61	1.56	1.55	1.54
7	34	1.93	1.87		1.92
8	18	3.20	3.21		2.40

region whereas the pion-energy losses change considerably as the thickness of Lucite absorber increases. Beyond the range of pions (i.e., for thicknesses greater than 8-5/8 in. of Lucite), the pion peak is absent and the electron peak persists.

The experimental values of the most probable energy losses of pions (both positive and negative) are given along with theoretical values in Table 2. Since for lower energies the Landau approximation breaks down at large detector thicknesses, probable energy loss must be computed by using the rigorous Vavilov expression (18), as tabulated by Seltzer and Berger (19). Values obtained by using the Landau approximation in this particular case would be about 3% higher than those obtained by using the Vavilov expression. The residual energy of the pion beam after passing through various thicknesses of Lucite absorbers is computed from range-energy tables (17).

The agreement between the Vavilov-derived values and the experimental values is within 2% down to a residual energy of 44 MeV (corresponding to a Lucite absorber thickness of 6 in.). At lower energies the agreement is very poor, as noted for 365-MeV π^-.

MEASUREMENT OF THE ENERGY DISTRIBUTION OF PION-PRODUCED STARS IN SILICON

We obtained the Bragg curve for the pion beam with the argon-CO_2-filled ionization chambers in the classical fashion, using one chamber as a monitor followed by different thicknesses of Lucite absorber and then using the second ionization chamber as a detector. For this beam the Bragg peak is obtained at 8-5/8 in. of Lucite absorber. Most of the pions stop in this region and create stars. The width of the Bragg peak at 50% level is approximately 1.89 g/cm^2 of Lucite.

The thickness of the semiconductor used in this study is 0.61 g/cm^2. Hence, if the detector were sitting at the Bragg peak position, a good portion of the pions would be stopped in the detector and create stars in silicon. In addition to the energy of stars formed in the

detector because of pions stopped there, the detector at this position would also see the energy loss of the pions, muons, and electrons passing through the detector.

In order for the detector to see the energy distribution of the pion star alone, the energy deposited by the pions, muons, and electrons while passing through the detector has to be eliminated. This is achieved by using another semiconductor detector in anticoincidence with the analyzing detector. The schematic diagram is shown in Fig. 1. In this way we can observe only the pions that stop in the analyzing detector (i.e., pion stars), and the rest of the events can be eliminated. However, sometimes one of the prongs of the stars in the first detector can pass through the second detector and cause anticoincidence, thereby losing some stars. This does not greatly affect the energy distribution of the pion stars. Figure 16 shows the energy distribution of the pion stars. The upper curve shows the distribution without using the second detector in anticoincidence, so that the detector sees, besides the energy of the stars, quite a few low-energy events due to pions, muons, and electrons passing through the detector. The bottom curve is obtained by using the anticoincidence detector, thereby giving the energy distribution of pion stars in silicon.

The thickness of the detector corresponds to the range of approximately 84-MeV α particles and 20-MeV protons. Therefore this energy distribution of pion stars does not correspond to the total energy of the star, but only to that fraction of the energy of the star fragments that is deposited in the detector. Most of the α-particle energy and that from heavier fragments would be stopped in the detector. Indeed, this is also true for the protons with the exception that some of the higher energy protons may escape the detector, depositing only a fraction of their energy. On the other hand, neutrons would escape the detector most of the time. It can be seen from Fig. 16 that the number of stars is a constantly decreasing function with increasing energy and that this star energy extends beyond 60 MeV. Since both the curves are for the same amount of charge collected in the monitor chamber, strictly speaking they should both coincide up to about 10 MeV. However, the lower curve (for the anticoincidence detector) is less than the upper curve (for a single detector), thereby indicating that some of the star events are lost when the anticoincidence detector is used, because some of the fragments pass through the analyzing detector and reach the anticoincidence detector.

CONCLUSIONS

The lithium-drifted silicon semiconductor detectors used in this study give very promising results in measuring energy loss of high-energy particles. Indeed, the agreement between the theoretical and experimental values of energy loss is within 2%. The behavior of the pion beam as it passes through various thicknesses of absorbing material is dramatically displayed with instrumentation that is relatively simple when compared with other instrumentation used with high-energy machines. The composite beam of pions, muons, and electrons of the same momentum can be differentiated. The pion-star energy spectrum is a constantly decreasing function with increasing energy, with the high-energy tail extending beyond 60 MeV. An attractive feature of these detectors is that they operate as true energy-measuring devices in that they do not exhibit the saturation effects of scintillator counters.

SUMMARY

Measurements were made of the most probable energy loss in silicon for pions of energies extending from 365 MeV to 50 MeV. The results agree within 2% with the theoretical values. The behavior of the pion beam with its inherent muon and electron contaminants, as it passes through various thicknesses of absorbing material, is displayed. Finally the energy distribution of negative pion stars in silicon is measured, and is found to be a constantly decreasing function with increasing energy, with the high-energy tail extending beyond 60 MeV.

ACKNOWLEDGMENTS

We wish to thank Professors John H. Lawrence and Cornelius A. Tobias for their continued interest and encouragement. Special thanks to D. Landis, R. Lathrop and H. Smith for supplying the detectors and helpful discussions on their use. Also, the discussions with Fred Goulding in preparation of this paper are most appreciated. Finally, we wish to thank Mr. Howard Maccabee for making the theoretical calculations.

This work was done under the auspices of the U. S. Atomic Energy Commission and the American Cancer Society.

REFERENCES AND NOTES

1. Richman, C.; unpublished data, 1952.
2. Fowler, R. H., and Perkins, D. H.; Nature, 189:524, 1961.
3. Richman, C.; Aceto, H., Jr.; Raju, M. R.; Schwartz, B., and Weissbluth, M.; Semi-annual Report, Donner Laboratory, Lawrence Radiation Laboratory, UCRL-11387, 1964.
4. Richman, C.; Aceto, H., Jr.; Raju, M. R., and Schwartz, B.; The Therapeutic Possibilities of Negative Pions—Preliminary Physical Experiments; in preparation.
5. Ammiraju, P., and Lederman, L. M.; Nuovo Cimento 4:283, 1956.
6. Menon, M. G. K.; Muirhead, H., and Rochat, O.; Phil. Mag. 41:583, 1950.
7. Goulding, F.; Lawrence Radiation Laboratory Report UCRL-11132, 1964.
8. Seventh Annual National Meeting on Solid State Radiation Detectors, in IRE Trans. Nucl. Sci. 8, No. 1 Jan., 1961.
9. Miller, G. L.; Foreman, B. M.; Yuan, L. C. L.; Donovan, P. F.; Gibson, W. M.; in IRE Trans. Nucl. Sci. 8, No. 1:73, 1961.
10. Van Putten, J. D.; Vander Velde, J. C.; in IRE Trans. Nucl. Sci. 8, No. 1:124, 1961.
11. Sternheimer, R. M.; Phys. Rev., 115:137, 1959.
12. Koch, L.; Messier, J., and Valin, J.; in Nuclear Electronics, Vienna, International Atomic Energy Agency, 1962, pp. 1, 465.
13. Goulding, F. S. and Hansen, W. L.; in IEEE Trans. Nucl. Sci. 11, No. 3:286, 1964.
14. Williamson, L., and Boujot, J. P.; Tables of Range and Rate of Energy Loss of Charged Particles of Energy 0.5 to 150 MeV, 1962.
15. Astbury, A.; Crowe, K. M.; Deutsch, J. G.; Maung, T. M., and Taylor, R. E.; Lawrence Radiation Laboratory Report UCRL-10120, 1962.
16. Landau, L.; Zh. Eksperim. i Teor. Fiz., 8:201, 1944.

17. Rich, M., and Madey, R.; University of California Radiation Laboratory Report UCRL-2301, 1954.
18. Vavilov, P. N.; Zh. Experim. i Teor. Fiz. 32:320, 1957.
English Transl: Soviet Phys. --JETP 5:749, 1957.
19. Seltzer, S. M., and Berger, M. J.; in Studies in Penetration of Charged Particles in Matter, N.A.S., Nat. Res. Council, Publ. No. 1113, 1964, p. 187.

This paper will be published in Nuclear Instruments and Methods.

Dr. Chaim Richman is professor of radiobiology at the Graduate Research Center, and the Department of Radiology, University of Texas Southwestern Medical School, Dallas, Texas.

Received May, 1965.

Differential Cytologic Effects of Negative Pion Beams in Plateau and "Star" Regions - Preliminary Report

William D. Loughman, H. Saul Winchell, Henry Aceto, Chaim Richman, Mudundi R. Raju and John H. Lawrence

LAF_1 mice carrying the Ly2 lymphoma as an ascites tumor were exposed to the negative pion beam of the 184-in. cyclotron (including its muon and electron contaminants). A complete description of the beam characteristics including dosimetric techniques is discussed elsewhere (1, 2). Mice exposed in the plateau region of the pion beam received 65 to 80 rads, with the beam estimated to contain about 64% pions. Mice exposed in the "star" region of the pion beam received 80 to 95 rads, with the beam estimated to contain less than 50% pions.

Cytological examination of lymphoma cells aspirated from mice at various time intervals following pion irradiation was performed. Four characteristics were scored: mitotic index; frequency of polyploid metaphase cells; frequency of anaphase cells displaying "bridges"; and chromosome counts of metaphase cells. Mitotic index determinations indicate a decrease in mitotic index with age of tumor. An immediate drop in mitotic index is seen after irradiation, followed by an increase, reaching control values on about the second day after irradiation. Polyploid cells, usually approximately tetraploid, increased in frequency shortly after irradiation, and subsequently decreased to near control values. The frequency of polyploid metaphase cells in tumors exposed in the "star" region of the beam exceeded that in tumors exposed in the plateau region for at least six days following irradiation (see Fig. 1).

Anaphase "bridges", irrespective of type, increased in frequency following irradiation and then decreased to control values five to six days later. The frequency of "bridges" in lymphoma cells exposed in the "star" region exceeded that seen in cells exposed in the plateau region (see Fig. 2). Aneuploidy is increased following irradiation, with a larger spread of chromosome numbers per cell in tumors exposed in the "star" region than in the plateau region of the beam. Chromatid breaks and metacentric chromosomes, which were sometimes seen in the irradiated cells, were never seen in the controls. The irradiated cells showed an increased percentage of cells with multiple nuclei, micronuclei, and giant and bizarre nuclei. At six days following irradiation, the irradiated cells showed more karyorrhexis than controls, and cells with multiple micronuclei were common.

The incidence of polyploidy and anaphase "bridges" was about five times higher in cells exposed in the "star" region of the beam than in cells exposed to the plateau region. It is difficult to interpret these findings in terms of RBE. However, since the radiation doses from plateau and "star" regions were similar, it would seem that "star" region negative pions have a greater RBE than those in the plateau region.

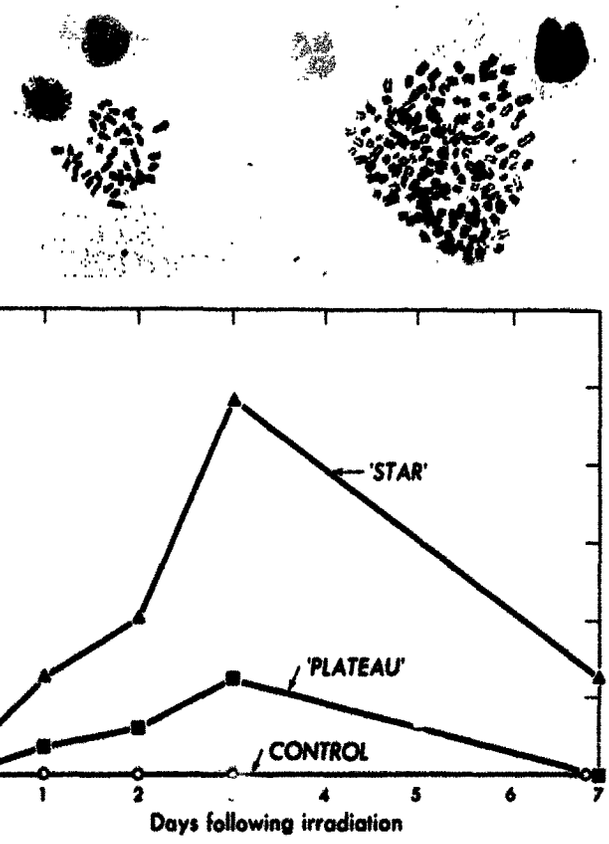

Figure 1. Polyploid metaphase cells as a percent of all metaphase cells scored in unirradiated control cells, cells exposed in the plateau region of a pi-meson beam, and cells exposed in the "star" region. Left Photograph = Normal Ly-2 metaphase. Right Photograph = Polyploid metaphase of extreme type.

MUB-6317

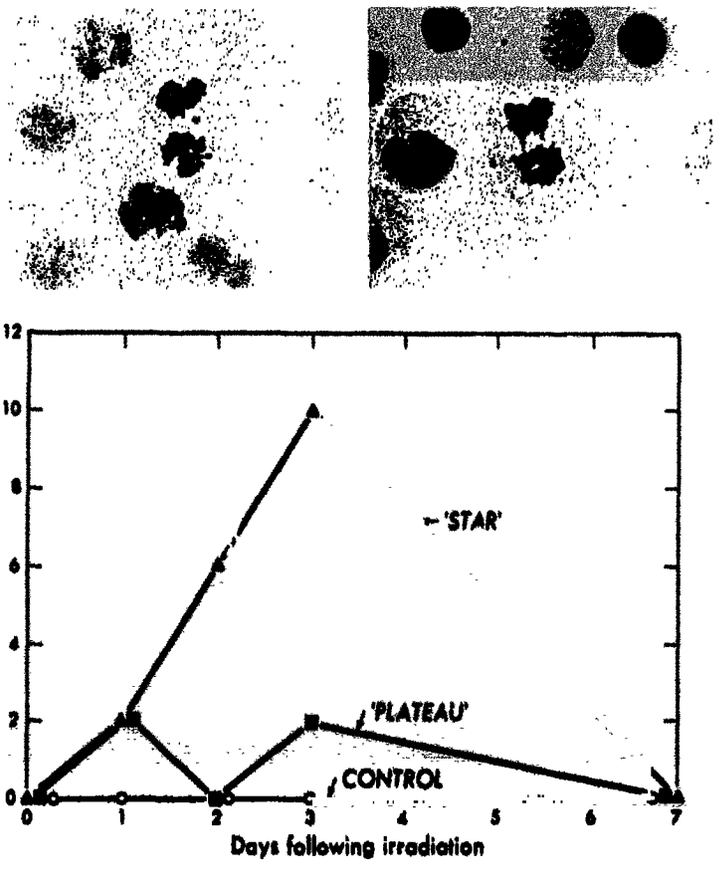

Figure 2. Anaphase "bridges" as a percent of all anaphase cells scored in unirradiated control cells, cells exposed in the plateau region of a pi-meson beam, and cells exposed in the "star" region. Photographs = Anaphase "bridges" found in irradiated cells.

MUB-6318

Present pion study efforts are directed toward a pion beam virtually free of contaminants. Further biological investigations are planned for such a beam.

REFERENCES

1. Richman, C.; Aceto, H.; Raju, M. R.; Schwartz, B., and Weissbluth, M.; Semiannual Report, Donner Laboratory, Lawrence Radiation Laboratory, UCRL-11387:114, 1964.
2. Richman, C.; Aceto, H.; Raju, M. R., and Schwartz, B.; The Therapeutic Possibilities of Negative Pions -- Preliminary Physical Experiments. To be published.

Received, July 1965.

Fluctuations of Energy Loss by Charged Particles in Silicon Detectors

Howard D. Maccabee and Mudundi R. Raju

The theory of energy loss of charged particles in matter has been studied extensively and is summarized well in a review article by Fano (1). The agreement between theoretical predictions of mean energy loss and experimental values is excellent. In certain ranges of particle energy and absorber thickness, however, fluctuations in energy loss differ significantly from the "expected" Gaussian distribution. These fluctuations have been studied theoretically by Landau (2) and others (3-7). Recently, Seltzer and Berger (8) have tabulated the rigorous theoretical distribution given by Vavilov (6). Approximate experimental verification of the Landau theory has been performed by Igo et al. (9) for 31.5 MeV protons in a gas proportional counter and by Galaktionov et al. (10) for minimum ionizing π-mesons and protons of momentum 600 MeV/c in a spark chamber.

The usefulness of semiconductor detectors in high-energy particle physics has been shown by Miller et al. (11), Labeyrie (12), Van Putten et al. (13), Koch et al. (14) and Raju et al. (15). Although all of the above experimenters have shown fair agreement in a limited range with the approximate theory of Landau (2) or Symon (3), none have attempted verification in detail of the rigorous Vavilov distribution in the important intermediate range of particle velocity and detector thickness. "Thick" lithium-drifted semiconductor detectors have certain inherent advantages for such an investigation: a) the density of the solid semiconductor is on the order of a thousand times that of a gas, yielding that many more energy-loss collisions per unit path length; b) the energy required to create a charge pair in silicon is 3.6 eV (approximately a tenth of the value for gas), yielding ten times as many charge pairs and thus improving statistics and resolution; c) absence of wall effect; d) short pulse duration, allowing high count rates, fast coincidence circuitry, etc.; e) relative uniformity of thickness of depletion layer as compared to "thin" p-n junction detectors.

The aim of the present investigation is to use thick lithium-drifted semiconductor detectors for a detailed experimental investigation of fluctuations of energy loss by particles of high and intermediate energy. Special consideration is being given to situations of significance for biomedical irradiation.

METHOD

Lithium-drifted silicon detectors as developed by Goulding and Hansen (16) are used in an experimental setup similar to that shown in Fig. 1 on page 86. Calibration of the system is done with an ^{241}Am alpha source and a ^{207}Bi internal-conversion electron source.

The thickness of the depletion layer is measured by the method described by Raju et al. in article beginning on page 84, and is checked operationally by exposing the detector to alpha particles of an energy whose energy-loss distribution is well known.

In a given experiment, the detector is mounted in a plane normal to the beam axis and bias is applied. The voltage pulses due to particles passing through the detector are then amplified, and analyzed in a multi-channel pulse-height analyzer. Information from the pulse-height analyzer is then printed out in the form of counts per channel versus channel number. This information may then be processed to yield a plot of relative probability versus energy loss in the detector, with the assumption that the pulse-height is directly proportional to the energy loss in the detector.

PRELIMINARY RESULTS

The results of two preliminary experiments are shown in Figs. 1 and 2. Figure 1 is a plot of the data from a run with the 730-MeV proton beam in the medical cave of the 184-in. cyclotron, with a silicon detector of thickness 0.48 g/cm^2. Figure 2 is a plot of the data from a run with the 370-MeV pion beam in the meson cave of the 184-in. cyclotron, with a detector of thickness 0.45 g/cm^2. It may be noted here that the plot of probability versus energy loss is similar to the familiar LET (linear energy transfer) spectrum. The theoretical curve of Fig. 1 is calculated by interpolation from the numerical data of Seltzer and Berger. The pion energy and detector thickness in Fig. 2 are in the range where the Landau theory is believed to be accurate, and thus the theoretical curve is computed directly from Landau's plot of $\phi(\lambda)$ versus λ, where $\phi(\lambda)$ is a parameter related to probability and λ is a parameter related to energy loss. Both theoretical curves are normalized such that their maximum heights are equal to those of the experiment. A Gaussian curve centered about the mean energy loss is shown for comparison, to indicate the failure of normal statistics to predict these highly asymmetrical energy-loss spectra.

DISCUSSION

The most probable energy losses measured are in excellent agreement with the theoretical predictions. There is also good agreement on the shape and height of the curves for moderate- and high-energy losses, but there is a significant deviation on the low-energy side. A possible explanation for this discrepancy is edge effects in the detector, i.e. the detector diameter is smaller than that of the beam and there is a certain probability that particles enter and leave the detector at its edges, without "seeing" the full detector thickness. This geometrical problem will be corrected in the future by the use of another small detector as a coincidence gate to define the beam. Other possible explanations for the discrepancy are capture of δ-rays created by the beam in the air in front of the detector and escape of δ-rays out the back of the detector. Each of these possibilities is being evaluated and will be eliminated if feasible. There has been some criticism of the Landau and Vavilov theories on the basis that their postulated collision spectrum does not take proper account of glancing collisions between the energetic particle and the electrons of the stopping material; this effect might also yield some deviation on the low energy side of the curve (17).

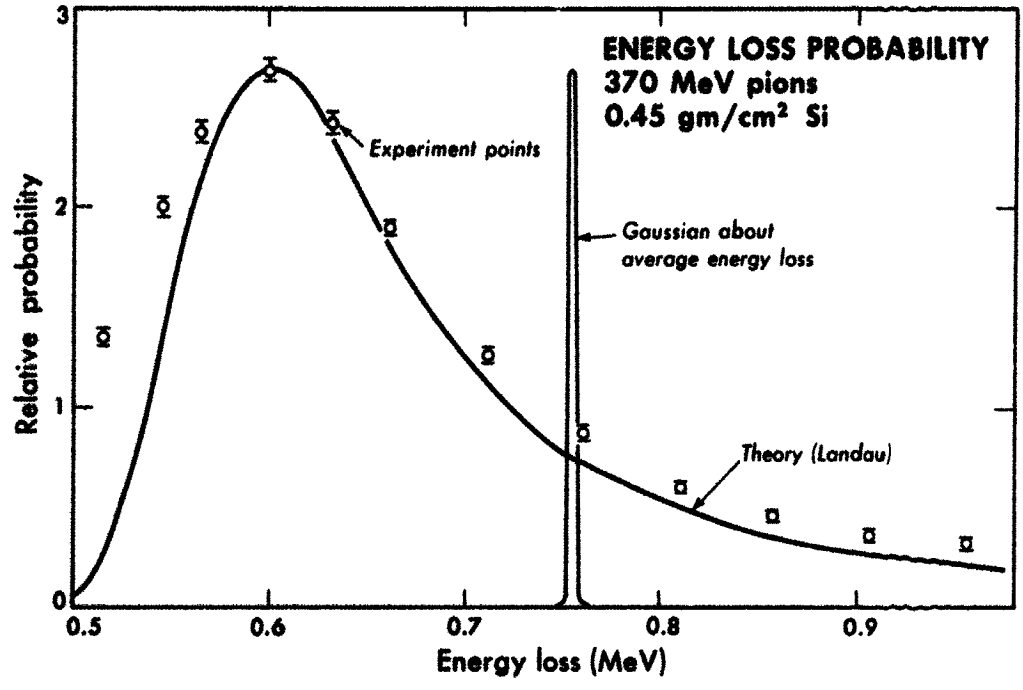

Figure 1 MUB-6728

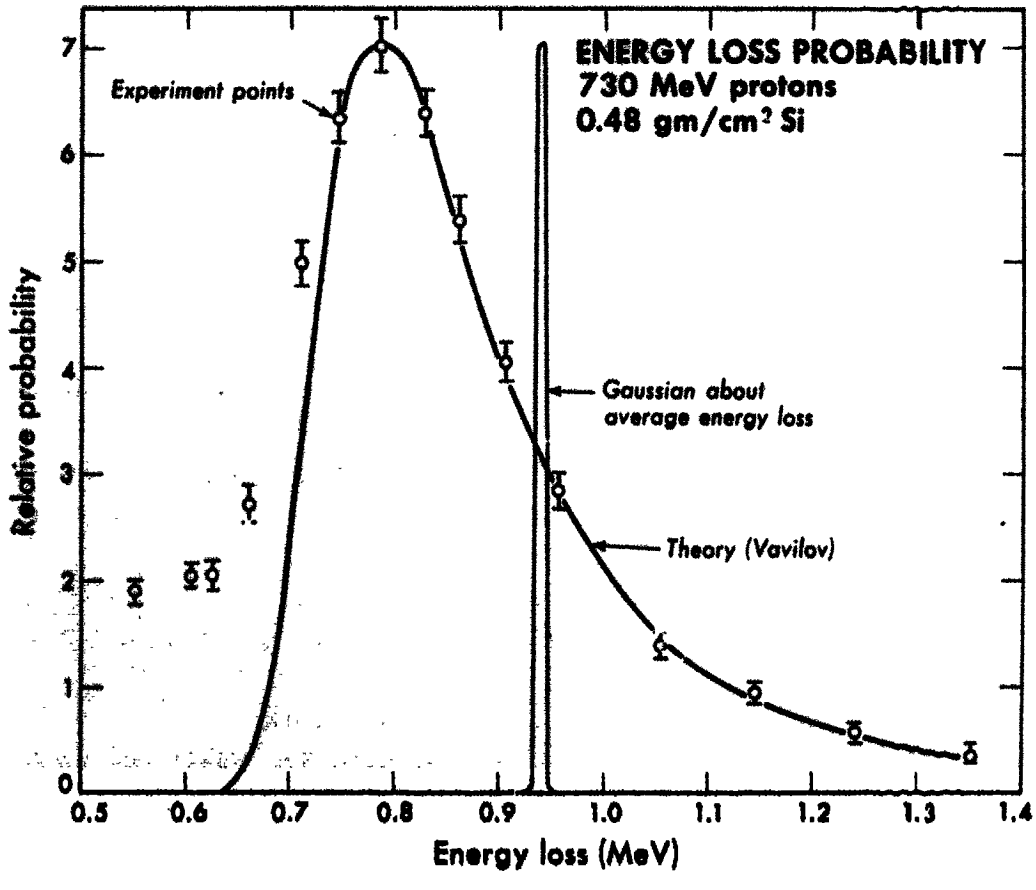

Figure 2 MUB-6727

Other errors may have been introduced by the uncertainty in measurement of detector thickness (judged to be less than 2%) and by the fact that the beam is not monoenergetic but spread over a finite range of energies. Work is continuing on several facets of this problem: a) refinement of the experiments, b) theoretical analysis, c) accumulation of data for a wide range of energies and thicknesses, and d) application of results to the prediction and measurement of characteristics of biomedical beams.

ACKNOWLEDGMENTS

We wish to thank Professor C. A. Tobias for his continued interest and encouragement. We are obliged to Drs. N. Oda, W. Barkas, H. Heckman, H. Mark, and F. Goulding for helpful discussions. Special thanks are due to D. Landis, R. Lathrop, and H. Smith for supplying the detectors and for discussions on their use.

This work was supported by the National Aeronautics and Space Administration. Mr. Maccabee wishes to thank the National Science Foundation and the Atomic Energy Commission for continued fellowship support.

REFERENCES

1. Fano, U.; Ann. Rev. Nucl. Sci. 13:1, 1963.
2. Landau, L.; J. Phys. USSR 8:201, 1944.
3. Symon, K. R.; Thesis, Harvard Univ., 1948, summary in High Energy Particles (Rossi), New York, Prentice-Hall, 1952, p. 32.
4. Williams, E. J.; Proc. Roy. Soc. (London) A125:420, 1929.
5. Moyal, J. E.; Phil. Mag. 46:263, 1955.
6. Vavilov, P. N.; Zh. Experim. i Teor. Fiz. 32:920, 1957; English transl: Soviet Phys. JETP 5:749, 1957.
7. Blunck, O., and Leisegang, S.; Z. Physik 128:500, 1950.
8. Seltzer, S. M., and Berger, M. J.; in Studies in Penetration of Charged Particles in Matter, NAS-NRC Pub. #1133, 1964, p. 187ff.
9. Igo, C. J.; Clark, D. D., and Eisberg, R. M.; Phys. Rev. 89:879, 1953.
10. Galaktionov, Y. V.; Yech, F. A., and Lyubimov, V. A.; Nucl. Inst. and Methods 33:353, 1965.
11. Miller, G. L.; Wagner, S., and Yuan, L. C. L.; Nucl. Inst. and Methods 20:303, 1963.
12. Labeyrie, J.; in Proc. Intl. School of Physics, Enrico Fermi Course XIX, New York, Academic Press, 1963, p. 187.
13. Van Putten, J. D., and VanderVelde, J. C.; IRE Trans, Nucl. Sci-8, No. 1:124, 1961.
14. Koch, L.; Messier, J., and Valin, J.; in Nuclear Electronics, Vol. 1, I. A. E. A. Vienna, 1962, p. 465.
15. Raju, M. R.; Aceto, H., and Richman, C.; this report, p. 84.
16. Goulding, F. G., and Hansen, W. L.; IEEE Trans. Nucl. Sci. NS-11:286, 1964.
17. Oda, N.; personal communication.

Received June, 1965.

Responsiveness of Hematopoietic Tissue to Erythropoietin in Relation to the Time of Administration and Duration of Action of the Hormone

John C. Schooley

The cells of blood and bone marrow are maintained in a steady state in spite of the fact that most of these cells are not self-maintaining populations. An enormous proliferative capacity is required to maintain this steady state. It has been postulated that there exists a self-maintaining population of stem cells in the bone marrow. The stem cell or stem cells differentiate and subsequently, through proliferation, give rise to the various blood cells. Although the identities of the stem cells are unknown, various investigators have proposed kinetic models which can explain and predict some characteristics of the stem cell population (1-3). Osgood (4) and Lajtha and co-workers (5) have published thorough discussions of their theoretical models of stem-cell kinetics.

The responsiveness after mild irradiation of the hypertransfused mouse to a standard dose of the hormone erythropoietin has been utilized by Gurney, Lajtha and Oliver (6) as an experimental system to test their theoretical model. Various aspects of this experimental system for investigating stem-cell kinetics have been discussed by Gurney (7). He points out that since no reliable simple method for quantitating the erythropoietic response exists, and since the challenge by erythropoietin of the stem cells cannot be instantaneous, the usefulness of their experimental model is seriously limited. The first of these limitations is primarily the time and effort required for more precise measurements. The second limitation, however is more serious and is due to the fact that erythropoietin has a prolonged biological half-life, and that an effective concentration of erythropoietin must exist. Thus, in studies of the stem-cell population utilizing the hypertransfused mouse, it is likely that the stimulating dose of exogenous erythropoietin generally used acts during the entire test period, while conditions within the stem-cell population and the developing erythroid population are changing as a result of the initial action of erythropoietin.

The recent development of an immune serum that can neutralize the biological activity of erythropoietin provides a means of limiting the availability of the stimulating dose of erythropoietin in the intact animal (8-11). In the present experiments changes in the responsiveness of the stem-cell population of the hypertransfused mouse, after erythropoietin stimulation, have been measured.

METHODS

Female C_3H mice weighing about 23 g were hypertransfused with two daily intraperitoneal injections of 1 ml of packed red blood cells obtained from isogenic donors. The donor red blood cells were washed three times with saline, and the buffy coat was removed after each wash. Normally, erythropoietin (sheep plasma erythropoietin Al-0336, No. 103194A obtained from the Hematology Study Section of the National Institutes of Health) was injected intravenously into the hypertransfused mice on the fifth day after the last transfusion. Fifty-six hours after the erythropoietin injection, 0.5 μCi of Fe^{59} as iron citrate (specific activity approximately 10 μCi/μg.) was injected intraperitoneally, and 72 hr later a sample of blood was taken by cardiac puncture. In all experiments the interval between the injection of Fe^{59} and the sampling of the blood of the assay animals was 72 hr, but the time of injection of erythropoietin and immune serum relative to the time of Fe^{59} injection was varied. Therefore, the time of these injections is always given relative to the time before or after the Fe^{59} injection. Thus, in one experiment groups of hypertransfused mice received injections of erythropoietin 56, 32, and 8 hr before and 16 hr after the injection of Fe^{59}, i.e., the normal time (56 hr before), and one, two, and three days later than normal. In another experiment groups of hypertransfused mice were injected intravenously with 0.25, 0.5, 1.0, 2.0, or 4.5 cobalt units of sheep-plasma erythropoietin 56 hr before the Fe^{59} injection, and at various times later enough immune serum (0.2 ml) to neutralize the biological activity of the largest dose of erythropoietin was injected intravenously into each mouse. Blood was collected from the mice of each group 72 hr after the Fe^{59} injection, regardless of the time of immune serum injection.

In another experiment 0.5 cobalt unit of sheep plasma erythropoietin was injected intravenously 56 hr before the Fe^{59}, and another similar injection of erythropoietin was made at various intervals after the first erythropoietin injection. In some cases immune serum was injected 6 hr after the second erythropoietin injection. The radioactivity in 0.5 ml of whole blood was measured in the assay mice, and the percent of the injected Fe^{59} in the total red-blood volume was calculated. It was assumed that the blood volume of the hypertransfused mice was 7% of the total body weight. Values from any animal that lost weight or whose hematocrit was less than 55% at the time of sampling were discarded. Each individual group in each experiment consisted of six to 10 mice. The standard error of the mean is indicated for each value.

Immune serum capable of neutralizing the biological activity of sheep plasma erythropoietin was obtained from rabbits immunized with human urinary erythropoietin. The schedule of immunizations and characterizations of the immune serum have been described previously (11).

RESULTS

The effects of varying the interval between the injection of erythropoietin and the injection of Fe^{59} were measured. If 0.5 cobalt unit of erythropoietin was given 56 or 32 hr before the injection of Fe^{59} (the normal time and one day later than normal), the uptake of Fe^{59} into the calculated blood volume 72 hr after the radioiron administration was

3.29 ± 0.31% and 3.16 ± 0.4% respectively. However, if the erythropoietin injection was given only 8 hr before the Fe^{59} injection (two days later than normal), the Fe^{59} uptake was decreased to 0.41 ± 0.08%. The Fe^{59} uptake observed when the stimulating dose of erythropoietin was given 16 hr after the Fe^{59} injection was 0.09 ± 0.01% which is indistinguishable from the values found in saline-injected controls. These results indicate that very little Fe^{59} is taken up by cells during the early development of the wave of erythropoiesis. After the wave of erythropoiesis has progressed for 56 hr, a significant uptake of Fe^{59} is observed, but this uptake is not significantly different from that observed when the wave has progressed for 32 hr. The Fe^{59} uptake found in the assay animal 72 hr after the injection of Fe^{59} is the result of a complex series of events such as the stage of the wave of erythropoiesis at the time of Fe^{59} injection, the hemoglobin synthesizing ability of the individual erythroid cells present at this time, the rate of disappearance of the injected Fe^{59}, the rate of release of the newly formed red cells into the peripheral blood, etc.

The effect of varying the interval between the injection of the two identical doses of 0.5 cobalt unit of erythropoietin on the erythropoietic response is shown in Fig. 1. The first injection of erythropoietin was given 56 hr before the injection of Fe^{59}, and the second dose of erythropoietin was given at various times after the first injection. The Fe^{59} uptake was determined 72 hr after the injection of Fe^{59}. The 72-hr uptakes are plotted as a function of the interval between the first and second erythropoietin injections. When the interval between the first and second dose of erythropoietin was 72 and 96 hr, the second dose of erythropoietin was given 16 and 40 hr after the injection of Fe^{59}. The values for the Fe^{59} uptake are given relative to the Fe^{59} uptake observed when no interval existed between the first and second erythropoietin injection, i.e., a total of 1 cobalt unit was injected in one dose. If 0.5 cobalt unit of erythropoietin is given at the usual time (56 hr before Fe^{59}) and again 24 hr later, the erythropoietic response is about two and one-half times greater than that observed when 1.0 cobalt unit of erythropoietin is injected 56 hr before Fe^{59}, or about five times the response found with only 0.5 cobalt unit of erythropoietin. The magnitude of the erythropoietic response observed when the total dose of erythropoietin is fractionated into two doses 24 hr apart is not only greater than that observed when the dose is not fractionated but is greater than the sum of the responses found when each dose is given singly at these times. The increased erythropoietic response observed when the total dose of erythropoietin is divided into two injections is evident even when the interval between the two injections is only 6 hr. It has been stressed previously that the Fe^{59} uptake observed in the assay animals is the resultant of a complex series of reactions occurring in the erythroid population before and during the time Fe^{59} is available. Obviously, the series of events becomes even more complex following multiple injections of erythropoietin, since the waves of erythropoiesis produced by each injection of erythropoietin will be at different stages of development when the Fe^{59} is injected. Presumably, this accounts for the observation that when the interval between the two fractionated doses is increased to 48 or 72 hr, the erythropoietic response is not greater than that observed when the dose is not fractionated. However, the responses in this case do tend to be greater than the sum of the individual responses observed when 0.5 cobalt unit of erythropoietin is injected at these times without fractionation. Gurney et al. (12) did, however, observe that a given dose of erythropoietin was about twice as effective when administered

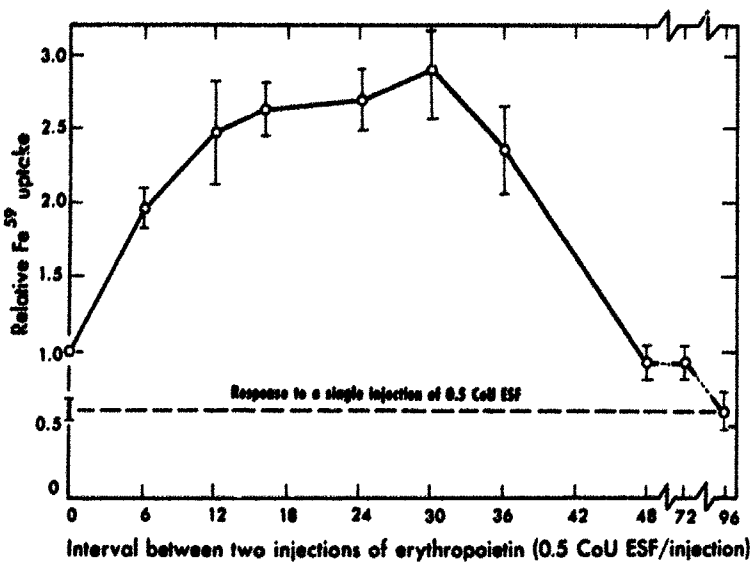

Figure 1. The effect of a divided dose of erythropoietin relative to the effect of the same total amount of erythropoietin given as a single dose. Unit response is defined as that observed following a single intravenous dose of 1.0 cobalt unit of erythropoietin. The curve represents the response, relative to this unit response, when the dose was divided into two 0.5 cobalt-unit doses given at times separated by the intervals (in hours) indicated on the abscissa.
MU-33706

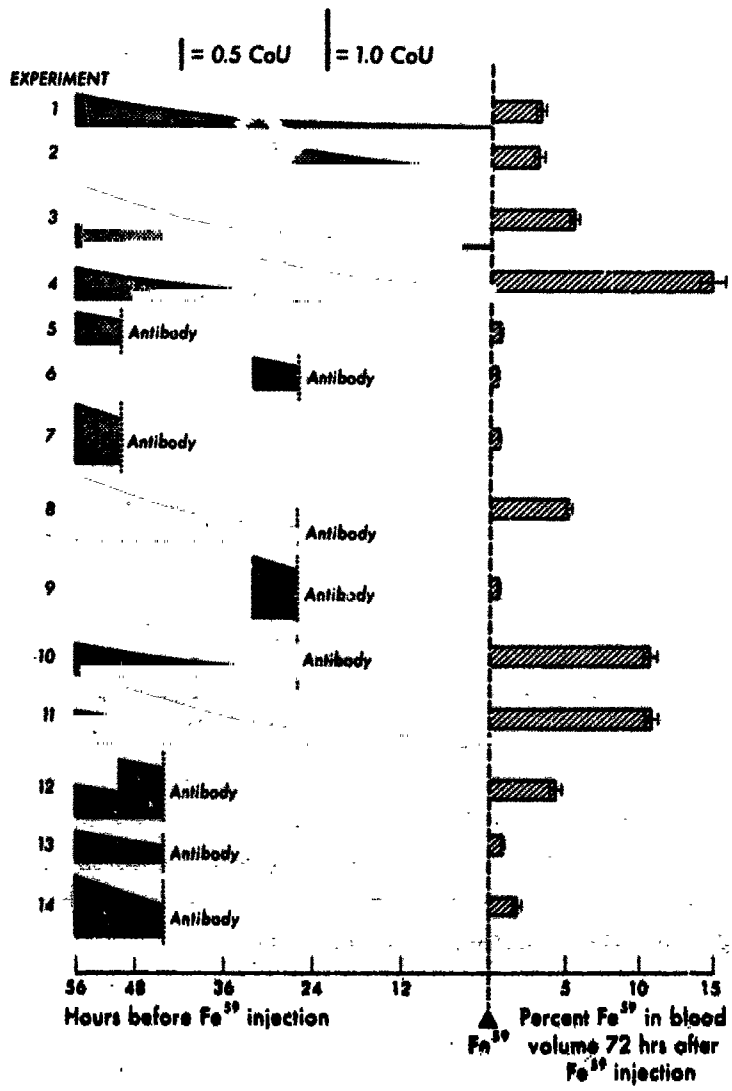

Figure 2. A diagrammatic representation of a series of experiments in which the time of injection of erythropoietin and antibody against erythropoietin is varied. The actual times of injection are indicated on the abscissa to the left. The amount of erythropoietin injected is indicated by the initial height of the shaded areas. The magnitude of the erythropoietic response is indicated for each experiment by the bars to the right.
MUB-2275

in two partial injections separated by 48 hr. The discrepancy between their findings and the present experiments is probably related to the fact that their dose of erythropoietin was greater than that used in the present experiments and their erythropoietin was injected subcutaneously rather than intravenously. These differences in dosage and route of injection suggest that an effective level of erythropoietin was maintained in their experimental animals for a longer interval of time following each erythropoietin injection than in the experiments reported here.

The above results suggest that the responsiveness of hematopoietic tissue to erythropoietin is increased after the initial exposure to erythropoietin. This possibility was further investigated by allowing the second dose of erythropoietin to act for the limited time of 6 hr. The results of these experiments are shown in Fig. 2. The times of injection of the doses of erythropoietin and antibody relative to the time of injection of Fe^{59} are shown to the left of this figure. The uptake of Fe^{59} into the calculated blood volume 72 hr later is indicated on the right. The amount of erythropoietin initially injected is indicated by the height of the vertical line. The decreasing amount of erythropoietin following injection is plotted for convenience as if the T-1/2 was 12 hr in these hypertransfused mice. The first experiments shown in this figure simply reemphasize the results already mentioned and show that fractionating the total dose of 1 cobalt unit into two injections 24 hr apart of 0.5 cobalt unit gives a much greater response (experiment 4) than 1 cobalt unit (experiment 3) or the sum of the responses observed when a total of 0.5 cobalt unit of erythropoietin is injected either 56 or 32 hr before Fe^{59} (experiment 1 and 2). Experiments 5, 6, 7, and 9 of Fig. 2 indicate that if 1.0 or 0.5 cobalt unit of erythropoietin is injected either 56 or 32 hr before the injection of Fe^{59} and allowed to act on the marrow for only 6 hr, measurable erythropoietic responses occur, but they are not different from one another. If 0.5 cobalt unit of erythropoietin is injected 56 hr before the Fe^{59} injection and allowed to act 30 hr before the injection of immune serum, the erythropoietic response is about the same as that observed when no immune serum is injected (experiments 3 and 8). If, however, 0.5 cobalt unit is injected 56 and 32 hr before the Fe^{59}, and immune serum is injected so that the first dose of erythropoietin acts for 30 hr and the second dose acts for 6 hr, then the erythropoietic response is significantly greater than that observed when 1 or 0.5 cobalt unit is injected without fractionation and allowed to act only 30 hr or during the entire assay (compare experiments 1, 3, and 10). But the response is not as great as that found when the fractionated dose acts during the entire assay period (experiment 4). The erythropoietic response given when 1 cobalt unit acts on the hypertransfused mouse marrow for 30 hr is shown in experiment 8. This is about two times the response seen when 0.5 cobalt unit of erythropoietin acts during the same interval. The response observed in experiment 10 with fractionated doses of 0.5 cobalt units each is much greater than the sum of the responses seen even with the larger dose of 1.0 cobalt unit in experiments 8 and 9. When 0.5 cobalt unit of erythropoietin acts for 30 hr (the period from 56 to 26 hr before the injection of Fe^{59}), the Fe^{59} uptake is 2.8 ± 0.27%, and when this same dose acts for 6 hr during the period 32 to 24 hr before the Fe^{59} injection, the Fe^{59} uptake is 0.42 ± 0.07%. The sum of these two values is 3.2 ± 0.28% which is considerably less than the 10.6 ± 0.45% observed when 0.5 cobalt unit is injected into the same animal 56 and 32 hr before the Fe^{59} injection and allowed to act until the 26th hour before Fe^{59} injection. Thus, the second injection of

0.5 cobalt unit of erythropoietin stimulated the marrow to give a response during the short interval of 6 hr of 10.6 - 3.2 or about 7%. This is almost eighteen times the response observed when 0.5 cobalt unit acts on the marrow during the same time interval in animals that have not received an earlier injection of erythropoietin. Similar results are shown in the last four experiments of Fig. 2. In these experiments 0.5 cobalt unit was injected 56 hr before the Fe^{59} followed by another similar injection 6 hr later. The erythropoietic response is shown in experiment 11. Notice that the response is about double that observed when both injections of 0.5 cobalt units are injected at the same time (experiment 3). If the action of both injections of erythropoietin is limited to 12 hr by the injection of immune serum 6 hr after the second injection of 0.5 cobalt unit of erythropoietin, a significant erythropoietic response results. This response is much greater than that observed when 0.5 (experiment 13) or 1.0 cobalt unit (experiment 14) acts on the marrow for 12 hr. Thus, even at this early time after the first injection of erythropoietin, the data indicate that a second injection stimulates the marrow to a greater extent than when the marrow has not been previously exposed to exogenous erythropoietin.

The above experiments were repeated using divided doses of 0.25 units of erythropoietin given with an interval of 24 hr before the first and second injection. When 0.5 unit of erythropoietin was given in two divided doses of 0.25 unit 56 and 32 hr before the Fe^{59} injection, the Fe^{59} uptake in the calculated blood volume of the mice 72 hr after the Fe^{59} injection was 10.4 ± 1.38%, but when the same dose was given undivided 56 hr before the Fe^{59}, the response was only 3.29 ± 0.31%, i.e., the response following the divided doses was about three times greater. If the divided doses were allowed to act for only 30 hr (56 to 26 hr before the Fe^{59} injection) by the injection of immune serum 6 hr after the second injection of erythropoietin, the response was 6.23 ± 1.06%.

The responsiveness of the stem-cell population to different doses of erythropoietin acting during limited periods of time was investigated. The results are shown in Fig. 3. The different doses of erythropoietin were injected 56 hr before the injection of Fe^{59}, and antibody was injected at various times after the injection of erythropoietin. The interval between the times of erythropoietin and antibody injection is indicated on the abscissa. The uptake of radioiron into the calculated blood volume 72 hr after the injection of radioiron is indicated on the ordinate. The erythropoietic response observed following the injection of 0.25, 0.5, 1.0, 2.0 and 4.0 cobalt units of erythropoietin when antibody was not injected is indicated by the appropriate horizontal lines. The erythropoietic response found when antibody was injected at various times following erythropoietin is indicated at each time for each dose of erythropoietin. These responses are connected with appropriate lines corresponding to the dose of erythropoietin injected. The Fe^{59} uptakes of 0.25 and 4.0 cobalt units of erythropoietin following intravenous injection are about 2% and 16% respectively, the other doses having intermediate values. These responses are submaximal; larger doses of erythropoietin do give larger Fe^{59} uptakes.

The injection of antibody 24 hr after the injection of 4.0 or 2.0 cobalt units of erythropoietin significantly reduced the subsequent development of the wave of erythropoiesis as

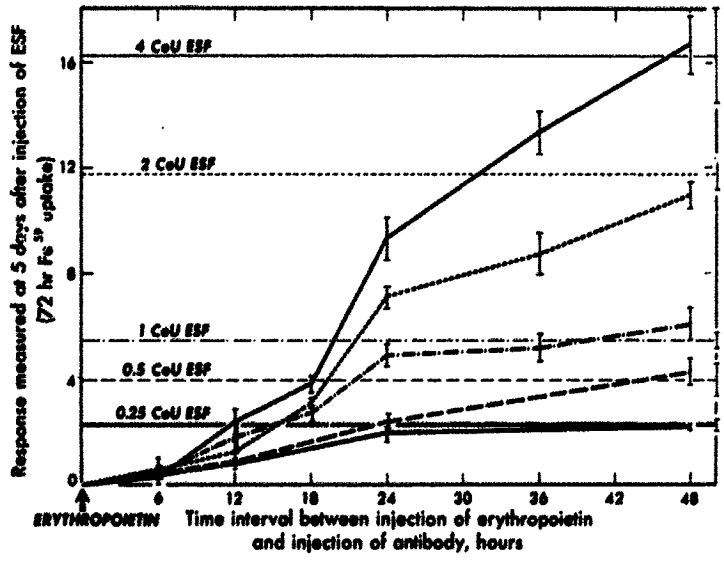

Figure 3. Erythropoietic response observed following the intravenous injection of different doses of erythropoietin. The horizontal lines represent the responses observed when the indicated doses of erythropoietin are allowed to act for the entire assay period. The curves represent the responses observed when the same respective doses act for the limited time indicated on the abscissa.

MU-33707

measured by the decreased Fe^{59} uptakes. Similar injections of antibody at this same time had little if any effect on the erythropoietic response seen with doses of erythropoietin of 1.0 cobalt unit or less. At 48 hr the injection of antibody had little effect on the erythropoietic responses given by the injection of 4.0 and 2.0 cobalt units of erythropoietin, i.e., the responses were not significantly different from those found when antibody was not injected. Presumably, the depression in the erythropoietic response following the injection of antibody is the result of the removal by neutralization of circulating erythropoietin that has not acted on the receptive cells of the bone marrow. Large numbers of immature erythroid cells are present in the marrow at the time of the antibody injection, and these cells must mature in order to give the erythropoietic response eventually seen. This indicates that the antibody has no effect on these maturing erythroid cells, and therefore that erythropoietin is not necessary for the maturation of erythroid cells.

Injection of antibody 6 hr after the injection of the different doses of erythropoietin markedly reduced the various erythropoietic responses; however, the responses found are small although measurable. They are not significantly different from one another, even though there is a sixteen-fold difference between erythropoietin doses. This finding suggests that during the first 6 hr following erythropoietin injection there is a limited number of receptive cells in the bone marrow, and all these cells are triggered to differentiate by even the smallest erythropoietin dose. When the doses are allowed to act for longer intervals, the erythropoietic responses given by each dose become more and more different. By the 24th hour all the doses except 0.25 and 0.5 cobalt units are significantly different from one another, and by the 48th hour the responses given by these small doses are also significantly different.

When 4 cobalt units of erythropoietin are allowed to act for 24 hr, the erythropoietic response of the mouse is much greater than four times the response seen when this dose is allowed to act only 6 hr, i.e., the response seen after 24 hr exposure of the marrow to

erythropoietin is about 30 times greater than that observed after a 6-hr exposure. During the time interval between 18 and 24 hr the erythropoietic response increased from 3.84 ± 0.25% to 9.30 ± 0.82%, an increase of about 5.5%. This increase is about one and one-half times greater than the erythropoietic response seen during the entire first 18 hr. This increase occurs in spite of the fact that the exogenous erythropoietin is disappearing from the assay animal. In nonhypertransfused animals the $T_{1/2}$ for this disappearance has been reported to be about 1 to 3 hr (13, 14). The present findings suggest that in the hypertransfused mouse the $T_{1/2}$ may be much longer. Regardless of how much of the injected erythropoietin has disappeared by the 18th hour, these data indicate that the marrow is much more sensitive to erythropoietin stimulation during the 18th to 24th hr following erythropoietin injection than during the entire first 18 hr. The magnitude of this increased sensitivity depends, of course, on the actual $T_{1/2}$ for the disappearance of exogenous erythropoietin in hypertransfused animals.

DISCUSSION

Erythropoiesis, measured either by the incorporation of radioiron or by the presence of identifiable erythroid cells in the hematopoietic tissues, virtually ceases in the mouse four or five days after the production of an increased red-cell volume by transfusion (15). The depression of erythropoiesis is probably due to the absence of erythropoietin production (16). The presence of an inhibitor of erythropoiesis in the plasma of polycythemic animals has been claimed (17); however, we have been unable to confirm this finding (Schooley and Garcia, unpublished observations).

The injection of exogenous erythropoietin into a polycythemic mouse gives rise to a predictable orderly wave of erythropoiesis. In the spleen (18) and bone marrow (10), this wave of erythropoiesis is characterized by the appearance of a peak percentage of proerythroblasts one day after erythropoietin injection which is followed on the second day by a peak percentage of basophilic erythroblasts. On the third day, a peak percentage of reticulocytes occurs in the peripheral blood. By the fifth day after a single injection of erythropoietin, the hematopoietic tissue is again devoid of identifiable erythroid cells. Two methods have been utilized to quantitate the erythropoietic response: the uptake of Fe^{59} in the blood volume of the hypertransfused mouse measured 128 hr after the injection of erythropoietin and 72 hr after the injection of Fe^{59}; and/or the percentage of reticulocytes is measured in the peripheral blood on the third day after erythropoietin injection. Measurements of either of these parameters give graded responses for doses of erythropoietin ranging from about 0.25 to 6.0 cobalt units. The magnitude of the response for any particular dose of erythropoietin depends somewhat on the route of injection as well as the vehicle of injection, i.e., subcutaneous injections give larger responses than intravenous injections, and subcutaneous injections in serum give larger responses than similar injections in saline (Garcia and Schooley, unpublished observations). It has been demonstrated that there is a smaller erythropoietic response to a single submaximal dose of erythropoietin than there is to the same amount given in divided doses (12). This fact has been utilized in one assay for erythropoietin (9).

A great deal of data indicates that erythropoietin regulates erythropoiesis primarily by regulating the differentiation of stem cells into the erythroid population (1, 2). Some

arguments, however, have been advanced which suggest that erythropoietin may, in addition, have an effect on nucleated erythroid cells (19, 20). Schooley and Garcia (10) have presented evidence consistent with experiments presented here, showing that erythropoietin is not necessary for the maturation of erythroid cells. Thus, the injection of antibody capable of neutralizing erythropoietin into polycythemic mice that have received erythropoietin does not prevent the development of the wave of erythropoiesis. The magnitude of the erythropoietic response depends on the dose of erythropoietin injected and the time of antibody injection. Eventually, with the doses used in the current experiments, a time occurs when the injection of antibody has no effect on the magnitude of the erythropoietic response, even though the hematopoietic tissue contains large numbers of nucleated erythroid cells at the time of the antibody injection. The finding that injections of large amounts of erythropoietin into young 14-day-old rats whose marrows contain large numbers of nucleated erythroid cells does not further stimulate erythropoiesis (21) also suggests that the injected erythropoietin has little effect on nucleated erythroid cells.

Jacobson et al. (22) demonstrated in an elegant experiment that when rat bone-marrow cells are injected into lethally irradiated polycythemic mice, the leukocytes of the chimera are rat type, but rat erythrocytes are not observed. Rat red cells were produced in such animals when erythropoiesis was stimulated. These workers suggested that the stem cells specific for rat red cells either remained dormant in the mouse until erythropoiesis was stimulated or that the stem cells of the rat are pluripotential. It is also possible that the specific stem cell for rat red cells was actively dividing in such animals but simply died when not stimulated to differentiate into an erythroid cell. More recent autoradiographic observations indicate that the stem cell, which differentiates into erythroid cells, is continuously proliferating in the polycythemic mouse, in spite of the fact that differentiation into erythroid cells does not occur (23, 24). The fate of these proliferation stem cells, if not triggered to differentiate into erythroid cells, cannot be resolved until the question of the pluripotential nature of the stem cell is settled.

Following the intravenous injection of erythropoietin into the polycythemic mouse, dispersion of the hormone must occur rapidly, and stem cells in various stages of their proliferative cycle must presumably encounter the hormone. When different doses of erythropoietin are injected and allowed to act in the polycythemic mouse for the limited period of 6 hr the erythropoietic response is stimulated to the same extent, even though the dose varies sixteen-fold. This suggests that only a small number of the stem cells stimulated by erythropoietin during these 6 hr is receptive to the differentiative action of the hormone. Which of the various stages in the proliferative cycle are receptive to the action of the hormone is an open question. Preliminary autoradiographic observations indicate that when H^3-thymidine and erythropoietin are injected into polycythemic mice at the same time, the nucleated erythroid cells present in the marrow two days later are rarely labeled; whereas, when the H^3-thymidine is injected at increasing intervals after the erythropoietin injection, increasing percentages of the nucleated erythroid cells are labeled. This suggests that the stem cells stimulated by the erythropoietin do not pass into the DNA synthetic phase of interphase (the S phase) either just before or after stimulation. Erslev (1) has shown in the rabbit that when mitotic

division was arrested by colchicine during a 20-hr period of anoxia, the onset of the reticulocyte response, though delayed one or two days, was not decreased. In similar unpublished experiments I have found that the injection of colcemid (1 mg/kg. body weight) into polycythemic mice simultaneously with exogenous erythropoietin has little effect on the development of the wave of erythropoiesis. However, the injection of the same dose of colcemid 24 hr after the erythropoietin injection almost completely depressed the erythropoietic response. This suggests that the stem cell is receptive to the action of erythropoietin sometime after metaphase and before the commencement of DNA synthesis. Lajtha et al. (5) recently proposed a model of stem-cell kinetics based on the concept that the stem cells are what he terms a Type IIb population. He defines this population as those cells capable of growth; at any single time only a random proportion of the cells are in this state of growth. The state of growth is defined as a cell cycle (G_1-S-G_2 periods) followed by cell division. The length of this cell cycle is constant. The cells not in cell cycle are in a state of dormancy or what Lajtha terms "G_0". He proposes that G_0 follows mitosis and is of an indeterminate length; and further, that differentiative actions on stem cells can occur only when the stem cells are in G_0, i.e., the cells are receptive only during G_0.

The fact that different doses of erythropoietin acting on the marrow for the limited period of 6 hr stimulate erythropoiesis to the same extent suggests, in terms of Lajtha's model, that all the cells in G_0 have been stimulated to differentiate. When, however, these same doses of erythropoietin are allowed to work longer periods of time, significant differences in the responses obtained for each individual dose of erythropoietin are observed. The increased erythropoietic response observed when 4.0 cobalt units act for an additional 6-hr interval, i.e., the dose acts for 24 hr instead of 18 hr, compared to the erythropoietic response observed when the same dose acts for the first 6-hr interval after injection, suggests that a continual recruitment of receptive stem cells occurs after the first exposure of the marrow to erythropoietin. The results obtained when divided doses of erythropoietin are injected also suggest that increased numbers of receptive cells are found in the marrow after the first exposure of the hypertransfused mouse to erythropoietin. This conclusion is also supported by the experiments in which the second dose of erythropoietin was allowed to act on the marrow for the limited period of 6 hr. Thus, it appears that very soon after the removal of receptive cells from the stem-cell population by the action of erythropoietin the stem-cell population detects the loss and recruits even larger numbers of receptive cells. How the stem-cell population detects this loss and directs the recruitment of more receptive cells is an intriguing problem for future work. The conclusion that a recruitment of stem cells occurs assumes that the increased erythropoietic responses observed in these cases are not the result of an action of erythropoietin on the differentiated but not yet identifiable erythroid stem cell, i.e., does not cause an increased number of divisions of cells that have already been committed towards the erythroid line of development. This assumption appears to be valid considering the effects of erythropoietin on the polycythemic mouse during the first 12 hr after the initial injection of erythropoietin, since the marrows of the erythropoietin injected and control mice cannot be distinguished cytologically from one another. However, at later times it cannot be assumed, on the basis of these experiments alone, that erythropoietin has no effect on early pro-erythroblasts. With these reservations, the results suggest that if most of

the stem-cell population is in a receptive state in the polycythemic mouse, i.e., in the state of G_0, the recruitment of even larger percentages of cells into G_0 from cells in cell cycle would be difficult to accomplish within 6 hr considering the time required for a proliferative cell cycle. In terms of Lajtha's model, it would appear necessary to postulate that if a large percentage of the stem-cell population is in G_0, these cells are receptive to the actions of differentiative agents only during limited times while in the state of G_0. Thus, the increased numbers of receptive cells in the present experimental situations could arise from divisions of stem cells, as well as an increase in the number of cells in a receptive stage of G_0.

Recently, Till, McCulloch and Siminovitch (25) have advanced a stochastic model of stem-cell kinetics, similar to Osgood's model (4), based on their experiments on the production of spleen colonies following the transplantation of hematopoietic tissue into lethally irradiated mice. They indicate that stem cells have a probability of either dividing and producing two stem cells or differentiating and leaving the population, i.e., a birth or a death process. They suggest that these probabilities are controlled. Either increased numbers of stem cells would occur if the probability of differentiation was decreased, or increased numbers of differentiated cells would result by decreasing stem-cell division. They conclude, however, that erythropoietin is not involved in regulating the "death" process but is involved in determining the path of differentiation, which the differentiated cell, produced as a result of the death process, will take (26). This conclusion, they claim, is necessary to explain the fact that the number of colonies formed by a cell suspension is not decreased in the presence of erythropoietin. Such a decrease would be expected in their model if the colony-forming cell is a stem cell. One could instead postulate that the differentiating effect of erythropoietin stem cells is simply decreased by an increase in the probability of a stem-cell division. The increased probability for stem-cell division may be regulated by the same mechanisms that bring about the recruitment of stem cells or erythropoietin sensitive cells.

SUMMARY

Following the injection of erythropoietin, either in a single large dose or in multiple doses, a change in the responsiveness of the hematopoietic tissue occurs. The fact that different doses of erythropoietin stimulate erythropoiesis to the same extent when the action of the hormone is limited to 6 hr by the injection of antibody suggests that the stem cells are receptive to the action of erythropoietin only at some limited time in their individual life cycle. It is suggested that this period is sometime after metaphase and before the commencement of DNA synthesis in the interphase state of individual stem cells. It is further suggested that the increased responsiveness of the hematopoietic tissue to erythropoietin following injection is due to recruitment of stem cells into this receptive state. This recruitment may be due to both the division of stem cells and the movement of cells through cell cycle into the receptive state. The results are discussed in relation to two recent models of stem-cell kinetics.

ACKNOWLEDGMENTS

The author wishes to express his appreciation for the valuable technical assistance of Linda N. Cantor and Virginia W. Havens.

This work was supported in part by the U. S. Atomic Energy Commission and in part by Cancer Research Funds of the University of California.

REFERENCES

1. Erslev, A. J.; Blood 14:386, 1959.
2. Alpen, E. L., and Cranmore, D.; in The Kinetics of Cellular Proliferation, edited by F. Stohlman, Jr., New York, Grune & Stratton, 1959, p. 290.
3. Stohlman, F. Jr.; Brecher, G., and Moores, R. R.; in Erythropoiesis, edited by L. O. Jacobson and M. Doyle, New York, Grune & Stratton, 1962, p. 162.
4. Osgood, E. E.; J. Nat. Cancer Inst. 18:155, 1957.
5. Lajtha, L. G.; Oliver, R., and Gurney, C. W.; Brit. J. Haematol. 8:442, 1962.
6. Gurney, C. W.; Lajtha, L. G., and Oliver, R.; Brit. J. Haematol. 8:461, 1962.
7. Gurney, C. W.; Perspectives in Biol. and Med. 6:233, 1963.
8. Garcia, J. F., and Schooley, J. C.; Proc. Soc. Expertl. Biol. Med. 112:712, 1963.
9. Schooley, J. C., and Garcia, J. F.; Proc. Soc. Expertl. Biol. Med. 109:325, 1962.
10. Schooley, J. C., and Garcia, J. F.; Proc. Soc. Expertl. Biol. Med. 110:636, 1962.
11. Schooley, J. C., and Garcia, J. F.; Blood 25:204-217, 1965.
12. Gurney, C. W.; Wackman, N., and Filmanowicz, E.; Blood 17:531, 1961.
13. Stohlman, F. Jr., and Howard, D.; in Erythropoiesis, edited by L. O. Jacobson and M. Doyle, New York, Grune & Stratton, 1962, p. 120.
14. Keighley, G.; in Erythropoiesis, edited by L. O. Jacobson and M. Doyle, New York, Grune & Stratton, 1962, p. 106.
15. Jacobson, L. O.; Goldwasser, E.; Plzak, L. F., and Fried, W.; Proc. Soc. Expertl. Biol. Med. 94:243, 1957.
16. Gurney, C. W., and Pan, C.; Proc. Soc. Expertl. Biol. Med. 98:789, 1958.
17. Krzymowski, T., and Krzymowska, H.; Blood 19:38, 1962.
18. Filmanowicz, E., and Gurney, C. W.; J. Lab. Clin. Med. 57:65, 1961.
19. Borsook, H.; Lingrel, J. B.; Sears, J. L., and Millette, R. L.; Nature 196:347, 1962.
20. Fruhman, G. J., and Fischer, S., Experientia 18:462, 1962.
21. Garcia, J. F., and Van Dyke, D. C.; Proc. Soc. Expertl. Biol. Med. 106:585, 1961.
22. Jacobson, L. O.; Goldwasser, E., and Gurney, C. W.; in Haemopoiesis: Cell Production and Its Regulation, edited by G. E. W. Wolstenholme and M. O'Connor, Boston, Little, Brown & Co., 1960, p. 423.
23. Gurney, C. W.; in Erythropoiesis, edited by L. O. Jacobson and M. Doyle, New York, Grune & Stratton, 1962, p. 194.
24. Schooley, J. C., and Giger, K.; Semiannual Report, Donner Laboratory, Lawrence Radiation Laboratory, UCRL-10683:176, 1962.
25. Till, J. E.; McCulloch, E. A., and Siminovitch, L.; Proc. Natl. Acad. Sci. 51:29, 1964.
26. Bruce, W. R., and McCulloch, E. A.; Blood 23:216, 1964.

Received December, 1964.

Microelectrophoretic and Enzymatic Studies Concerning the Carbohydrate at the Surface of Rat Erythrocytes

Robert M. Glaeser and Howard C. Mel

In recent years interest has increased in the degree to which carbohydrates play a role in the structure and function of mammalian cell surfaces. It has been reported that human red-blood-cell (RBC) stroma (ghosts) contain 4.4% by weight of carbohydrate, the principal sugars being sialic acid, hexoses (galactose, glucose, mannose, and fucose), and hexosamine (1). Similarly, plasma membranes from rat liver cells have been found to contain 0.065 μmole hexose, 0.050 μmole hexosamine, and 0.03 to 0.04 μmole sialic acid (N-acylated neuraminic acid) per milligram of protein (2). Furthermore, combined enzymatic and microelectrophoretic experiments have strongly indicated that the carbohydrate, sialic acid, exists at the outermost surface of a variety of RBC's (3), of Ehrlich ascites tumor cells (4, 5, 6), and of rat ascites tumor cells (liver carcinoma), normal human leukocytes, and human bone-marrow cells (7).

One specific function has already been assigned to surface carbohydrates of human RBC: Morgan (8), Watkins (9) and many others have shown that various simple sugars and some small polymers thereof help to determine the blood group antigens. Antigen carbohydrates, however, apparently comprise only a small fraction of the total surface carbohydrates (a present estimate would be about one part in 10,000), and the function of the remainder is largely unknown. In discussing his theoretical model of the plasma membrane, Bell (10) has suggested some possibilities in this regard.

In this paper we report a combined microelectrophoretic and biochemical study pertinent to carbohydrate constituents at the surface of rat RBC. The relation between electrophoretic mobility and cell charge, whether total or surface charge, has been discussed elsewhere (11). The most common interpretation, that mobility is determined by surface charge (from external ζ potential), will be adopted in this paper. Hydrodynamic and other factors being constant, the mobility should be proportional to the charge per unit area of the cell surface.

MATERIALS AND METHODS

RBC were obtained by withdrawing blood from the vena cava of ether-anesthetized adult Sprague-Dawley rats. Disposable plastic syringes were used without rinsing with anticoagulants. The blood was immediately delivered into 10 to 20 vol of buffer and centrifuged for 10 min at approx. $250 \times g$ in an International PR-1 refrigerated centrifuge. The supernatant fluid was removed by vacuum suction, and the cells were washed as before. The buffer solution used in this work was 0.145 M NaCl maintained at pH 7.3 ± 0.2 by 3×10^{-4} M $NaHCO_3$.

The enzyme preparations used are described in Table 1. RBC were incubated at 37°C at pH 7.3 ± 0.2 for the desired length of time, in a certain v/v concentration and enzyme concentration, as indicated in the section on results.

When chemical assays for enzymatically split products were desired, the cell suspension was centrifuged, the supernatant fluid pipetted off and any hemoglobin in the fluid was flocculated by heating for 3 min in boiling water. A clear solution was thus obtained by filtration through Whatman No. 42 filter paper. Free sialic acid was determined by the method of Warren (12), except that the final chromophore was extracted into 1.5 ml of cyclohexanone to increase the sensitivity of the assay, and the absorption spectrum was taken with a Beckman DK-1 recording spectrophotometer. Bound sialic acid was released in the free form (when necessary) after hydrolysis with 0.1 M H_2SO_4 at 80°C.

For the determination of electrophoretic mobilities, aliquots of cell suspension were withdrawn after various periods of enzyme treatment, and the cells were immediately washed twice with buffer. The apparatus and techniques used in the microelectrophoretic studies were the same as those previously described (13).

RESULTS

Electrophoretic mobilities were measured before and after incubation with enzyme. Unless otherwise stated, concentrations were 1% or 2% v/v for RBC, 1 mg/ml for enzyme. In the case of receptor-destroying-enzyme (RDE) treatments, the cell concentration was always 33% v/v, and the enzyme solution was diluted 1:1 with buffer.

RECEPTOR-DESTROYING ENZYME In two experiments the absolute value of the mobility decreased from 1.00 ± 0.03 to 0.70 ± 0.02 μ-cm per volt-sec, the cells being negatively charged at pH 7.3. Under these conditions the decrease in mobility required about an hour to come to completion. (Errors quoted are maximum deviations. According to our experience, mobility differences of less than about 0.05 mobility units are not significant.)

α-AMYLASE In three experiments the (negative) mobility decreased from 1.20 ± 0.05 to 0.55 ± 0.05 micron-cm per volt-sec (in two of these experiments the cell concentration during incubation was 33% v/v). In two further experiments the kinetics of the mobility decrease was studied. At an enzyme concentration of 0.5 mg/ml the (negative) mobility decreased from 1.25 to 0.69 micron-cm per volt-sec in less than 5 min, and no subsequent decrease occurred. At an enzyme concentration of 0.01 mg/ml the (negative) mobility decreased exponentially with time, from an initial value of 1.25 to a final value of 0.64 μ-cm per volt-sec. The half-time for the change was a little over 15 min. Further evidence for a change in the surface properties of α-amylase-treated RBC was observed in these studies. First, it was noted that the treated RBC had a tendency to stick to the surface of a glass container, and could not be readily detached from the glass (e.g., by swirling the liquid). Secondly, the RBC had a considerable tendency to adhere to one another when centrifuged, so that there was some difficulty in resuspending the pellet during the washing operations. This tendency to agglutinate was discovered to be much more severe at lower temperatures, when

Table 1. Name and characterization of enzymes used in this study

Name of enzyme	Specificity of enzyme action	Source of enzyme and purity	Enzymatic activity (manufacturer's quotation)	Range of pH optimum	Manufacturer and form available
Receptor-destroying enzyme (RDE)	The specific α-glycosidase cleaving the α-ketosidic linkage joining the potential keto group of a terminal N-acylated neuraminic acid to an adjacent sugar residue in a disaccharide, trisaccharide or polysaccharide; will cleave both a 2 → 3 and a 2 → 6 linkage.	Culture fluid *Vibrio cholerae* (unpurified)	Titer of 1:1,600 is the end-point dilution, using influenza PR-8 in the virus hemagglutination test.		Microbiological Associates (frozen solution)
α-amylase	An α(1 → 4)-glycosidase that attacks glycosidic linkages in the interior of a polysaccharide chain, with the formation of oligosaccharides. Hydrolysis can occur on either side of a branching point; i.e., at (1→6) glycosidic bonds.	Bacterial (B grade)	5,000 SKB units/g at 30°C	6.8-8.0	Calbiochem (dry powder)
β-amylase	An α(1 → 4) glycosidase that splits off disaccharides; action initiates at the non-reducing end of a polysaccharide chain, and action stops at branching point; i.e., at (1→6) glycosidic bonds.	Sweet potato(?) (B grade)	2,000 °C Lintner (α-amylase free)	4-6	Calbiochem (dry powder)
Hyaluronidase	Specific for the hydrolysis of glycosidic bonds involving the reducing group of N-acetylglucosamine.	Bovine testes (B grade)	> 300 U.S.P. units/mg	5.5-6.2	Calbiochem (dry powder)

an attempt was made to slow down the enzyme action by incubation at zero degrees C. In that case agglutination began even before centrifugation and was so severe afterwards that the pellet could not be resuspended. By contrast, neither the normal nor the RDE-treated cells showed such stickiness or adhesion.

After establishing that α-amylase could induce a reduction in the mobility of RBC, as well as induce changes in other surface properties, experiments were carried out to determine whether or not sialic acid was released from the RBC by this enzyme. In all cases a 33% v/v suspension of RBC in a 1 mg/ml solution of α-amylase was incubated at 37°C for 1 hr. Estimates of the amount of sialic acid present were obtained by assuming the molar extinction coefficient at maximum absorption ($\approx$ 553 mμ) to have the value 57,000, as reported by Warren (12).

Free sialic acid was not present in the supernatant liquid of α-amylase-treated RBC, as evidenced by a negative Warren test. Similar experiments with RDE showed a release of about 0.2 μmoles of sialic acid per 10^{10} RBC. Upon acid hydrolysis, free sialic acid did appear in the supernatant solution of α-amylase-treated RBC. The amount of free sialic acid present rose exponentially with time, reaching a maximum of 0.2 to 0.3 μmoles per 10^{10} RBC after 2 hr of hydrolysis of the supernatant material. Acid hydrolysis of the supernatant from RDE-treated RBC showed only a small degradation of free sialic acid under these conditions (about 4% per hr).

OTHER ENZYMES In one experiment with β-amylase, no change in mobility was observed, even after 120 min incubation. In another experiment with hyaluronidase, no change in mobility was observed, even after 85 min incubation. These negative results suggested that these enzymes were not acting upon the RBC surface structure, or at least not at pH 7.3.

DISCUSSION

INTERPRETATION OF THE OBSERVED SURFACE CHANGES As previously indicated in this paper, enzymatically induced changes in mobility are interpreted as resulting from changes in the surface of the RBC. Removal of sialic acid by either of the enzymes α-amylase or RDE coincides with a decrease in the (negative) mobility of RBC; this implies that sialic acid is responsible for at least part of the surface charge.

If sialic acid were to be completely responsible for the surface charge of untreated RBC, we could only conclude that the residual surface charge after enzyme treatment derives from ionogenic groups exposed upon removal of this carbohydrate. However, it cannot yet be determined to what extent a structural unfolding, if any, would accompany such an exposure of new groups.

A more profound alteration in the surface is produced by α-amylase than by RDE, since α-amylase-treated RBC show evidence of both stickiness and adhesion, as defined by Coman (14). Indeed, a larger carbohydrate moiety should be taken off by this enzyme, so it is not surprising to see greater changes in the surface properties.

For the α-amylase experiments, other possible interpretations of the mobility reduction should be considered: 1) adsorption of enzyme onto the RBC surface, and 2) action of a contaminant (e.g., a proteolytic enzyme) that might be present in the α-amylase preparation An adsorption mechanism seems unlikely, partly because of the kind of enzyme-concentration dependence observed for the kinetics of mobility decrease, but particularly in view of the known release of (bound) sialic acid by the enzyme. Regarding a possible active impurity in the 5,000 SKB unit/g α-amylase, such an impurity would presumably comprise less than 10% of the α-amylase present. Yet even at the 0.01 mg/ml α-amylase concentration a fairly rapid mobility decrease was noted. By contrast, Seaman and Uhlenbruck (15) report that 20 to 40 min incubation at 37°C is required for a similar mobility reduction with proteolytic enzymes, used at concentrations of 1 mg/ml or higher. Furthermore, a contaminant, if any, might reasonably be expected to be present in the other B grade enzymes used (see Table 1). Even at concentrations of 1.0 mg/ml, however, these latter produced no mobility change. A final cautionary word may be added. Certain glycoproteins associated with human red-cell membranes may not be affected by α-amylase (3).

STRUCTURAL PICTURE OF CARBOHYDRATE AT THE RBC SURFACE By a combination of microelectrophoretic and enzymatic techniques it has been strongly indicated that sialic acid exists at the outermost surface of RBC (16). No evidence has been found for the existence of ionizable surface groups with a pK 6.0 to 11.0 (see ref. 13 and others quoted there). One must therefore conclude that protein and phospholipid groups with pK's in this range (amino group of lysine, imidazolyl group of histidine, sulfhydryl group of cystein, hydroxyl group of tyrosine, the amino groups of serine and ethanolamine) probably lie deeper in the membrane structure than does sialic acid. It has in fact been suggested that the various ionogenic groups of sialic acid may be solely responsible for the surface charge of rat RBC in the pH range from 0.9 to 12.3, at ionic strength 0.145, see (13).

One might suppose that carbohydrate formed a continuous layer on the outer surface of RBC, allowing the ionic groups of sialic acid to dominate the surface charge. Yet simple calculations based on Ludewig's determination of total carbohydrate (1), and on the dimensions of the simple sugars involved, have indicated that carbohydrate could cover at most 1/4 to 1/2 of the total surface area (11). We have thus been led to believe that carbohydrate must be non-uniformly distributed and must stand out, on the whole, a bit farther than other ionogenic substances. Charge from ionized groups on proteins and phospholipids, lying sufficiently interior to the surface so that their counter-ions move with the cell as a whole (at least at ionic strength 0.145), would not be reflected in the electrophoretic mobility.

From the specificity of RDE, sialic acid must occupy the terminal position of an oligosaccharide. From the specificity of α-amylase, it must be concluded that this oligosaccharide contains at least two simple sugars for each molecule of sialic acid: at least one still bound to sialic acid after the action of α-amylase, and at least one remaining bound to the RBC surface. Conversely, using Ludewig's estimate that sialic acid constituted 25% by weight of the total carbohydrate (1), and using molecular weights of 309 and 180, respectively, for sialic acid and the other simple sugars, we would conclude that on the average the

oligosaccharide cannot contain more than five simple sugars for each sialic acid molecule. Proteolytic enzymes have also been shown to remove charge-determining carbohydrate, in the form of a sialomucoid (mucopeptide), from several kinds of RBC's (5, 15). We are now left with the intriguing biochemical prospect that the split products, cleaved from the RBC surface by the action of α-amylase and the various proteolytic enzymes, may be isolated and analyzed to give the sequence of simple sugars in the oligosaccharide, and the sequence of amino acids in the vicinity of its attachment to protein.

At the moment one can only speculate as to the possible function of carbohydrate at the cell surface, apart from its role as antigen. There hardly appears to be sufficient carbohydrate in mammalian RBC surfaces for it to be a major structural element, as in plant cells. Perhaps the carbohydrate lends specificity to intercellular contacts, just as it is responsible for the specificity of the blood group antigens (8). The probable position of the sialic acid-containing oligosaccharide at the outermost portion of the RBC surface is further reason to suggest that carbohydrate could play a role in determining the strength (or weakness) and specificity of intercellular contacts. Perhaps a function is to lend structural stability to the membrane proteins, which together with lipids are the major structural elements of cellular membranes. The carbohydrate might also play a physicochemical protective role for selected surface sites; glycoproteins are well known for their resistance to heat and other agents. The elucidation of the function of carbohydrate on the cell surface as well as the detailed mode of its incorporation into the surface structure are some of the most interesting problems for future study.

SUMMARY

The negative electrophoretic mobility of rat erythrocytes is reduced when these cells are incubated with bacterial α-amylase, indicating that the surface charge of the cells has been reduced by the action of this enzyme. Release of sialic acid in a bound form results from the enzymatic treatment. The α-amylase-treated cells also exhibit stickiness and adhesion, whereas the untreated cells do not. These alterations in surface properties are believed to be associated with the enzymatic cleavage of a sialic acid-containing oligosaccharide, probably located at the outermost portion of the erythrocyte surface. The possible role of surface carbohydrate on mammalian cells is discussed.

REFERENCES

1. Ludewig, S.; Proc. Soc. Exptl. Biol. Med. 104:250, 1960.
2. Emmelot, P.; Bos, C. J.; Benedetti, E. L., and Rümke, P.; Biochim. Biophys. Acta 90:126, 1964.
3. Eylar, E. H., and Matioli, G. T.; Science 147:869, 1965.
4. Cook, G. M. W.; Heard, D. H., and Seaman, G. V. F.; Exptl. Cell Res. 28:27, 1962.
5. Langley, O. K., and Ambrose, E. J.; Nature 204:53, 1964.
6. Wallach, D., and Eylar, E. H.; Biochim. Biophys. Acta 52:594, 1961.
7. Ruhenstroth-Bauer, G.; Fuhrmann, G. F.; Granzer, E.; Kübler, W., and Rueff, F.; Naturwiss. 49:363, 1962
8. Morgan, W. T. J.; Proc. Roy. Soc. (London) Ser. B. 151:308, 1960.

9. Watkins, W. M.; in The Red Blood Cell, New York, Academic Press, 1964, p. 359.
10. Bell, L. G. E.; J. Theoret. Biol. 3:132, 1962.
11. Glaeser, R. M.; Ph. D. Thesis, University of California, Lawrence Radiation Laboratory, UCRL-10898, July 1963 (unpublished).
12. Warren, L.; J. Biol. Chem. 234:1971, 1959.
13. Glaeser, R. M., and Mel, H. C.; Biochim. Biophys. Acta 79:606, 1964.
14. Coman, D. R.; Cancer Res. 21:1436, 1961.
15. Seaman, G. V. F., and Uhlenbruck, G.; Arch. Biochem. Biophys. 100:493, 1963.
16. Eylar, E. H.; Madoff, M. A.; Brody, O. V., and Oncley, J. L.; J. Biol. Chem. 237:1992, 1962.

Received April, 1965.

Effects of Simulated Altitude on Iodine Metabolism I. Acute Effects on Serum and Thyroid Turnover

Gilles LaRoche and Clarence L. Johnson

Studies on organ weights and histology have led Gordon et al. (1) to recognize the possibility of a slight reduction in thyroid activity associated with simulated altitude (250 to 280 mm Hg for 14 to 20 days). Van Middlesworth (2) demonstrated a definite change in the 24-hour ^{131}I distribution of rats submitted to simulated altitude (268 mm Hg for 36 hr). The author then interpreted the significant drop in the 24-hr plasma protein-bound radioiodine and thyroid uptake as evidence of decreased thyroidal activity. Verzar et al. (3) have indicated that an acute decrease in ^{131}I thyroid uptake can be noted in rats placed at reduced pressures of 490 mm Hg or lower. It was also pointed out that after four or five days of exposure to reduced pressures the uptakes were returned to levels observed in animals at 732 mm Hg. Recently De Bias and Yen (4) have indicated that rats exposed to simulated altitude (282 mm Hg for 6 hr) demonstrate evidence of increased thyroid function.

A preliminary investigation by La Roche, as reported by Siri et al. (5), on the effects of simulated altitude (395 mm Hg for four days) in a human male showed a significant change in serum stable iodine. Protein-bound iodine (PBI) and total iodine determinations were performed before, during and after exposure to simulated altitude. A rise in both values (Table 1) was noted. This change was found to persist throughout the period of simulated altitude. Upon closer examination the PBI values were showing an impressive rise, and total iodine increase only appeared as the dampened result of this phenomenon. As calculated by difference (Table 1), serum iodide decreased significantly and accounted for the less dramatic changes in total iodine. From this it seemed that the PBI rises were accompanied by a depletion of circulating iodide reserves. It was also noticeable that after one month at sea level, following exposure to simulated altitude, the PBI determinations were practically back to their original values, but serum iodide had only shown a partial recovery. Thus, simulated altitude might have induced an acute rise in thyroid-hormone synthesis, as indicated by the increase in serum protein-bound iodine. This conclusion seemed further warranted by the dramatic depletion of serum iodide which remained affected for at least one month following a return to sea-level environment. The present report will show that simulated altitude (395 mm Hg for a period of up to 15 days) induces a significant change in iodine turnover, as observed through combined ^{125}I and ^{127}I studies in rats.

MATERIALS AND METHODS

Sixty five 300-g male albino rats (Sprague-Dawley purchased from Charles River) were received in February, 1964. The animals were kept four per cage and held five weeks for

Table 1. Effect of decompression on serum iodine in human (μgm I/100 ml).

Treatment	PBI	Iodide*	Total
October 22			
Sea-level	3.4	1.7	5.1
October 23			
Sea-level	3.7	1.7	5.4
October 24			
Decompression	4.8	0.5	5.3
October 25			
Decompression	6.6	0.4	7.0
October 26			
Decompression	6.2	---	---
October 27			
Decompression	5.7	0.4	6.1
October 29			
Sea-level	4.8	0.4	5.2
November 21			
Sea-level	4.0	0.7	4.7

*Obtained by difference

environmental and dietary adjustments. During the entire period all rats received ad libitum a commercial pelleted diet (Simonsen & Co., Gilroy, California) containing 1.8 μg I per gram and tap water containing 0.03 μg I per 100 ml. Five rats were used to measure the level of intrathyroidal stable iodine.

Each of the sixty animals received a single intraperitoneal injection containing 60 μCi ^{125}I in 0.5-ml normal saline medium. Thirty control animals remained at atmospheric pressure until scarificed. Thirty experimental animals were immediately placed in an altitude chamber containing a dehumidifying unit, and the pressure was lowered to a simulated altitude of 17,000 feet (395 mm Hg). Every day, sea-level pressure was reinstated for periods of 10 to 15 min to allow for removal of animals and/or cleaning.

Five or six animals from each group were sacrificed at 1, 2, 3, 8 and 15 days following the injection. At the time of sacrifice the animals were anesthetized with ether and weighed. Then the blood was removed by puncture of the aorta at the apex of the bifurcation leading to the legs. The thyroids were excised, weighed and immediately homogenized in

0.5 ml NaCl-Tris buffered solution, and the homogenates were placed in an ice bath. These homogenates were hydrolyzed with 2.5 mg pronase. Two drops toluene were added to inhibit bacterial growth and possible interferences. Hydrolysis proceeded at 37°C for 4 hr. Upon completion duplicate 50-μl aliquots were placed on Whatman number 3 mm paper for ascending chromatography by the method of Rosenberg, et al. (6). Duplicate 100-μl aliquots were taken for microchemical analysis of iodine content, and 10-μl aliquots for determining thyroid ^{125}I uptakes. Following chromatographic separation and radioautographic resolution, individual bands corresponding to thyroidal iodinated amino acids were cut out and placed in plastic counting vials for ^{125}I counting. Microiodine determinations were performed on the same fractions. (Intrathyroidal distribution of iodine (^{125}I and ^{127}I) will be presented in another paper of this series.)

The blood obtained at sacrifice was centrifuged at 2,500 rpm for 15 min. The serum was collected and 500-μl aliquots were taken for total serum microiodine determinations. Similarly, 500-μl aliquots, passed through 3-cm anionic exchange resin columns (CG-400), were collected for protein-bound (NAI) microiodine determinations, La Roche, et al. (7). Varying amounts of serum were used to estimate the total ^{125}I concentrations (50- to 200-μl aliquots) and protein-bound ($NA^{125}I$) (100- to 500-μl aliquots).

The combined results of thyroidal ^{125}I and $NA^{125}I$ were submitted to a mathematical analysis, Rescigno (8) and Resigno and Segre (9), and estimates of the acute effects of simulated altitude on the glandular secretion rate and turnover time were estimated.

RESULTS

Body weights (Fig. 1) of animals placed in the altitude chamber were significantly depressed after two days ($P < 0.01$). This effect appeared to persist throughout the exposure which lasted for 15 days.

The total thyroid ^{127}I content (Fig. 2) becomes significantly higher ($P < 0.05$) on the 3rd and 8th day of exposure to simulated altitude. However there were no significant differences on the 1st, 2nd and 15th days. In addition, a significant but ephemerous rise in the thyroid ^{127}I concentration (Fig. 3) seems to precede this phenomenon and to occur on the 2nd day only. When both series of values (total thyroidal ^{127}I contents and thyroidal ^{127}I concentrations) are corrected for animal size (Fig. 4), significant increases in stable iodine can be observed from the 2nd day and including the 15th day. Both of these corrected glandular total values and ^{127}I concentration values have decreased considerably and indicate a return to a relationship generally found between thyroid ^{127}I content and body weight.

The glandular ^{125}I uptake was significantly increased by simulated altitude on the 2nd, 3rd and 8th day. The controls had an average maximum uptake of 3.8% of the injected dose at 24 hr and an average retention of 0.8% at 15 days (Fig. 5).

Serum ^{127}I concentrations of rats exposed to simulated altitude show drastic declines which lasted at least eight days after the beginning of treatment (Fig. 6). Total serum ^{127}I,

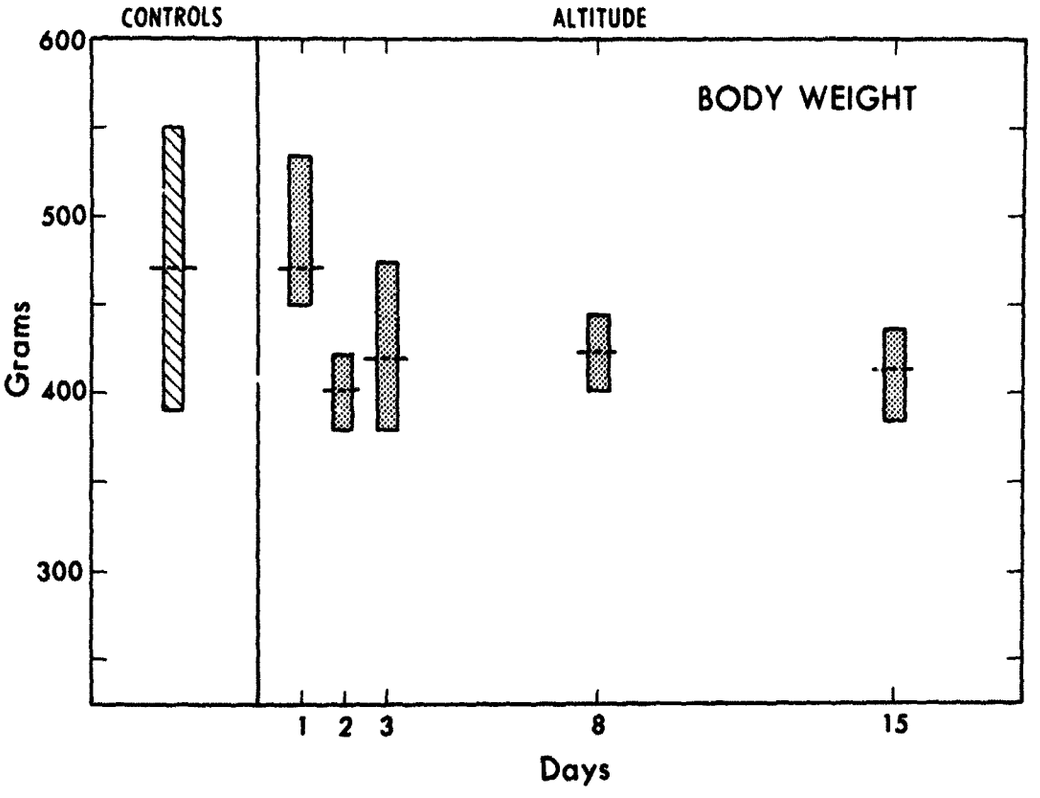

Figure 1 MUB-4394

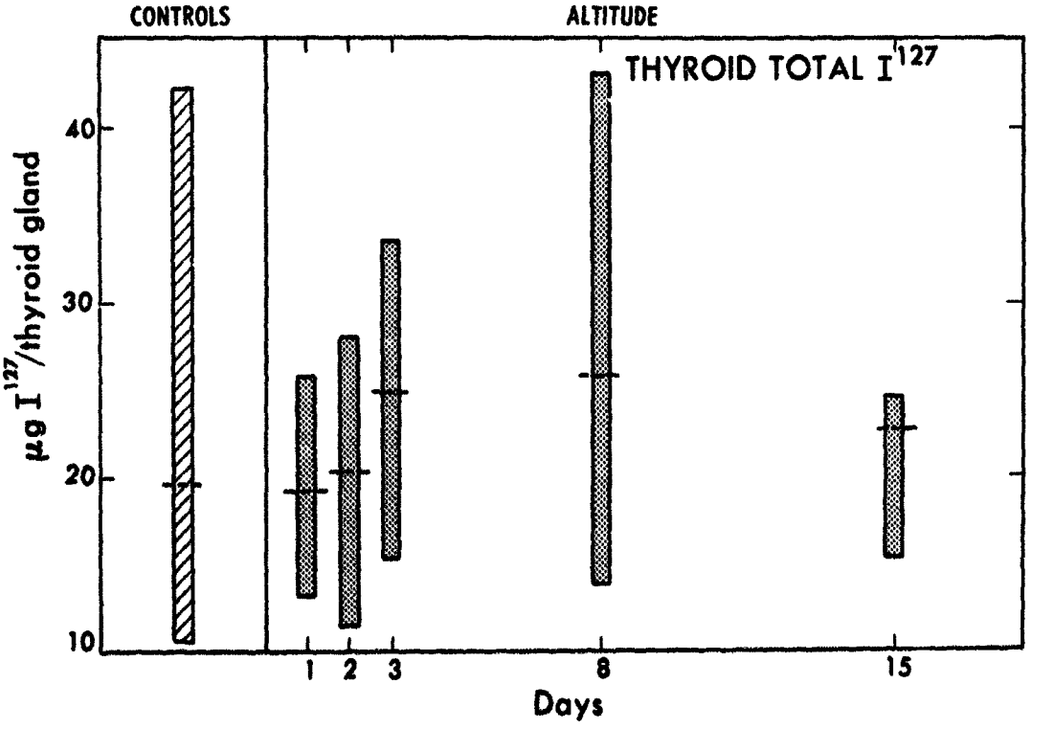

Figure 2 MUB-4396

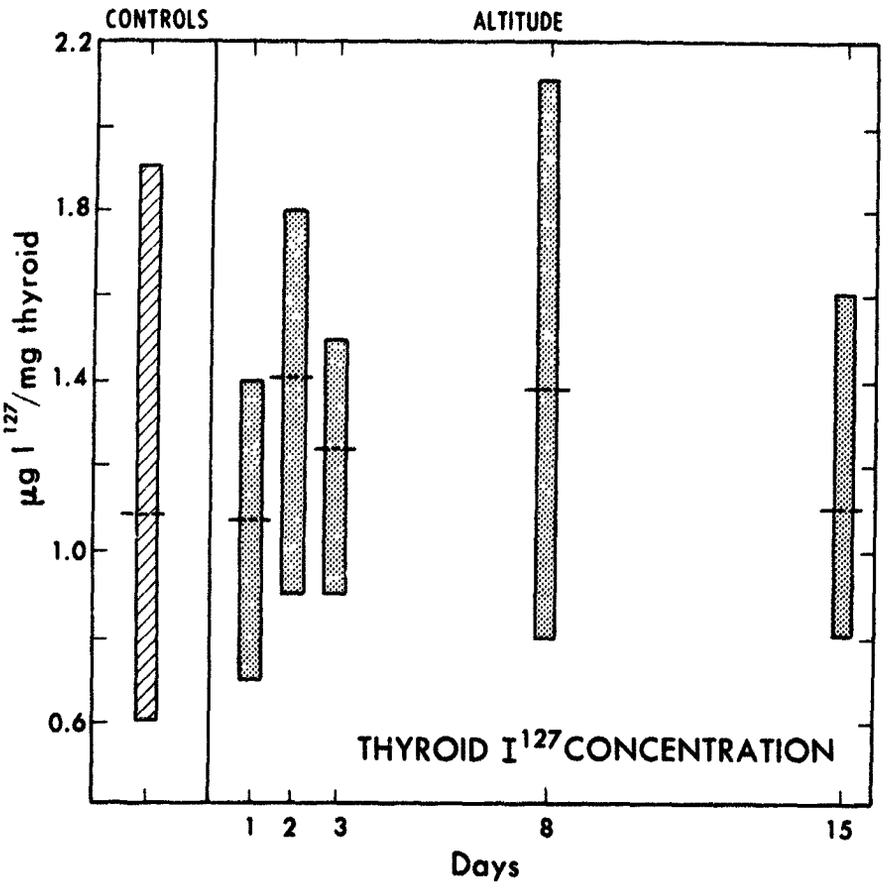

Figure 3

MUB-4395

protein-bound ^{127}I ($NA^{127}I$) and iodide (^{127}I) were significantly ($P < 0.05$) lower for all days except the 15th. However ^{125}I serum parameters varied in quite a different manner. During the first two days of simulated altitude the total serum ^{125}I did not appear significantly different from control values (Fig. 7). On the other hand, the serum $NA^{125}I$ and iodide (^{125}I) for these same periods were respectively lower ($P < 0.01$) and higher ($P < 0.05$) (Fig. 7). On the 3rd, 8th and 15th day of exposure to simulated altitude the total serum ^{125}I was significantly higher ($P < 0.01$) (Fig. 7). The $NA^{125}I$ was not affected on the 3rd and 8th day of exposure, but this value became significantly higher ($P < 0.02$) on the 15th day (Fig. 7). As for the iodide (^{125}I), there was no significant difference on the 3rd and 15th day, but on the 8th day of altitude exposure there was a significant rise of this parameter ($P < 0.01$) (Fig. 7). In controls, the maximum $NA^{125}I$ level was reached at approximately 2 days whereas this value was not reached before the 3rd day in animals submitted to altitude. The maximum serum $NA^{125}I$ of controls at 2 days (Fig. 7) seems to follow closely the maximum thyroidal ^{125}I uptake at 1 day (Fig. 5). However the maximum $NA^{125}I$ of altitude-treated rats (Fig. 6) occurred at approximately the same time as the maximum thyroidal ^{125}I uptake (Fig. 5), i. e. at 3 days.

Estimates of thyroid secretion rates (8, 9) were 2.2% of the injected dose of ^{125}I for controls and 0.5% for treated rats. Similarly, the thyroidal-iodine-turnover time was 23 and 100 days for controls and treated respectively.

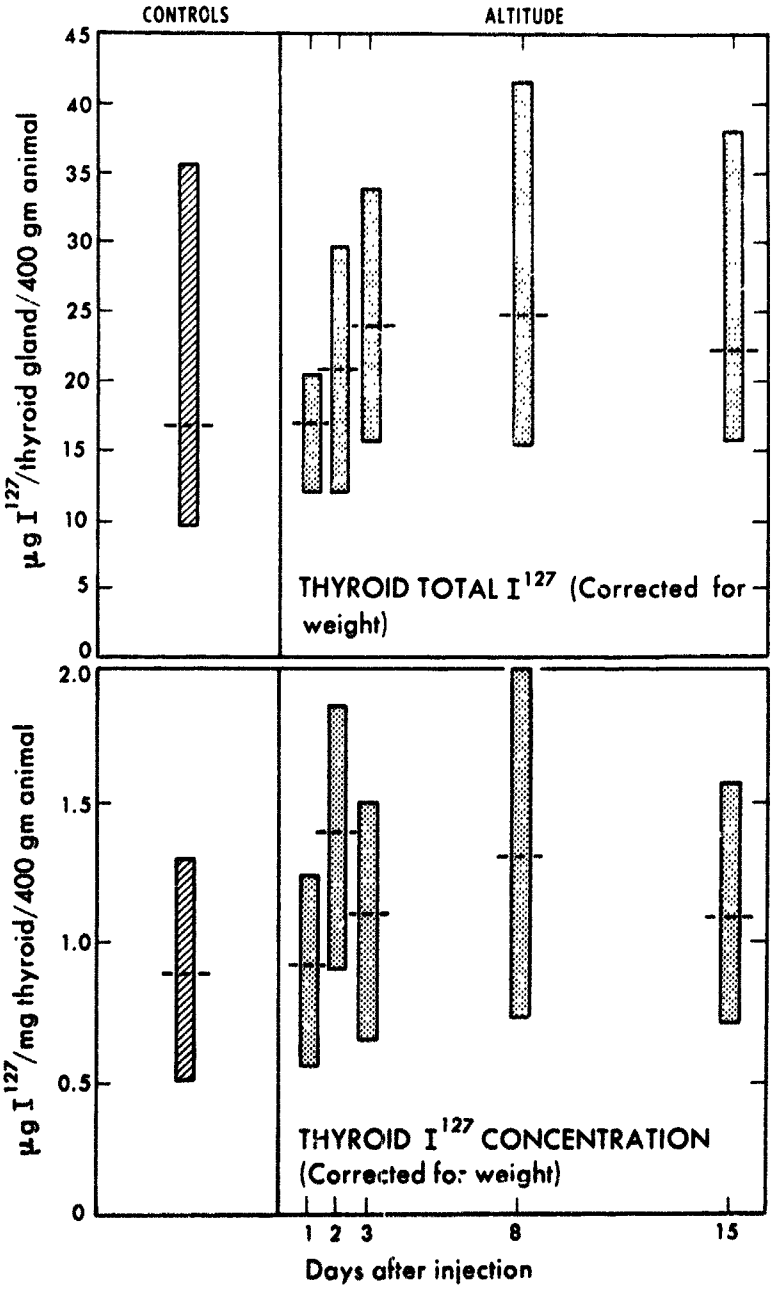

Figure 4

MUB-4617

DISCUSSION

The loss of weight ($P < 0.01$) noticed on the second day of decompression (Fig. 1) is undoubtedly related to a loss of appetite and a loss of depot fat that are generally associated with hypoxia. The last effect is possibly the result of extensive triglyceride lipolysis as noted, under similar conditions, by Uspenskii and Chou-Su (10). Figure 4 represents values of Figs. 2 and 3, corrected for animals size. The observations can be made here that the acute weight loss is not immediately followed by a compensatory loss of thyroidal iodine. However, it would seem that at 15 days the thyroid gland began to readjust its iodine content to a lower level (Fig. 4) commesurate with the loss of body weight that persists (Fig. 1).

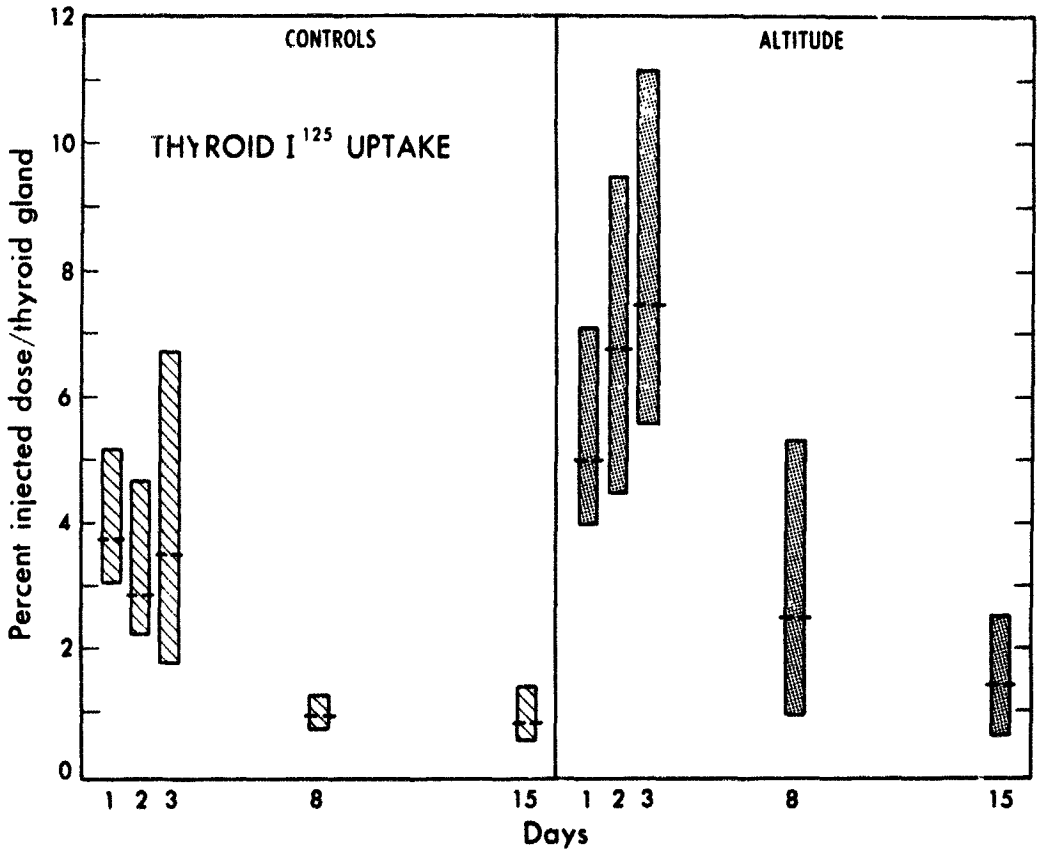

Figure 5

MUB-4537

An ultimate increase in thyroidal-secretion rate at or around 15 days appears confirmed by the increased levels of NA^{127}I (Fig. 6) and NA^{125}I (Fig. 7).

According to the changes in thyroid ^{127}I content, ^{127}I concentration and ^{125}I uptakes, it appears that altitude stimulates acute responses that do not appear to extend far beyond 15 days (Fig. 4). First there is an ^{125}I thyroidal uptake, which keeps rising beyond 24 hr and remains significantly higher from the 2nd day through the 8th day (Fig. 5). Second, a significant increase in thyroid ^{127}I concentration occurs on the second day and matches the extended rise in ^{125}I uptake. Finally there is an increase in total ^{127}I content of the gland which is significant on days three through eight. None of these parameters are significantly different between treated and controls on either the 1st or the 15th day of treatment. From these results it is suggested that altitude stimulates a prolonged and higher uptake of iodide, which results in an increase in thyroid-tissue iodine concentration on the 2nd day only (Fig. 3). The increase in total iodine content would then be overshadowed on days three through eight by a compensatory hypertrophy or hyperplasia of the gland, which would bring the thyroidal ^{127}I concentration back to control levels (Fig. 3).

Concentrations of the two isolated serum ^{127}I fractions are depressed from the 1st through the 8th day of decompression (Fig. 6). This may result from either an increase in thyroid ^{127}I concentration, appearing on the second day (Fig. 3), or possibly a stimulated iodine excretion, or both.

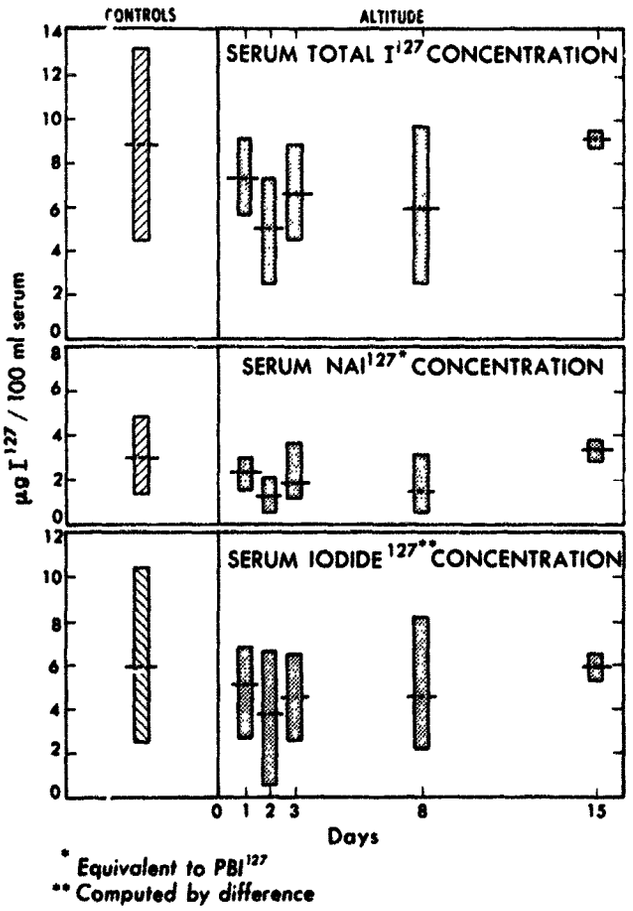

Figure 6

MUB-4397

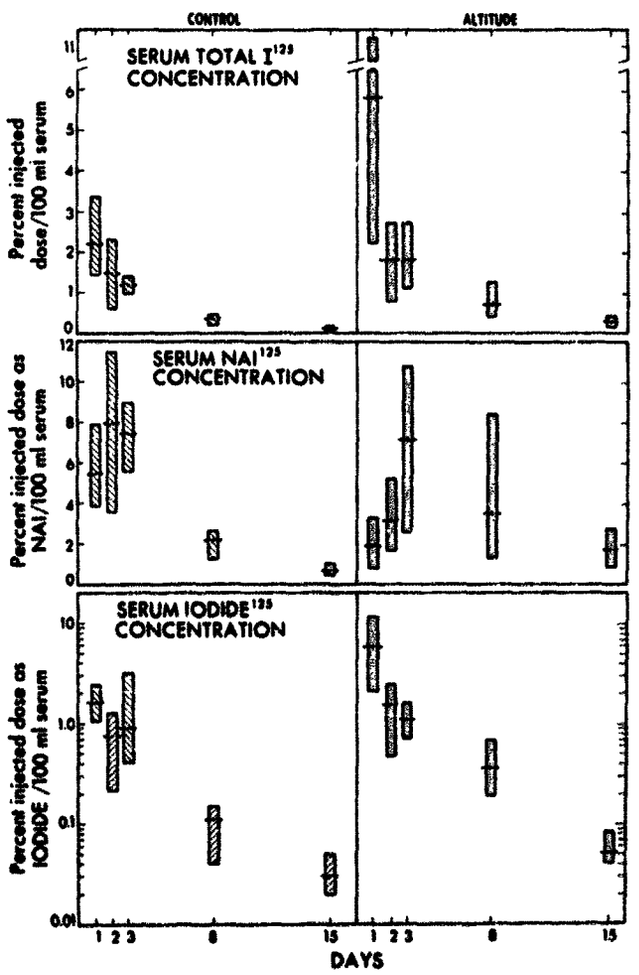

Figure 7

MUB-4398

Figure 7 indicates that serum total ^{125}I is not affected during the first two days of simulated altitude. On the other hand, for this same period of time NA^{125}I's are significantly reduced ($P < 0.01$) and iodide (^{125}I) values are increased ($P < 0.05$) (Fig. 7). Thus the cumulated differences nullify changes in serum total ^{125}I at these time periods. Again, serum ^{125}I turnover changes (Fig. 7) may reflect some thyroidal involvements, but it is not possible at this time to eliminate possible changes in iodine excretion associated with simulated altitude.

As observed by Van Middlesworth (2), the 24-hr concentration of serum protein-bound iodine is lower in treated animals than controls. However, it should be stressed that observations extending over a longer period of time reveal a more gradual iodine binding as well as delayed protein-bound iodine turnover in anoxic rate. Therefore it would appear premature to claim a suppression of thyroid activity, Van Middlesworth (2), on the basis of a single series of observations at 24 hr.

The work of Verzar et al. (3) is difficult to analyze and compare, in view of certain technical liberties which included their re-use of some experimental animals and the presentation of uptakes in counts per minute rather than percent of the injected dose. Nevertheless, the authors claim a reduction in thyroid activity identified by a decrease in the rate of thyroid ^{131}I uptake over a period of 48 hr. Also mentioned is the effect of dietary iodine on thyroid metabolism. However there are no reports on iodine intakes of these rats. In spite of these uncertainties it appears that an acute slowing in the rate of thyroid uptake can be associated with high altitude.

De Bias and Yen (4) have cl d an increase in thyroid function associated with decompression. In this case, measurements at a specific time (either 24 or 54 hr) were made without consideration to possible changes in patterns of thyroidal uptake or release over an extended period, which might have led the authors to reach an opposite conclusion.

Fregly (11) has shown that anoxia (13% oxygen over 100 hr) at 760 mm Hg reduces thyroid activity, as suggested by a lower thyroid to serum ^{131}I-conversion ratio. On the other hand, Felig et al. (12) have demonstrated a significant lowering in the PBI values of rats exposed to 99% oxygen. In this last instance it is tempting again to claim a reduction in thyroid gland activity, whether the phenomenon is induced by a direct glandular effect or mediated through the pituitary or adrenal glands. However, as indicated by these authors, exposure to high oxygen levels may also have marginal effects, such as increasing thyroid-hormone clearance or decreasing thyroxine-binding capacity, among several possibilities.

PBI's (or NAI's) alone should not be regarded as definitive indications of thyroid activity. They may furnish an indirect measure of thyroid function, as the oversimplified diagram (Fig. 8) shows, but should never be the sole criterion to be relied upon. The PBI (or NAI) is a concentration of transient serum organically-bound iodine that can vary without changes in thyroid output (Fig. 8, flow through A would remain constant): a) NAI or PBI would rise if the rate of flow through B remains temporarily lower than that through A;

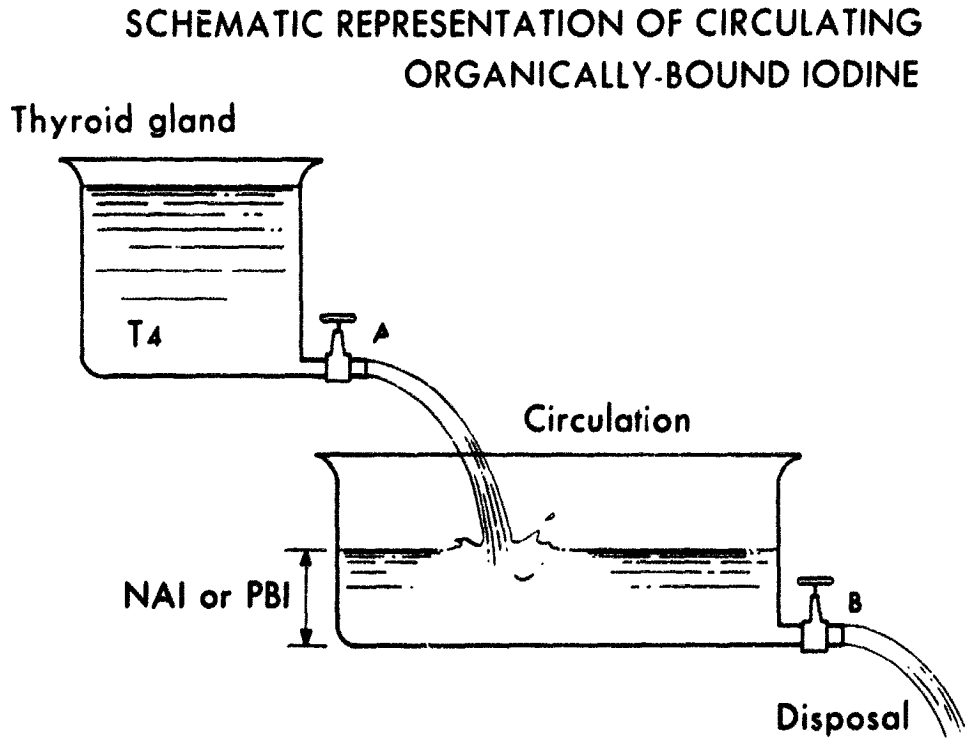

Figure 8 MU-30156

b) NAI or PBI would decrease if the rate of flow through B would become greater than that A. This simplified representation is functionally complex, even without introducing the possibility of an independent increase or decrease recirculation of metabolized T_3 and/or T_4 as sulfates or glucuronides, Roche et al. (13), for instance. However, this simple diagram is chosen deliberately in order to emphasize the limits of a momentary indirect serum on concentration estimate in evaluating thyroid function.

A situation, without changes in thyroxine binding capacity, can thus be summarized as follows: 1) in an uncomplicated rise in thyroid output without a corresponding increase in the rate of hormonal disposal, an increase in NAI or PBI can be expected; 2) if the rate through B rises or falls proportionally to that through A, NAI or PBI would remain normal even though goitrous states might be present; 3) an increased rate of thyroid metabolite disposal (increase in iodine excretion through B while A remains constant) would erroneously suggest an inadequate thyroidal output through a lowering of NAI or PBI.

As can be noted, it is rather fortunate when NAI or PBI can be associated with changes in thyroid activity. At best this parameter can be a cumulative rather than instantaneous sign of thyroid malfunction. This conclusion is all the more plausible when considering that chemical NAI or PBI estimates are often made on 0.5 ml of serum with an accuracy of approximately 5%, and that thyroidal secretion rates would likely be followed by a compensating change in disposal rates that might only bring a slight differential and/or temporary change in concentrations of transient metabolites. It is obvious that small changes

in protein-bound iodine might pass unnoticed and that it is only through a multiplicity of indirect tests that a thyroid gland status can be assessed with any degree of certainty.

From the present results it appears that a functional dichotomy exists between thyroidal iodine uptake (^{127}I: Fig. 2, days two and three; ^{125}I: Fig. 5, days two, three and eight) and thyroidal-secretion rates as evidenced by serum NAI levels (^{127}I: Fig. 6, days one, two, three and eight; ^{125}I: Fig. 7, days one and two). It would therefore be preferable to avoid identifying states of thyroid activity by uptakes alone or by PBI's (or NAI's) alone. Further, examination of one thyroidal parameter at various times after exposure to simulated altitude or several thyroidal parameters at only one time period is not sufficient to serve as measures of thyroid activity with any degree of accuracy.

Thus, in rats on an adequate iodine intake, sudden exposure 17,000 ft induces a temporary increased thyroidal iodine uptake (Figs. 2, 3, 4 and 5) and a decrease in serum iodine (Fig. 6). These early changes are also associated with what appears to be a lower thyroxine secretion rate, as suggested by NA^{127}I and NA^{125}I, which remains significantly lower on the first and second day of exposure to altitude (Fig. 7). A mathematically derived thyroid-secretion rate also reveals an acute four-fold reduction associated with simulated altitude. This reduction in the thyroid secretion rate of rats exposed to the above mentioned altitude is difficult to conciliate with a sudden rise in PBI observed in a man submitted to similar conditions (Table 1). However, it would not be unlikely that this phenomenon in man could result from decrease in the rate of circulating-thyroid-hormone utilization. If similar to the findings in rats, an increased thyroidal ^{127}I-uptake could then account for a decrease in circulating iodide concentration (Table 1).

ACKNOWLEDGMENTS

The authors wish to acknowledge the cooperation of William Siri and the assistance of Dorothy Carpenter, Georgia Reichert and J. M. London.

REFERENCES

1. Gordon, A. S.; Tornetta, F. J.; D'Angelo, S. A., and Charipper, H. A.; Endocrinology 33:366, 1943.
2. Van Middlesworth, L.; Science 110:120, 1949.
3. Verzar, F.; Sailer, E., and Vidovic, V.; J. Endocrinol. 8:308, 1951-52.
4. De Bias, D. A., and Yen, Wang; U. S. A. F. Tech. Docum. Report (SAM-TDR-63-101), 1963.
5. Siri, W.; Van Dyke, D. C.; Winchell, H. S.; Pollycove, M., and Parker, H. G.; Semiannual Report, Donner Laboratory, Lawrence Radiation Laboratory, UCRL-10683:59, 1962.
6. Rosenberg, L. L.; Dimick, M. K., and La Roche, G.; Endocrinology 72:749, 1963.
7. La Roche, G.; Carpenter, D., and Coxworth, A.; Semiannual Report, Donner Laboratory, Lawrence Radiation Laboratory, UCRL-11387:152, 1964.
8. Rescigno, A.; Ann. N. Y. Acad. Sci. 108:204, 1963.

9. Rescigno, A. and Segre, G.; Semiannual Report, Donner Laboratory, Lawrence Radiation Laboratory, UCRL-11184:141, 1963.
10. Upenskii, V. I., and Chou-Su; Patol. Fiziol. Eksper. Terap. 7:60, 1963.
11. Fregly, M. J.; U. S. A. F. Tech. Docum. Rep. (SAM-TDR-63-4), 1963.
12. Felig, P.; Goldman, J. K., and Lee, W. L. Jr.; Science 145:601, 1964.
13. Roche, J.; Michel, R.; Closon, J. and Michel, O.; Biochim. Biophys. Acta 33:461, 1959.

Received December, 1964.

Fertilization in Drosophila II.
Time of Inactivation of a Gene Effect

Philip E. Hildreth

The discovery that X irradiation of Drosophila melanogaster embryos can inactivate the effect of a suppressor gene and thus influence developmental processes that are to unfold several days later was reported by Glass and Plaine in 1950 (1). In the same report it was also shown that irradiation of fertilized eggs, still in meiotic stages, produced similar results, the effect of the suppressor gene having been negated by X rays. Specifically, the experiments involved the gene er (erupt eyes) and its suppressor Su-er. Flies homozygous for er in most cases have large outgrowths of nonfaceted material near the center of one or both eyes, and in some cases several bristles may be present; in weaker manifestations of this character the facets may be merely disarranged, or there may be only an extra bristle at the anterior margin of the eye. When er/er individuals are homozygous for Su-er, the effect of the erupt gene is suppressed almost completely, but occasionally flies may show either the weak or extreme erupt phenotype. The above authors observed that when eggs or larvae from parents homozygous for both er and Su-er were irradiated with 1,000 R of X rays, the effect of the suppressor gene was inactivated. As a result, about 90 to 100% of the treated individuals had erupt eyes. Even when eggs only 8±8 min old were irradiated, there was 100% inactivation of the Su-er effect, but irradiation of eggs and sperm prior to fertilization failed to cause such inactivation. Assuming that these 8±8-min-old eggs "could hardly have reached the first cleavage division, on the average," Glass and Plaine concluded that the entrance of the sperm into the egg immediately activates it to produce "at least one specific gene-initiated substance or morphogenetic system," and that this is inactivated by X rays. During the second and third larval instars, X rays had a progressively diminishing inhibitory effect on the action of Su-er, indicating "either that the primary gene product or substrate is gradually being used up, or that the morphogenetic system in which the product (or substrate) participates has advanced beyond the stage at which the product or substrate can modify it." Since this report, Su-er has been often considered the earliest-acting gene in the development of a multicellular organism (2). Glass and Plaine stated further that "the target altered in nature by irradiation is probably to be identified as a product of the suppressor gene, ..." In 1957, however, the senior author (3) pointed out that an alternative interpretation is possible according to which "the sensitive substance" may be "an essential substrate or precursor for the gene's action," and if the latter is the case then "the action of the suppressor might actually be concurrent with differentiation of the eye."

Recent cytological evidence (4) has shown that, even when females are induced to lay eggs rapidly and collection periods are only five minutes, still a certain percentage of eggs are already in cleavage stages at the time of fixation. The mortality rate of irradiated eggs is known to vary with treatment during meiosis and early cleavage stages (5), but the eclosion frequencies taken from the data of Glass and Plaine do not appear to be what one would expect if their egg samples were homogeneous in age when treated and the dose given were 1,000 R. Accordingly, it is possible that their samples contained some eggs that might have been retained for several hours after fertilization by the females, and that only these eggs survived and were induced to have the erupt phenotype. It was decided to repeat their experiments, with special effort being made to accurately time the developmental stages of the treated eggs. If the hypothesis is correct that the effect of the suppressor is not inactivated in very early stages, then the present methods should produce no, or very few, erupt-eyed flies. The results to be reported herein tend to support this expectation.

MATERIALS AND METHODS

STOCKS The flies used in these experiments were kindly supplied by the California Institute of Technology and by Professor Bentley Glass. The first stock, B82, homozygous for the genetic markers Su-er, tu (tumor), bw (brown eyes) on the second chromosome and st (scarlet eyes), er, su-tu (suppressor of tumor) on the third chromosome was used without modification. Stock B92A, Su-er bw; st er originally had attached-X chromosomes and the males carried a genetically marked free X; unmarked and nonattached-X's were substituted for these. The third stock, B91;83, was synthesized by combining Su-er bw from stock 91 with st er from stock 83; this stock also had free and unmarked X chromosomes.

EGG COLLECTIONS AND CULTURES Virgin females and males were collected and aged separately for six to eight days in vials containing well-yeasted cornmeal-molasses-agar medium. About 30 females and 60 males were stored in their separate vials and were transferred to fresh culture vials two or three times during the aging period. Early in the morning on the day the experiments were to be carried out, the stored females were shaken into the vials with the males. Between 2 and 3 hr later the flies from each vial were shaken into the egg-collecting tubes (Hildreth and Brunt (4)). Eggs collected during the first hour were discarded in order to reduce the number of eggs that might have been retained by the females. Collection periods for the experiment were from 5 to 30 min, depending on whether the samples were to be irradiated immediately, aged, or used for controls. After the "immediate" irradiations, eggs were transferred to small squares of water-soaked green blotting paper, lined up for easy counting and placed in culture vials containing yeasted cornmeal-molasses-agar medium. The control samples and those to be irradiated later were transferred as soon as each collection was terminated. Not more than 50 to 60 eggs were placed in any control or late-irradiation vial to ensure that cultures would be uncrowded, but up to 100 or more were placed in a few immediate-irradiation cultures as the irradiation would prevent the great majority of eggs from hatching. Upon eclosion, the eyes of the adults were examined with the aid of a binocular dissecting microscope at a magnification of 37.5. The eyes were classified as normal, weak erupt, or extreme erupt. The cultures were kept until it was apparent that

no more adults would eclose and in no culture did any eclose after the fourteenth day. Some collections were made at room temperature and others at 25° C. All cultures were kept at 25° C.

IRRADIATIONS To eliminate the possibility that the intensity or wave length of X rays used might account for the differences that became apparent between my results and those of Glass and Plaine, it was decided to use three machines, each with different kilovoltage, milliamperage, and filtration. In most experiments an Andrex industrial machine with a Eureka tube having 1.5-mm aluminum inherent filtration was used; operated at 140 kV, 4 mA, with no added filtration at a target distance of 9-1/4 in., the machine delivered about 105 R/min. The second was a Philips X-ray machine with a Philips tube having 1.4-mm aluminum inherent filtration. This tube delivered about 110 R/min when operated with no added filtration at 60 kV, 15 mA, and at a target distance of 12 in. The third, a Picker X-ray machine with a Machlett tube having 2-mm beryllium inherent filtration, delivered about 250 R/min at a target distance of 6-3/8 in. when operated at 50 kV, 16 mA, with 1.0-mm aluminum added filtration. The total dose given with any of these machines was 1,000 or 1,500 R. Irradiations of the immediate and 30-min groups were terminated late in the afternoon so that even if a female was inseminated as soon as placed with the males, and a fertilized egg was retained until just prior to the last irradiation, such an egg could not have been more than about 8-1/2 hr old when treated.

CYTOLOGY In order to estimate the frequency of eggs that might be in meiosis or in stages prior to the first cleavages when treatment was initiated, eggs were taken from 10-min collection periods, placed on cover slips, and fixed within the next 8 to 10 min. The eggs were then stained by the Feulgen whole-mount procedure (6) and scored as to their stages of development.

RESULTS

When eggs from stock B82 were irradiated, the results were quantitatively different from those of Glass and Plaine. Eggs treated when 16 to 21 hr old yielded only about 18% erupt-eyed individuals, with 11% being of the extreme phenotype (Table 1). However, when young eggs were irradiated, none of the surviving individuals showed the erupt phenotype. Since Glass and Plaine obtained high yields of extreme erupt when eggs were irradiated during any developmental stage, it was decided to try a second stock derived from one supplied by Professor Glass. This stock, B92A, produced results similar to those from B82. When eggs 10 hr and 17 to 19-1/2 hr old were irradiated, the yield of individuals with erupt eyes was low (Table 1) when compared with the results obtained by the earlier authors, and irradiation of young eggs, even up to 141 min old, failed to produce the erupt phenotype in any of the adults.

The stock B91;83 was then synthesized, and the results for eggs irradiated when about 18 hr old were comparable to those of Glass and Plaine, see Table 2; they obtained 88% erupt with 65.8% being of the extreme phenotype, while I had a yield of 72.2% to 95% extreme erupt, dependent upon the X-ray machine used. However, when eggs were irradiated immediately

Table 1. Effect of X rays on the Su-er; er system

Age when irrad. started	Number of Eggs	Adults	% Eclosion	% Nonerupt	Extreme erupt Number	%
Stock B82 Su-er tu bw; st er su-tu						
Control	632	344	54.4	98.8	0	0
$3\frac{1}{2} \pm 3\frac{1}{2}$ min	269	5	1.9	100	0	0
16 - 21 hr	499	248	49.7	82.3	27	10.9
Stock B92A Su-er bw; st er						
Control	2,086	1,326	63.6	97.8	0	0
6 ± 6 min	900	76	8.4	100	0	0
	*501	25	4.9	100	0	0
28 - 90 min	505	0	0			
120 - 141 min	144	4	2.8	100	0	0
10 hr	914	458	50.1	91.5	7	1.5
17 - $19\frac{1}{2}$ hr	618	449	72.7	88.2	34	7.6

*A total dose of 1,000 R was given with the Andrex machine except where marked * (Philips machine *). See Materials and Methods for description of output and technique used.

Table 2. Effect of X rays on the Su-er; er system

Age when irrad. started	Numbers of Eggs	Adults	% Eclosion	% Nonerupt	Extreme erupt Number	%
Stock B91;83 Su-er bw; st er						
Control	2,070	1,153	55.7	97.1	9	0.8
1000 R						
$5\frac{1}{2} \pm 5\frac{1}{2}$ min	3,134	133	4.2	97.0	3	2.3
	*626	36	5.8	97.2	0	0
30 ± 5 min	1,334	6	0.4	83.3	0	0
18 hr ± 15 min	1,163	641	55.1	14.7	463	72.2
	*58	20	34.5	0	19	95.0
1500 R						
$5 \pm 5\frac{1}{2}$ min	197	1	0.5	100	0	0
	*639	3	0.5	100	0	0
18 hr ± $5\frac{1}{2}$ min	120	16	13.3	0	16	100
	*160	8	5.0	0	8	100

*See Materials and Methods for description of X-ray machines and the techniques used. The Andrex machine was used except where marked * (Picker machine *).

after 10-min collection periods or when approximately 30 min old, the frequency of erupt-eyed individuals was comparable with that of the control samples. Thus, irradiation of these early stages did not result in the inactivation of the effect of the suppressor gene.

Amongst the 179 eggs examined cytologically, 129 (72.1%) were fertilized. These 129 included 84 that were in meiosis or in prophase of syngamy and 12 that were undergoing the first cleavage at the time of fixation. Thus, at the maximum, not more than 96 (74.4%) could have been in precleavage stages if irradiation were started immediately after the collections were terminated. Of the remaining eggs 23 were in the second cleavage, 6 in the third, 2 in the fourth and 2 probably in the seventh or eighth cleavage divisions. (Two of the 84 presyngamy eggs had two sperms, and the rest were monospermic.)

DISCUSSION

The immediate problem is to determine the cause for the differences between the results presented herein and those obtained by Glass and Plaine. The first reason that comes to mind is that obviously the stocks used in the present experiments are not the same, and at least 15 years elapsed between the original and repeat tests. The results of irradiations of the present stocks indicate that there are differences between either the suppressors or the erupt alleles, or that modifiers of either gene have appeared. The fact remains, that irradiation of late egg stages from stock B91;83 produces the erupt phenotype with high frequency, but irradiation of early stages does not. This might indicate that the suppressor has changed so that its effect can be inactivated in the late but not in the early stages of embryonic development. Alternatively, one might assume that an enhancer of Su-er has appeared in the stock and that this protects the suppressor effect from inactivation by X rays in the early stages but, perhaps because of complete utilization of the enhancer product or inactivation of the enhancer gene during embryonic development, the same protection is not available in later stages. Either of these interpretations may prove to be correct, but unless a stock can be found that will produce results similar to those originally obtained by Glass and Plaine, the alternative explanation presented below appears to be more plausible.

Basing their assumption that the 8-min embryos "could hardly have reached the first cleavage division, on the average" on the embryological studies of the timing of meiotic and mitotic divisions done by Rabinowitz (7), Glass and Plaine did not take into account the fact that he used a "highly inbred vigorous Florida stock" and "When an egg was laid later than 5 min after the preceding egg deposited by the same female, it was usually discarded." There is no a priori reason to assume that all strains of flies oviposit at the same rate, and it is extremely unlikely that a female lays eggs at 5-min intervals for a very long period. Even by using vigorous stocks and methods that highly stimulate laying, an average yield of only three to four eggs per female per hour was obtained over a 2- to 3-hr period; after this the rate falls off considerably. Females of the Su-er;er stocks tested would not be considered especially rapid layers, and in the present experiments the average was 1.4 eggs per female per hour for those samples irradiated immediately. Of course, this rate includes eggs from the noninseminated females that are also induced to lay rapidly. Also, if the females used in the experiments by Glass and Plaine were placed with males the day or night before the eggs were

collected, it would be possible that some were retained for 10 or more hours and that irradiation of these could account for the erupt phenotypes, the young eggs being killed by the treatment. It should be pointed out that the frequencies of eclosion, from egg to adult, in their experiments were similar when eggs were irradiated at 1, 3, and 5 hr (3.2, 2.0, and 3.2%, respectively) and at 10 and 18 hr (15.2% each), and that it was only 6.8% at 15 hr; the number of eggs irradiated at 8 ± 8 min is not given. In the present experiments there is only a slight reduction below that of the control rates when eggs were irradiated at 10 or 18 hr. In fact, when eggs from stock B92A were irradiated at 17 to 19-1/2 hr, the eclosion rate was higher than that for the controls; this, undoubtedly, was because of a slightly higher frequency of fertilized eggs in the irradiated than in the control groups. In contrast, in a sample of 3,014 eggs irradiated when 1 hr ± 5 min old (unpublished data), the eclosion rate was 1/132 that of the control, yet, in the Glass and Plaine experiments, eggs irradiated at a similar stage had an eclosion rate about 1/30 that of their controls. This might be explained if their samples contained some eggs in advanced stages less sensitive to the killing effects of X rays than the early stages.

The difference in wavelength produced by the three X-ray machines had no apparent effect when eggs were irradiated immediately after being collected (Tables 1 and 2) but the longer wavelengths (Table 2) appear to have been more effective than the short ones when eggs were treated during the late developmental stages. The differences in sample size (641 vs 20 adults examined) may account for the discrepancy in the results produced by the two machines when 1,000 R of X rays were given at 18 hr. The high dose (Table 2), of course, had a greater killing effect in both early and late stages, but the frequency of erupt individuals was not increased above that for the control or for the lower dose when young eggs were treated.

Failure to produce the erupt phenotype when Su-er;er eggs were irradiated immediately after fertilization removes support for the theory that gene action of Su-er is determined at this early stage or that a substrate upon which this gene may act is inactivated at this time by X rays. Further experiments are in progress to determine more accurately at which stage the suppressor effect can be inactivated. Discussion of the influence of irradiation on the Su-er;er system will be postoned until this is established.

SUMMARY

Experiments of Glass and Plaine (1950) yielded inactivation of the effect of a suppressor gene in Drosophila melanogaster when eggs in early stages after fertilization were irradiated. A repetition of these experiments with presently available stocks did not confirm the original findings. The data do not support the view that the gene action of Su-er is determined very early, or the alternative view that a substance upon which the gene Su-er acts is inactivated by X rays after fertilization of the egg but before cleavage divisions have begun.

ACKNOWLEDGMENTS

I am grateful to Dr. Curt Stern for his comments and suggestions, Cole Ulrichs for her help in conducting the experiments, and Lydell Williams for preparing the culture media and glassware.

REFERENCES

1. Glass, B., and Plaine, H. L.; Proc. Nat. Acad. Sci. 36:627, 1950.
2. Physiology of Insect Development, edited by F. L. Campbell, Chicago, The University of Chicago Press, 1959, p. 12.
3. Glass, B; Science, 126:683, 1957.
4. Hildreth, P. E., and Brunt, C.; Drosophila Information Service 36:128, 1962.
5. Würgler, F. E.; Ulrich, H., and Schneider-Minder, A.; in Repair from Genetic Damage and Differential Radiosensitivity in Germ Cells, edited by F. H. Sobels, London, Pergamon Press, 1963, p. 101.
6. von Borstel, R. C., and Lindsley, D. L.; Stain Technol. 34:23, 1959.
7. Rabinowitz, M. J.; J. Morphol., 69:1, 1941.

Received June, 1965.

Single-Strand Breaks in Duplex DNA of Coliphage T7 as Demonstrated by Electron Microscopy

David Freifelder and Albrecht K. Kleinschmidt

In the original helical model of double-stranded DNA it was assumed that the two strands are continuous, Watson and Crick (1). However, Davison, Freifelder and Holloway (2), studying DNA from several bacteriophages, have presented evidence that these polynucleotide strands are not always continuous in each DNA duplex but often contain interruptions, or single-strand breaks. The argument was the following: Bacteriophage DNA, which is relatively homogeneous in molecular weight, Rubenstein, Thomas and Hershey (3), Davison et al. (4), shows a single sharp boundary when sedimented in the analytical ultracentrifuge, whereas single-stranded material obtained by denaturation of this DNA (under conditions that avoid hydrolysis of phosphodiester bonds) has a multicomponent boundary. Since fractionation of denatured DNA by zonal centrifugation through a sucrose gradient yields samples which, when recentrifuged, possess different sedimentation coefficients, the sedimentation heterogeneity is real. Since sedimentation heterogeneity can reflect differences only in molecular weight, shape, or amount of bound material and since in solvents of various ionic strengths, pH, and compositions, the relative proportions of each of the different sedimenting components are unchanged, it was concluded that there is molecular weight heterogeneity of the DNA single strands. Hence, the native DNA must contain either pre-existent single-strand breaks or a small number of special bonds, not of the phosphodiester type, which could be broken by the denaturation technique.

The interpretation of these centrifugation experiments has been challenged, Berns and Thomas (5), because of earlier conflicting results of molecular weight determinations of denatured DNA by CsCl density gradient centrifugation. The cause of the disagreement is unclear at present. To resolve this controversy, it is necessary to demonstrate unambiguously that the sedimentation heterogeneity is a consequence of molecular weight heterogeneity.

It is now possible to demonstrate molecular weight heterogeneity by directly measuring the lengths of DNA single strands as seen in electron micrographs. In the present paper, a protein monolayer technique first described by Kleinschmidt and Zahn (6), has been modified so that electron micrographs of single-stranded DNA can be obtained routinely; this is a further modification of the method used to study the circularity of the single-stranded DNA of phage ϕX-174, Freifelder et al. (7), and the structure of denatured trout sperm DNA, Lang et al. (8). Using this technique, we have shown that the lengths of T7 single strands are not identical, and, have concluded that T7 DNA contains a small number of either single-strand breaks or highly labile bonds.

MATERIALS AND METHODS

The preparation and purification of coliphage T7 are described elsewhere, Davison and Freifelder (9). Single-stranded DNA was obtained by putting freshly prepared, viable phage directly into 0.1 M NaOH for 20 sec and adding sequentially 1/2 volume of 37% HCHO and 1/8 volume of 1 M KH_2PO_4. In one case, it was prepared from native DNA by heating for 2 min at 70 °C in 9% HCHO, pH 7.8. Native double-stranded DNA was prepared by heating the phage for 5 min at 70°C in 0.01 M PO_4, pH 7.8, 1 M NaCl. In every case the final concentration of the DNA was 20 μg/ml. Single-stranded DNA was fractionated in a sucrose gradient as previously described, Davison et al. (2).

An improved procedure for preparation of the DNA in a protein monolayer, Kleinschmidt et al. (10), was further modified as follows:

1. The DNA (20 μg/ml) was diluted to less than 2 μg/ml into 1 M NH_4Ac + 0.5% neutralized HCHO. 2. Cytochrome C (Nutritional Biochem. Corp.) was added to the DNA to give a concentration of 0.01%. The protein-DNA film was formed by flowing 0.2 - 0.4 ml of the solution down a wet glass ramp (microscope slide at an angle of ca. 30°) onto a clean solution of 0.3 M NH_4Ac + 0.5% HCHO. Because of partial denaturation of the protein by HCHO, the film covered a slightly larger area than if HCHO were absent, i.e., somewhat greater than the limiting area of 1 m^2/mg protein, Cheesman and Davies (11). 3. The film was picked up by the usual method onto carbon-coated Formvar support films mounted onto Pt grids. 4. Since preparations of single-stranded DNA have significantly lower contrast than native DNA, the shadowing procedure is critical. To minimize coarseness of the background, only grids and support films were used which showed no irregularities when examined with a light microscope. To prepare for shadowing, 30 mg of uranium foil were placed on a tungsten wire support about 15 cm distant from the specimen holder. The grazing angle of shadowing was 5 to 8 degrees. Prior to shadowing, the uranium was preheated to fuse the metal into a small bead. This was then covered with a 40-mg sheet of uranium (ca. 8×8 mm) bent to form a tent-like structure over the bead. The samples were then placed in the chamber and rotated at 60 rpm for the duration of the shadowing operation. Shadowing was done slowly (up to 10 min for total evaporation) with the pressure always maintained below 10^{-4} mm Hg. Faster evaporation resulted in coarser crystallization of the uranium and thereby lower contrast. 5. The procedures for photographing, determining the magnification, and for tracing and measuring are described elsewhere, Kleinschmidt et al. (10).

RESULTS

Figures 1a and b show tracings of the ultracentrifuge diagrams of the samples of native and alkali-denatured T7 DNA used in the present experiments. The native DNA shows the characteristic sharp boundary while the denatured DNA consists half of homogeneous material (assumed to be intact single strands) and half slower heterogeneous material (fragments) in quantitative agreement with previous results, Davison et al. (2). The minimum sedimentation coefficient ($S_{20,w}$) of the denatured DNA is 17 ± 2 which, according to a rough calibration (Freifelder and Davison (12)), corresponds to a molecular weight of 20% of the intact strand. Slower material could not be detected unless it amounted to at least 10% of the total concentration.

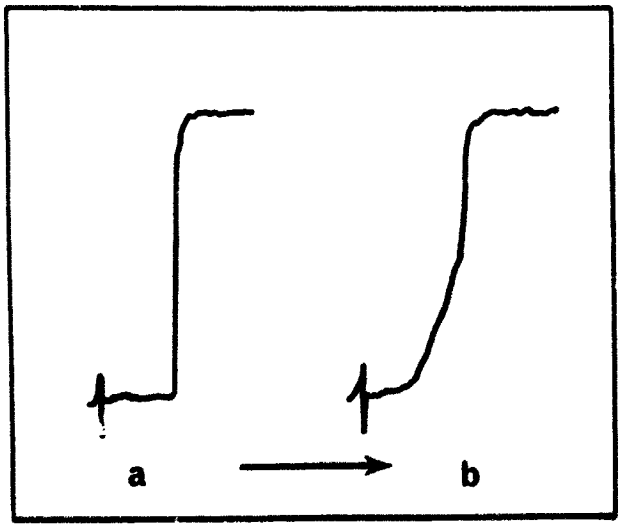

Figure 1. Photometric trace of ultraviolet absorption diagram of (a) native and (b) alkali-denatured T7 DNA. Ultracentrifugation was in a 30-mm Kel-F cell, 33450 rpm. The diagram shows the boundary after 20 min of centrifugation. The arrow shows the direction of sedimentation. The $S_{20,w}$ of the native and denatured material were 29 and 39 respectively. DNA concentration: 20 μg/ml.

MUB-5939

Figure 2 shows an electron micrograph of a mixture of single- and double-stranded T7 DNA, obtained by adding native heat-released T7 DNA to alkali-denatured, formaldehyde-stabilized T7 DNA just before adding to cytochrome C and prior to spreading. When compared to double-stranded DNA, the single strands are more tangled and thinner, though often irregular in width, and have sharper, angular bends. There is rarely any difficulty in distinguishing single from double strands. The same conformational differences were seen earlier for native and denatured trout sperm DNA, Lang et al. (8). In Fig. 3a, a micrograph of single-stranded T7 DNA mixed with circular, naturally single-stranded DNA from coliphage ϕX-174, Freifelder et al. (7), is shown to demonstrate that these DNA's have a similar appearance (i.e., width and conformation).

Figures 3b-e and 4 show micrographs with higher contrast and more extended molecules from the spreading of the single-stranded T7 DNA characterized in Fig. 1b. The different lengths of the various filaments are readily apparent and are indicated.

Figure 5a shows the contour length distribution of the native double-stranded DNA of Fig. 2. The mean length is 12.2 μ. This has been plotted with an interval of 0.5 μ for easy comparison to single-stranded DNA; the distribution plotted with an interval of 0.1 μ (not shown) is approximately Gaussian with a standard deviation of 5%. In Fig. 5b and c the length distribution for the single strands of the sample characterized in Fig. 1a is shown. All measurable filaments have been plotted. Two histograms have been given. In the first the interval has been chosen to be 1 μ; in the second, 0.1. The second represents the reproducibility of the tracing and measuring operation and is therefore a lower limit to the accuracy of the values given. The former (1 μ) is the interval in which, judging from the length distribution of ϕX-174 DNA, a given value will fall with high probability (93%). The broad distribution of Fig. 5b clearly contrasts with the relatively narrow one in Fig. 5a for double-stranded DNA. The distribution in Fig. 5c is merely given to present the raw data and so that the possibility of discrete size classes will not be totally ignored.

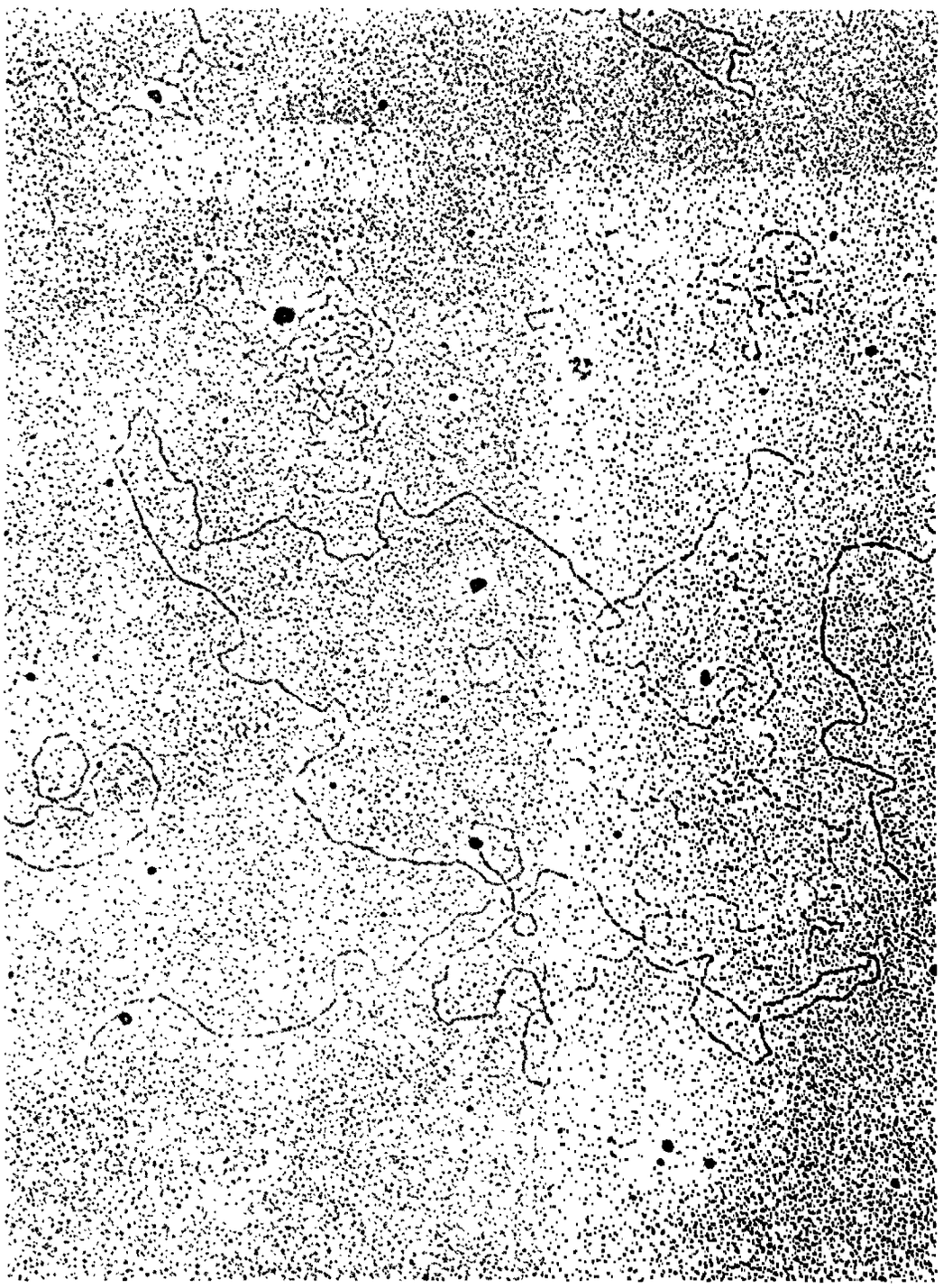

Figure 2. Electron micrograph of a mixture of native and denatured T7 DNA. Magnification x47,000. For discussion, see text. The contour lengths of one filament each of native (123 μ) and of denatured (8.3 μ) DNA are indicated.

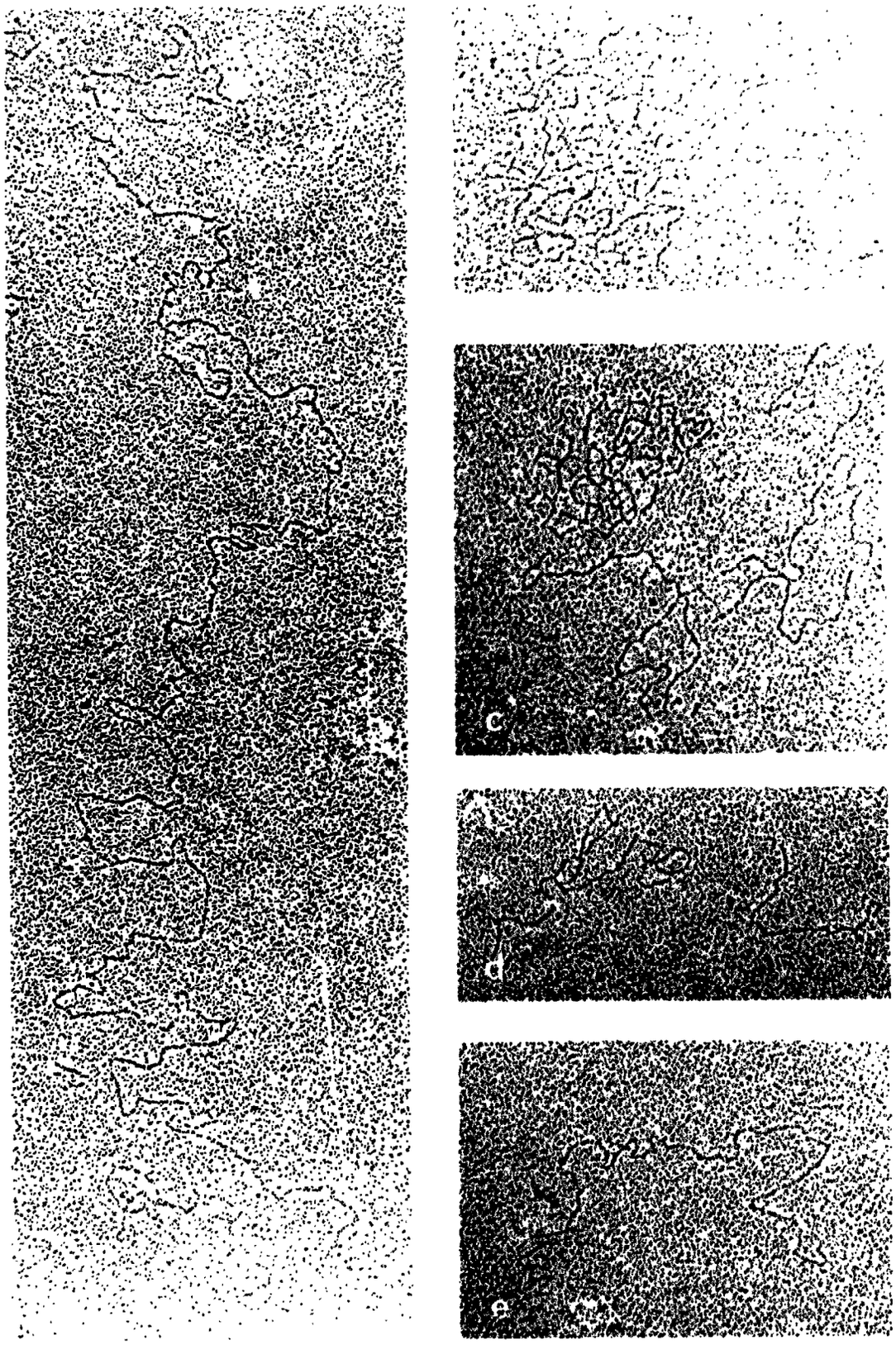

Figure 3. (a) Electron micrograph of a mixture of single-stranded T7 DNA (the 9.4 μ filament) and circular DNA from phage ØX 174 (the 1.5 μ circle). See text for discussion of arrows. Magnification x62,000. (b, c, d and e) Electron micrographs of single strand T7 DNA. Contour lengths are indicated for the untangled, measurable molecules.

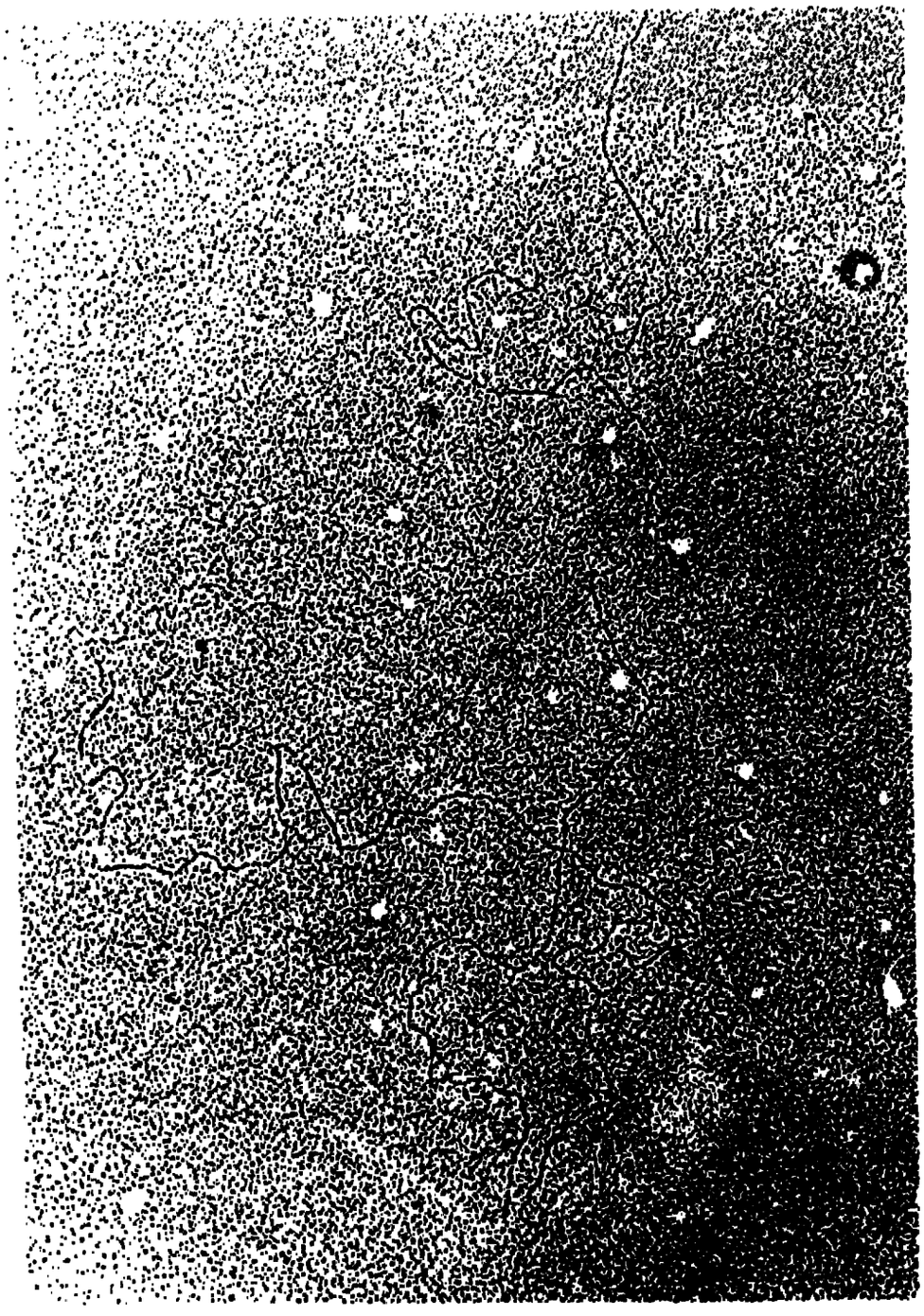

Figure 4. Electron micrograph showing two filaments of single-stranded T7 DNA obtained from the preparation characterized in Fig. 1b. Magnification x52,000.

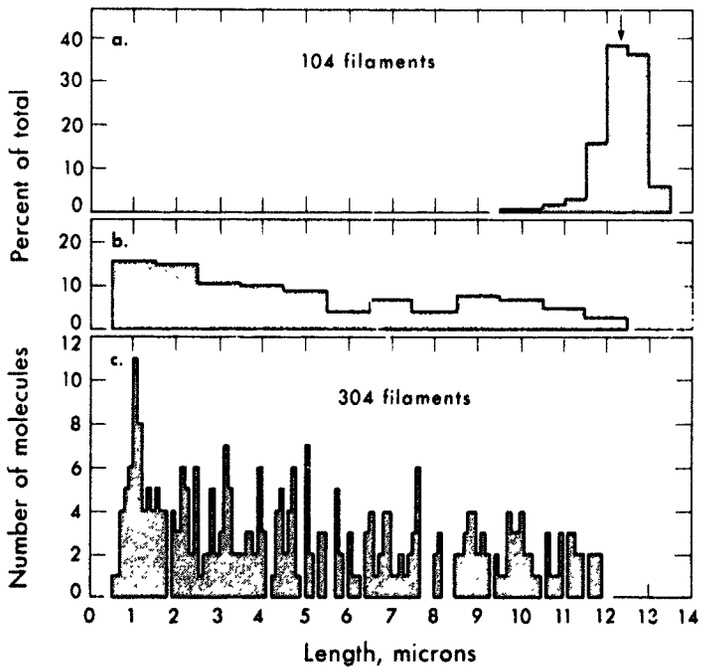

Figure 5. (a) Histogram showing the length distribution of native, double-stranded T7 DNA from the spreading shown in Fig. 4. Only untangled molecules (no branch points with more than 4 branches) were measured. Spreading was on 0.3 M NH_4 Acetate + 0.5% HCHO. (b) Histogram showing the length distribution of single-stranded T7 DNA of the preparation characterized in Fig. 1b. The measurements have been grouped in intervals of 1 μ for reasons given in text. (c) Histogram showing the length distribution of single-stranded T7 DNA of the preparation characterized in Fig. 1b. This is the same data as in Fig. 5b, but the grouping is in intervals of 0.2 μ (see text for discussion).

MUB-7822

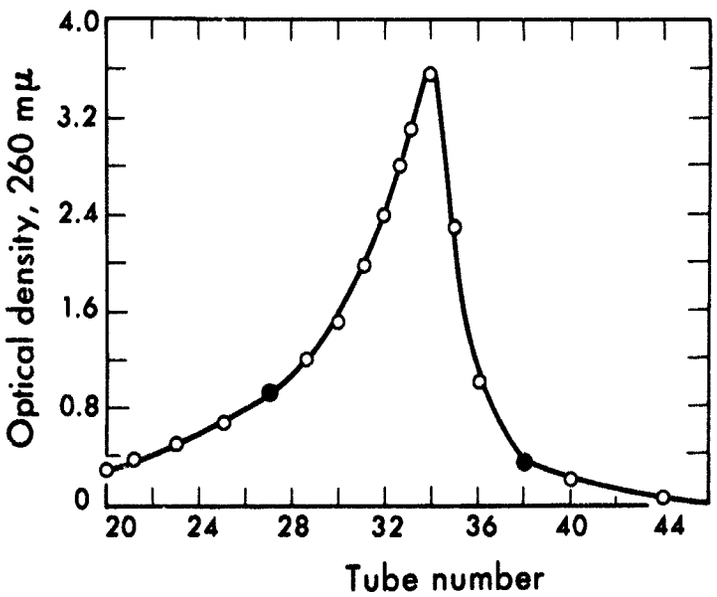

Figure 6. Optical density (260 mμ) profile of denatured T7 DNA sedimented through a sucrose gradient (5-20%) for 16 hr at 2500 rpm in the SW 25 rotor of the Spinco Model L Preparative Ultracentrifuge. The solvent was 1 M NaCl, 0.01 M PO_4, pH 7.8, 9% HCHO. Eighty fractions were collected by drop collecting. The direction of sedimentation is to the left. The solid circles represent the samples, shown in Fig. 7, used for electron microscopic analysis.

MUB-5941

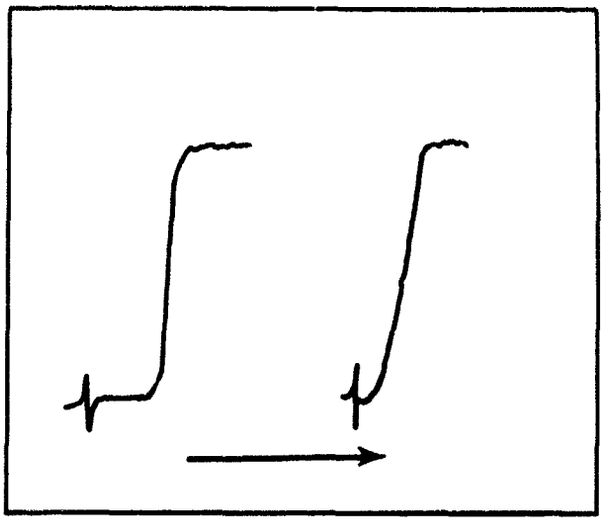

Figure 7. Photometric traces of ultraviolet absorption diagrams of denatured T7 DNA samples 27 (left) and 38 (right) from Fig. 6. Conditions of centrifugation are as in Fig. 1.

MUB-5940

It should be pointed out that a sampling error has distorted the shape of the distribution, which is noticeably deficient in intact single strands (length ca. 11 - 12 μ). If the distribution of Fig. 5b is plotted as a weight instead of a number distribution, only 16% of the material is in the 10.5 - 12.5 μ range, as opposed to the 50% intact single strands predicted from the centrifuge diagram of Fig. 1b. Approximately 30 to 40% of the filaments are badly tangled (cf. Fig. 3), and only untangled molecules and those with clearly defined ends have been measured. A second kind of unmeasurable molecules are those which run out of the field of view. That these two difficulties result in a selective loss of long molecules was seen by roughly measuring these "unmeasurable" molecules (tangled molecules and those only partially in the field of view); more than 80% of several hundred of these "unmeasurable" molecules were longer than 6 μ, which is larger than half of the length of the intact strand. Although a complete length distribution was not determined, qualitatively the same results were obtained for single-stranded material prepared by heat denaturation.

A broad molecular weight distribution could result from fragmentation of intact single strands during the preparation for electron microscopy. To show that this is not the case, micrographs were taken of single-stranded DNA fractionated according to their sedimentation coefficient and presumably by molecular weight before spreading. Single-stranded DNA (alkali-denatured) was centrifuged through a sucrose gradient in the presence of formaldehyde, and fractions were obtained by drop collection. The distribution of material in the gradient is shown in Fig. 6. Samples # 27 and 38 were dialyzed against 1 M NaCl, 0.01 M PO_4, pH 7.8, 6% HCHO, to remove sucrose and were then re-run in the analytical centrifuge. The sedimentation diagrams are shown in Fig. 7. The fast sample (# 27) consisted almost entirely of material having intact single strands ($S_{20,w}$ = 39), whereas the slow sample (# 38) was composed of small pieces ($S_{20,w}$ = 12 - 18). It should be noticed that whereas in Fig. 1b the minimum S was 17, sample 38 has material of S = 12; this corresponds to molecules having a molecular weight of approximately 10% of the intact single strands, in agreement with the minimum lengths in Figs. 5b and c. These two samples were individually spread and electron micrographs obtained. Sample 27 consisted primarily of large tangles and

molecules running out of the field of view, although a few long (> 8 μ) measurable filaments were found; there were no short filaments. Fraction 38 consisted entirely of filaments shorter than 2 μ. Hence, the single strands do not break during sample preparation and the sedimentation heterogeneity represents heterogeneity in molecular weight, as previously suggested.

DISCUSSION

Ultracentrifugal analysis using sedimentation velocity and zonal sedimentation has led to the conclusion that the DNA of coliphage T7, as well as of other phages, contains single-strand breaks Davison et al. (2). This conclusion disagrees with the results for phage T4 by Berns and Thomas (5) and has also more recently been challenged by Tomizawa and Anraku (13). However, the existence of breaks in phage T5 DNA in specific positions demonstrated by sedimentation studies, Davison et al. (2) has been confirmed by Hershey et al. (14), Rubenstein (15) and Rhoades et al. (16). Single-strand breaks have also been found in T7 by Studier (17), using band centrifugation (Vinograd et al. (18)), although there may be quantitative differences with the results of Davison et al. (2). It seems obvious that the question has not been resolved by sedimentation analysis.

The essential assumption on which the interpretation of all sedimentation velocity studies rests is that the observed sedimentation heterogeneity (a fact upon which all workers agree) is a manifestation of heterogeneity in molecular weight. That this is the case has been previously inferred only by elimination of other possibilities, Davison et al. (2). The validity of this assumption is shown in the present electron microscopic studies in that (a) the single strands do have a broad spectrum of lengths and (b) faster sedimenting fractions contain longer and more tangled molecules and the slower fractions have the shorter. However, the significance of the length measurements is contingent upon the assumption that the mass per unit length of each polynucleotide filament seen in the electron microscope is roughly constant. Evidence that this assumption is reasonable comes from the observed equality in the lengths of single-stranded rings of phage ϕX-174 and the double-stranded rings of its replicative form, Kleinschmidt et al. (19) and Freifelder et al. (7), and from the small standard deviation for these measurements of only 7%. However, several factors can influence the mass per unit length, and these effects might be greater for long molecules. For instance, the single strands may still be somewhat coiled as in the native molecule. This certainly occurs since, if the single-stranded ring of ϕX-174 were fully extended, it would probably be two to three times longer than the replicative form, which is not the case. This is probably also true in the present case since the longest filaments of single-stranded T7 seen were 11.8 μ, which is similar to the value of 12.2 μ for native DNA. Presumably this coiling results from the tendency for the nucleotide bases to stack, Hamaguchi and Geiduschek (20). This stacking, however, means that the molecules are probably not very rigid and could be stretched or further contracted by possible effects of HCHO, salts, cytochrome C or surface forces during spreading and drying on the support film. Furthermore, the stacking tendency need not be constant along the filament. A second major problem of a more practical sort is the difficulty in tracing and measuring a molecule that is slightly kinked (e.g., invisible "microkinks") or shows sharp, acute angles.

In this regard, we have remeasured the molecule shown in Fig. 3a, on the assumption that at the positions marked by the arrows the molecule is doubled over; the length is increased by about 10%. Other molecules have been tested in the same way with similar results; this error, if it exists, would not affect the conclusion that heterogeneity exists.

With these reservations it is possible to state 1) that the lengths of single-stranded DNA obtained from T7 are not uniform so that there must be either single-strand breaks or bonds broken both by the alkali and heat denaturation procedures, and 2) that the sedimentation heterogeneity of single-stranded DNA is a result of molecular weight heterogeneity. These conclusions are based both upon the assumption that the errors in length measurement inherent in the technique could not possibly broaden the distribution to ten-fold that of native DNA and the fact that the strands of different length can be separated by gradient sedimentation. An additional conclusion is that there is not a single centrally-located break in each molecule, or, more generally, that the molecules do not have a single break that can occupy only one position.

It was hoped that it would be possible to compare the length distribution to the sedimentation diagram. However, with the present technique this has not been possible because of selective loss of long fragments from the class of measurable molecules. Although tangling of double-stranded DNA and the presence of flower-like molecules can now be avoided by an appropriate choice of salt concentration (Kleinschmidt and Freifelder, in preparation), this problem persists for longer molecules of single-stranded DNA. This effect skews the distribution toward the short side, as shown by a measurement of the minimum length of tangled molecules, in which it was found that long molecules are preferentially tangled and also have a greater probability of running out of the field of view. The best one can say is that (i) the slowest molecules seen in the sucrose gradient experiment have an $S_{20,w} = 12$ which corresponding to a molecular weight of ca. one million and (ii) since the smallest molecules seen in the electron micrographs are 1 μ long, contrasted to the intact, single strands of length 11.5 μ and of molecular weight 10 - 12.5 million, they should have a molecular weight of circa one million.

SUMMARY

Previous work based on ultracentrifugal studies had led to the hypothesis that there are gaps in the single polynucleotide strands of the DNA of coliphage T7. To investigate this further, the length distribution of the single strands derived from native T7 DNA by alkaline denaturation has been obtained. An improved technique for electron microscopic visualization of single strands of DNA in a cytochrome C monolayer was used for this measurement. In contrast with the narrow length distribution for native, double-stranded DNA, the length distribution of the single strands was found to be very broad (about eight-fold greater than for the native material). Single-stranded T7 DNA was then fractionated according to sedimentation coefficient by sucrose gradient centrifugation, and these various fractions were examined with the electron microscope. It was found that the more rapidly and slowly moving fractions consist of longer and shorter filaments respectively, from which it has been concluded that sedimentation heterogeneity of single-stranded DNA is a reflection of molecular weight heterogeneity. Hence, the electron microscopic studies confirm the original hypothesis that T7 DNA contains single-strand breaks. An attempt was made to determine the position of these

breaks and the number per molecule; however, it could only be said that the breaks can occur in many places and that the number per molecule is small.

ACKNOWLEDGMENTS

We wish to thank Susan Johnson for patient help with the electron microscopy and Katherine Le Blanc, who prepared the phage samples and aided in the length measurements. Dr. Bruce Trumbo, Stanford University, and Dr. Thomas Trautner, University of California, Berkeley, were particularly helpful in the interpretation of the data. This work was done while one of us (A. K. K.) was a research biophysicist on leave from the University of Frankfurt am Main, Germany, in the laboratory of Dr. Robley C. Williams, whose cooperation we gratefully acknowledge.

This work was supported by the Atomic Energy Commission, the National Institute of Allergy and Infectious Diseases, the National Cancer Institute and the National Institutes of Health.

REFERENCES

1. Watson, J. D., and Crick, F. H. C.; Nature 171:737, 1953.
2. Davison, P. F.; Freifelder, D., and Holloway, B. W.; J. Mol. Biol. 8:1, 1964.
3. Rubenstein, I.; Thomas, C. A., and Hershey, A. D.; Proc. Nat. Acad. Sci. 47:1113, 1961.
4. Davison, P. F.; Freifelder, D.; Hede, R., and Levinthal, C.; Proc. Nat. Acad. Sci. 47:1123, 1961.
5. Berns, K. I., and Thomas, C. A.; J. Mol. Biol. 3:289, 1961.
6. Kleinschmidt, A. K., and Zahn, R. K.; Z. Naturforsch. 14b:770, 1959.
7. Freifelder, D.; Kleinschmidt, A. K., and Sinsheimer, R. L.; Science 146:252, 1964.
8. Lang, D.; Kleinschmidt, A. K., and Zahn, R. K.; Biophysik 2:73, 1964.
9. Davison, P. F., and Freifelder, D.; J. Mol. Biol. 5:635, 1962.
10. Kleinschmidt, A. K.; Kass, S. J.; Williams, R. C., and Knight, C. A.; J. Mol. Biol., in press.
11. Cheesman, D. F., and Davies, J. T.; Advan. Protein Chem. 9:439, 1954.
12. Freifelder, D., and Davison, P. F.; Biophys. J. 3:49, 1962.
13. Tomizawa, J., and Anraku, N.; J. Mol. Biol. 11:509, 1965.
14. Hershey, A. D.; Goldberg, E.; Burgi, E., and Ingraham, L.; J. Mol. Biol. 6:230, 1963.
15. Rubenstein, I.; Abstracts, Biophysical Society (San Francisco), 1965.
16. Rhoades, M. M.; Abelson, J.; Pinkerton, T. C., and Thomas, C. A.; Abstracts, Biophysical Society (San Francisco), 1965.
17. Studier, F. W.; J. Mol. Biol. 11:373, 1965.
18. Vinograd, J.; Bruner, R.; Kent, R., and Weigle, J.; Proc. Nat. Acad. Sci. 49:902, 1963.
19. Kleinschmidt, A. K.; Burton, A., and Sinsheimer, R. L.; Science 142:961, 1963.
20. Hamaguchi, K., and Geiduschek, E. P.; J. Amer. Chem. Soc. 84:1329, 1962.

Received June, 1965.

Mechanism of Inactivation of Coliphage T7 by X rays

David Freifelder

When bacteriophages are X-irradiated, plaque-forming ability is lost. The specific chemical or physical changes that are responsible for this inactivation have never been positively identified, although the damage is undoubtedly in the DNA. The difficulty in the past has been that to make the X-ray damage measurable in DNA required very large radiation doses. Therefore, identification of the lethal change necessitated a difficult extrapolation of the data to the lower "biological" doses. However, some alterations in DNA can be detected at the level of one per molecule, e.g., strand breakage. In the present experiments the number of X-ray-induced single- and double-strand breaks per phage has been measured at high (20-100%) survival levels by ultracentrifugal analysis of the DNA of irradiated and titered phage T7. This is possible because the percentage of broken molecules in an initially homogeneous DNA sample is the percentage of material sedimenting more slowly than the main boundary of intact molecules (1) so that centrifugal analysis of native DNA yields the percentage of molecules that have received a double-strand break. To measure single-strand breaks, the DNA is denatured in formaldehyde to obtain single polynucleotide strands (2), and the analysis is then the same as for native DNA. The results of these studies are that after irradiation in buffer at least 90% of the nonviable phage particles have been inactivated by a double-strand break whereas in broth only 40% of the phages are killed by this mechanism. The remaining 60% have probably suffered pyrimidine damage.

MATERIALS AND METHODS

Coliphage T7M was grown and purified as described earlier (3). Radioactive phage were prepared by infection of E. coli B thy- in minimal medium containing 2 μg/ml C^{14}-thymine (10 μc/μmole). Viable counts were determined by the soft agar layer technique (4) using Difco nutrient agar and E. coli B(B). When the phages were irradiated in buffer, survival continued to decrease after the irradiation was completed. This after-effect, which amounts to an effective doubling of dose after 1 hr at 4°C, has a 5 to 10 min lag and was avoided by immediate dilution into 0.8% nutrient broth. For physical experiments, the phages remained in buffer since the physical properties of the DNA showed no after-effect.

The X-ray source was a Norelco Mg 150 operating at 150 kV, 12 mA. The phages were suspended (at an OD_{260} of 1.6) in either 0.01 M PO_4, pH 7.8, or phosphate + 10^{-3} M *l*-histidine, or 0.8% nutrient broth. Native DNA was isolated from phage by heating for 5 min at 70° in 0.01 M PO_4, pH 7.8, 0.4 M NaCl. To obtain single-stranded DNA, one volume of phage in phosphate was mixed sequentially with equal volumes of 0.2 M NaOH (20 sec) and 37% HCHO (pH 11), and 1/3 volume 1 M KH_2PO_4. The same result was obtained when the

DNA was first heat-released and then denatured by 2 min, 70°C in 9% HCHO. These techniques for release and denaturation do not damage DNA (5). The high OD_{254} of broth prevented its use in centrifugation experiments. However, as shown by Watson (6) for T-even phages, 10^{-3} M *l*-histidine, which has an OD_{254} of 0.03, also protects against indirect effects, as depicted in Fig. 1, so that this was used in place of broth.

The effect of nitrogen and sulfhydryl groups was studied as follows. Phages were suspended in 10^{-2} M PO_4, pH 7.8, 10^{-3} M *l*-histidine, 10^{-2} M *l*-cysteine (necessarily freshly prepared), and samples were removed for titering. Four-tenths of a milliliter was placed in a 2-ml ampoule and nitrogenated for 2 min; the ampoule was sealed while still in the nitrogen stream. Immediately after irradiation, the ampoule was broken and samples were taken for titering. If the DNA was then heat-released, it continued to be degraded for the next few hours. If the sample was flushed with N_2 for 2 min prior to DNA release (ca. 1 min after the strong H_2S smell was gone), this aftereffect was avoided.

The percentage of broken DNA molecules was measured by analytical ultracentrifugation with UV optics. After irradiation the sharp boundary characteristic of intact phage DNA (1) gives way to a more slowly sedimenting component (Fig. 2). Since the sedimentation diagram is an integral distribution function of DNA concentration along the centrifuge cell, the height of the boundary at a given value of sedimentation coefficient (S) divided by the total height is the fraction of material with $S \leq$ that particular value (1). Therefore, the height of the slow boundary gives the percentage of molecules that are broken, and the fast boundary represents the intact fraction. The mean number of breaks per strand was calculated from a crude curve relating S and molecular weight (2). This number is a minimum value since in this analysis one break cannot be distinguished from two very near one another in the same strand, and breaks near the ends of the strands are not detected (see Discussion).

RESULTS

The effect of X irradiation on the survival of phage T7 is shown in Fig. 1. The curves are typical of most phages in that (i) sensitivity is higher in buffer than in either broth or 10^{-3} M *l*-histidine and (ii) the curve is sigmoidal in buffer and exponential in broth; the D_{37} in broth (84,000 rads) is the same as Watson's value (6). This solvent effect on curve shape and sensitivity implies either that X rays can produce at least two types of lethal damage or that there are several mechanisms for producing the same damage. In a study of coliphages T2, T4 and T6, Watson favored the idea of different chemical lesions and hypothesized that, in buffer, phage protein was damaged because of an apparent loss of adsorptive capacity, whereas in broth DNA is primarily affected. Hence, exponential (one-hit) inactivation in broth could be explained by the phage having a single DNA molecule whereas the sigmoidal kinetics in buffer was a result of the multiplicity of the phage proteins involved in adsorption. This proposal does not, however, hold for T7 since the adsorptive ability of T7 is unaffected by irradiation in either broth or buffer, as next demonstrated.

When C^{14}-thymine-labeled T7 phages were irradiated at several doses (to 1% survival) in either buffer or histidine, titered and allowed to adsorb to a tenfold excess of *E. coli* B(B),

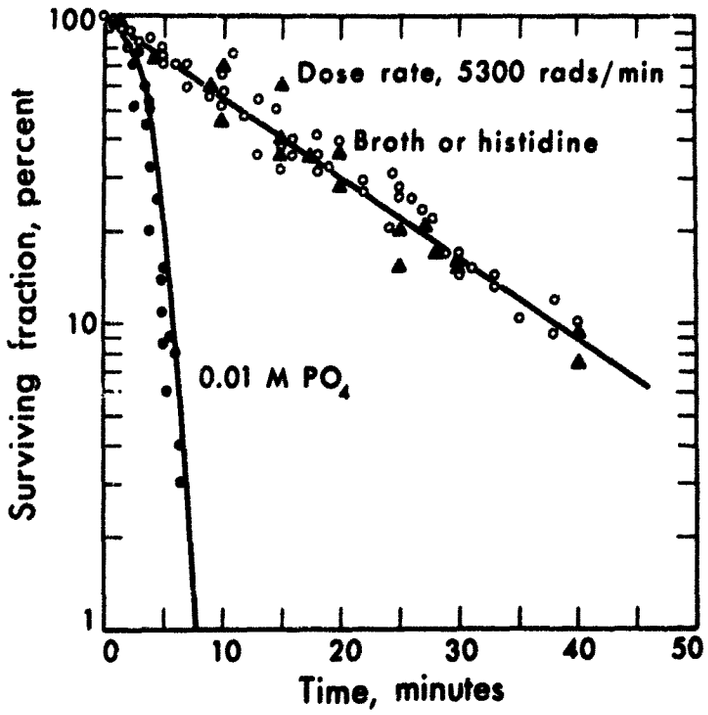

Figure 1. Survival of coliphage T7 following X irradiation in 0.01 M PO_4, pH 7.8: closed circles; nutrient broth: open circles; and phosphate containing 10^{-3} M *l*-histidine: triangles.
MUB-3700

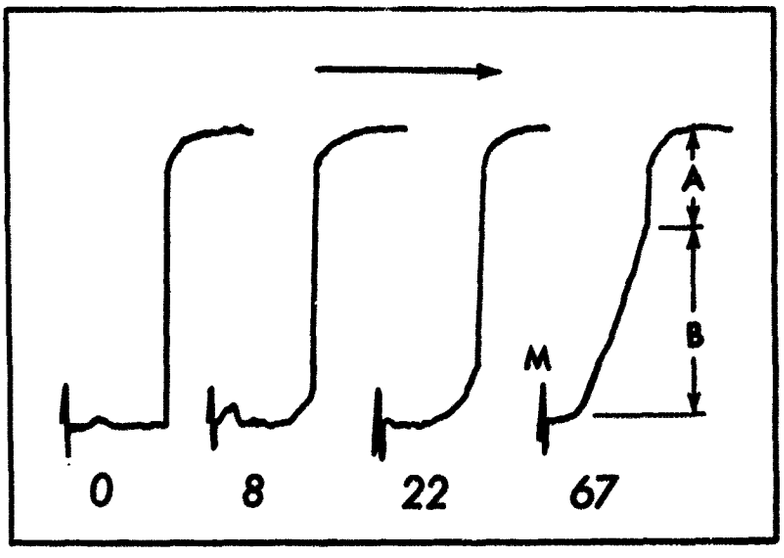

Figure 2. Sedimentation diagrams for DNA extracted from T7 phage irradiated to various survival levels. The arrow indicates the direction of sedimentation. The meniscus is at M. The diagram, a photometric trace of an ultraviolet photograph, shows concentration of DNA along the cell after 20 min at 33,450 rpm. The main nearly vertical boundary (A) is that of the intact molecules. The trailing boundary (B) represents broken molecules. The numbers indicate the percent broken molecules.
MUB-3703

Table 1

% Dead phage	% Broken molecules
14	14
16-18	16-17
22	21-23
28	28-29
61	60

in both media there was a small decrease in the adsorbed radioactivity but never enough (< 10%) to account for the observed loss of viability. The nonadsorbing material was identified as free DNA in the following experiments. (i) C^{14}-thymine phages were irradiated, treated with DNA-ase and precipitated with trichloracetic acid. In both buffer and histidine, acid-insoluble counts decreased with dose, indicating that the nonadsorbing material is DNA-ase sensitive. (ii) Phages were irradiated and centrifuged without releasing the DNA. In an unirradiated suspension all of the UV-absorbing material sediments at a single rate (S = 480), that of free phage, but with increasing dose there appeared material with $15 < S < 29$, which was DNA-ase sensitive. This was mainly broken DNA molecules since intact molecules have S = 29. These experiments show that X irradiation does not reduce the ability of T7 to adsorb to host bacteria and that the DNA which does not adsorb is free DNA released into the medium by rupture of the phage head.

In order to investigate directly the relation between DNA damage and phage inactivation, the DNA of irradiated and titered phage was examined in the ultracentrifuge for double- and single-strand breaks. In Fig. 3 the percent broken double-stranded molecules is plotted against the percent dead phage in the 20- to 100% survival range for irradiation in buffer and in histidine. A straight line of slope 1 ± 0.07 results for the buffer case from which it is inferred that each (> 93%) dead particle has received a double-strand break. For irradiation in histidine, the slope is 0.4 so that only 40% of the dead phages contain double-strand breaks.

The nature of the damage to the remaining 60% of the nonviable particles is suggested by the following. When phage T2 is irradiated under nitrogen in thiourea (or histidine) containing 10^{-2} M cysteamine, the sensitivity is reduced approximately two-fold compared to thiourea alone (7). This effect is also true of T7 in nitrogenated histidine-cysteine. When the percent broken double-stranded molecules is compared to percent dead phage for these conditions, they are now found to be equal, as shown in Table 1. Therefore under these conditions, all dead phages contain broken molecules, and the cysteine and N_2 must prevent the occurence of the damage which inactivates the 60% nonviable phages with unbroken molecules. The possible identity of this lesion will be discussed below.

For both buffer and histidine, single-strand breaks accumulate more rapidly than viability decreases. This is shown in Fig. 4 in which the average number of single-strand breaks per phage is given as a function of dose for irradiation in buffer. With a 1-min dose

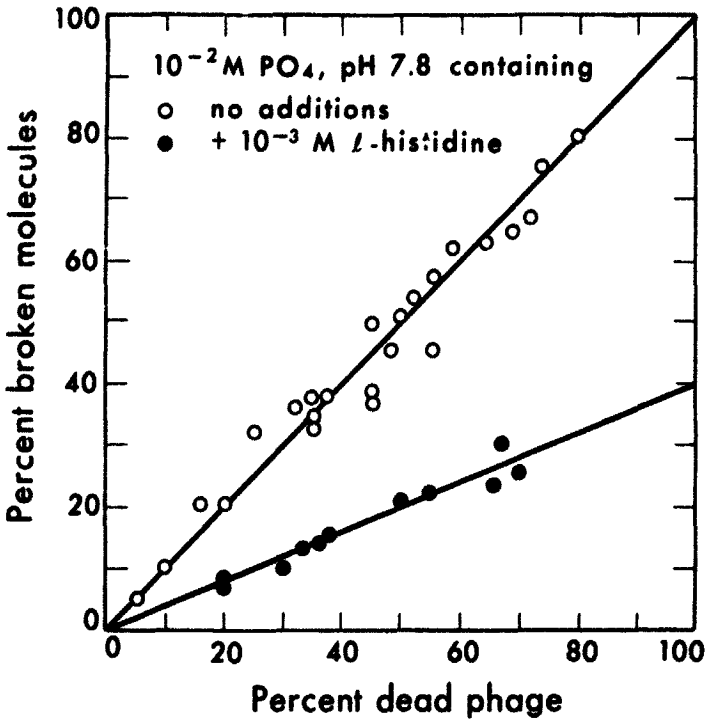

Figure 3. Percentage of dead T7 phage vs. percentage of broken DNA molecules for phages in 10^{-2} M PO_4, pH 7.8, ± 10^{-3} M ℓ-histidine. Phage samples were irradiated and titered to determine the percentage of dead particles. The DNA was then extracted by heating 5 min at 70°C and was centrifuged to measure the percentage of broken molecules.

MUB-5076

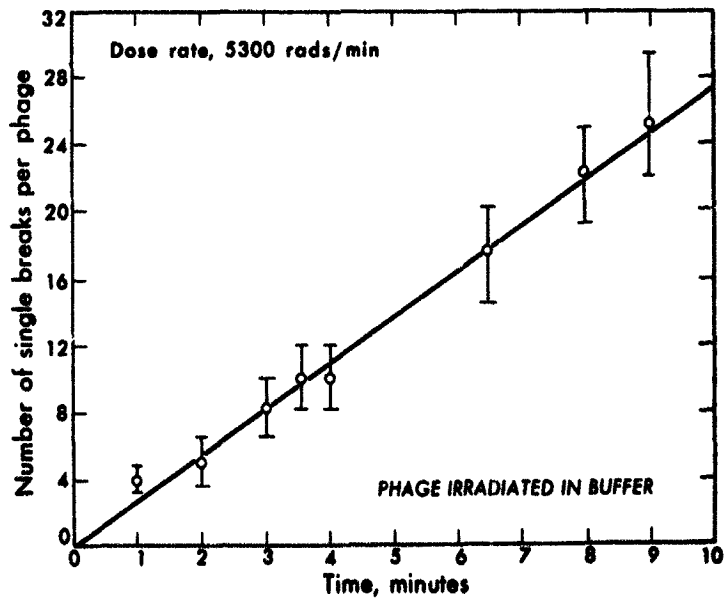

Figure 4. Average number of well-separated (see text) single-strand breaks per phage as a function of dose of X rays in buffer. DNA was extracted from irradiated phage, denatured in alkali, and ultracentrifuged. The number of breaks was calculated from the mean molecular weight.

MUB-3702

there are ca. three breaks per phage, yet the survival is greater than 90%. For histidine the result is similar, and the ratio of single to double breaks produced in histidine is approximately 10 to 15. Clearly, single-strand breaks have little or no effect on viability.

DISCUSSION

When T7 phages are irradiated in buffer, inactivation results almost entirely from the production of double strand breaks in the DNA. If the phages are protected by histidine, 40% of the phages are inactivated by double-strand breaks and 60% by other damage. If the phage is further protected by nitrogenated histidine-cysteine, these 60% survive, and again, all dead phages have double-strand breaks. The cysteine and N_2 have eliminated the "other damage."

The identity of the damage avoided by cysteine and N_2 can only be presumed from the fact that if free DNA is X-irradiated, sugar attack is unaffected by nitrogenation, although destruction of pyrimidine bases is reduced 2.5-fold (8). The lack of effect of nitrogenation on the sugar moiety is consistent with the fact that inactivation in buffer is also independent of the presence of oxygen since only double-strand breaks are involved in this medium. (Indeed, if free DNA is irradiated in buffer, strand breakage shows no O_2 effect (9).) We presume then it is pyrimidine damage that is avoided by the cysteine-N_2 conditions.

It seems clear therefore that the lethal damage is double-strand breakage, although a continuing problem in radiobiology is whether an observed chemical change is the lethal lesion or merely a concomitant. In this case such a logical question probably does not arise since a double-strand break alone would certainly inactivate the phage because either only a part of the genome would be injected or, if the entire genome were actually injected in two pieces, a recombinational event would be required to restore viability. That at least part of the DNA of irradiated phages penetrates the host bacterium has been shown by genetic experiments with T4 irradiated with γ-rays (10). It is also possible that some double-strand breaks do not inactivate, for instance, those very near the end of the molecule. However, such end breaks are not measurable and hence would not affect these results.

It is odd that under protected conditions (histidine) only a single hit is required, whereas in the more sensitive situation (buffer), many hits are necessary for inactivation to occur. Therefore, the histidine must prevent the multi-hit process from acting. Hence, the sigmoidal vs. exponential kinetics requires that there be two mechanisms for production of double-strand breaks since the same lesion is produced. One can hypothesize that: 1) under protected conditions (histidine), only ionizations occurring within the phage head are lethal and, although both single and double breaks are produced, single breaks can never be made without double breaks also being produced. This is a necessary stipulation because otherwise a particle could be inactivated by two independnet sublethal ionizations (i.e., single breaks without lethality) which would result in sigmoidal inactivation. This idea is not untenable since the mean energy of an ion cluster produced by X rays in water ca. 100 eV which is enough energy to break 20 to 30 phosphoester bonds.

2) In the absence of protective conditions, reactive substances produced in the buffer by ionizations external to the phage diffuse in the head and make single breaks which accumulate until a matched pair results.

There is one difficulty with this model, namely the number of single breaks per dead phage in buffer is very small. At 50% survival there are ca. 10 to 20 single breaks per dead phage or per double-strand break which is not very different from the hit number. If the single breaks are randomly distributed, then a double break would be the result of two single breaks separated by as many as 100 base pairs, which seems improbable (11). However, only widely spaced breaks are counted in this analysis since nearby breaks or breaks near the ends would not have a detectable effect on the molecular weight. Furthermore, the distribution of breaks need not a priori be random since the partial opening of the double helix after a break is produced could easily make that region more susceptible to attack. An influence of the DNA packing in the phage head is also possible. Therefore, clustering of single breaks that would remain undetected could explain the result. Evidence that this may be the case comes from our experiments using a Pseudomonas phage similar in size to T7, in which case the number of single breaks measured by the rate of breakage of intact strands is twice that calculated from the molecular weight (9).

It should be noted that rupture of particles is not to be considered a cause of death (although they are certainly nonviable) since the DNA so released always consists of broken molecules. Therefore, the ruptured phages are probably the result of a small fraction of intra-head ionizations that apparently are sufficiently energetic so that both DNA and the head protein are damaged. The lack of effect of single-strand breaks deserves a brief comment. This is consistent with the fact that viable phages already contain natural single-strand breaks (5), but yet transforming DNA is inactivated by DNA-ase with exponential kinetics (12). However, this may be related to the mechanism of fixation of transforming DNA which apparently involves single strands (13).

SUMMARY

When coliphage T7 is X irradiated in buffer, the number of nonviable particles equals the number of particles that have suffered a double-strand break. If the irradiation is in histidine, an equivalent to nutrient broth, only 40% of the nonviable phages contain double-strand breaks. The remaining 60% can be protected by cysteine and N_2 and are probably inactivated by pyrimidine base damage. Individual single-strand breaks are ineffective.

ACKNOWLEDGMENTS

I wish to thank Katherine Le Blanc, Kristin Chung, and John Polachek for excellent technical aid during the course of this work.

REFERENCES

1. Davison, P. F., and Freifelder, D.; J. Mol. Biol. 5:643, 1962.
2. Freifelder, D., and Davison, P. F.; Biophys. J. 3:49, 1963.
3. Davison, P. F., and Freifelder, D.; J. Mol. Biol. 5:635, 1962.

4. Adams, M.: The Bacteriophage, New York, Interscience, 1959, p. 450.
5. Davison, P. F.; Freifelder, D., and Holloway, B. W.; J. Mol. Biol. 8:1, 1964.
6. Watson, J. D.; J. Bact. 60:697, 1950; J. Mol. Biol. 63:473, 1952.
7. Howard-Flanders, P.; Nature 186:485, 1960.
8. Hems, G.; Nature 186:710, 1960.
9. Freifelder, D.; unpublished data.
10. Foss, H. M., and Stahl, F. W.; Genetics 48:1659, 1963.
11. Trumbo, B.; unpublished calculations.
12. Lerman, L. S., and Tolmach, L. J.; Biochim. Biophys. Acta 33:371, 1959.
13. Fox, M. S., and Allen, M. K.; Proc. Nat. Acad. Sci. 52:412, 1964.

Received March, 1965.

A Technique for Starvation of E. coli of Thymine

David Freifelder

It is often expedient to stop DNA synthesis by depriving a thymine-requiring bacterium of exogenous thymine. Membrane filtration is the most effective procedure although intracellular pools fail to be depleted. These pools should be rapidly consumed by synthesis of a small amount of DNA yet it is not impossible that instead DNA synthesis continues at a low and undetectable rate. This uncertainty complicates the interpretation of experiments dealing with biological processes that require at best very little DNA synthesis, e.g., genetic transfer, phage induction, and recombination. In this paper a procedure is described for suppressing utilization of thymine (but which does not work for thymidine).

The bacterium used was a thymine-requiring Escherichia coli B/r (ATCC 12407). Liquid growth medium was tris-glucose minimal medium supplemented with 2 μg/ml thymine; viability was assayed on nutrient agar plates. E. coli B/r thy- undergoes thymineless death (1) when incubated in medium complete except for thymine. With low thymine concentrations, the death rate is reduced, as shown in Fig. 1; at 0.1 μg/ml all cells survive. However, if the cells are in medium containing 0.1 μg/ml thymine and 5-50 μg/ml uridine, the thymineless death proceeds normally. In Fig. 2 this effect of uridine concentration is shown. This same antagonism of low thymine protection is found for adenosine, guanosine, and cytidine. The free bases, adenine, guanine, cytosine, and uracil, at 50 μg/ml, are only half as effective as the ribosides and are inactive at 20 μg/ml. The deoxyribosides, ribose, and deoxyribose, are ineffective even at 100 μg/ml. Since free bases, but not deoxyribosides, can be easily converted to ribosides, the ribosides seem to be the active thymine antagonists. When thymidine replaces thymine, death is totally inhibited by 0.03 μg/ml; however, neither free bases, ribosides, and deoxyribosides, separately at 100 μg/ml each, nor in groups of four can antagonize low thymidine protection.

Thymineless death can be restored at any time by riboside addition. That is, when 10 μg uridine are added per ml to a culture preincubated in 0.1 μg/ml thymine for up to two hours, death ensues after the usual 30 to 40 min lag. Furthermore, the reversible nature of the protection by low concentration of thymine against thymineless death can be shown by adding thymine (0.1 μg/ml) for up to one hour after periods of no thymine. Death stops immediately but when uridine is added (10 μg/ml) the death curve resumes with that segment of the curve below the survival level at which death has been stopped.

Since, when 0.1 μg/ml thymine is used, thymineless death begins slowly after three hours, protection might result from a low rate of DNA synthesis (thymine concentration being

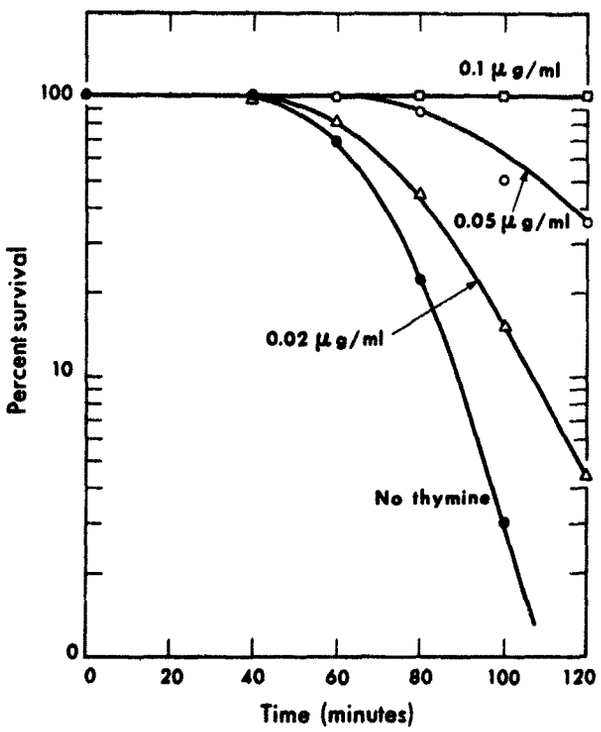

Figure 1. Survival of E. coli B/r thy- when incubated in growth medium containing various concentrations of thymine.
MUB-5935

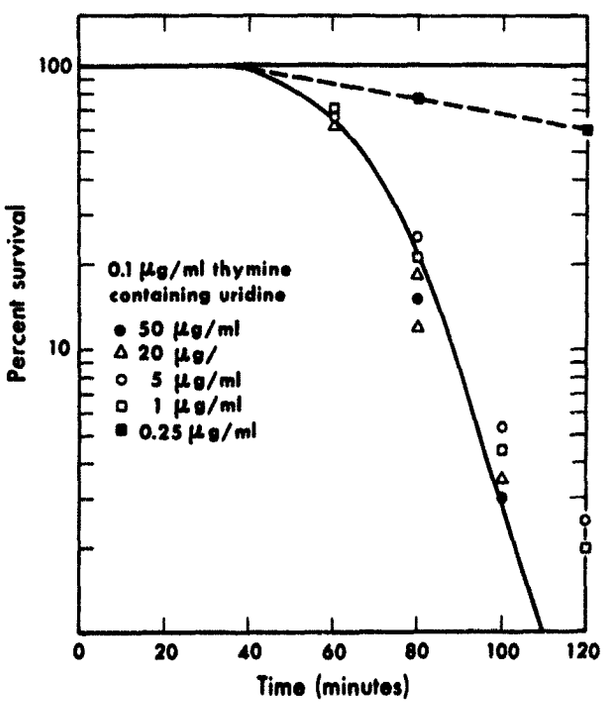

Figure 2. Antagonism of protection by 0.1 μg/ml thymine against thymineless death by various concentrations of uridine.
MUB-5936

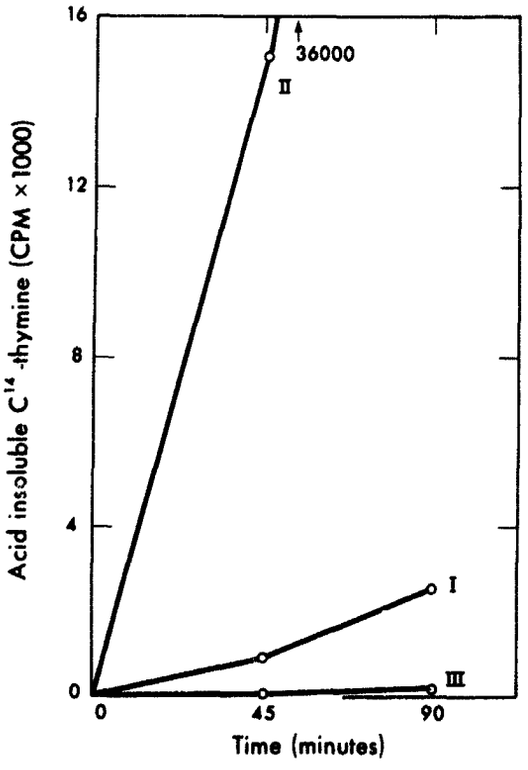

Figure 3. Incorporation of C^{14}-thymine into acid-soluble material by E. coli B/r thy- incubated in 1.0 and 0.1 μg/ml thymine and 0.1 μg/ml thymine + 20 μg/ml adenosine.
MUB-5934

rate-determining) which would ultimately stop when the thymine was (nearly?) exhausted. To test this, DNA synthesis was measured by incorporation of C^{14}-thymine into an acid-insoluble fraction, as shown in Fig. 3. Curve I shows the incorporation for 0.1 μg/ml C^{14}-thymine. In curve II, 0.9 μg/ml unlabeled thymine was added to raise the concentration to 1 μg/ml. The observed incorporated radioactivity has been multiplied by 10 since the specific activity was 10-fold lower in this case. It is clear that the concentration of thymine limits the rate of incorporation. In curve III, adenosine (20 μg/ml) has been added to 0.1 μg/ml C^{14}-thymine. The rate of incorporation has been reduced to 13% of that in curve I. At 50 μg/ml adenosine or other ribosides, the incorporation is not detectable. The mechanism of this inhibition has not been examined directly but is presumably the conversion of thymine to ribosyl thymine by transribosylation (2). It is unlikely that the inhibition is a result merely of prevention of uptake of thymine by the cells from the growth medium since thymine and thymidine are presumably taken up by the cell in the same way (probably passively) and thymidine utilization cannot be inhibited. Antagonism by such low concentrations of uridine as 0.25 μg/ml (Fig. 2) also argues against this idea.

These experiments suggest that utilization of thymine pools can be stopped by the addition of 50 μg/ml of any riboside. Any remaining activity of thymidylate synthetase in thymineless auxotrophs can probably be inhibited by the addition of 5 μg/ml fluorouridine deoxyriboside, a potent inhibitor of this enzyme (3).

ACKNOWLEDGMENT

I wish to thank Katherine Le Blanc, who performed these experiments.

REFERENCES

1. Barner, H. D., and Cohen, S. S.; Proc. Natl. Acad. Sci. 40:885, 1954.
2. Mantsavinos, R., and Zamenhof, S.; J. Biol. Chem. 236:876, 1961.
3. Cohen, S. S.; Flaks, J. G.; Barner, H. D.; Loeb, M. R.; and Lichtenstein, J.; Proc. Natl. Acad. Sci. 44:1004, 1958.

Received June, 1965.

Ultracentrifuge Rotor Temperature and Speed Measurement by Radio Telemetry

Stephen J. Fabricant and Frank T. Lindgren

The ultracentrifugal analysis of serum lipoprotein distributions (1, 2) has been difficult, in part, because of the enormous range in physical properties exhibited by the human lipoprotein spectra. For instance, the density range of human serum lipoproteins is indeed wide, ranging from 0.93 g/ml to 1.16 g/ml, and with molecular weights of the various lipoprotein components extending from 10^5 to 10^{11} units. Normally, for the sake of convenience and efficiency, both a low- and high-density lipoprotein fraction are run s multaneously in the Spinco Model E analytic ultracentrifuge. However, in order to gain significant information about the relative concentrations of the lipoproteins of high molecular weight and very low-density, which float rapidly in the ultracentrifuge, the first Schlieren photograph must be taken during the early part of the run, frequently while the rotor is still accelerating or just as the final speed of 52,640 rpm has been reached. To obtain information on the lower molecular weight low-density lipoproteins and the high-density lipoprotein fraction, the analytical run must proceed for an hour or more, during which time additional Schlieren photographs are taken.

In ultracentrifugal analysis, temperature control is complicated by the rapid adiabatic expansion and cooling (3) of the rotor during acceleration to full speed. These cooling effects are most pronounced at the periphery of the rotor near the analytic cell and lead to thermal gradients during the critical early phase of ultracentrifugation. Within the ultracentrifuge cell itself, temperature changes result in solution viscosity changes on the order of 2% per degree Centigrade (at 26°C), which result in an approximately corresponding change in measured sedimentation and flotation rates. In addition, rapid temperature changes cause convection effects that result in striations or gross irregularities on the Schlieren pattern, contributing to inaccuracies and difficulties in the lipoprotein analysis. Since our measurements and those of earlier investigators (3-5) have shown the acceleration period to be one of rapid and relatively great temperature change, and the remainder of the run period to be subject to significant temperature variations, it is desirable to monitor accurately and/or closely control the temperature to some fixed, repeatable value.

Several workers in the past have devised methods of measuring the temperature of the rapidly rotating ultracentrifuge rotor. These methods have fallen into three categories. One type of measurement, performed by Svedberg and Pedersen (4) and others (5-7), employed the direct optical observation of the melting of organic compounds in the ultracentrifuge cell. While this method provides accurate and valuable data on the thermal environment of

the cell, as opposed to the body of the rotor, it is clearly unsuitable for routine monitoring of regular analytical runs, in which samples are present in the cells of the analytical rotor.

A second method, devised by Waugh and Yphantis (3), used a radiation thermocouple to measure the temperature of the bottom of the rotor. Although this method was accurate and did not in any way impede the motion of the rotor, it nonetheless required sensitive equipment, a rather elaborate calibration technique, and a reference block, the temperature of which had to be known at all times.

The third general method employs some type of rotating contact to the rotor, to either transfer heat (8) or electrical information as from a thermistor (9) to a stationary contact. The most commonly used commercially available temperature monitor-controller, the Spinco R. T. I. C. unit (10), employs such a method, using a tungsten-steel needle dipping into a pool of mercury as a rotating contact for a thermistor attached at the bottom at the central axis of the rotor. This device has been used at this laboratory until recently when it was felt that certain disadvantages, primarily the inconvenience of mechanical non-interchangeability for different types of rotors, warranted the development of an entirely new temperature monitoring and controlling system.

Mackay and Jacobson (11) have perfected techniques of building small radio transmitters and used them to measure several physiological parameters of living subjects, thereby eliminating the need for direct electrical or mechanical connections to the subject. In particular, temperatures were measured readily, with an accuracy which depended largely on the sophistication of the equipment used. It was felt that such an approach might be applied to the problem of measuring rotor temperature and speed.

Our system under development applies some of the basic principles of radio telemetry to the problem of measuring the rotor temperature. The frequency of a small, temperature-sensitive transmitter, attached to the bottom of the rotor is measured by a radio receiver. This frequency is then correlated to the rotor temperature through a calibration procedure. Angular variations in the coupling between the transmitter antenna and receiving antenna produce amplitude modulation on the frequency-modulated carrier. The amplitude modulation is detected and its frequency counted electronically to indicate rotor revolutions per unit time.

THE TRANSMITTER

The transmitter consists of a transistorized Colpitts oscillator operating in the standard FM band. The capacitors in the frequency-determining LC circuit are inexpensive disc ceramic units that have been specially selected for high negative temperature coefficients, in the vicinity of -4000 ppm/°C. The RCA 2N709 transistor also has a net negative temperature coefficient of frequency in this circuit, but of a much smaller magnitude than that of the capacitors. The tuned circuit inductance, which serves as the antenna, concists of two turns of No. 30 wire inclined 45 degrees to the spin axis. The frequency of the transmitter

changes at a rate of approximately +60 kc per degree centigrade. The circuit of the transmitter is shown in Fig. 1.

The components of the transmitter are assembled symmetrically about its vertical axis and are then completely encapsulated in a mixture of powdered aluminum and epoxy cement. This ensures great mechanical rigidity and good thermal conductivity to the sensitive components, while still providing electrical insulation. The thermal response time of the encapsulated transmitter is about 5 sec. Two electrical contacts for battery power are brought out from the encapsulated transmitter. A brass ring at the midsection of the transmitter serves as the positive contact and is grounded by the retaining ring. A brass button at the end opposite the antenna loop serves as the negative battery contact. The transmitter is shown in Fig. 2.

The transmitter is powered by two Mallory RM-312 mercury cells in series, which provide 2.8 V at approximately 1 mA. These cells were found to be the most satisfactory ones available because of their small diameter (0.312 in.) that minimizes centrifugal stress (maximum force at the periphery of these cells at full speed is approximately 10,000 g). Two cells have powered the transmitter for as long as 26 hr, but they normally are replaced after about 5 hr to provide a safety factor. An experiment was performed to measure cell voltage under load at normal ultracentrifuge operating speed, with a modified Spinco mercury-cup RTIC rotating-contact device. The results of this experiment showed that the voltage produced by the cells remains constant within 2% during acceleration, at full speed (52,640 rpm), and during deceleration. Under load, the voltage drops very slowly, to about 80% of its initial value after some 24 hr, then drops rapidly to zero in less than one hour. The frequency of the transmitter is only slightly sensitive to operating voltage, and, if the system is calibrated at the start of each 70-min ultracentrifuge run, errors due to variations in battery voltage are of the order of ± 0.01°C. The fixture by which the transmitter is attached to the rotor is shown in Fig. 3. Several different fixtures have been made and tried, but it is difficult to evaluate how well the transmitter reflects the true thermal environment of the rotor sample cells. However, Gropper and Boyd (12) have measured the temperature gradient in aluminum rotors and found it to be quite small, on the order of 0.1°C. In the future, the rotors can be bored out to accommodate the transmitter, thereby eliminating the need for a bolt-on fixture and in addition placing the temperature-sensitive elements in the body of the rotor. A fixture that fastens the transmitter to the top of a preparative ultracentrifuge rotor has also been made and used in the Spinco Model L preparative machine.

Another possible source of frequency error may arise from centrifugal forces acting on the transmitter, and mechanically distorting components of the tuned circuit. No experiment to demonstrate or disclaim this possibility has been made as yet, but we feel that this effect would be extremely small owing to the great rigidity of the epoxy-aluminum casting material and the small radius (0.227 in.) of the transmitter.

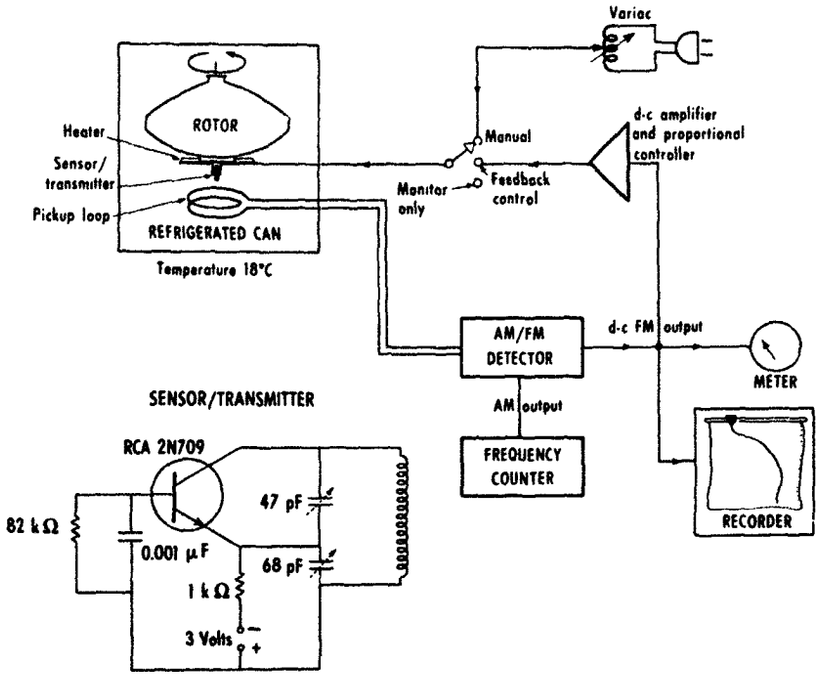

Figure 1. Block diagram of the ultracentrifuge temperature monitor/controller and speed indicator. Circuit diagram of the transmitter is shown in lower left.

MUB-6736

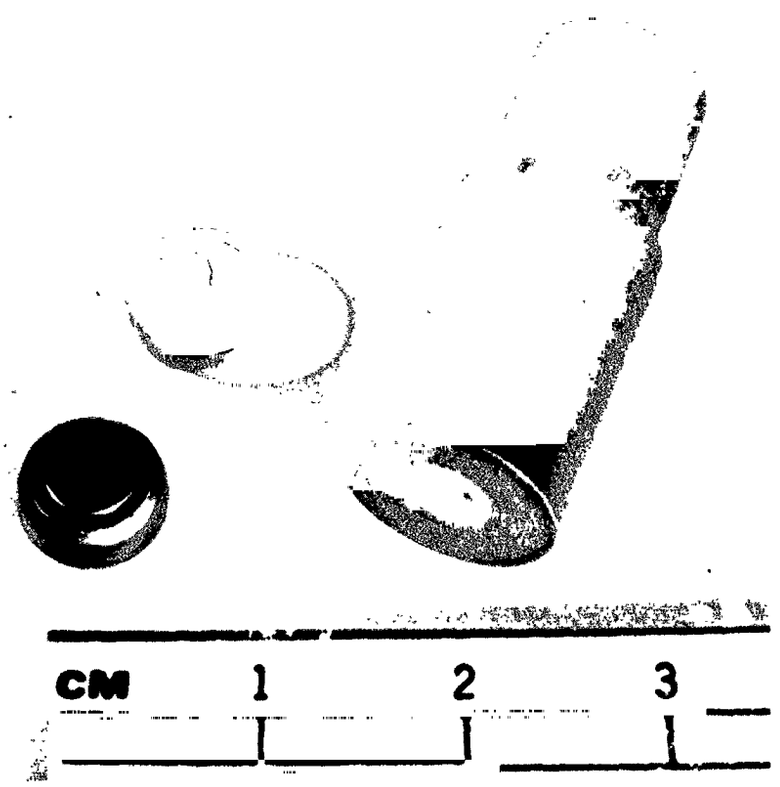

Figure 2. The telemetry transmitter used to monitor ultracentrifuge rotor temperature, and the two batteries that power it.

JHL-5098

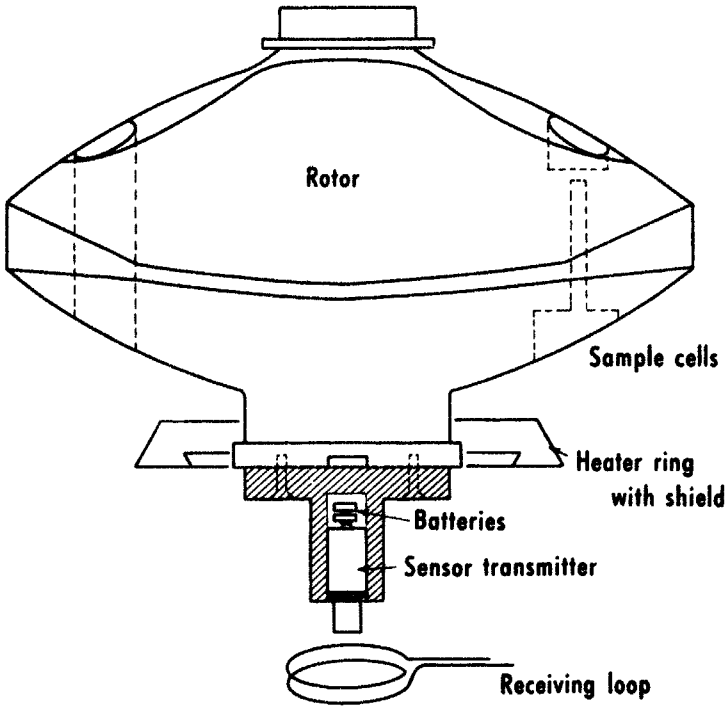

Figure 3. Schematic diagram of the transmitter and fixture attached to the ultracentrifuge rotor, showing the receiving antenna and control heater.
MUB-6658

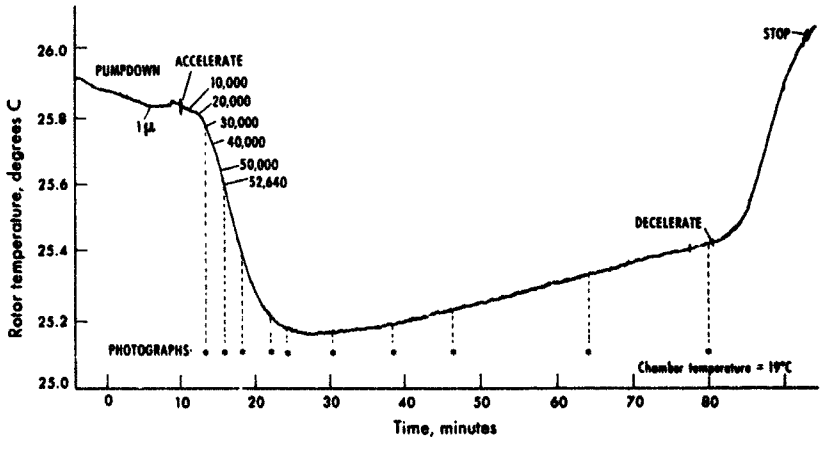

Figure 4. Recording of uncontrolled rotor temperatures, measured with the telemetry system, during a standard analytical run.
MUB-6659

THE RECEIVER

The signal from the transmitter is coupled to a stationary pickup coil consisting of two turns of wire one inch in diameter, mounted about one inch below the transmitter in the rotor chamber. This signal is fed via coaxial cable to the receiving equipment. The receiving equipment presently in use has been built around an inexpensive high-fidelity FM tuner, an Eico Model HF-90A. This tuner has been rack-mounted and modified electrically so that the dc voltage from the discriminator stage may be read on a zero-center panel meter as relative signal frequency, and fed to a strip-chart recorder. In addition, the incoming amplitude-modulated signal is tapped off before the limiter stages, and is detected and amplified for

rotor rpm measurement. The FM demodulator produces plus and minus approximately five volts over its linear range, corresponding to a frequency range of plus and minus 150 kc from the center frequency. This allows a range of temperature measurement of approximately ± 2°C without resetting the receiver tuning dial. While this receiving apparatus leaves something to be desired in the realm of absolute frequency calibration, linear frequency range, and resettability, frequency stability and signal sensitivity are entirely adequate for the task at hand. Future plans include more sophisticated frequency-measuring equipment.

TEMPERATURE CONTROL

The equipment described thus far is all that is needed to monitor rotor temperature. Once the temperature of the rotor is known, it is a relatively simple task to control it at any given temperature. To accomplish this, the dc signal from the receiver FM demodulator is fed into a dc amplifier that applies power to a heater in the rotor chamber. The heater power is thus proportional to the negative temperature error signal, and may go as high as 200 W when a large error signal is present, as occurs when a cold rotor is introduced to the centrifuge chamber. The specially fabricated heater is in the shape of a ring around the midsection of the rotor (Fig. 3) and is carefully shielded so it heats only a narrow band, approximately thermally equidistant from the sensing transmitter and the sample cells in the periphery of the rotor. This arrangement tends to minimize the effect of the small thermal gradient that exists between the cell and the rotor body.

RESULTS

TEMPERATURE MEASUREMENT Preliminary results have indicated that this telemetry system is capable of great temperature resolution. With little effort toward refinement, rotor temperature may be read with a precision of 0.01°C, once the system has been properly calibrated. Our present calibration procedure consists merely of immersing the transmitter and fixture in a water bath and measuring the temperature of the fixture with a thermistor probe while simultaneously monitoring the transmitter frequency. Water temperature is varied slowly and the voltage output from the telemetry receiver recorded on a strip-chart recorder. The temperature measured by the thermistor probe is marked on the chart at frequent intervals, and from this data a calibration curve is obtained. Absolute accuracy of calibration then depends solely on the accuracy of the thermistor device. Other errors in the system contribute an estimated ± 0.02°C. Since accurate data on the steady-state temperature gradient between cell and rotor bottom are available (12) for various types of analytic rotors, we feel our measurements of cell temperature are accurate to ± 0.05 °C. Rotor temperature was measured during a typical analytical run, as shown in Fig. 4. These results show a sharp temperature drop of about 0.7°C during acceleration, a slow rise due to frictional heating and finally a sharp rise on rotor deceleration. These results are very similar to those of Waugh and Yphantis (3), who used a radiation thermocouple to measure the temperature of the bottom of the rotor.

TEMPERATURE CONTROL When it is desired to control the temperature of the rotor to 26.0°C during an analytical run, the transmitter and mounting fixture are first immersed in a water bath held at the desired temperature, and the signal is tuned at the receiver

after thermal equilibrium has been reached, so the panel meter and chart recorder read at the center of their ranges. This fixture is then removed and attached to the rotor, which is placed in the ultracentrifuge vacuum chamber. When the chamber is closed, the signal from the pickup antenna in the chamber is fed to the receiver. The control loop is then closed by turning on the dc amplifier (Fig. 1). Preliminary results indicate that excellent temperature control may be obtained after some adjustment of the control-loop parameters, although some sort of manual control or automatic nonlinear control of the heater power may be necessary to compensate for the abrupt temperature drop due to adiabatic expansion of the rotor during acceleration, as shown in the "open-loop" recording of Fig. 4. It is anticipated that for future application a refrigerated, black-walled vacuum chamber and a black-anodized rotor should give better results because of increased efficiency of radiation heating and cooling.

RPM MEASUREMENT The sinusoidal amplitude-modulated signal produced by varying coupling between transmitter and receiver antennas during rotation is detected and amplified in the receiver. The frequency of the sine wave is the rotational frequency of the rotor, and is counted for either 0.6, 6.0, or 60 sec by a Hewlett-Packard Preset Counter Model 5214L, depending on the time period over which it is desired to integrate rpm. This provides a continuous digital display of rotor rpm, having far greater accuracy than that obtainable with the usual ultracentrifuge tachometer. When 5-digit accuracy is desired in a shorter counting time, the period of the sine wave may be measured. We plan to use this capability as a part of a control circuit that will automatically accelerate the rotor from rest to 52,640 rpm according to a pre-determined time-velocity profile.

SUMMARY

The principles of radio telemetry have been applied in achieving a unique solution to the problem of analytic ultracentrifuge rotor temperature measurement, eliminating the necessity for a direct electrical connection to the rotor. A small transmitter operating in the standard FM band and powered by batteries is mounted in a fixture that is bolted to the rotor. The frequency of the transmitter is a function of rotor temperature, and the amplitude of the received carrier is dependent on the angular relationship of the transmitter to a pickup loop mounted several inches below the rotor. This composite AM and FM signal is detected by an ordinary FM tuner. The output of the FM detector is read on a voltmeter or a recorder as temperature; the AM signal is counted by an electronic counter to display rotor speed in digital form. This system is capable of repeatable temperature measurements accurate to ± 0.05°C after appropriate calibration. Also, the system has been used in conjunction with a heater in a feedback loop to provide accurate temperature control of the rotor during the analytical run.

ACKNOWLEDGMENTS

We particularly wish to thank Frank T. Upham, and Alfred A. Windsor, of the Electronics Department, and Edward F. Dowling, of the Machine Shop, Lawrence Radiation Laboratory, for their valuable assistance.

This work was supported in part by research grant HE 02029-10 from the National Heart Institute, U. S. Public Health Service, and by the Atomic Energy Commission.

REFERENCES

1. deLalla, O., and Gofman, J.; in Methods of Biochemical Analysis, Vol. 1., edited by D. Glick, New York, Interscience, 1954, p. 459.
2. Ewing, A. M.; Freeman, N. K., and Lindgren, F. T.; in Advances in Lipid Research, Vol. 3, edited by R. Paoletti and D. Kritchevsky, New York, Academic Press Inc., 1965, Chpt. 11.
3. Waugh, D. F., and Yphantis, D. A.; Rev. Sci. Instr. 23:609, 1952.
4. Svedberg, T., and Pedersen, K. O.; The Ultracentrifuge, Oxford, Clarendon Press, 1940, p. 226.
5. Biancheria, A., and Kegeles, G.; J. Am. Chem. Soc. 76:3737, 1954.
6. Baldwin, R. L.; Biochem. J. 65:603, 1957.
7. Cecil, R., and Ogston, A. G.; Biochem. J. 43:592, 1948.
8. Bauer, J. H., and Pickels, E. G.; J. Exptl. Med. 65:565, 1937.
9. Ecker, P. G.; Blum, J., and Hiatt, C. W.; Rev. Sci. Instr. 20:799, 1949.
10. R. T. I. C. Operating Manual, Beckman Instruments Spinco Div., Palo Alto, Calif.
11. Mackay, R. S., and Jacobson, B.; Nature 179:1239, 1957.
12. Gropper, L., and Boyd, W.; Anal. Biochem. 11:238, 1965.

Received July, 1965.

Particle-Size Distribution of Very Low-Density Plasma Lipoproteins

Thomas L. Hayes, Frank T. Lindgren, James N. Hawkins, Alicia M. Ewing and Edwin L. Bierman

The very low-density plasma lipoproteins (S_f 20-10^5) represent an important fraction of the serum lipids, especially with regard to the early phases of fat absorption and metabolism. Their size range, extending from approximately 250 to 10,000 Å, makes them particularly suitable for study with the electron microscope (1-5). In addition to particle size, the lipoprotein surface properties, including net electrical charge, allow fractionation of these very large S_f 20-10^5 lipoproteins by starch-block electrophoresis (6, 7). Subsequent ultracentrifugal flotation permits isolation of these lipoprotein-containing fractions from other plasma macromolecules possessing the same electrophoretic properties.

Preliminary estimates (7, 8) of the physical properties for both the primary and secondary particle have placed them in the size range of from 700 Å to 2,000 Å in particle diameter. However, a more definitive analysis of both the particle size and flotation-rate distribution of these two electrophoretic classes of very low-density lipoproteins is needed. It is hoped that such information regarding lipoprotein particle-size distributions may be useful in furthering our understanding of the structure and function of the very low-density lipoproteins.

METHODS

Postprandial human plasma was obtained from normal subjects three to four hours after the feeding of 250 cc of corn oil blended with skim milk. In addition, eight subjects were given butterfat in place of corn oil; two of these subjects had recieved corn oil in a previous experiment. Samples of fresh, unrefrigerated plasma, measuring 8 to 17 cc, were fractionated by starch block electrophoresis under the conditions previously described (7). The turbidity peaks of primary and secondary particles, as determined by nephelometry (Coleman Model 14) of eluted starch block segments, migrated (relative to albumin) within the normal range (.60 ± .10 and .23 ± .08 respectively) (7). Large starch segments containing primary-particle (PP) and secondary-particle (SP) fractions were eluted with isotonic saline by aspiration through a coarse sintered glass filter. Eluates were concentrated and washed twice by ultracentrifugal flotation through saline for approximately 3×10^6 g x min in a Spinco SW 39 rotor. The fractions were stored at 4 to 10 °C until analyzed. These primary- and secondary-particle fractions (PP and SP) were analyzed by analytic ultracentrifugation and electron microscopy in order to determine flotation-rate characteristics and particle-size distribution, respectively. Total lipoprotein content of each fraction was estimated from a total-lipid extraction and gravimetric assay.

One primary and three secondary particle fractions were studied in the analytic ultracentrifuge to determine, if possible, the low end of the S_f-rate distribution. For this purpose, 87.1 mg of solid NaCl was added to 1 ml of each fraction, bringing the solvent density at 26 °C to 1.0613 g/ml (1.700 molal NaCl). Although a diffuse turbidity boundary rapidly migrated in each lipoprotein fraction during acceleration, no resolvable concentration of lipoproteins less than S_f 400 was observed. Unfortunately, the turbidity of particles of 750 Å and larger (corresponding to S_f values of 400 and greater) effectively interferes with resolution in the Schlieren optical system. Nonetheless, these ultracentrifugal findings definitely indicate that the S_f-rate distributions of the primary and secondary particle fractions studied are essentially above S_f 400.

In order to evaluate further the nature of the particle-size distribution as well as lipoprotein stability to preparative ultracentrifugation, a secondary-particle fraction was subfractionated on a density gradient (9). The conditions of low-speed centrifugation (3,800 ×g for 23 min at 20 °C) were such as to permit recovery of the S_f 20,200 and higher lipoprotein classes in the top milliliter of the preparative tube. In all, 17 fractions (one milliliter and 16 half-milliliter fractions) were taken from the 1/2- by 3 1/2-in. preparative tube. Prior to centrifugation, a half milliliter of a secondary-particle fraction in 1.70 molal NaCl was introduced separately at the bottom of a preformed nonlinear NaCl gradient, using a spinal needle and a syringe. A control NaCl gradient was used to evaluate by refractometry the density and viscosity in each region of the preparative tube. The top of the gradient tube had a density of 1.0065 g/ml and the bottom 1.0650 g/ml (unless otherwise indicated, all densities are given at 20 °C). Particle-size distributions for each fraction were determined using a Model HU-11 Hitachi electron microscope.

The fixation process for electron microscopy utilized 1% of OsO_4 in a buffer at pH 7.4. After exposure for one-half hour, the fixed lipoproteins were placed on the electron microscope grid for viewing. Particle-diameter measurements were made from prints with a total magnification of about 15,000 x. Data obtained in this way were analyzed in order to yield particle-size distribution, mass distribution and sedimentation-rate distribution, as well as average values of these parameters. Conversion of particle-diameter distributions to mass distribution and flotation-rate distribution was achieved using a computer.

The experimental data, consisting of measurements of each individual particle diameter, were punched on Standard IBM cards and analyzed by a program for the IBM 7094 computer. The approximate computer procedure was as follows:

1) reading the data for a single electron microscope plate;
2) performing a desired calculation on each data item; e.g., converting measured diameter to actual diameter in angstroms, calculating molecular weights and calculating flotation rates;
3) generating a histogram for such a series of newly calculated values. The size of the histogram intervals was easily changed by an input card at the beginning of each use of the program.

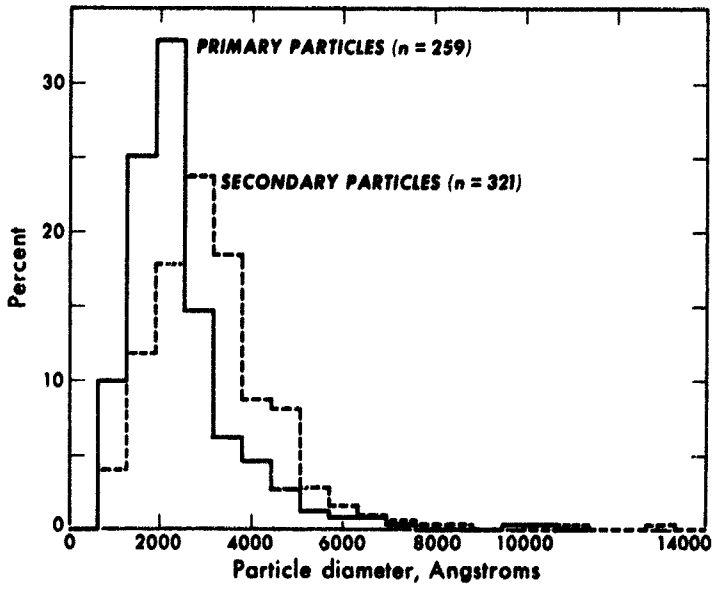

Figure 1. Comparison of a primary- and secondary-particle diameter distribution obtained from the same plasma (Sample # 2).

MUB-2604

The program was written in Fortran and was easily modified to calculate any values for which histogram distributions were desired.

RESULTS

Figure 1 shows a comparison of particle-size distribution of a primary- and secondary-particle fraction obtained from the same plasma (PP-2, SP-2). In each fraction, the particle size ranged from approximately 750 to 6,000 Å in diameter. Three similar pairs of primary and secondary particles were analyzed, and it would appear that the particle-size distribution for each of these fractions are comparable. Further, in each of the three pairs, the secondary particles have a somewhat larger particle diameter than the primary particles. Typical electron micrographs used in the study of PP-2 (Fig. 2) and SP-2 (Figs. 3 and 4) are shown.

The anticipated and experimental recoveries of subfractions from the density-gradient flotation experiment is shown in Fig. 5. Before centrifugation, the secondary-particle fraction (SP-3) in 1.70 molal NaCl was introduced into region 17 of the preparative tube.

Table 1 presents the average particle size, molecular weight and S_f rate for 17 fractions obtained from this density gradient separation. Figure 6 shows the detail of the particle-diameter distributions obtained for the 3rd, 7th, 11th, and 15th fractions, and Fig. 7 shows a typical electron micrograph for fraction 13. Although there is a considerable overlap in size distribution for adjacent fractions, the results are consistent with anticipated recovery (somewhat smaller particle sizes were obtained experimentally than by calculation from ultracentrifugal flotation). This comparison is made with the calculated threshold recovery, 100% recovery and limiting recovery, assuming a continuous distribution of lipoprotein particle size of constant hydrated density (0.93 g/ml). The calculations were made with a computer treating each of the 17 regions of the gradient as a homogenous medium of constant density and

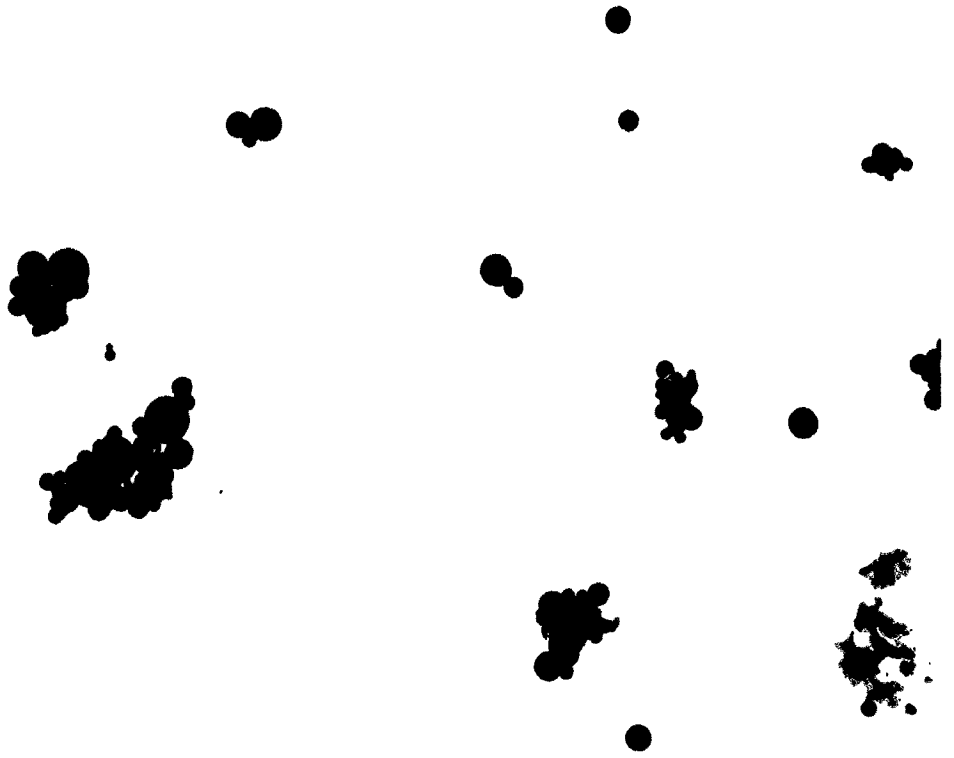

Figure 2. Typical electron micrograph of primary-particle fraction (PP-2). Magnification is 11,400 x.

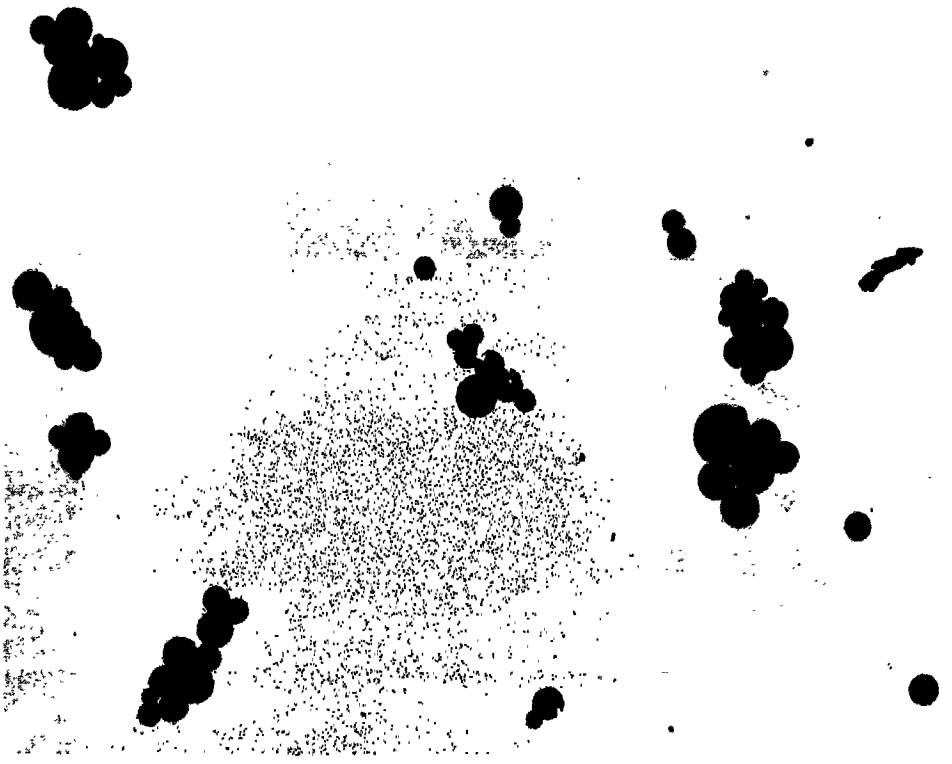

Figure 3. Typical electron micrograph of secondary-particle fraction (SP-2). Magnification is 11,400 x.

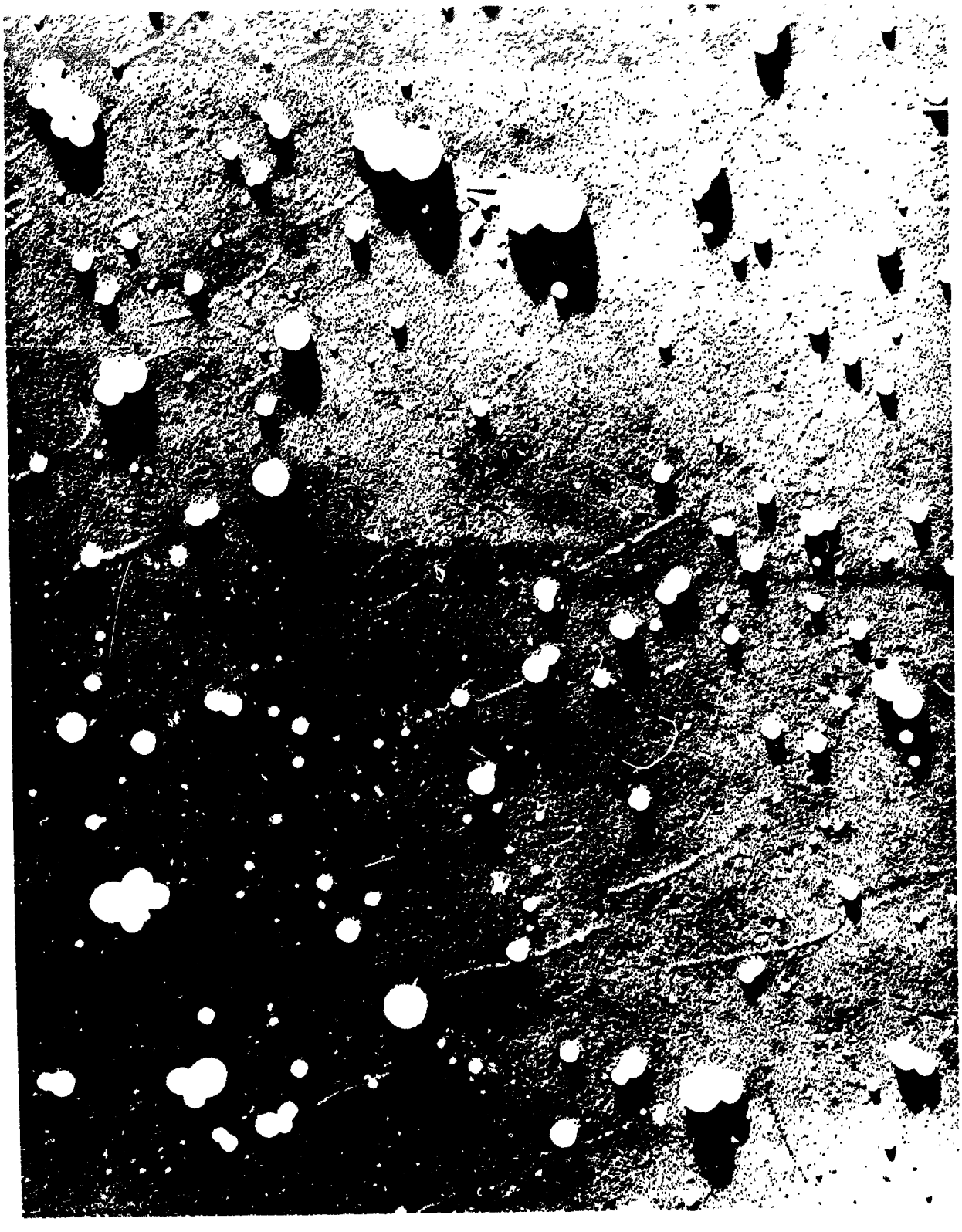

Figure 4. Chromium shadowed preparation on secondary-particle fraction (SP-2). Magnification is 16,600 x.

Table 1. Subfractionation of secondary particle sample (SP-3)

Subfraction		n	Lipoprotein particle diameter		Molecular weight in 10^6 molecular weight units		S_f rate (Svedbergs)	
			Average diameter	Standard deviation	Mass average	Standard deviation	S_f rate average	Standard deviation
1	a	52	4,240 Å	± 1,500	30,500	± 25,700	15,200	± 9,440
	b	80	4,150	± 1,420	28,100	± 23,400	14,400	± 8,750
2	a	58	3,870	± 897	19,700	± 12,600	11,800	± 5,180
	b	36	3,510	± 959	15,400	± 10,100	9,850	± 4,740
3	a	68	4,010	± 984	22,400	± 19,600	12,700	± 8,650
	b	52	4,010	± 1,110	23,700	± 26,800	12,900	± 8,220
4	a	30	3,480	± 606	13,400	± 5,770	9,270	± 2,930
	b	62	3,550	± 966	16,500	± 19,900	10,100	± 6,560
5	a	151	3,440	± 864	14,300	± 13,500	9,350	± 5,040
	b	85	3,690	± 674	16,300	± 9,980	10,500	± 4,070
6	a	94	3,190	± 667	10,900	± 8,690	7,880	± 3,630
	b	83	3,060	± 824	10,100	± 6,440	7,440	± 3,530
7	a	120	2,930	± 698	8,790	± 8,950	6,710	± 3,760
	b	54	2,940	± 453	7,990	± 3,290	6,350	± 1,910
8	a	67	2,860	± 770	8,720	± 12,900	6,480	± 4,780
	b	63	3,840	± 577	7,700	± 8,060	6,200	± 3,270
9	a	50	2,720	± 747	7,690	± 12,700	5,890	± 4,710
	b	46	2,710	± 521	6,480	± 4,180	5,500	± 2,270
10	a	78	2,220	± 387	3,510	± 1,860	3,720	± 1,320
	b	143	2,430	± 482	4,820	± 5,930	4,510	± 2,480
11	a	120	1,950	± 376	2,420	± 1,350	2,880	± 1,100
	b	139	2,010	± 303	2,550	± 1,360	3,010	± 975
12	a	90	1,980	± 307	2,450	± 1,090	2,940	± 901
	b	-	-	-	-	-	-	-
13	a	300	1,700	± 324	1,530	± 1,450	2,190	± 978
	b	349	1,850	± 323	2,010	± 966	2,560	± 861
14	a	120	1,720	± 270	1,610	± 712	2,210	± 673
	b	339	1,640	± 315	1,450	± 828	2,030	± 778
15	a	150	1,610	± 174	1,260	± 395	1,900	± 407
	b	120	1,270	± 194	650	± 293	1,190	± 367
16	a	150	1,160	± 208	504	± 280	997	± 365
	b	150	1,160	± 250	523	± 313	1,010	± 425
17	a	249	1,150	± 215	489	± 266	975	± 364
	b	235	1,132	± 214	472	± 267	950	± 365

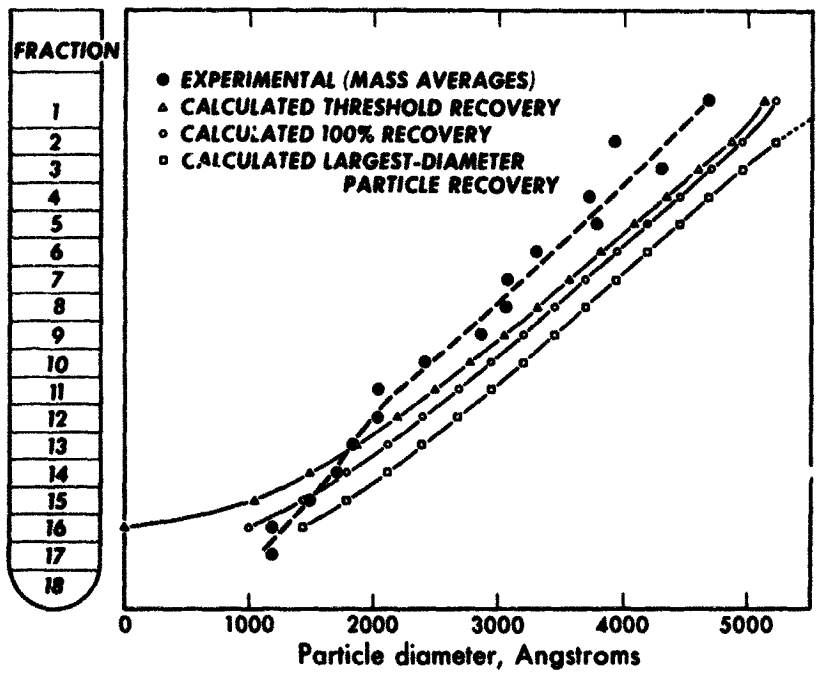

Figure 5. Comparison of experimental recovery with calculated recovery for the density-gradient flotation experiment.
MUB-2603

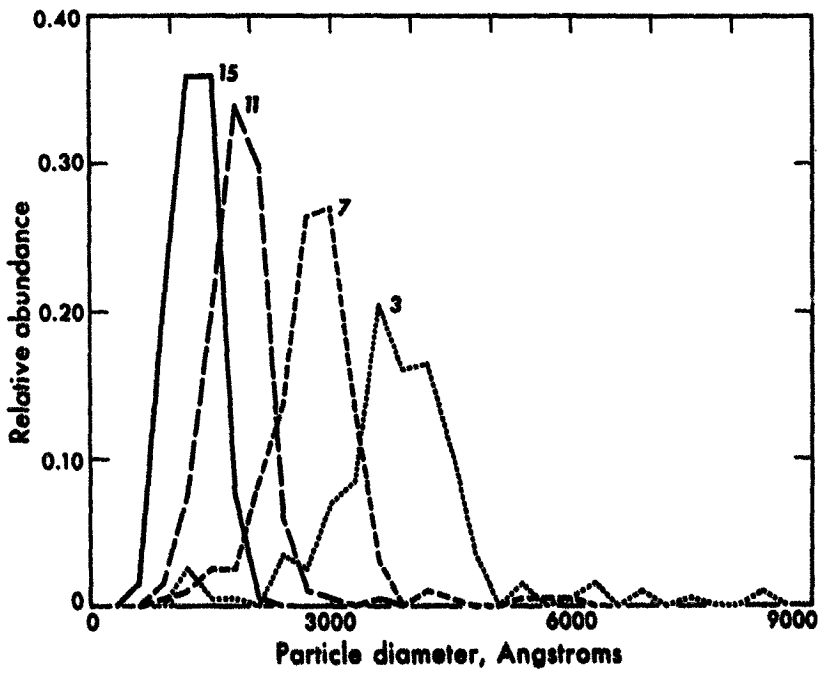

Figure 6. Distribution of particle diameter for the 3rd, 7th, 11th, and 15th subfractions as obtained from the density-gradient flotation of a secondary-particle fraction (SP-3). For clarity of presentation, the histograms have been converted to an estimate of continuous particle-diameter distribution.
MUB-2605

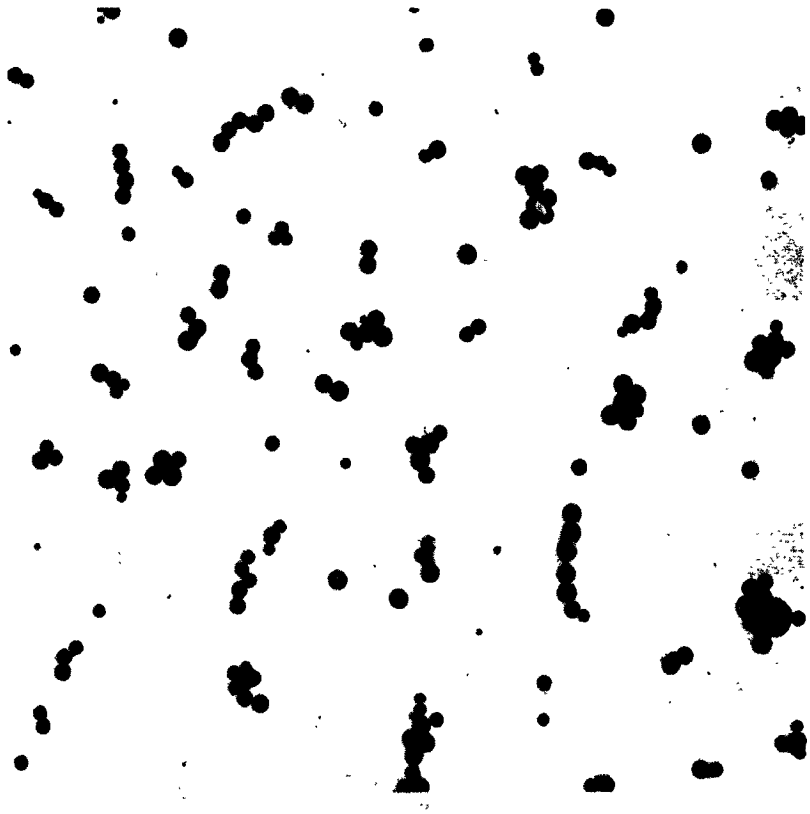

Figure 7. Electron micrograph of ultracentrifugal subfraction 13 (SP-3). Magnification is 11,400 x.

viscosity. These results also suggest that preparative centrifugation, osmium fixation and dispersion in the initial preparation for the fractions, as well as in this analysis, do not significantly alter the particle-size distribution.

It may be of considerable significance that in no case of butterfat-produced chylomicrons were we able to visualize the particles in the electron microscope, using our usual techniques of osmium fixation.

DISCUSSION

The particle-size distributions of electrophoretically and ultracentrifugally fractionated very low-density plasma lipoproteins from subjects receiving corn oil have been determined using the electron microscope. The results obtained on four secondary-particle fractions and three primary-particle fractions indicate a considerably broader particle-size distribution than was previously estimated (7). These preliminary data suggest that both primary and secondary particles have a size distribution that includes most of the known serum-lipoprotein spectrum above S_f 400. Further, from the comparable primary- and secondary-particle distribution observed in a given plasma sample, it would appear that significantly different surface properties may exist for lipoproteins of the same particle size.

By using only the measurement of diameter, it has been possible to calculate molecular-weight distribution and flotation-rate distributions of each lipoprotein fraction and subfraction studied with the electron microscope. However, in these calculations it has been assumed that no change in particle size occurs as a result of osmium fixation. Since at one-half hour the stoichiometry of the fixation reaction (10) with very low-density lipoproteins requires approximately 1 to 2 moles osmium per mole fatty acid double bond, the lipoproteins might be expected to increase their size by an amount approximately equivalent to the added volume of osmium. Because of the very small partial specific volume of osmium, it is estimated that the size of the fixed lipoproteins is on the order of 5% larger than the native unfixed lipoproteins. The importance of the degree of lipid unsaturation in the osmium tetroxide-lipoprotein reaction has been pointed out (10, 11). The failure of the osmium to fix butterfat-produced chylomicrons may reflect a significant change in amount or location of fatty acid double bonds in particles from subjects fed butterfat instead of corn oil. Further experiments are in progress to determine the effect of diet and certain disease states on the particle size of these very low-density plasma lipoproteins.

SUMMARY

The size distributions of electrophoretically isolated subfractions of the very low-density human plasma lipoproteins have been determined, using electron microscopic techniques. By this method, the primary and secondary particles show size distributions that are essentially the same. Very low-density lipoproteins produced by corn-oil feeding can be fixed by osmium tetroxide reaction whereas those produced by butterfat feeding could not be fixed or visualized by this technique. Evidence is presented that shows a good agreement between particle size as measured by electron microscopy and particle size as predicted by ultracentrifugal analysis.

ACKNOWLEDGMENTS

These studies have been carried out as a cooperative study with the Department of Medicine, University of Washington School of Medicine and Veterans Administration Hospital, Seattle, Washington. The work described in this paper was supported in part by Research Grant HE-02029-09 from the National Heart Institute, Public Health Service, and AM-06670-01 from the U. S. Public Health Service, Bethesda, Md., and by the U. S. Atomic Energy Commission.

REFERENCES AND NOTES

1. Hayes, T. L., and Hewitt, J. D.; J. Appl. Physiol. 2:425, 1957.
2. Lindgren, F. T.; Nichols, A. V.; Hayes, T. L.; Freeman, N. K., and Gofman, J. W.; Ann. N. Y. Acad. Sci. 72:826, 1959.
3. Hayes, T. L.; Lindgren, F. T., and Schooley, J. C.; Semiannual Report, Donner Laboratory, Lawrence Radiation Laboratory, UCRL-9897, 1961.
4. Jones, R.; Thomas, W. A., and Scott, K. F.; Exptl. and Mol. Pathol. 1:65, 1962.
5. Casley-Smith, J. R.; J. Cell. Biol. 15:259, 1962.
6. Kunkel, H. G., and Trautman, R.; J. Clin. Invest. 35:641, 1956.

7. Bierman, E. L.; Gordis, E., and Hamlin, J. T. (III); J. Clin. Invest. 41:2254, 1962.
8. Dole, V. P., and Hamlin, J. T. (III); Physiol. Rev. 42:674, 1962.
9. Lindgren, F. T.; Nichols, A. V.; Upham, F. T., and Wills, R. D.; J. Phys. Chem. 66:2007, 1962.
10. Hayes, T. L.; Lindgren, F. T., and Gofman, J. W.; J. Cell. Biol. 19:251, 1963.
11. Hayes, T. L., and Hawkins, J. N.; Semiannual Report, Donner Laboratory, Lawrence Radiation Laboratory, UCRL-11184:110, 1963.

Edwin L. Bierman is associate professor of Medicine and Chief, Metabolic Disease Service, University of Washington School of Medicine and Veterans Administration Hospital, Seattle, Washington.

Received December, 1964.

STAFF PUBLICATIONS

Anger, H. O.; Van Dyke, D. C.; Gottschalk, A.; Yano, Y., and Schaer, L. R.: The Scintillation Camera in Diagnosis and Research, Nucleonics 23:57-62, 1965.

Berlin, N. I., and Siri, W. E.: Isotopic Determination of Body Composition in Man, in Progress in Atomic Medicine, Vol. I, edited by J. H. Lawrence, New York, Grune & Stratton, 1965, Chap. 2, pp. 34-52.

D'Angio, G. J.; Lawrence, J. H.; Gottschalk, A., and Lyman, J.: Relative Efficiency of High-LET Radiation (Bragg-Peak Lithium Ions) on Normal Rabbit Skin, Using Integral Dose as a Basis for Comparison, Nature 204:1267-1268, 1964.

Freifelder, D.: A Novel Method For the Release of Bacteriophage DNA, Biochem. Biophys. Res. Commun. 18:141-144, 1965.

Gottschalk, A., and Anger, H. O.: Letter to the Editor, J. Nucl. Med. 5:569-570, 1964.

Gottschalk, A., and Anger, H. O.: Progress in Radioisotope Scanning: Clinical Application of the Scintillation Camera, in Progress in Atomic Medicine, Vol. I, edited by J. H. Lawrence, New York, Grune & Stratton, 1965, Chap. 4, pp. 78-106.

Gottschalk, A., and Anger, H. O.: Renal Scintiphotography with the Gamma-Ray Scintillation Camera and Hg^{203}-Neohydrin, Radiology 84:861-867, 1965.

Gottschalk, A.; McCormack, K. R.; Adams, J. E., and Anger, H. O.: A Comparison of Results of Brain Scanning Using Ga^{68}-EDTA and the Positron Scintillation Camera, with Hg^{203}-Neohydrin and the Conventional Focused Collimator Scanner, Radiology 84:502-506, 1965.

Grendon, A.: Federal Radiation Guides and Other Exposure Standards, Am. J. Public Health 55:738-747, 1965.

Hanawalt, P. C., and Haynes, R. H.: Repair Replication of DNA in Bacteria: Irrelevance of Chemical Nature of Base Defect, Biochem. Biophys. Res. Commun. 19:462-467, 1965.

Haynes, R. H.: Radiobiology, Macromolecular Aspects Of, in McGraw-Hill Yearbook of Science and Technology, 1965 edition, New York, McGraw-Hill Inc., 1965, pp. 353-354.

Hildreth, P. E.: Doublesex, A Recessive Gene that Transforms Both Males and Females into Intersexes, Genetics 51:659-678, 1965.

King, J. L.: The Effect of Litter Culling - or Family Planning - on the Rate of Natural Selection, Genetics 51:425-429, 1965.

La Roche, G.; Johnson, C. L., and Woodall, A. N.: Thyroid Function in the Rainbow Trout (Salmo gairdneri, Rich.) I. Biochemical and Histological Evidence of Radiothyroidectomy, Gen. Comp. Endocrinol. 5:145-159, 1965.

Lawrence, J. H.: Nuclear Techniques in Biomedical Research, Nucleonics 23:48-49, 1965.

Lawrence, J. H., and Tobias, C. A.: Heavy Particles in Medicine, in Progress in Atomic Medicine, Vol. I, edited by J. H. Lawrence, New York, Grune & Stratton, 1965, Chap. 6, pp. 127-146.

Lawrence, J. H.; Tobias, C. A.; Linfoot, J. A.; Born, J. L.; Manougian, E., and Lyman, J.: Heavy Particles and the Bragg Peak in Therapy, Ann. Internal Med. 62:400-407, 1965.

Lindgren, F. T.; Freeman, N. K., and Nichols, A. V.: Physical and Chemical Properties of the Low-Density Lipoproteins and Their Analysis by Refractometry, in Metabolism of Lipids as Related to Atherosclerosis, compiled by F. A. Kummerow, Springfield, Ill., Charles C. Thomas, 1965, pp. 1-14.

Low-Beer, A. de G., and Parker, H. G.: Decreased Recovery of Gross Alpha Determinations by Alkaline Phosphate Precipitation in the Presence of DTPA, Health Phys. 11:61-62, 1965.

Mel, H. C.; Mitchell, L. T., and Thorell, B.: Continuous Free-Flow Fractionation of Cellular Constituents in Rat Bone Marrow, Blood 25:63-72, 1965.

Nichols, A. V., and Smith, L.: Effect of Very Low-Density Lipoproteins on Lipid Transfer in Incubated Serum, J. Lipid Res. 6:206-210, 1965.

Pollycove, M.: Iron Metabolism, in Thannhauser's Textbook of Metabolism and Metabolic Disorders, 2nd edition, edited by N. Zöllner. American edition translated and edited by S. Estren, New York and London, Grune & Stratton, 1964, Vol. II, Chap. 15, pp. 809-842.

Schooley, J. C.: Responsiveness of Hematopoietic Tissue to Erythropoietin in Relation to the Time of Administration and Duration of Action of the Hormone, Blood 25:795-808, 1965.

Schooley, J. C., and Garcia, J. F.: Some Properties of Serum Obtained From Rabbits Immunized with Human Urinary Erythropoietin, Blood 25:204-217, 1965.

Schooley, J. C., and Kelly, L. S.: Influence of the Thymus on the Output of Thoracic-Duct Lymphocytes, in The Thymus in Immunobiology; Structure, Function, and Role in Disease, edited by R. A. Good, New York, Evanston, London, Harper & Row, 1964, Chap. 11, pp. 236-254.

Snyder, N. J.: Iodine 131 in the Treatment of Thyroid Cancer and its Use for Thyroid Ablation in Certain Nonthyroid Diseases, in Progress in Atomic Medicine, Vol. I, edited by J. H. Lawrence, New York, Grune & Stratton, 1965, Addendum to Chap. 8, pp. 219-226.

Strisower, E. H.; Nichols, A. V.; Lindgren, F. T., and Smith, L.: The Effect of Sf 20-10^5 Concentration Changes Induced by Ethyl Chlorophenoxyisobutyrate on High-Density Lipoprotein Lipid Composition, J. Lab. Clin. Med. 65:748-755, 1965.

Tokunaga, C., and Stern, C.: The Developmental Autonomy of Extra Sex Combs in Drosophila melanogaster, Develop. Biol. 11:50-81, 1965.

Tym, R., and Todd, P. W.: The Sensitization by Iododeoxyuridine of Cultured Human Cells to the Lethal Effect of X-rays and Heavy Ions, Intern. J. Radiation Biol. 8:589-603, 1964.

Van Dyke, D., and Anger, H. O.: Patterns of Marrow Hypertrophy and Atrophy in Man, J. Nucl. Med. 6:109-120, 1965.

Winchell, H. S.; Pollycove, M.; Kusubov, N., and Fawwaz, R.: Kinetics of ^{131}I-albumin and ^{131}I-transferrin in Lymph, in Symposium on the Preparation and Biomedical Application of Labeled Molecules, Venice, Aug. 1964, Proceedings, edited by M. Sirchis, Brussels, Euratom, 1965, pp. 273-286.

Yano, Y., and Anger, H. O.: Production and Chemical Processing of Fe^{52} for Medical Use, Intern. J. Appl. Radiation Isotopes 16:153-156, 1965.